

ROBUST COMPUTATIONS OF TURBULENT FLOWS

Submitted by Simone Mandica
for the degree of
Doctor of Philosophy
of the University of Bath
Department of Mathematical Sciences
August 2006

COPYRIGHT

Attention is drawn to the fact that copyright of this thesis rests with its author. This copy of the thesis has been supplied on condition that anyone who consults it is understood to recognise that its copyright rests with its author and no information derived from it may be published without the prior written consent of the author.

This thesis may be made available for consultation within the University library and may be photocopied or lent to other libraries for the purposes of consultation.

Signature of Author

Simone Mandica

A Roberta, la mia stella polare.

Abstract

We consider the numerical solution to the stationary Reynolds averaged Navier-Stokes equations coupled with the k - ε turbulence model. These form a second-order system of partial differential equations which is used in engineering applications to model the mean properties of turbulent flows; this set of equations is highly nonlinear and presents the additional complication that the variable ε (the dissipation rate of mean turbulent energy) blows-up as the parameter $h_+ \rightarrow 0$. (The parameter h_+ is the distance of artificial boundaries (“walls”) from physical boundaries and, for modelling reasons, approaches zero as the Reynolds number increases).

Using the standard Galerkin finite element method, we discretise the equations on a mesh which is carefully refined in the direction of the ε blow-up, and is designed to approximate, accurately and efficiently, the unknowns in an appropriate sense. The mesh grading depends on h_+ . This dependence is investigated in detail theoretically and by numerical experiments. Through numerical experiments on $1D$ problems and $2D$ straight channel flows, we show that, by using this graded mesh, very little computational effort is needed to obtain accurate solutions, even in the case of very small values of h_+ .

Not only is the mesh very satisfactory from the point of view of the accuracy of the numerical solutions and of the practicality of their computation but it also improves drastically the robustness of iterative methods for solving the discrete nonlinear system. In fact, on the graded, h_+ -dependent mesh the convergence ball of Newton’s method for the nonlinear finite element system does not shrink to zero as $h_+ \rightarrow 0$. We show this theoretically for $1D$ flows, by exploiting the invariance of the iterative method under affine covariant and affine contravariant transformations of the underlying nonlinear system, and give experimental evidence for $1D$ flows and flows in straight channels. Newton’s method is also shown to outperform the often used inner-outer iterative scheme for the problem under investigation. This is of prime importance in industrial applications where existing solvers and ad hoc meshes have been observed to be very unreliable.

We also consider the finite element computation of fully developed turbulent flows in $2D$ expanding channels. We discretise these flow domains by orthogonal meshes which, in the direction where ε blows-up, have the graded, h_+ -dependent points’ distribution we have identified. We experimentally show that on such grids it is possible to resolve, accurately and practically, complex flow features, such as recirculation, even for widely expanded channels and small values of h_+ .

Acknowledgements

My thanks go first to my supervisor Ivan Graham. I could not have imagined having a better mentor for my PhD; his dedication to work and competence will always be an example in my future career. On top of this Ivan is a very kind and interesting person. I would also like to thank Bill Morton. Not only did he contribute to this project with his deep mathematical insights, but he was also an inexhaustible source of energy and enthusiasm. Furthermore, I will always be extremely grateful to Andrew Cliffe, my industrial advisor at Serco Assurance. Despite his numerous engagements, Andrew has always found the time to come to Bath for a meeting, to answer my questions and to help me with ENTWIFE. Thank you all!

Great thanks go to all the staff and students of the Department of Mathematical Sciences, in particular to all my mates, for making life easier. Special thanks go to Patrick, Stefano, Zhivko, Melina, André, Richard, Dave and Andy.

I would like to say a big “thank-you” to all those people with whom I have had fruitful discussions: Christine Bernardi, Bijan Mohammadi, Chris Budd, Victor Galaktionov, Adrian Hill, Alastair Spence, Bob Russel, Robert Scheichl and Jeff Williams. Special thanks are also due to Paul Smith, for his understanding and help in the last months, and to the Department, the EPSRC and Serco Assurance plc. for sponsoring this project.

I would like to particularly thank my brother Andrea, my mother and my father for all their support and encouragement throughout my undergraduate and postgraduate studies, their appreciation has meant a lot to me. A warm thank also to Fabio, Franco and Assunta, not only for being sure that I can count on them.

Last but certainly not least, my biggest thank goes to Roberta, my wife. A Long time ago she spotted things in me I was not aware of and since then her love has been my real strength (grazie, Robi, ti amo!).

Contents

Preface	vi
1 Turbulent flows, properties and modelling	1
1.1 The physical nature of turbulence	1
1.1.1 The Navier-Stokes equations	3
1.2 Kolmogorov's theory	5
1.3 Statistical description of turbulent flows	8
1.3.1 RANS equations	11
1.4 Eddy viscosity k - ε model	12
1.4.1 Modelled k transport equation	14
1.4.2 Modelled ε transport equation	16
1.4.3 The closed system of dynamical and model equations	17
1.5 Near-wall turbulence	19
1.5.1 Log-law for the mean velocity profile	20
1.5.2 Wall functions for k and ε	23
1.6 Known mathematical results on the k - ε model	24
2 The k-ε model for stationary turbulent flows in straight channels	27
2.1 2D formulation of the problem	28
2.2 1D formulation of the problem	31
2.3 Stationary turbulent Couette flow	34
2.3.1 A possible scaling	36
2.3.2 Analytical solution	36
2.4 Couette flow in the limit $h_+ \rightarrow 0$	39
2.4.1 Computation of u_*	42
2.5 Stationary turbulent Poiseuille flow	45
2.6 Weak formulation of the problem	46
2.6.1 Weak form of the RANS	47
2.6.2 Implementation of the law of the wall for the stress	49
2.6.3 Weak form of the k - ε equations	52
2.7 Galerkin Finite Element Method equations	55

3	The finite element mesh	59
3.1	Equidistributed meshes	60
3.2	The finite element error	64
3.3	Optimal monitor functions	66
3.4	Monitor functions for specific classes of functions	69
3.5	A particular case	75
3.6	Close-up of the approximation of $f(y)=1/y$	79
3.6.1	Uniform mesh	81
3.6.2	Alternative derivation of the optimal mesh for approximating $f(y)=1/y$	83
3.7	Numerical tests for the accuracy and practicality of the mesh	85
3.7.1	Equidistributed mesh vs. uniform mesh	85
3.7.2	Equidistributed mesh vs. exponentially graded mesh	88
4	Affine invariant properties of Newton's method	92
4.1	Local convergence theory of Newton's method	93
4.1.1	Termination of the iteration	97
4.2	Affine covariant transformation	98
4.3	Affine contravariant transformation	100
4.4	Discrepancy between the theory for Newton's method and its affine properties	102
4.5	A weighted norm	105
5	Iterative procedures for the discretised $k-\varepsilon$ model	107
5.1	Newton's method for a model reduced 2×2 problem	108
5.1.1	Convergence analysis in the weighted norm	110
5.1.2	Convergence analysis in the standard norm	114
5.1.3	Practical properties of Newton's method	119
5.2	Robustness of Newton's method for the discretised $1D$ turbulence equations	124
5.2.1	Newton's method for the RANS and $k-\varepsilon$ equations	128
5.2.2	Newton's method for the $k-\varepsilon$ equations	138
5.3	An inner-outer iteration	142
5.3.1	Numerical experiments	148
5.3.2	Convergence analysis for a model problem	150
6	Fully developed turbulent flows in expanding channels	157
6.1	Formulation of the problem	157
6.1.1	The flow domain	158
6.1.2	Boundary conditions and weak form	161
6.1.3	The numerical strategy	166
6.2	A graded boundary-fitted orthogonal mesh	168
6.2.1	Orthogonal mapping technique	168
6.2.2	Numerical experiments	171

Preface

The aim of this project is to improve the robustness of the finite element CFD code FEAT (Finite Element Analysis Toolbox); this is a multiphysics industrial code, containing solvers for fluid flows, heat transfer and structural analysis. Due to the lack of robustness, the solver for turbulent flows, which solves the Reynolds averaged Navier-Stokes equations coupled with the k - ε turbulence model, has been unreliable and unpractical. We have solved this non-convergence problem by devising a robust solution method for turbulent flows, which relies on the use of a specific family of meshes in combination with Newton's method.

Chapter 1

Turbulent flows, properties and modelling

The focus of this chapter is on providing an overview of some of the physical and modelling issues related to the study of turbulent flows.

Initially, we will discuss the physical properties of turbulence and very briefly review the Navier-Stokes equations, the governing equations of turbulent flows (§1.1). In §1.2, we will outline Kolmogorov's theory, one of the few theoretical results available in the field of turbulence, and then, in §1.3, present the basic statistical analysis of turbulent flows together with the derivation of the Reynolds-averaged Navier-Stokes (RANS) equations (see §1.3.1). In §1.4 we will discuss Boussinesq's hypothesis (a possible way to close the RANS equations) and the related k - ε model of turbulence, and in §1.5 we will illustrate the "wall function" technique used in turbulence modelling for determining the behaviour of the variables in the proximities of solid boundaries. In particular, we will discuss one of the major landmarks in turbulence theory: the logarithmic "law of the wall" for the velocity profile (see §1.5.1). Finally, in §1.6, we will outline the mathematical results on the k - ε model which we are aware of.

The physical and theoretical considerations on turbulent flows presented in this chapter have been elaborated mainly bearing in mind the results discussed in [1], [2], [3] and [4], while the part concerned with turbulence modelling is based on [5], [2] and [6].

Due to the extent and complexity of the subject, the following summary can only be partial and simply aims at giving a hint of the physical, engineering and mathematical issues involved in the description of turbulent flows.

1.1 The physical nature of turbulence

Turbulent flows exist in nature as well as in industrial environments, where they represent the vast majority of flows in practical applications. For example, flows around airplanes and cars, in gas/coal burning furnaces and in cooling systems are turbulent, even the blood flowing past prosthetic heart valves is turbulent. Turbulent flows also occur in oceans, rivers, the atmosphere and in the lungs of human beings. The prediction of their properties is therefore crucial to many

1.1. The physical nature of turbulence

scientific and engineering activities.

A fully satisfactory definition of turbulence is not yet available, and flows are regarded as turbulent if they exhibit the following properties:

Irregularity Randomness is one of the main characteristics of turbulent flows. For example, the velocity field of a turbulent flow varies significantly and irregularly in both position and time (this makes the statistical approach to the problem of turbulent flows quite natural, see §1.3).

Large Reynolds number Turbulent flows always occur at high Reynolds number¹. Turbulence often originates as instability of laminar flows if the Reynolds number becomes too large.

Wide range of length scales In turbulent flows a number of different length scales exists, these are bounded from above by the dimension of the flow field (the imposed length scale) and from below by the diffusive action of molecular viscosity.

Three-dimensional vorticity fluctuations Turbulent flows are three dimensional and their vorticity field (defined as the curl of the velocity field) is characterized by intense, fine-scale, random fluctuations. The random vorticity fluctuations could not maintain themselves if the velocity field was two dimensional, since an important vorticity-maintenance mechanism, known as vortex stretching, is absent in two dimensional flows (for a discussion of this phenomenon see [1] §3.3). (It should be made clear that a turbulent flow can nonetheless be two-dimensional in a statistical sense, that is its statistical properties are independent of one of the three spatial directions with zero mean-velocity component in that direction).

Diffusivity The diffusivity of turbulence, which causes rapid mixing and increased rates of momentum, heat, and mass transfer, is another important feature of all turbulent flows. If a flow pattern looks random but does not exhibit spreading of velocity fluctuations through the surrounding fluid, it is surely not turbulent.

Dissipation Turbulent flows are always dissipative. Viscous shear stress perform deformation work which increases the internal energy of the fluid at the expense of kinetic energy of the turbulence. Turbulence needs a continuous supply of energy to make up for these viscous losses. If no energy is supplied, turbulence decays rapidly. (We will argue that dissipation acts on the finest scales of turbulent flows where viscosity becomes effective).

¹If U and L are respectively a representative velocity and a representative length of a particular flow whose kinematic viscosity is ν , then the Reynolds number is defined to be $Re := UL/\nu$. It can be interpreted as a measure of the relative magnitude of inertial and viscous forces in the flow (see §1.1.1).

1.1. The physical nature of turbulence

Continuum Turbulence is a continuous phenomenon, governed by the equations of fluid mechanics. Even the smallest scales occurring in a turbulent flow are ordinarily far larger than any molecular length scale.

Turbulence is a feature of flows, not of fluids The major characteristics of turbulent flows are not controlled by the molecular properties of the fluid in which turbulence occurs, therefore most of the dynamics of turbulence is the same in all fluids, whether they are liquids or gases, if the Reynolds number is large enough.

1.1.1 The Navier-Stokes equations

First, for clarity and reduction of ambiguity, we explain the tensor notation which we will employ in the rest of this thesis and which is also used and reviewed in [2] and [7]. In the following the summation convention over repeated indices is assumed. Let us consider the vector (or rank-one tensor) \mathbf{b} , then by $\nabla\mathbf{b}$ we will denote a rank-two tensor which, in the Cartesian base-vector notation, is expressed as:

$$\nabla\mathbf{b} = \mathbf{e}_i\mathbf{e}_j \frac{\partial b_j}{\partial x_i} .$$

Clearly $\nabla\mathbf{b}$ can also be interpreted as a matrix with entries $(\nabla\mathbf{b})_{ij} := \partial b_j / \partial x_i$. Also, if \mathbf{A} is a rank-two tensor, then the inner product of \mathbf{A} and \mathbf{b} is the vector:

$$\mathbf{A} \cdot \mathbf{b} = (\mathbf{e}_i\mathbf{e}_j A_{ij}) \cdot \mathbf{e}_k b_k = \mathbf{e}_i \delta_{jk} A_{ij} b_k = \mathbf{e}_i A_{ij} b_j ,$$

where δ_{jk} is the Kronecker delta which is equal to zero for $i \neq j$ and equal to 1 if $i = j$. $\mathbf{A} \cdot \mathbf{b}$ can also be interpreted as the product of the matrix \mathbf{A} , with entries $(\mathbf{A})_{ij} := A_{ij}$, and the vector \mathbf{b} . The divergence of the rank-two tensor \mathbf{A} is the inner product of ∇ and \mathbf{A} :

$$\nabla \cdot \mathbf{A} = \left(\mathbf{e}_k \frac{\partial}{\partial x_k} \right) \cdot (\mathbf{e}_i\mathbf{e}_j A_{ij}) = \mathbf{e}_j \frac{\partial A_{ij}}{\partial x_i} ,$$

correspondingly the vector $(\nabla \cdot \mathbf{A})_j := \partial A_{ij} / \partial x_i$ can be interpreted as the divergence of the matrix \mathbf{A} . Finally we define the dot product of two rank-two and rank-three tensors. Let \mathbf{B} be a rank-two tensor, then the dot product between \mathbf{A} and \mathbf{B} is given by:

$$\mathbf{A} : \mathbf{B} = (\mathbf{e}_i\mathbf{e}_j A_{ij}) : (\mathbf{e}_k\mathbf{e}_l B_{kl}) = \delta_{jk}\delta_{il} A_{ij} B_{kl} = A_{ij} B_{ji} ,$$

in matrix notation $\mathbf{A} : \mathbf{B}$ is given by the trace of the product of the matrices \mathbf{A} and \mathbf{B} , while if \mathbf{C} and \mathbf{D} are two rank-three tensors, then their dot product is given by:

$$\mathbf{C} : \mathbf{D} = (\mathbf{e}_i\mathbf{e}_j\mathbf{e}_k C_{ijk}) : (\mathbf{e}_l\mathbf{e}_m\mathbf{e}_n D_{lmn}) = \delta_{kl}\delta_{jm}\delta_{in} C_{ijk} D_{lmn} = C_{ijk} D_{kji} ,$$

the last quantity has no correspondent in matrix notation and will be needed in §1.4.2.

We now present the equations describing the dynamical properties of turbulent flows. Due

1.1. The physical nature of turbulence

to the continuum assumption (see above), the dynamics of a turbulent, Newtonian, incompressible flow, with uniform initial density and no external body force acting on it, is represented by the Navier-Stokes equations:

$$\nabla \cdot \mathbf{u} = 0 \quad (1.1)$$

$$\frac{\partial \mathbf{u}}{\partial t} + \mathbf{u} \cdot \nabla \mathbf{u} = \nabla \cdot \boldsymbol{\sigma} \quad (1.2)$$

where $\mathbf{u} = \mathbf{u}(\mathbf{x}, t)$ is the (unknown) velocity field and $\boldsymbol{\sigma}$ is the Cauchy stress tensor per unit mass, given by:

$$\boldsymbol{\sigma} := -p\mathbf{I} + \nu [\nabla \mathbf{u} + (\nabla \mathbf{u})^T] , \quad (1.3)$$

with $p = p(\mathbf{x}, t)$ the (unknown) hydrodynamic pressure per unit mass and ν the kinematic viscosity, a property of the particular fluid which is being considered. Equation (1.1) expresses the conservation of mass in incompressible fluids and is also known as continuity equation, equation (1.2) represents the conservation of linear momentum (for a derivation of (1.1)-(1.2)-(1.3) see [8]).

It should be noted that equations (1.1)-(1.2), subject to appropriate initial and boundary conditions, apparently represent a perfectly deterministic system for \mathbf{u} and p , therefore the question of how they can describe turbulent flows, which are random phenomena (see §1.3 for a discussion on the randomness of turbulence), has represented a major conceptual obstacle to the progress in the theory of turbulence. A fully satisfactory mathematical answer to this problem has not been provided yet, but it has been shown that nonlinear equations may exhibit acute sensitivity to initial conditions, and hence unpredictability (see [9], [10], [11] and also the books [12], [13] and [14]). This issue is well beyond the scope of this thesis, and we will readily accept, as commonly done, that the Navier-Stokes equations also govern the motion of turbulent flows.

Next, for the sake of illustrating the meaning of the Reynolds number, which has a key role in the dynamics of turbulent flows, we give an alternative formulation of (1.2). By substituting the expression (1.3) for $\boldsymbol{\sigma}$ into the right-hand side of (1.2) and using the vector identity $\nabla \cdot (\nabla \mathbf{u})^T = \nabla(\nabla \cdot \mathbf{u})$ together with (1.1), it is possible to express (1.2) as follows:

$$\frac{\partial \mathbf{u}}{\partial t} + \mathbf{u} \cdot \nabla \mathbf{u} = -\nabla p + \nu \Delta \mathbf{u} . \quad (1.4)$$

The nonlinear convective term $(\partial/\partial t + \mathbf{u} \cdot \nabla)\mathbf{u}$ on the left-hand side of (1.4) (and of (1.2)) is called the inertial term, while the diffusive linear term $\nu \Delta \mathbf{u}$, on the right-hand side of (1.4), is the viscous term. Now, let U and L be respectively a representative velocity and a representative length of a particular flow. If (1.4) is expressed in nondimensional form, using U , L and L/U respectively as reference velocity, length and time, then the nondimensionalised equation will explicitly contain the Reynolds number Re which can then be interpreted as an estimate

1.2. Kolmogorov's theory

of the relative magnitude of inertial and viscous terms:

$$Re := \frac{UL}{\nu} \sim \frac{|Du_i/Dt|}{|\nu\Delta u_i|},$$

where

$$\frac{Du_i}{Dt} := \left(\frac{\partial \mathbf{u}}{\partial t} + \mathbf{u} \cdot \nabla \mathbf{u} \right)_i$$

and $\Delta u_i := (\Delta \mathbf{u})_i$. Usually L is the imposed length scale, that is some large-scale length related to the domain occupied by the fluid (for example, for a channel flow, L can be the width of the channel) while U can be related to the boundary conditions. As said at the beginning of this section, a distinctive feature of turbulent flows is $Re \gg 1$, for example for the flow of air around a glider of characteristic length $1m$ cruising at speed $1 m \cdot s^{-1}$, $Re \approx 6 \times 10^4$; for cars of characteristic length $4 m$ running at $30 m \cdot s^{-1}$, $Re \approx 7 \times 10^6$ and for airplanes of length $50 m$ cruising at $270 m \cdot s^{-1}$, $Re \approx 8 \times 10^8$.

Finally, in order to form an intuitive impression of the existence in turbulent flows of different characteristic lengths, consider that, broadly speaking, the viscous diffusive term in the Navier-Stokes equations scales with distance (generically denoted by x) as $1/x^2$ whilst the inertial term scale as $1/x$, therefore the former increase in relative importance as the length scale considered decreases. So viscous force becomes effective on length scales much smaller than the imposed length scale on which, at high Reynolds number, the inertial term dominates. Moreover, in the case of wall-bounded flows, viscosity, no matter how small it is, enforces the no-slip condition at the physical walls and viscous forces become then dominant in very thin boundary layers adjacent to the solid surfaces. In §1.5 the structure of turbulent boundary layers will be briefly discussed in the context of the “laws of the wall” for the mean properties of turbulent flows.

1.2 Kolmogorov's theory

In this section, we briefly outline a cornerstone in the field of turbulence: Kolmogorov's theory (originally discussed in [15], [16], [17]). This theory, by representing turbulent flows in terms of a *cascade of kinetic energy* from large to small scales, provides an estimate of the size of the finest scales and an expression for the energy spectrum in the so called *inertial range* (see below). (The cascade metaphor was not used by Kolmogorov, but is due to Onsager [18]).

As it is presented here and was originally formulated, Kolmogorov's theory is based on heuristic arguments and on scaling properties and has no explicit reference to the Navier-Stokes equations. Some work has recently been done in order to obtain some of its results in a mathematically rigorous way starting from the Navier-Stokes equations, see [19], [20], [21].

In the framework of Kolmogorov's theory, turbulent flows are qualitatively regarded as a cascade of large eddies (large-scale components of the flow) breaking up successively into ever smaller sized eddies (fine-scale components of the flow). This cascade process entails a trans-

1.2. Kolmogorov's theory

fer of kinetic energy from one length scale to a smaller one and is associated with the “vortex stretching mechanism”, a phenomenon strictly related to changes in the length scales and solely due the presence of the nonlinear inertial term in the Navier-Stokes equations (see §3.3 of [1] for a detailed discussion). The flow of kinetic energy, however, does not continue to arbitrarily small length scales, in fact, as the length scale becomes smaller and smaller the relative importance of molecular viscous diffusion increases and eventually becomes dominant and prevents the generation of infinitely small scales of motion by dissipating small-scale energy into heat (the range of length scales where dissipation occurs is called the *dissipation range*).

From the observation that at high Reynolds number there is little direct interaction between the large eddies governing the energy transfer and the small dissipating eddies, Kolmogorov proposed his first similarity hypothesis: “*small-scale motions are isotropic and statistically independent of the large-scale turbulence and of the mean flow*”. In terms of the cascade representation, this can be interpreted saying that at high Reynolds number the cascade is very long (that is there is a large difference in the eddy sizes at its ends) and, as kinetic energy flows from one scale to a smaller one, all information about the anisotropy of the large energy-containing scales is lost and the small-scales then show a universal behaviour. Therefore, being independent of initial and boundary conditions (which affect large-scale motions), small-scale motions can depend only on the rate at which they are supplied with energy by the large-scale motion and on the kinematic viscosity ν , related to the dissipation of kinetic energy into heat occurring at the finest scales. Since it is also assumed that the rate of energy supply is equal to the rate of dissipation, it then follows that the dynamics of small scale motion is governed by the viscosity ν and the dissipation rate (which we denote by ε). With these two parameters, one can form length, time and velocity scales, as now shown. The dimensions of ε are $\text{length}^2 \cdot \text{time}^{-3}$:

$$[\varepsilon] = \frac{l^2}{t^3} ,$$

where l means length, and its unit of measurement is meter, and t means time, and its measure is second, and the dimensions of ν are $\text{length}^2 \cdot \text{time}^{-1}$:

$$[\nu] = \frac{l^2}{t} .$$

Therefore the relation between l and $[\varepsilon]$, $[\nu]$ can be obtained by setting:

$$l = [\varepsilon]^\alpha [\nu]^\beta = \frac{l^{2\alpha} l^{2\beta}}{t^{3\alpha} t^\beta} = \frac{l^{2(\alpha+\beta)}}{t^{3\alpha+\beta}}$$

from which $\alpha = -1/4$ and $\beta = 3/4$. It then follows that the characteristic length of the smallest eddies is:

$$\varepsilon^{-1/4} \nu^{3/4} = \left(\frac{\nu^3}{\varepsilon} \right)^{1/4} := \eta . \quad (1.5)$$

Similarly one can obtain the characteristic time and velocity of the smallest eddies, which are

1.2. Kolmogorov's theory

respectively:

$$\tau := \left(\frac{\nu}{\varepsilon}\right)^{1/2} \quad \text{and} \quad \frac{\eta}{\tau} = (\nu\varepsilon)^{1/4} := v . \quad (1.6)$$

The scales η , τ and v , typical of the dissipation range, are referred to as *Kolmogorov microscales* of length, time and velocity.

As said before, the flow of kinetic energy from large to small scales is assumed to be due only to the vortex stretching mechanism which is a nonlinear phenomenon totally unrelated to viscous effects. This consideration is at the basis of Kolmogorov's second similarity hypothesis: "*the cascade process occurs in a regime at lengths sufficiently large for the effects of viscosity to be inconsequential*". It is then assumed that there exists in the flow a range of length scales, called *inertial range*, where viscous forces have no effect on the removal of energy from one length scale to a smaller one, and there is then an equilibrium between energy flowing in from above to a given scale and that flowing out to a lower scale (experimentally it turns out that 90% of the energy that is fed into the large eddies is finally dissipated at the smallest eddies). The fact that in the inertial range the energy fed to the largest eddies is merely transmitted to the smallest eddies, where dissipation occurs, allows us to relate ε to the length and velocity scales of the large-scale turbulence, as now explained. Let L represent the size of the largest eddies or the width of a particular flow, and u the characteristic turbulent velocity of the largest eddies. It is plausible to assume that the rate at which large eddies supply energy to small eddies is proportional to the reciprocal of the time scale of the large eddies L/u , moreover, since the amount of turbulent kinetic energy per unit mass in the large-scale eddies is proportional to u^2 , the rate of energy supply to the small scale eddies can be estimated to be of the order: $u^2 \cdot u/L = u^3/L$. This energy is dissipated at a rate ε , which should be equal to the supply rate. Hence,

$$\varepsilon \sim \frac{u^3}{L} , \quad (1.7)$$

the viscous dissipation of energy is then estimated from the large-scale dynamics, which do not involve viscosity. Dissipation is clearly seen as a passive process, in the sense that it proceeds at a rate dictated by the inviscid inertial behaviour of the large eddies. We can now use (1.7) to form an impression of the differences between the large-scale and small-scale aspects of turbulence. In order to do so we first define the Reynolds number:

$$Re = \frac{uL}{\nu} , \quad (1.8)$$

based on the representative velocity and length of the large eddies. Then, substituting the

1.3. Statistical description of turbulent flows

expression (1.7) for ε into (1.5) and into (1.6) and using (1.8) yields:

$$\eta \sim \left(\nu^3 \frac{L}{u^3} \right)^{1/4} = L \left(\frac{\nu^3}{u^3 L^3} \right)^{1/4} = L \text{Re}^{-3/4} \Rightarrow \frac{\eta}{L} \sim \text{Re}^{-3/4}, \quad (1.9)$$

$$\tau \sim \left(\nu \frac{L}{u^3} \right)^{1/2} = \frac{L}{u} \left(\frac{\nu}{u L} \right)^{1/2} = \frac{L}{u} \text{Re}^{-1/2} \Rightarrow \tau \frac{u}{L} \sim \text{Re}^{-1/2}, \quad (1.10)$$

$$v \sim \left(\nu \frac{u^3}{L} \right)^{1/4} = u \left(\frac{\nu}{u L} \right)^{1/4} = u \text{Re}^{-1/4} \Rightarrow \frac{v}{u} \sim \text{Re}^{-1/4}. \quad (1.11)$$

These relations indicate that the length, time and velocity scales of the smallest eddies are very much smaller than those of the largest eddies. From (1.9)-(1.11) it is clear that the separation in scales widens as the Reynolds number increases, in accordance with the assumption that at high Reynolds number the cascade is long and there is little direct interaction between the large eddies and the small ones.

The other aspect of Kolmogorov's theory is concerned with the distribution of the energy spectrum $E(k)$, where k is the wave number (which carries dimension length^{-1}). In the inertial range, $E(k)$ must be a function of the rate at which energy is transmitted from one length scale to a smaller one (ε) and of the wave number and must be independent of the viscosity. Therefore, dimensional considerations again dictate that this dependence can only be of the form

$$E(k) = C \varepsilon^{2/3} k^{-5/3}, \quad (1.12)$$

where C is a dimensionless constant. (1.12) is known as *Kolmogorov $-5/3$ law*. The first experimental verification of (1.12) was carried out by Grant, Stewart and Moilliet [22], who conducted their experiments in a tidal channel between Vancouver Island and mainland Canada where $Re \sim 10^8$. A spectral exponent of $-5/3$ has since been measured many times in materially different flow with very high Reynolds number (see [23]) and the dimensionless constant C in (1.12) appears to be a universal constant with a value close to 1.5 (see [24]).

1.3 Statistical description of turbulent flows

In this section we give a very brief account of the statistical description of turbulent flows on which turbulence modeling relies (for more details see Chapter 6 of [1], Chapter 3 of [2] and Chapter 2 of [4] and [25]). We will discuss the physical and practical reasons for introducing a statistical representation of turbulent flows, trying to highlight its drawbacks and advantages, especially in comparison with the two techniques which, in the last two decades, have been increasingly successful in correctly predicting the properties of turbulent flows: direct numerical simulation (DNS) and large eddy simulation (LES).

DNS and LES are both based on fully three-dimensional and time dependent calculations which need to be conducted over long periods of time in order to obtain stable and signifi-

1.3. Statistical description of turbulent flows

cant statistics. The first approach (DNS) pursues a thorough three-dimensional resolution of all scales present in the turbulent flow under investigation by solving the Navier-Stokes equations (1.1)-(1.2). Therefore, in the case of turbulent flows without wall boundaries, the DNS technique requires a number of mesh cells in each spatial direction of the order of $Re^{3/4}$ (this follows from the length scale estimate (1.9)). In this case in 3D the total number of cells then scales like $Re^{9/4}$ (the dependence on Re is more severe in the case of turbulent channel flows, see the discussion in [2]). Moreover, considering that the number of time steps over which the equations have to be integrated is at least of the order of the number of grid cells in one direction, we obtain a total computing expense for a simulation which varies at least as Re^3 . This is clearly totally unpractical already for flows with $Re = 10^5$, which are very common in engineering applications.

LES is a more practical alternative in which the large-scale part of turbulent quantities is computed explicitly, while the small scales are treated by some approximate parametrization or model. Clearly LES is less costly than DNS, but, like DNS, has the drawback of always requiring three-dimensional and time-dependent calculations even for flows which are two- or one-dimensional in the mean. The use of LES is becoming more and more popular in engineering applications, but complex turbulent flows still cannot yet be tackled by this technique due to the high requirements in computer memory and central-processing-unit time.

When a study of the detailed physics of the flow is the goal, then DNS or LES, if feasible, should be the methods of choice, but, in most circumstances, what engineers would like to know is the mean effect of the turbulent quantities and they are not so concerned with the instantaneous fluctuations. Thus, a more practical approach to describing turbulent flows would be to couple the Reynold-averaged Navier-Stokes (RANS) equations (which, as it will be shown in the next subsection, represent a system of equations for the mean properties of the flow) with a turbulence model. This technique will be illustrated in the next sections and is based on the statistical representation of turbulent flows which is now briefly discussed.

The reason for modelling turbulent flows by suitable average quantities, has its foundation in the fact that, as a matter of definition, we are supposing that in turbulent flow regimes, the physical properties are randomly varying (see §1.1). By saying, for example, that the velocity \mathbf{u} is a random function of position \mathbf{x} and time t we mean that at a given point (\mathbf{x}, t) of space-time the velocity \mathbf{u} is not predictable in practice from the data of the problem. Thus, if an experiment is repeatedly carried out, a different velocity field is obtained in each *realization* even if the experimental conditions are nominally the same (we will refer to a collection of realizations as an *ensemble*). Physically, this is due to the fact that the detailed behaviour of the flow in any one realization is extremely sensitive to small changes in the initial or boundary conditions, that cannot be controlled to infinite precision.

We also observe that it is implicit in the use of the phrase “random function” that the values assumed by \mathbf{u} at any point (\mathbf{x}, t) are distributed according to certain definite probability laws. We shall assume that the probability laws describing the velocity fluctuations are determined by the data of the problem. Therefore, we could define the turbulent motion at (\mathbf{x}, t) to be such that as the number of realizations tends to infinity the probability distribution of \mathbf{u} tends to a

1.3. Statistical description of turbulent flows

limiting form which depends only on the data of the problem.

This interpretation of \mathbf{u} as random variable applies for every point (\mathbf{x}, t) and in general there will exist a statistical connection between the random values of \mathbf{u} that occur at different points in space-time. Therefore the full statistical properties of the velocity field are characterized by the joint-probability distribution of the values $\mathbf{u}_1, \mathbf{u}_2, \dots, \mathbf{u}_N$ of \mathbf{u} , at the points $(\mathbf{x}_1, t_1), (\mathbf{x}_2, t_2), \dots, (\mathbf{x}_N, t_N)$ in space-time, and this for arbitrary values of N . Furthermore the pressure field should also be considered and its joint distribution with velocity should then be taken into account. It is then clear that, in principle, a vast amount of statistical information is contained in a turbulent flow. But, usually correlations between different time-space points and different variables are not taken into account and the flow is described only through single-point statistics. In the case of incompressible flows (when no variations in the density of the fluid have to be considered), this is done as now explained. The velocity and pressure fields are split into a mean and a fluctuating part:

$$\mathbf{u}(\mathbf{x}, t) = \bar{\mathbf{u}}(\mathbf{x}, t) + \tilde{\mathbf{u}}(\mathbf{x}, t) , \quad p(\mathbf{x}, t) = \bar{p}(\mathbf{x}, t) + \tilde{p}(\mathbf{x}, t) , \quad (1.13)$$

(the decomposition (1.13) is referred to as *Reynolds decomposition*), where $\tilde{\mathbf{u}}$ and \tilde{p} are the fluctuating velocity and pressure at (\mathbf{x}, t) and are usually identified with the turbulence, whilst $\bar{\mathbf{u}}$ and \bar{p} are respectively the average over the ensemble at (\mathbf{x}, t) of \mathbf{u} and p and define the “mean flow”:

$$\bar{\mathbf{u}} := \int \mathbf{u} F_{\mathbf{u}}(\mathbf{u}, \mathbf{x}, t) d\mathbf{u} \quad \bar{p} := \int p F_p(p, \mathbf{x}, t) dp , \quad (1.14)$$

with $F_{\mathbf{u}}(\mathbf{u}, \mathbf{x}, t)$ the probability distribution of \mathbf{u} at (\mathbf{x}, t) and similarly $F_p(p, \mathbf{x}, t)$. In (1.14) the integration is carried out over all possible values of \mathbf{u} and p respectively. Then, a system of equations for $\bar{\mathbf{u}}$ and \bar{p} is determined by computing the “Reynolds average” of (1.1)-(1.2), as will be shown in §1.3.1. For this, we first need to introduce the *Reynolds average* operator $\langle \cdot \rangle$, which is a linear operator such that, for any function f of the flow variable φ ,

$$\langle f(\varphi) \rangle = \overline{f(\varphi)} , \quad (1.15)$$

where $\overline{f(\varphi)}$ is the average over the ensemble at (\mathbf{x}, t) of $f(\varphi)$. The following properties of the Reynolds average operator are also assumed:

- (a) $\left\langle \frac{\partial \varphi}{\partial t} \right\rangle = \frac{\partial \langle \varphi \rangle}{\partial t} , \quad \left\langle \frac{\partial \varphi}{\partial x_i} \right\rangle = \frac{\partial \langle \varphi \rangle}{\partial x_i} ,$
- (b) $\langle \langle \varphi \rangle \rangle = \langle \varphi \rangle ,$
- (c) $\langle \langle \varphi_1 \rangle \varphi_2 \rangle = \langle \varphi_1 \rangle \langle \varphi_2 \rangle .$

Note that from linearity and property (b) it follows that:

$$\langle \tilde{\mathbf{u}} \rangle = \langle \mathbf{u} - \bar{\mathbf{u}} \rangle = \langle \mathbf{u} \rangle - \langle \bar{\mathbf{u}} \rangle = \mathbf{0} , \quad (1.16)$$

and similarly

$$\langle \tilde{p} \rangle = 0 , \quad (1.17)$$

1.3. Statistical description of turbulent flows

moreover (1.16)-(1.17) together with property (c) imply that the Reynolds average of the product of a fluctuating and a mean quantity is zero. For example, using again linearity and also (a), we have:

$$\langle \tilde{\mathbf{u}} \cdot \nabla \bar{\mathbf{u}} \rangle = \langle \tilde{\mathbf{u}} \cdot \langle \nabla \mathbf{u} \rangle \rangle = \langle \tilde{\mathbf{u}} \rangle \cdot \langle \nabla \mathbf{u} \rangle = 0$$

The equations for the mean flow will be derived in the next section. Here we observe that if, on one hand, by considering one-point statistics, information about the flow is reduced to what might be presumed its essentials (e.g., mean velocities) and the flow description is consequently simplified, on the other hand, one-point averaged quantities do not encompass the full statistics of the flow, since multipoint averages cannot be deduced from one point data. Statistical information is thus lost in going to one-point averages, information that may be crucial to an understanding of certain aspects of the flow. In what follows, we will see that the incompleteness of the one-point statistics will prevent the system of equations for the mean flow from being closed, so that approximations will have to be introduced in order for the set of equations to be complete.

Finally, it should be noted that we have introduced a statistical representation of turbulent flows based on the assumption that suitable probability distribution functions exist, assuring then the existence of meaningful ensemble averages. But, in practice, measurements of various aspects of turbulent flows are actually measurements of time-averaged quantities. The relation between the two types of average is usually dealt with by assuming the ‘‘ergodic hypothesis’’. Then, in the case of statistically steady turbulence (all mean quantities are invariant under translation in time), for example, time averages are precisely equal to ensemble averages and there is then a correspondence between experiments and theoretical results.

1.3.1 RANS equations

Now, by taking the Reynolds average of the Navier-Stokes equations (1.1)-(1.2) we derive the Reynolds-averaged Navier-Stokes (RANS) equations for $\bar{\mathbf{u}}$ and \bar{p} . We shall see that the RANS equations are not closed, due to the fact that the averaging process will introduce a new unknown: the Reynolds stress, which involves second order moments of the fluctuating velocity field. The lack of closure reflects the incompleteness of the one-point statistics which does not encompass the full multipoint statistics of the flow.

In the following we will use the properties (a), (b), (c) of the filter $\langle \cdot \rangle$, without making explicit reference to them. We have that the Reynolds average of equation (1.1) yields:

$$\nabla \cdot \bar{\mathbf{u}} = 0 , \tag{1.18}$$

and taking the difference of (1.1) and (1.18) we obtain:

$$\nabla \cdot \tilde{\mathbf{u}} = 0 . \tag{1.19}$$

We then observe, from (1.18) and (1.19), that the mean and fluctuating velocities satisfy the

1.4. Eddy viscosity k - ε model

continuity equation as they were assumed to be independent flows. This decoupling, however, does not extend to equation (1.2), due to the presence of the nonlinear term $\mathbf{u} \cdot \nabla \mathbf{u}$, as now shown. Reynolds averaging equation (1.2) gives:

$$\frac{\partial \bar{\mathbf{u}}}{\partial t} + \langle \mathbf{u} \cdot \nabla \mathbf{u} \rangle = \nabla \cdot \bar{\boldsymbol{\sigma}}, \quad (1.20)$$

with

$$\bar{\boldsymbol{\sigma}} := -\bar{p}\mathbf{I} + \nu [\nabla \bar{\mathbf{u}} + (\nabla \bar{\mathbf{u}})^T], \quad (1.21)$$

then, also using the expression (1.13) for \mathbf{u} and equation (1.19), we write:

$$\begin{aligned} \langle \mathbf{u} \cdot \nabla \mathbf{u} \rangle &= \langle (\bar{\mathbf{u}} + \tilde{\mathbf{u}}) \cdot \nabla (\bar{\mathbf{u}} + \tilde{\mathbf{u}}) \rangle \\ &= \bar{\mathbf{u}} \cdot \nabla \bar{\mathbf{u}} + \langle \tilde{\mathbf{u}} \cdot \nabla \tilde{\mathbf{u}} \rangle + \langle \tilde{\mathbf{u}} \cdot \nabla \bar{\mathbf{u}} \rangle + \langle \bar{\mathbf{u}} \cdot \nabla \tilde{\mathbf{u}} \rangle \\ &= \bar{\mathbf{u}} \cdot \nabla \bar{\mathbf{u}} + \langle \tilde{\mathbf{u}} \cdot \nabla \tilde{\mathbf{u}} \rangle \\ &= \bar{\mathbf{u}} \cdot \nabla \bar{\mathbf{u}} + \langle \nabla \cdot \tilde{\mathbf{u}} \tilde{\mathbf{u}} \rangle \\ &= \bar{\mathbf{u}} \cdot \nabla \bar{\mathbf{u}} + \nabla \cdot \widetilde{\tilde{\mathbf{u}} \tilde{\mathbf{u}}}. \end{aligned}$$

The last expression for $\langle \mathbf{u} \cdot \nabla \mathbf{u} \rangle$ can be used in (1.20) to obtain:

$$\frac{\partial \bar{\mathbf{u}}}{\partial t} + \bar{\mathbf{u}} \cdot \nabla \bar{\mathbf{u}} = \nabla \cdot (\bar{\boldsymbol{\sigma}} + \boldsymbol{\tau}) \quad (1.22)$$

with

$$\boldsymbol{\tau} := -\widetilde{\tilde{\mathbf{u}} \tilde{\mathbf{u}}} \quad (1.23)$$

the Reynolds stress tensor per unit mass, a second order moment of the velocity components at single point in space and time.

It is now clear that the equations (1.18) and (1.22) for the mean flow are not closed since they are coupled to the fluctuations through $\boldsymbol{\tau}$. This represents the mean transport of fluctuating linear momentum per unit mass due to turbulent velocity fluctuations and is interpreted as an additional stress tensor by which the fluctuating part of the flow interacts with the mean flow.

In order to close the equations (1.14)-(1.22), it is then necessary to tie $\boldsymbol{\tau}$ to the global history of the mean velocity $\bar{\mathbf{u}}$ in a physical consistent fashion, i.e.:

$$\boldsymbol{\tau}(\mathbf{x}, t) = \mathbf{F}(\bar{\mathbf{u}}(\mathbf{x}', t'); \mathbf{x}, t), \quad \mathbf{x}' \in \mathcal{V}, \quad t' \in (-\infty, t)$$

where \mathcal{V} is the fluid volume. This is discussed in the next section.

1.4 Eddy viscosity k - ε model

Here we will consider the eddy viscosity k - ε turbulence model (where k is the turbulent kinetic energy and ε its dissipation rate), which is a two-equations first-order closure model based on

1.4. Eddy viscosity k - ε model

Boussinesq's hypothesis (introduced in 1877):

$$\boldsymbol{\tau} = \nu_T (\boldsymbol{\nabla} \bar{\mathbf{u}} + (\boldsymbol{\nabla} \bar{\mathbf{u}})^T) - \frac{2}{3} k \mathbf{I} , \quad (1.24)$$

where ν_T is a positive scalar coefficient to be specified, called the *eddy viscosity* or *turbulent viscosity* and k is given by

$$k := \frac{1}{2} \overline{\mathbf{u} \cdot \mathbf{u}} ,$$

the expression for ε is given in (1.34) (the reasons for defining the k - ε model a two-equations first-order closure model will become clear in the following).

The (questionable) assumption behind (1.24) is that the Reynolds stress can be related to the gradient of the mean velocity field in a similar manner as in Newtonian incompressible fluids the stress is related to the gradient of the total velocity field (compare (1.24) with (1.3)). Then, by substituting (1.24) and (1.21) into (1.22), and by using the vector identity $\boldsymbol{\nabla} \cdot (f \mathbf{I}) = \boldsymbol{\nabla} f$ (where f is a scalar function), it is not difficult to obtain:

$$\frac{\partial \bar{\mathbf{u}}}{\partial t} + \bar{\mathbf{u}} \cdot \boldsymbol{\nabla} \bar{\mathbf{u}} = \boldsymbol{\nabla} \cdot [(\nu + \nu_T) (\boldsymbol{\nabla} \bar{\mathbf{u}} + (\boldsymbol{\nabla} \bar{\mathbf{u}})^T)] - \boldsymbol{\nabla} \left(\bar{p} + \frac{2}{3} k \right) , \quad (1.25)$$

finally, defining the modified mean pressure:

$$\mathcal{P} := \bar{p} + \frac{2}{3} k ,$$

(1.25) can be written as:

$$\frac{\partial \bar{\mathbf{u}}}{\partial t} + \bar{\mathbf{u}} \cdot \boldsymbol{\nabla} \bar{\mathbf{u}} = \boldsymbol{\nabla} \cdot [(\nu + \nu_T) (\boldsymbol{\nabla} \bar{\mathbf{u}} + (\boldsymbol{\nabla} \bar{\mathbf{u}})^T)] - \boldsymbol{\nabla} \mathcal{P} . \quad (1.26)$$

We then have two dynamical equations, (1.26) and (1.18), for the mean variables $\bar{\mathbf{u}}$ and \mathcal{P} , there still remains the task of expressing ν_T in terms of known or calculable quantities. We now discuss the solution to the problem of determining ν_T provided by the k - ε turbulence model.

An expression for ν_T is determined by observing that it carries dimensions $\text{length}^2 \cdot \text{time}^{-1}$ (as it can be deduced from (1.24)):

$$[\nu_T] = \frac{l^2}{t} ,$$

therefore, since ν_T , unlike the kinematic viscosity ν , is not a property of the fluid but is expected to be determined by the structure of the turbulence at the point (\mathbf{x}, t) in question, it is expressed as:

$$\nu_T = C_\mu \frac{l_T^2}{t_T} , \quad (1.27)$$

where C_μ is a constant (whose value will be given in §1.4.3) and $l_T = l_T(\mathbf{x}, t)$ and $t_T = t_T(\mathbf{x}, t)$ are respectively the turbulent length and time scales. In the framework of the k - ε turbulence

1.4. Eddy viscosity k - ε model

model, l_T and t_T are built up from k and ε as follows:

$$l_T = \frac{k^{3/2}}{\varepsilon}, \quad t_T = \frac{k}{\varepsilon} \quad (1.28)$$

and the turbulent quantities k and ε in turn are determined by way of transport equations, see (1.41) and (1.45) (this is the reason for referring to the k - ε model as a two-equations model, in contrast to zero-equation models where ν_T is found by way of algebraic formulae or to one-equation models in which the determination of ν_T entails the solution of a differential equation for only one property of the turbulence). Then, combining (1.27) with (1.28) yields

$$\nu_T = C_\mu \frac{k^2}{\varepsilon}. \quad (1.29)$$

Note that it is also possible to construct l_T and t_T using variables other than (k, ε) , and in fact turbulence models with various combination of variables have been proposed. The k - ε model has emerged as the most widely used turbulence model, and is included in most commercial CFD codes. As for all turbulence models, its details and the concepts which it relies on, have evolved over time; but Jones and Launder [26] are credited with developing the “standard” k - ε model, with Launder and Sharma [27] providing improved values of the model constants (see Postulation 5 below and the discussion in §1.4.3).

Before sketching the derivation of the governing differential equations for k and ε (see §§1.4.1, 1.4.2), we summarize the basic postulations which, together with the “ k - ε turbulence scale hypothesis” (1.28), are adopted by the k - ε model (some of the following assumptions underlie most turbulence models):

1. The diffusion of turbulent transport properties by turbulence is proportional to the gradient of transport properties (*diffusion gradient model*)
2. Small turbulent eddies are isotropic (*isotropic dissipation model*)
3. All turbulent transport quantities are local functions of Reynolds stress, turbulence kinetic energy, rate of dissipation of turbulent kinetic energy, mean-flow variables $(\overline{\mathbf{u}\mathbf{u}}, k, \varepsilon, \overline{\mathbf{u}}, \overline{p})$ (*one-point correlation closure statement*).
4. All modeled turbulent phenomena must be consistent in symmetry, invariance, permutation, and physical observations (*consistency and realizability requirement*).
5. All turbulence model constants, $C_\mu, \sigma_k, \sigma_\varepsilon, C_{\varepsilon 1}, C_{\varepsilon 2}$ (these are the constants appearing in (1.29), (1.49) and (1.50)) require experimental calibration and determination (*uniqueness of constants*).

1.4.1 Modelled k transport equation

In this and next section we will derive the modelled transport equations respectively for k and ε , following mainly the study presented in [5].

1.4. Eddy viscosity k - ε model

We now describe the governing equation for the turbulent kinetic energy k and the modelling procedure related to the diffusion gradient model hypothesis (Postulation 1). Subtracting the mean flow equation (1.22) from equation (1.2) for the total field, yields

$$\frac{\partial}{\partial t}(\mathbf{u} - \bar{\mathbf{u}}) + \mathbf{u} \cdot \nabla \mathbf{u} - \bar{\mathbf{u}} \cdot \nabla \bar{\mathbf{u}} = \nabla \cdot [(\boldsymbol{\sigma} - \bar{\boldsymbol{\sigma}}) - \boldsymbol{\tau}] , \quad (1.30)$$

then, using the expressions for \mathbf{u} and p in (1.13), those for $\boldsymbol{\sigma}$, $\bar{\boldsymbol{\sigma}}$ and $\boldsymbol{\tau}$ respectively in (1.3), (1.21) and (1.23), and using also (1.19), it is not difficult to obtain from (1.30) the following equation for the fluctuating part of the velocity field:

$$\frac{\partial \tilde{\mathbf{u}}}{\partial t} + \bar{\mathbf{u}} \cdot \nabla \tilde{\mathbf{u}} + \tilde{\mathbf{u}} \cdot \nabla \bar{\mathbf{u}} + \tilde{\mathbf{u}} \cdot \nabla \tilde{\mathbf{u}} + \nabla \tilde{p} - \nu \Delta \tilde{\mathbf{u}} - \nabla \cdot \overline{\tilde{\mathbf{u}} \tilde{\mathbf{u}}} = \mathbf{0} , \quad (1.31)$$

which is formally written in operator notation as:

$$\mathcal{N} \tilde{\mathbf{u}} = \mathbf{0} . \quad (1.32)$$

From (1.32), we then construct the Reynolds average:

$$\langle (\mathcal{N} \tilde{\mathbf{u}}) \cdot \tilde{\mathbf{u}} \rangle = 0$$

which, by using (1.19) together with some vector identities and the properties of the filter $\langle \cdot \rangle$, yields the “exact” transport equation for k :

$$\frac{\partial k}{\partial t} + \bar{\mathbf{u}} \cdot \nabla k = \nabla \cdot \left(-\overline{\tilde{k} \tilde{\mathbf{u}}} - \overline{\tilde{p} \tilde{\mathbf{u}}} + \nu \nabla k \right) - \overline{\tilde{\mathbf{u}} \tilde{\mathbf{u}}} : \nabla \bar{\mathbf{u}} - \nu \overline{\nabla \tilde{\mathbf{u}}} : (\nabla \tilde{\mathbf{u}})^{\text{T}} , \quad (1.33)$$

where

$$\tilde{k} := \frac{1}{2} \tilde{\mathbf{u}} \cdot \tilde{\mathbf{u}}$$

is the fluctuating kinetic energy.

The left-hand side of (1.33) clearly represents the total derivative of k following the motion of the mean flow with velocity $\bar{\mathbf{u}}$, we now give a physical interpretation of the terms on the right-hand side of equation (1.33) and discuss the modelling procedure needed for the new unknowns $\overline{\tilde{k} \tilde{\mathbf{u}}}$ and $\overline{\tilde{p} \tilde{\mathbf{u}}}$. The last term on the right-hand side of (1.33) represents the rate of dissipation of turbulent kinetic energy:

$$\varepsilon := \nu \overline{\nabla \tilde{\mathbf{u}}} : (\nabla \tilde{\mathbf{u}})^{\text{T}} , \quad (1.34)$$

note that ε is always positive (the ε -transport equation will be derived in §1.4.2), the term

$$-\overline{\tilde{\mathbf{u}} \tilde{\mathbf{u}}} : \nabla \bar{\mathbf{u}} = \boldsymbol{\tau} : \nabla \bar{\mathbf{u}} \quad (1.35)$$

represents, instead, the production of turbulent kinetic energy due to the interaction of the Reynolds stress with the gradient of the mean flow (the energy exchange between the mean

1.4. Eddy viscosity k - ε model

flow and the turbulence usually involves loss to the mean flow and a profit to the turbulence), and finally we observe that the diffusion of turbulent kinetic, given by

$$\nabla \cdot \left(-\overline{\tilde{k}} \tilde{\mathbf{u}} - \overline{\tilde{p}} \tilde{\mathbf{u}} + \nu \nabla k \right), \quad (1.36)$$

is due both to fluctuating motions (first two terms in (1.36)) and to the molecular properties of the fluid (third term in (1.36)). The first two terms in (1.36) are new unknowns and are modelled according to Postulation 1. Hence, we take them proportional to the gradient of k , as follows:

$$-\overline{\tilde{k}} \tilde{\mathbf{u}} - \overline{\tilde{p}} \tilde{\mathbf{u}} = C_k \left(\frac{l_T^2}{t_T} \right) \nabla k \quad (1.37)$$

$$= C_k \frac{k^2}{\varepsilon} \nabla k. \quad (1.38)$$

In the expressions above, which simulate isotropic diffusivity, C_k is a dimensionless scalar coefficient, while the coefficient l_T^2/t_T in (1.37) must be attached to ∇k in order to keep the dimensions consistent and it is easy to see that (1.38) follows from (1.37), by using (1.28). Substituting (1.38) into (1.36) then gives:

$$\begin{aligned} \nabla \cdot \left(-\overline{\tilde{k}} \tilde{\mathbf{u}} - \overline{\tilde{p}} \tilde{\mathbf{u}} + \nu \nabla k \right) &= \nabla \cdot \left[\left(C_k \frac{k^2}{\varepsilon} + \nu \right) \nabla k \right] \\ &= \nabla \cdot \left[\left(\frac{\nu_T}{\sigma_k} + \nu \right) \nabla k \right] \end{aligned} \quad (1.39)$$

where, in order to obtain (1.39), we have used (1.29) and introduced the coefficient $\sigma_k := C_\mu/C_k$ (whose value will be specified in §1.4.3).

Equation (1.33) requires no additional modelling and, using (1.34), (1.35) and (1.39), can be rearranged into:

$$\frac{\partial k}{\partial t} + \bar{\mathbf{u}} \cdot \nabla k = \nabla \cdot \left[\left(\frac{\nu_T}{\sigma_k} + \nu \right) \nabla k \right] + \boldsymbol{\tau} : \nabla \bar{\mathbf{u}} - \varepsilon. \quad (1.40)$$

Finally, substituting for $\boldsymbol{\tau}$ on the right-hand side of (1.40) its expression (1.24) and observing that $\mathbf{I} : \nabla \bar{\mathbf{u}} = \nabla \cdot \bar{\mathbf{u}} = 0$, because of (1.18), yields the modelled transport equation for k :

$$\frac{\partial k}{\partial t} + \bar{\mathbf{u}} \cdot \nabla k = \nabla \cdot \left[\left(\frac{\nu_T}{\sigma_k} + \nu \right) \nabla k \right] + \nu_T (\nabla \bar{\mathbf{u}} + (\nabla \bar{\mathbf{u}})^T) : \nabla \bar{\mathbf{u}} - \varepsilon. \quad (1.41)$$

with ν_T given in (1.29).

1.4.2 Modelled ε transport equation

The transport equation for ε , the rate of dissipation of turbulent kinetic energy, is obtained by the following approach.

1.4. Eddy viscosity k - ε model

From (1.32), we construct the Reynolds average:

$$2\nu\langle(\mathcal{N}\tilde{\mathbf{u}}):\nabla\tilde{\mathbf{u}}\rangle = 0 \quad (1.42)$$

then, similarly to the derivation of the k -equation, by using (1.19) together with some vector identities and the properties of the filter $\langle \cdot \rangle$, it is possible to obtain from (1.42) the “exact” transport equation for ε :

$$\begin{aligned} \frac{\partial\varepsilon}{\partial t} + \bar{\mathbf{u}}\cdot\nabla\varepsilon &= \nabla\cdot\left(-\tilde{\varepsilon}\tilde{\mathbf{u}} - 2\nu\overline{\nabla\tilde{p}\cdot\nabla\tilde{\mathbf{u}}} + \nu\nabla\varepsilon\right) - 2\nu\overline{[\nabla\tilde{\mathbf{u}}\cdot(\nabla\tilde{\mathbf{u}})^T]:\nabla\tilde{\mathbf{u}}} - \\ &\quad - 2\nu\overline{\nabla\tilde{\mathbf{u}}:(\nabla\tilde{\mathbf{u}}^T\cdot\nabla\tilde{\mathbf{u}} + \nabla\tilde{\mathbf{u}}\cdot\nabla\tilde{\mathbf{u}}^T)} - 2\nu\overline{\nabla\tilde{\mathbf{u}}:[\tilde{\mathbf{u}}\cdot\nabla(\nabla\tilde{\mathbf{u}})^T]} - \\ &\quad - 2\nu^2\overline{[\nabla(\nabla\tilde{\mathbf{u}})^T]:[\nabla(\nabla\tilde{\mathbf{u}})^T]}, \end{aligned} \quad (1.43)$$

where

$$\tilde{\varepsilon} := \nu\nabla\tilde{\mathbf{u}}:(\nabla\tilde{\mathbf{u}})^T$$

is the fluctuating dissipation rate.

Unlike the k -equation, where only the diffusive term is modelled, in the case of the transport equation for ε each term on the right-hand side of (1.43) must be modelled (this will clearly reduce the general validity of the modelled ε -equation). The modelling procedure involves a lot of heuristic arguments and is discussed in detail in [5], here we give the final modelled ε -equation:

$$\frac{\partial\varepsilon}{\partial t} + \bar{\mathbf{u}}\cdot\nabla\varepsilon = \nabla\cdot\left[\left(\frac{\nu_T}{\sigma_\varepsilon} + \nu\right)\nabla\varepsilon\right] + C_{\varepsilon 1}\frac{\varepsilon}{k}\boldsymbol{\tau}:\nabla\bar{\mathbf{u}} - C_{\varepsilon 2}\frac{\varepsilon^2}{k}. \quad (1.44)$$

Then, substituting (1.24) into the right-hand side of (1.44) and using the fact that $\mathbf{I}:\nabla\bar{\mathbf{u}} = \nabla\cdot\bar{\mathbf{u}}=0$, yields:

$$\frac{\partial\varepsilon}{\partial t} + \bar{\mathbf{u}}\cdot\nabla\varepsilon = \nabla\cdot\left[\left(\frac{\nu_T}{\sigma_\varepsilon} + \nu\right)\nabla\varepsilon\right] + C_{\varepsilon 1}\frac{\varepsilon}{k}\nu_T(\nabla\bar{\mathbf{u}} + (\nabla\bar{\mathbf{u}})^T):\nabla\bar{\mathbf{u}} - C_{\varepsilon 2}\frac{\varepsilon^2}{k}. \quad (1.45)$$

The values of the constants σ_ε , $C_{\varepsilon 1}$ and $C_{\varepsilon 2}$ will be given in the next section.

1.4.3 The closed system of dynamical and model equations

We finally summarize the closed system of dynamical and model equations which describe the mean properties of turbulent flows in the framework of the eddy viscosity k - ε model.

Below we will show that:

$$\frac{\nu}{\nu_T} \ll 1, \quad (1.46)$$

and hence $\nu + \nu_T$ can be well approximated by ν_T . Using this and the expression (1.29) for ν_T , the differential equations (1.26), (1.18), (1.41) and (1.45) for the variables $\bar{\mathbf{u}}$, \mathcal{P} , k and ε ,

1.4. Eddy viscosity k - ε model

can be written as:

$$\frac{\partial \bar{\mathbf{u}}}{\partial t} + \bar{\mathbf{u}} \cdot \nabla \bar{\mathbf{u}} = \nabla \cdot \left[C_\mu \frac{k^2}{\varepsilon} (\nabla \bar{\mathbf{u}} + (\nabla \bar{\mathbf{u}})^T) \right] - \nabla \mathcal{P} , \quad (1.47)$$

$$\nabla \cdot \bar{\mathbf{u}} = 0 , \quad (1.48)$$

$$\frac{\partial k}{\partial t} + \bar{\mathbf{u}} \cdot \nabla k = \nabla \cdot \left(\frac{C_\mu}{\sigma_k} \frac{k^2}{\varepsilon} \nabla k \right) + C_\mu \frac{k^2}{\varepsilon} (\nabla \bar{\mathbf{u}} + (\nabla \bar{\mathbf{u}})^T) : \nabla \bar{\mathbf{u}} - \varepsilon , \quad (1.49)$$

$$\frac{\partial \varepsilon}{\partial t} + \bar{\mathbf{u}} \cdot \nabla \varepsilon = \nabla \cdot \left(\frac{C_\mu}{\sigma_\varepsilon} \frac{k^2}{\varepsilon} \nabla \varepsilon \right) + C_{\varepsilon 1} C_\mu k (\nabla \bar{\mathbf{u}} + (\nabla \bar{\mathbf{u}})^T) : \nabla \bar{\mathbf{u}} - C_{\varepsilon 2} \frac{\varepsilon^2}{k} . \quad (1.50)$$

This is the form of the dynamical and model equations that we will consider in the rest of this thesis. It should be noted that (1.46) is valid for large Reynolds numbers and sufficiently far from physical walls and both conditions are satisfied by k - ε model in its formulation presented here (see the comment below and §1.5 for an explanation of how the turbulence model describes the properties of flows near solid walls).

Equations (1.47)-(1.50) form a system of coupled PDE's and must be provided with appropriate initial and boundary conditions. In the next section we will see that in the case of wall-bounded flows, the boundary conditions for the mean flow variables are not imposed at the solid surfaces, where some assumptions behind the k - ε model fail to be valid, but are prescribed some distance away from the physical walls, by using the “wall function” technique (see §1.5).

Note that, according to Postulation 5 (see §1.4), the values of the constants C_μ , σ_k , σ_ε , $C_{\varepsilon 1}$ and $C_{\varepsilon 2}$, introduced by the modelling procedure, are to be determined from experiments. It should be remarked that if the k - ε model was complete then the turbulence model constants would be unique and valid for any turbulent flow geometry and conditions. However, at present time, no such turbulence model is available, and although the model coefficients are called constants, they can nevertheless depend on fluid properties and nondimensional parameters, such as the Reynolds number. Moreover for any particular flow it is likely that the accuracy of the model calculation can be improved by adjusting the values of the constants. In this thesis we will use the values recommended in [27]:

$$C_\mu = 0.09 , \quad \sigma_k = 1.0 , \quad \sigma_\varepsilon = 1.3 \quad C_{\varepsilon 1} = 1.44 , \quad C_{\varepsilon 2} = 1.92 , \quad (1.51)$$

these represent a sensible compromise which gives model equations acceptably accurate for a relatively wide range of flows. Also from these considerations it is clear that turbulence models should be regarded as engineering correlations or approximations rather than scientific laws; moreover since models can be “tuned” for particular features that may arise in individual turbulent flows, many variations of turbulence models, and hence model constants, are in existence under the postulations indicated in §1.4, for example high- Re turbulence models, low- Re turbulence models, near-wall turbulence model, two-scale turbulence models, and so forth.

We now show (1.46). As in §1.2, let u and L be respectively the characteristic turbulent velocity and characteristic length of the largest eddies of a particular flow whose viscosity is ν ,

1.5. Near-wall turbulence

and let

$$Re = \frac{uL}{\nu} \gg 1$$

be the Reynolds number based on these representative quantities. Then, assuming that $k \sim u^2$ (which is justified by the fact that most of the energy of the flow is contained in the large eddies) and using the expression for the Kolmogorov microscale of velocity v in (1.6) and the relation (1.11) between u and v , we obtain:

$$\frac{\nu}{\nu_T} = \frac{1}{C_\mu} \frac{\varepsilon \nu}{k^2} \sim \frac{1}{C_\mu} \frac{\varepsilon \nu}{u^4} \sim \frac{1}{C_\mu} \frac{v^4}{u^4} \sim \frac{1}{C_\mu} \frac{1}{Re} \ll 1.$$

We finally mention the fact that there are flows, such as flows with strong curved surfaces or three dimensional flows, for example, for which the k - ε model cannot perform well because their Reynolds stress cannot be approximated sufficiently accurately by Boussinesq's hypothesis (1.24). In order to describe correctly the features of these classes of flows, turbulence models which bypass Boussinesq's hypothesis (1.24), have been introduced. One of these is the second order two-equation *Reynolds stress model*, which represents the highest level of closure that is currently feasible for practical computations and involves the solution of modelled transport equations for each component of the Reynolds stress $\tau = -\widetilde{\mathbf{u}\mathbf{u}}$, along with the RANS equations (1.47)-(1.48) and the transport equations (1.40)-(1.44) for k and ε . The other is the *algebraic stress model* which still entails the solution of the RANS and k - ε equations but, by some approximations, reduces the differential transport equations for τ to a set of algebraic equations which implicitly determines the Reynolds stress as a local function of \mathbf{u} , k and ε . nd have better predictive These models have certainly better capabilities than the eddy viscosity k - ε model but require much more computational effort.

1.5 Near-wall turbulence

Most turbulent flows are bounded (at least in part) by one or more solid surfaces. For example, consider flows through pipes and ducts, flows around aircraft and ships' hulls, flows of rivers and the atmospheric boundary layer. The presence of solid walls imposes constraints which complicate the structure of the flow; most notably, the viscosity of the fluid enforces the no-slip condition, which requires that the velocity of the fluid at a solid surface is equal to the velocity of the surface, and this viscous constraint gives rise to a viscosity-dominated layer adjacent to the solid wall. It is then clear that, as already noticed, (1.46) cannot be true at physical walls or in their closest proximities, and in fact solid boundaries cause a number of different effects which would necessitate modifications of the k - ε model as presented in §1.4 (some postulations adopted in the formulation of the turbulence model, such as isotropic dissipation and isotropic diffusion, become questionable when the flow is studied near a wall). This problem is overcome by a special near-wall treatment: the "wall function" technique. This consists in determining distribution functions (based on the properties of the log-law region of the flow which are discussed in §1.5.1) which describe the variation of k and ε some distance

1.5. Near-wall turbulence

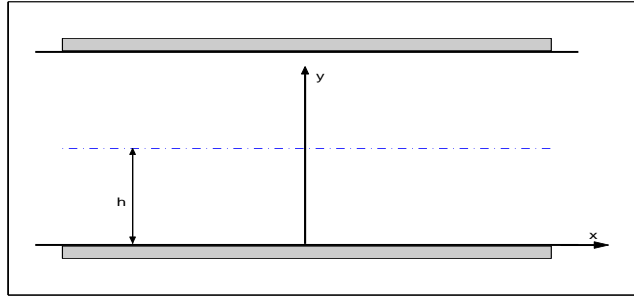


Figure 1.1: Flow in a channel with parallel walls.

away from the wall and in applying boundary conditions in this region. Thus the turbulence model equations are not solved very close to the wall (i.e. they are not solved between the physical wall and the location at which boundary conditions are applied, which later we call the “artificial wall”).

The wall function for ε is derived by using one of the major landmarks in turbulence theory: the logarithmic law for the component of the mean velocity field parallel to the wall. This is briefly discussed in §1.5.1 below, while the wall functions for the turbulence variables k and ε are presented in §1.5.2. The logarithmic law of the wall is also used explicitly in practical implementations of the k - ε model as discussed in §2.6.2 and in §6.1.2.

1.5.1 Log-law for the mean velocity profile

In this subsection we will sketch the derivation of the logarithmic law of the wall for the mean velocity profile following Chapter 5 of [1]. The study presented in [1] consists of a thorough multiple scales analysis of the dynamics of turbulent boundary-layer flows. We will see, in fact, that turbulent boundary layers are characterized by the coexistence of a very thin sublayer adjacent to the physical wall where the viscous stress is dominant, of an external sublayer where the viscous stress is negligibly small and of an overlap region between the two sublayers (a more refined subdivision of the boundary layer can also be considered, for this see §5.2 of [1] and §7.1.4 of [2]).

Tennekes and Lumley [1] consider the particular case of flows in channels with parallel walls which are infinitely long and wide and at rest with respect to the coordinate system used, see Figure 1.1. The mean flow, governed by the equations (1.18), (1.22), is assumed to be in the (x, y) plane and steady, and all derivatives of mean quantities normal to that plane are assumed to be zero. All derivatives with respect to the streamwise coordinate x are also assumed to be zero, except for the pressure gradient $\partial\bar{p}/\partial x$ which drives the flow. Under these conditions it is shown that there exists a region of the flow where the x -component of $\bar{\mathbf{u}} = (\bar{u}, \bar{v})$ can be expressed as:

$$\frac{\bar{u}(y)}{u_*} = \frac{1}{\kappa} \ln \left(\frac{u_* y}{\nu} \right) + C, \quad (1.52)$$

and where the x -component of the force exerted by the Reynolds stress (per unit mass) is

1.5. Near-wall turbulence

constant and has the form:

$$-\overline{uv} = u_*^2 . \quad (1.53)$$

In (1.52) and (1.53), u_* is called friction velocity and its square gives the value of the x -component of the total stress vector $(\overline{\sigma} + \tau) \cdot \mathbf{e}_y$ at the physical wall:

$$u_*^2 := \{\mathbf{e}_x \cdot [(\overline{\sigma} + \tau) \cdot \mathbf{e}_y]\}_{y=0} = \left(\nu \frac{\partial \overline{u}}{\partial y} - \overline{uv} \right)_{y=0} = \left(\nu \frac{\partial \overline{u}}{\partial y} \right)_{y=0} , \quad (1.54)$$

where we have used the fact that $\overline{uv}(0) = 0$, due to the no-slip boundary condition for the fluctuating velocity. In (1.52), C and κ are constants (κ is called von Kármán's constant) and their experimentally determined values are approximately 5.1 and 0.41, respectively. Experiments in turbulent channel flows show an excellent agreement between (1.52), (1.53) and the corresponding measured quantities for $u_* y / \nu > 30$.

We now illustrate, in general terms, the argument used by Tennekes and Lumley to derive (1.52). In [1], it is first shown that (1.18) yields:

$$\overline{v} = 0 \quad \forall y \in [0, 2h]$$

(h is half of the width of the channel, see Figure 1.1) and that the x -component of (1.22) can be expressed as

$$\nu \frac{d\overline{u}}{dy} - \overline{uv} = u_*^2 \left(1 - \frac{y}{h} \right) , \quad (1.55)$$

then the following study is based on the observation that, for large values of the Reynolds number $R_* = u_* h / \nu$, two different nondimensionalisations of (1.55) should be considered. One which holds in the *wall layer* or *surface layer*, which is a very thin inner layer confined to the immediate vicinity of the wall of representative scaled length

$$y_+ = \frac{u_* y}{\nu} = O(1) ,$$

where the viscous term does not become small as $R_* \rightarrow \infty$, and the another which is valid in the *core region* (or “outer layer”) of characteristic length

$$\eta = \frac{y}{h} = O(1) ,$$

where the viscous stress is negligibly small as $R_* \rightarrow \infty$. From the analysis of the governing equation in the surface layer, the following similarity expressions for the velocity field and the Reynolds stress are then deduced:

$$\left(\frac{\overline{u}}{u_*} \right) (y) = f(y_+) , \quad (1.56)$$

$$-\left(\frac{\overline{uv}}{u_*^2} \right) (y) = g(y_+) , \quad (1.57)$$

1.5. Near-wall turbulence

for some well behaved functions f and g such that $f(0) = 0 = g(0)$ (due to the no-slip condition at the solid wall). The relations (1.56) and (1.57) are called *law of the wall*. In the core region, instead, also from the analysis of the time-independent version of (1.33), it is deduced that:

$$\frac{d\bar{u}}{dy}(y) = \frac{u_*}{h} \frac{dF}{d\eta}(\eta) , \quad (1.58)$$

where $dF/d\eta$ is the derivative of some unknown function F . It is then shown that, as $R_* \rightarrow \infty$, the limits $y_+ \rightarrow \infty$ and $\eta \rightarrow 0$ can be taken simultaneously, that is there exists a *region of overlap* (or *matched layer*) between the wall layer and the core region. The result (1.52) then follows from matching the velocity gradient of the wall layer and the core region, as now shown. From (1.56) we have:

$$\frac{d\bar{u}}{dy} = \frac{u_*^2}{\nu} \frac{df}{dy_+} , \quad (1.59)$$

then, by equating (1.58) and (1.59), keeping in mind that we are considering a limit process where $y_+ \rightarrow \infty$ and $\eta \rightarrow 0$ simultaneously, we obtain:

$$\frac{u_*}{h} \frac{dF}{d\eta} = \frac{u_*^2}{\nu} \frac{df}{dy_+} ,$$

and multiplying both sides of the last expression by y/u_* yields:

$$\eta \frac{dF}{d\eta} = y_+ \frac{df}{dy_+} . \quad (1.60)$$

Since the left-hand side of (1.60) can be only a function of η and the right-hand side can be only a function of y_+ , in the region of overlap it must be

$$\eta \frac{dF}{d\eta} = \frac{1}{\kappa} = y_+ \frac{df}{dy_+} \quad (1.61)$$

where $1/\kappa$ is a universal constant. (1.61) can finally be integrated to get:

$$\begin{aligned} F(\eta) &= \frac{1}{\kappa} \ln \eta + \text{const} , \\ f(y_+) &= \frac{1}{\kappa} \ln y_+ + \text{const} , \end{aligned} \quad (1.62)$$

which are valid only if $\eta \ll 1$ and $y_+ \gg 1$. The logarithmic law of the wall (1.52) then clearly follows from substituting (1.62) into (1.56).

A similar matching process for the Reynolds stress yields (1.53).

It should be noted that for curved solid walls the above results are valid only locally, and generalisation of (1.52) to the case of expanding channels, will be given in §6.1.2.

1.5. Near-wall turbulence

1.5.2 Wall functions for k and ε

We now determine the wall functions for k and ε in the region of the flow where (1.52) and (1.53) hold ($u_*y/\nu > 30$).

First we observe that in the case of the straight channel geometry we are considering, we can use Boussinesq's hypothesis (1.24) to express $-\overline{uv}$ as:

$$-\overline{uv} = \nu_T \frac{\partial \bar{u}}{\partial y},$$

and therefore, using (1.46) and (1.53), we have that in the log-law region of the flow the following holds:

$$C_\mu \frac{k^2}{\varepsilon} \frac{\partial \bar{u}}{\partial y} = u_*^2. \quad (1.63)$$

This is the wall function for the component of the Reynolds stress vector parallel to the wall which, in the framework of the k - ε model is employed as boundary condition for the velocity field, see (2.14).

Next we derive the wall functions for k and ε . For this, consider that, for a stationary straight channel flow, the "exact" transport equation for k (1.33) becomes:

$$0 = \frac{\partial}{\partial y} \left(-\overline{k\tilde{v}} + \overline{p\tilde{v}} + \nu \frac{\partial k}{\partial y} \right) - \overline{uv} \frac{\partial \bar{u}}{\partial y} - \varepsilon, \quad (1.64)$$

and, since experiments show that in the log-law region ($u_*y/\nu > 30$), the dominant balance in (1.64) is between the production and dissipation terms, we have that, in this region, (1.64) reduces to

$$0 = -\overline{uv} \frac{\partial \bar{u}}{\partial y} - \varepsilon. \quad (1.65)$$

This is then used to derive the "law of the wall" for k :

$$k = C_\mu^{-1/2} u_*^2, \quad (1.66)$$

and the "law of the wall" for ε :

$$\varepsilon = \frac{u_*^3}{\kappa y}. \quad (1.67)$$

To obtain (1.66), use (1.63) to get the following expression for ε

$$\varepsilon = C_\mu \frac{k^2}{u_*^2} \frac{\partial \bar{u}}{\partial y}, \quad (1.68)$$

then substituting (1.53) and (1.68) into (1.65) yields:

$$0 = u_*^2 \frac{\partial \bar{u}}{\partial y} - C_\mu \frac{k^2}{u_*^2} \frac{\partial \bar{u}}{\partial y},$$

from which, by performing simple operations, (1.66) follows.

1.6. Known mathematical results on the k - ε model

To obtain (1.67) first rearrange (1.65) into:

$$\varepsilon = -\overline{\overline{uv}} \frac{\partial \overline{u}}{\partial y}, \quad (1.69)$$

then note that, in the log-law region, $-\overline{\overline{uv}}$ can be expressed as in (1.53) while an expression for $\partial \overline{u} / \partial y$ can be derived by differentiating (1.52) (or combining (1.59) and (1.61)):

$$\frac{\partial \overline{u}}{\partial y} = \frac{u_*}{\kappa y}. \quad (1.70)$$

Finally substituting (1.53) and (1.70) into (1.69) yields (1.67).

We will see, in §§2.1, 2.2, that the wall functions (1.63) and (1.67) are used as boundary conditions for \overline{u} and ε at the *artificial wall* $y = h_+$, with h_+ such that $u_* h_+ / \nu > 30$. In practical implementations of the k - ε model, the wall functions (1.52) and (1.66) are not imposed as boundary conditions but used to obtain expressions for u_* which are then substituted into (1.63) and (1.67), this is discussed in §§2.6.2, 2.6.3.

We also observe, from (1.67), that ε is in inverse proportion to the distance from the physical wall. This, as we will see in detail in §2.4, determines the blow-up of ε at the artificial wall, in fact, for large Reynolds numbers ($Re \approx 10^7$), values of h_+ as small as 10^{-4} satisfy the condition $u_* h_+ / \nu > 30$ (in §2.4.1 we will show that u_* grows with the Reynolds number).

1.6 Known mathematical results on the k - ε model

The system of coupled PDE's (1.47)-(1.50) certainly represents a major challenge both analytically and numerically. In fact, the high nonlinearity of the equations not only makes the task of proving the existence and uniqueness of their solution extremely difficult (such result has not been obtained yet) but also complicates the design of robust numerical methods. In this section we give a brief overview of the mathematical studies of (1.47)-(1.50) we are aware of; these, as we shall see, concern the transport equations (1.49)-(1.50) and assume that velocity field \overline{u} is known. This ‘‘simplification’’ of the problem (consider that the k - ε equations alone are, anyway, very complicated to analyse) reflects the extremely common approach to solving the discretised version of (1.47)-(1.50) by an iterative method based on the decoupling of (1.47)-(1.48) from (1.49)-(1.50) (in §5.3 we will discuss the reason for the widespread use of this scheme, but we will also show that it is much less effective than Newton's method for the system of fully coupled equations).

When the k - ε model was initially incorporated into fluid dynamics codes based on the standard Galerkin finite element technique, several difficulties were immediately encountered, as reported by Smith in [28] and [29] and by Hutton, Smith and Hickmott in [30]. The iterative method for the discretised equations (based on the decoupling of RANS and k - ε equations) soon proved to be highly unstable, in particular, the occurrence of negative values of k and ε during the solution procedure made the iterative scheme diverge or converge to unphysical solutions (the physics requires both k and ε to be positive). This last phenomenon even generated

1.6. Known mathematical results on the k - ε model

some controversy about the existence of meaningful solutions to the k - ε equations for some flow configurations. These concerns were partly dissipated by the argument of Mohammadi and Pironneau [31] (see also [32]), who, on the assumption that the velocity field $\bar{\mathbf{u}}$ is known, showed that *if the system (1.49)-(1.50), defined on the domain Ω for $t > 0$, has a smooth solution, then, for strictly positive Dirichlet conditions on $\partial\Omega$ and strictly positive initial data, k and ε stay positive and bounded at any $t > 0$* . The proof of Mohammadi and Pironneau is based on the introduction of the variable

$$\theta = \frac{k}{\varepsilon}, \quad (1.71)$$

and proceeds as follows. First, from (1.49) and (1.50), a transport equation is derived for θ , which, by a maximum principle type argument, is shown to be strictly positive (note that from the assumption that the boundary and initial conditions on k and ε are strictly positive, it follows that $\theta(t, \mathbf{x}) > 0$ on $\partial\Omega$ and $\theta(0, \mathbf{x}) > 0$). Then, (1.71) is used to eliminate ε from (1.50) and the strict positivity of θ is used in another maximum principle argument to show that $k(t, \mathbf{x}) > 0$. Finally, the fact that $\theta(t, \mathbf{x}) > 0$ and $k(t, \mathbf{x}) > 0$ for all $\mathbf{x} \in \Omega$ and $t > 0$ implies, through (1.71), $\varepsilon(t, \mathbf{x}) > 0$ for all $\mathbf{x} \in \Omega$ and $t > 0$.

More recently an equivalent positivity result has been obtained by Wu and Fu [33]. The study presented in [33] makes the same assumptions as in [31], but relies on the construction of an iterative method for solving the k - ε equations written in the form (1.41), (1.45). We shall now briefly outline this iterative method, which produces strictly positive iterates k^n , ε^n by exploiting an operator splitting technique

Let k^n and ε^n be the known approximations to k and ε , respectively, at time level t^n , then k^{n+1} and ε^{n+1} , approximations to k and ε at time $t^{n+1} = t^n + \Delta t$, are determined from k^n and ε^n as follows:

1. Solve the *advection-diffusion step*

$$\frac{\partial \hat{k}}{\partial t} + \bar{\mathbf{u}} \cdot \nabla \hat{k} = \nabla \cdot \left[\left(\frac{C_\mu}{\sigma_k} \frac{\hat{k}^2}{\hat{\varepsilon}} + \nu \right) \nabla \hat{k} \right], \quad (1.72)$$

$$\frac{\partial \hat{\varepsilon}}{\partial t} + \bar{\mathbf{u}} \cdot \nabla \hat{\varepsilon} = \nabla \cdot \left[\left(\frac{C_\mu}{\sigma_\varepsilon} \frac{\hat{k}^2}{\hat{\varepsilon}} + \nu \right) \nabla \hat{\varepsilon} \right], \quad (1.73)$$

on $[t_n, t_{n+1}] \times \Omega$ for \hat{k} and $\hat{\varepsilon}$ with strictly positive initial conditions $\hat{k}(t_n, \mathbf{x}) = k^n(\mathbf{x})$, $\hat{\varepsilon}(t_n, \mathbf{x}) = \varepsilon^n(\mathbf{x})$ and strictly positive Dirichlet boundary conditions on $\partial\Omega$.

2. Solve the *point-source step*

$$\frac{dk^{n+1}}{dt} = C_\mu \frac{(k^{n+1})^2}{\varepsilon^{n+1}} (\nabla \bar{\mathbf{u}} + (\nabla \bar{\mathbf{u}})^T) : \nabla \bar{\mathbf{u}} - \varepsilon^{n+1}, \quad (1.74)$$

$$\frac{d\varepsilon^{n+1}}{dt} = C_{\varepsilon 1} C_\mu k^{n+1} (\nabla \bar{\mathbf{u}} + (\nabla \bar{\mathbf{u}})^T) : \nabla \bar{\mathbf{u}} - C_{\varepsilon 2} \frac{(\varepsilon^{n+1})^2}{k^{n+1}}, \quad (1.75)$$

1.6. Known mathematical results on the k - ε model

on $[t_n, t_{n+1}] \times \Omega$ for k^{n+1} and ε^{n+1} with initial conditions $k^{n+1}(t_n, \mathbf{x}) = \widehat{k}(t_{n+1}, \mathbf{x})$ and $\varepsilon^{n+1}(t_n, \mathbf{x}) = \widehat{\varepsilon}(t_{n+1}, \mathbf{x})$. (Note that (1.74)-(1.75) is a system of ODE's at every point in space).

In [33], the solution $(\widehat{k}, \widehat{\varepsilon})$ to (1.72)-(1.73) is shown to be strictly positive by the maximum principle, while the strict positivity of k^{n+1} and ε^{n+1} (the solutions to (1.74)-(1.75)) is proved by the same technique used in [31]. That is, first the variable

$$\theta^{n+1} := \frac{k^{n+1}}{\varepsilon^{n+1}} \quad (1.76)$$

(compare (1.76) with (1.71)) is shown to be strictly positive, by the analysis of its point-source equation derived from (1.74)-(1.75), then, from the study of the point-source equation for k^{n+1} , obtained by eliminating ε^{n+1} from (1.74) using (1.76), it is also shown that $k^{n+1}(t, \mathbf{x}) > 0$. The positivity of ε^{n+1} finally follows. The proof is then concluded by showing the convergence of the scheme, that is $(k^{n+1}, \varepsilon^{n+1}) \rightarrow (k(t_{n+1}), \varepsilon(t_{n+1}))$, in the limit as $\Delta t \rightarrow 0$.

It should be remarked that both positivity results, in [31] and [33], rely on the assumption that a solution to the k - ε equations exists and is smooth. It seems very hard to prove this. However, existence results have been established for a reduced model: the φ - θ model. The transport equations for φ and θ are derived from (1.49)-(1.50) by the change of variables:

$$\varphi = \frac{\varepsilon^2}{k^3}, \quad \theta = \frac{k}{\varepsilon},$$

and by some extra modelling, see [34] (or [35]) and also [36], [37].

Finally we mention the fact that an analytical solution to the stationary k - ε model is available in the case of turbulent Couette flow in straight channels. This was presented by Cliffe [38] and, independently, by Henry and Reynolds [39]. These works will be discussed in some detail in Chapter 2.

Chapter 2

The k - ε model for stationary turbulent flows in straight channels

This chapter is devoted to a thorough discussion of turbulent Couette and Poiseuille flows between two parallel planes, as described by the k - ε turbulence model.

First we formulate the boundary value problem representing a stationary turbulent flow through a straight channel, both in the case when the flow is driven by the relative motion of two parallel walls of the channel (Couette flow) and in the case when the flow is driven by the pressure difference between the inlet and the outlet of the channel (Poiseuille flow), see §§2.1, 2.2 and also §2.5. Then, bearing in mind the work done in [38] and [39], we give the analytic solution to the system of equations describing Couette flow and analyse its behaviour in the limit as the distance between the artificial and the physical wall approaches zero, see §§2.3, 2.4 respectively. In §2.5, we discuss the continuation strategy we will use in the numerical computation of Poiseuille flow. This does not have a known analytic solution. In §2.6, we then introduce the specific weak forms of the RANS and k - ε equations and, in §2.7, we use these to generate the Galerkin finite element equations.

The following detailed analysis of turbulent Couette flow in straight channels is motivated by the fact that this flow (together with the Poiseuille one, whose solution can be confidently computed numerically using that of the Couette flow as an initial guess) will represent, throughout this thesis, a very important benchmark. In fact, as far as we know, plane Couette flow is the only case when the analytical solution to the k - ε model is available and moreover, far from being trivial, it encompasses the main features of every turbulent flow described by the k - ε model: the high nonlinearity of the governing equations (see §2.3), the blow up of the ε -variable at the artificial wall, together with the local predominance of source terms over diffusion terms (see §2.4) and the “ad hoc” implementations of the laws of the wall for the component of the stress parallel to the wall and for ε (see §§2.6.2, 2.6.3). The analysis of Couette flow will provide us with important insights in the understanding of more complex situations, and which will be used to test the efficiency of the numerical algorithms. The results of these tests then will guide us to the design of robust solvers for more general and realistic flows. In Chapter 6, in fact, the solution techniques developed for flows in straight channels will be applied to flows

2.1. 2D formulation of the problem

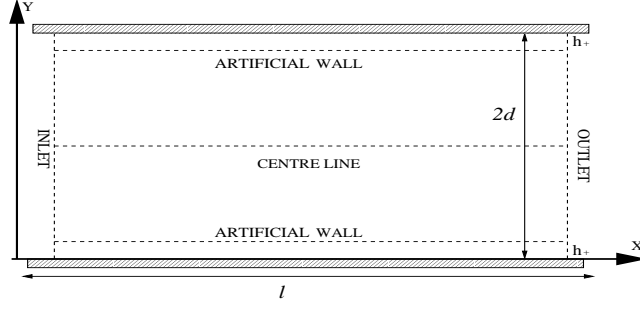


Figure 2.1: The geometry of the channel

in expanding channels.

2.1 2D formulation of the problem

In this section we specify the domain of the problem, give the two-dimensional formulation of the PDE's which describe the mean properties of the flow and discuss the boundary conditions. Figure 2.1 shows the geometry of the channel and some of the notation that will be employed in what follows. The channel width is taken as $2d$ and its length as l , we are supposing that l is much larger than d and that the other two walls of the channel, in the z -direction, are so distant that they have negligible effects on the flow in the region of interest. The last assumption implies that the flow is two-dimensional and all variables depend only on (x, y) . The distance between the physical walls and the artificial walls (where the boundary conditions are prescribed) is given by h_+ .

The stationary dynamical equations for the mean velocity field $\mathbf{u}(x, y) = (U(x, y), V(x, y))^T$ and the modified mean pressure field $p = p(x, y)$ (in Chapter 1, these quantities were denoted respectively by $\bar{\mathbf{u}}$ and \mathcal{P}) can be obtained from the RANS equations (1.47)-(1.48), by setting $\partial \bar{\mathbf{u}} / \partial t = 0$, and are expressed here as:

$$\begin{cases} \mathbf{u} \cdot \nabla \mathbf{u} = \nabla \cdot \boldsymbol{\sigma} \\ \nabla \cdot \mathbf{u} = 0 \end{cases}, \quad (2.1)$$

where the second-rank tensor

$$\boldsymbol{\sigma} := \nu_T [\nabla \mathbf{u} + (\nabla \mathbf{u})^T] - p \mathbf{I} \quad (2.2)$$

is the total stress tensor, with turbulent kinematic viscosity ν_T given by:

$$\nu_T = C_\mu \frac{k^2}{\varepsilon}, \quad (2.3)$$

((2.2) represents the sum of the mean Cauchy stress (1.21) and of the Reynolds stress (1.24) when $\nu + \nu_T$ is approximated by ν_T , by virtue of (1.46)).

In (2.3), k is the mean turbulent kinetic energy and ε its dissipation rate. $k = k(x, y)$ and

2.1. 2D formulation of the problem

$\varepsilon = \varepsilon(x, y)$ are the solutions to the stationary version of the transport equations (1.49)-(1.50):

$$\begin{cases} \mathbf{u} \cdot \nabla k - \nabla \cdot \left(C_\mu \frac{k^2}{\varepsilon} \nabla k \right) = C_\mu \frac{k^2}{\varepsilon} S(\mathbf{u}) - \varepsilon \\ \mathbf{u} \cdot \nabla \varepsilon - \nabla \cdot \left(\frac{C_\mu k^2}{\sigma_\varepsilon \varepsilon} \nabla \varepsilon \right) = C_{\varepsilon 1} C_\mu k S(\mathbf{u}) - C_{\varepsilon 2} \frac{\varepsilon^2}{k} \end{cases}, \quad (2.4)$$

where

$$S(\mathbf{u}) := \nabla \mathbf{u} : [\nabla \mathbf{u} + (\nabla \mathbf{u})^T], \quad (2.5)$$

and $:$ denotes the dot product of two second-rank tensors. C_μ , in (2.3) and (2.4), and σ_ε , $C_{\varepsilon 1}$ and $C_{\varepsilon 2}$, in (2.4), are all positive constants whose values are specified in (1.51).

Due to the symmetry of the channel with respect to the centre line $y = d$ (see Figure 2.1), the system of PDE's (2.1)-(2.4) will be considered only in the lower half of the channel, over the domain $\Omega = [0, L] \times [h_+, d]$.

We now give the boundary conditions for (2.1)-(2.4); these will be formulated in such a way as to encompass both cases of Couette and Poiseuille flow. On Γ_{in} , the inlet boundary of the channel at $x = 0$, the variables (U, V) , p , k and ε must satisfy the boundary conditions:

$$p - \nu_T \frac{\partial U}{\partial x} = p_{\text{in}}, \quad (2.6)$$

$$\frac{\partial V}{\partial x} = 0, \quad (2.7)$$

$$\frac{\partial k}{\partial x} = 0, \quad (2.8)$$

$$\frac{\partial \varepsilon}{\partial x} = 0, \quad (2.9)$$

and similarly on Γ_{out} , the outlet boundary at $x = L$,

$$p - \nu_T \frac{\partial U}{\partial x} = p_{\text{out}}, \quad (2.10)$$

$$\frac{\partial V}{\partial x} = 0, \quad (2.11)$$

$$\frac{\partial k}{\partial x} = 0, \quad (2.12)$$

$$\frac{\partial \varepsilon}{\partial x} = 0. \quad (2.13)$$

p_{in} and p_{out} , respectively in (2.6) and (2.10), are parameters of the problem (we will see that in the case of Couette flow $p_{\text{in}} - p_{\text{out}} = 0$, while for Poiseuille flow $p_{\text{in}} - p_{\text{out}} > 0$). (2.6)-(2.13) are the natural boundary conditions for the specific weak form of the RANS and k - ε equations

2.1. 2D formulation of the problem

that will be considered, see §2.6. On the artificial wall Γ_w , at $y = h_+$, we impose the following boundary conditions:

$$\nu_T \frac{\partial U}{\partial y} = u_*^2 , \quad (2.14)$$

$$V = 0 , \quad (2.15)$$

$$\frac{\partial k}{\partial y} = 0 , \quad (2.16)$$

$$\varepsilon = \frac{1}{\kappa} \frac{u_*^3}{h_+} . \quad (2.17)$$

Equation (2.14) is the “law of the wall” for the x -component of $\mathbf{t} = \boldsymbol{\sigma} \cdot \mathbf{e}_y$, the stress vector at the artificial wall (with $\boldsymbol{\sigma}$ given in (2.2), and \mathbf{e}_y the unit vector in the y -direction), and (2.17) is the “law of the wall” for ε . In (2.14) and (2.17), u_* is the wall-friction velocity, which depends on the Reynolds number Re (see §2.4.1 where an expression is given for u_* in terms of Re and the other constants of the problem), and finally κ , in (2.17), is von Kármán’s constant. In our study we will assume the following value for κ

$$\kappa := \sqrt{\sigma_\varepsilon C_\mu^{1/2} (C_{\varepsilon 2} - C_{\varepsilon 1})} = 0.4326 \dots , \quad (2.18)$$

which is compatible with the experimentally determined one $\kappa \approx 0.41$. The relation between κ and the other constants in (2.18) is a necessary condition for the existence of a solution to the turbulent Couette flow, see §§2.3, 2.4.

In order to formulate the boundary conditions on the centre line Γ_{cl} in a way to include both Couette and Poiseuille flow, we now introduce the parameter α which can take the value either 0 or 1 and then express the symmetry boundary conditions on Γ_{cl} , at $y = d$, as follows:

$$\alpha \frac{\partial U}{\partial y} = (1 - \alpha)(U_{CL} - U) , \quad (2.19)$$

$$V = 0 , \quad (2.20)$$

$$\frac{\partial k}{\partial y} = 0 , \quad (2.21)$$

$$\frac{\partial \varepsilon}{\partial y} = 0 . \quad (2.22)$$

In (2.19), U_{CL} is the value of U at $y = d$ (set $\alpha = 0$ in (2.19)) and this is related to the Reynolds number Re by

$$U_{CL} = \frac{\nu Re}{d} , \quad (2.23)$$

where ν is the kinematic viscosity of the fluid.

In §2.3 it will be shown that when $p_{in} - p_{out} = 0$ and $\alpha = 0$, equations (2.1) and (2.4),

2.2. 1D formulation of the problem

together with the boundary conditions above, describe a stationary turbulent flow driven by the relative motion of the walls of the channel with velocity $2U_{CL}$ (turbulent Couette flow). On the other hand when $p_{in} - p_{out} > 0$ and $\alpha = 1$, the flow under investigation is driven by the pressure difference between the inlet and the outlet of the channel (turbulent Poiseuille flow). In order to compute numerically the solution to the Poiseuille flow, we will use continuation with respect to the parameters $p_{in} - p_{out}$ and α . This is discussed in §2.5.

We finally observe that when $\alpha = 0$, (2.19) becomes a Dirichlet boundary condition for the longitudinal component of the velocity \mathbf{u} :

$$U(d) = U_{CL} ,$$

while when $\alpha = 1$, the boundary condition (2.19) reduces to

$$\frac{\partial U}{\partial y}(d) = 0 . \quad (2.24)$$

(2.24) derives from the commonly used boundary condition that at the symmetry line (the centre line with normal $\mathbf{n} = \mathbf{e}_y$, for the geometry under consideration) the mean shear stress vanishes:

$$[\nabla \mathbf{u} + (\nabla \mathbf{u})^T] \cdot \mathbf{n} - \{ \mathbf{n} \cdot [\nabla \mathbf{u} + (\nabla \mathbf{u})^T] \cdot \mathbf{n} \} \mathbf{n} = \mathbf{0} .$$

2.2 1D formulation of the problem

In this section, following a standard procedure, that, for example, can be found in [40], we give the 1D reduction of the 2D problem formulated in §2.1.

Since we are considering here a straight channel invariant under translations in the x -direction, all the mean properties of the flow, with the exception of the mean pressure, can be assumed to be independent of the x -variable:

$$\mathbf{u} = \mathbf{u}(y) = (U(y), V(y)) , \quad p = p(x, y) , \quad k = k(y) , \quad \varepsilon = \varepsilon(y) . \quad (2.25)$$

The dependence of the mean pressure on the x -variable cannot be excluded because the streamwise component of the pressure gradient ∇p is usually necessary for the flow to develop. ∇p appears as a source term in the first equation of (2.1) once the divergence of the stress tensor is computed explicitly. (We will show that, for flows in straight channels, ∇p is constant; in particular, in the case of the Couette flow, when the flow momentum can be maintained by the relative motion of the walls of the channel, the pressure gradient can be set to zero).

We now determine what the PDE's and the boundary conditions, introduced in the previous section, reduce to when a solution with \mathbf{u} , k , ε depending only on the y -coordinate is sought. Substituting the profiles in (2.25) into (2.1) and (2.4), we get respectively the differential equa-

2.2. 1D formulation of the problem

tions (2.26)-(2.28) and (2.29)-(2.30) below:

$$V \frac{dU}{dy} - \frac{d}{dy} \left(C_\mu \frac{k^2}{\varepsilon} \frac{dU}{dy} \right) = -\frac{\partial p}{\partial x} , \quad (2.26)$$

$$V \frac{dV}{dy} - 2 \frac{d}{dy} \left(C_\mu \frac{k^2}{\varepsilon} \frac{dV}{dy} \right) = -\frac{\partial p}{\partial y} , \quad (2.27)$$

$$\frac{dV}{dy} = 0 , \quad (2.28)$$

$$V \frac{dk}{dy} - \frac{d}{dy} \left(C_\mu \frac{k^2}{\varepsilon} \frac{dk}{dy} \right) = C_\mu \frac{k^2}{\varepsilon} \left(\frac{dU}{dy} \right)^2 - \varepsilon , \quad (2.29)$$

$$V \frac{d\varepsilon}{dy} - \frac{d}{dy} \left(\frac{C_\mu k^2}{\sigma_\varepsilon \varepsilon} \frac{d\varepsilon}{dy} \right) = C_\mu C_{\varepsilon 1} k \left(\frac{dU}{dy} \right)^2 - C_{\varepsilon 2} \frac{\varepsilon^2}{k} . \quad (2.30)$$

When a solution of the type given in (2.25) is sought, then the boundary conditions (2.7)-(2.9) and (2.11)-(2.13) are automatically satisfied, while the boundary conditions (2.6) and (2.10) simply reduce to the specification of the value of the mean pressure at the inlet and at the outlet of the channel:

$$p(0, y) = p_{\text{in}} , \quad p(L, y) = p_{\text{out}} . \quad (2.31)$$

(2.31) will be used to determine the constant value of the pressure gradient whose components appear in (2.26) and (2.27) (see Lemmata below).

The system (2.26)-(2.30) is then to be solved for U , V , p , k , ε over the interval $[h_+, d]$, under the boundary conditions (2.14)-(2.17) and (2.19)-(2.22), that are now recalled (using in (2.14) the expression for ν_T given in (2.3)):

$$\left(C_\mu \frac{k^2}{\varepsilon} \frac{dU}{dy} \right) (h_+) = u_*^2 , \quad (2.32)$$

$$V(h_+) = 0 ,$$

$$\frac{dk}{dy}(h_+) = 0 ,$$

$$\varepsilon(h_+) = \frac{1}{\kappa} \frac{u_*^3}{h_+} ,$$

$$\alpha \frac{dU}{dy}(d) = (1 - \alpha)(U_{CL} - U(d)) , \quad (2.33)$$

$$V(d) = 0 , \quad (2.34)$$

$$\frac{dk}{dy}(d) = 0 ,$$

$$\frac{d\varepsilon}{dy}(d) = 0 .$$

2.2. 1D formulation of the problem

We now show that, for turbulent flows in straight channels, the variable V vanishes and the variable p is a function of x only and has got a constant gradient in the x -direction.

The following Lemma is evident.

Lemma 2.2.1. *Equation (2.28) together with the boundary condition (2.32) or (2.34) has the solution*

$$V = 0 \ , \quad \forall \ y \in [h_+, d] \ . \quad (2.35)$$

Under the assumption that V is given by (2.35), we then have:

Lemma 2.2.2. *The mean pressure p depends only on the x -coordinate:*

$$\frac{\partial p}{\partial y} = 0 \ ,$$

and has a constant gradient in the x -direction:

$$\frac{dp}{dx} = \text{constant} \ .$$

Proof. Using (2.35) and (2.27) we obtain:

$$\frac{\partial p}{\partial y} = 0 \ ,$$

which implies

$$p = p(x) \ . \quad (2.36)$$

Also, combining (2.35) with (2.26) we get

$$-\frac{d}{dy} \left(C_\mu \frac{k^2}{\varepsilon} \frac{dU}{dy} \right) (y) = -\frac{dp}{dx} (x) \ .$$

Since k , ε and U are constrained to be functions of y only, this last equation can be satisfied only if both terms are equal to the same constant \mathcal{G} :

$$-\frac{d}{dy} \left(C_\mu \frac{k^2}{\varepsilon} \frac{dU}{dy} \right) (y) = \mathcal{G} \ , \quad (2.37)$$

$$-\frac{dp}{dx} (x) = \mathcal{G} \ . \quad (2.38)$$

In fact, integrating (2.38) over the interval $[0, L]$ and using (2.31), we obtain:

$$\mathcal{G} = \frac{p_{\text{in}} - p_{\text{out}}}{L} \ . \quad \square$$

Lemmas 2.2.1-2.2.2 lead to a great simplification of the equations (2.26)-(2.30). In fact, using (2.35) and (2.36), we can eliminate equations (2.27) and (2.28), and (2.26)-(2.28) reduce

2.3. Stationary turbulent Couette flow

then to the single equation (2.37) for U . Imposing $V = 0$ in (2.29) and (2.30), the system of ODE's (2.26)-(2.30) finally becomes:

$$-\frac{d}{dy} \left(C_\mu \frac{k^2}{\varepsilon} \frac{dU}{dy} \right) = \mathcal{G} , \quad (2.39)$$

$$-\frac{d}{dy} \left(C_\mu \frac{k^2}{\varepsilon} \frac{dk}{dy} \right) = C_\mu \frac{k^2}{\varepsilon} \left(\frac{dU}{dy} \right)^2 - \varepsilon , \quad (2.40)$$

$$-\frac{d}{dy} \left(\frac{C_\mu k^2}{\sigma_\varepsilon \varepsilon} \frac{d\varepsilon}{dy} \right) = C_\mu C_{\varepsilon 1} k \left(\frac{dU}{dy} \right)^2 - C_{\varepsilon 2} \frac{\varepsilon^2}{k} , \quad (2.41)$$

which are three second order nonlinear ordinary differential equations, subject to the six boundary conditions:

$$\left(C_\mu \frac{k^2}{\varepsilon} \frac{dU}{dy} \right) (h_+) = u_*^2 , \quad (2.42)$$

$$\frac{dk}{dy}(h_+) = 0 , \quad (2.43)$$

$$\varepsilon(h_+) = \frac{1}{\kappa} \frac{u_*^3}{h_+} , \quad (2.44)$$

$$\alpha \frac{dU}{dy}(d) = (1 - \alpha)(U_{CL} - U(d)) , \quad (2.45)$$

$$\frac{dk}{dy}(d) = 0 , \quad (2.46)$$

$$\frac{d\varepsilon}{dy}(d) = 0 , \quad (2.47)$$

with u_* , κ , U_{CL} as discussed above and $\alpha = 0$ or 1 .

2.3 Stationary turbulent Couette flow

We now discuss the analytical solution of the equations describing turbulent Couette flow. This solution is also found in the unpublished report [38] and was in fact published independently in [39].

Couette flow is driven by the relative motion of the walls of the channel. As such the flow will suffer no pressure change along the channel. Moreover, the value of U at $y = d$ is given by half of the velocity of the relative motion of the walls. The first condition is met by setting $\mathcal{G} = 0$ in (2.39) and the second by choosing $\alpha = 0$ in (2.45). Therefore we consider the system

2.3. Stationary turbulent Couette flow

of ODE's:

$$-\frac{d}{dy} \left(C_\mu \frac{k^2}{\varepsilon} \frac{dU}{dy} \right) = 0 \quad (2.48)$$

$$-\frac{d}{dy} \left(C_\mu \frac{k^2}{\varepsilon} \frac{dk}{dy} \right) = C_\mu \frac{k^2}{\varepsilon} \left(\frac{dU}{dy} \right)^2 - \varepsilon \quad (2.49)$$

$$-\frac{d}{dy} \left(\frac{C_\mu k^2}{\sigma_\varepsilon \varepsilon} \frac{d\varepsilon}{dy} \right) = C_\mu C_{\varepsilon 1} k \left(\frac{dU}{dy} \right)^2 - C_{\varepsilon 2} \frac{\varepsilon^2}{k} , \quad (2.50)$$

over the interval $[h_+, d]$, with boundary conditions:

$$\left(C_\mu \frac{k^2}{\varepsilon} \frac{dU}{dy} \right) (h_+) = u_*^2 , \quad (2.51)$$

$$\frac{dk}{dy}(h_+) = 0 , \quad (2.52)$$

$$\varepsilon(h_+) = \frac{1}{\kappa} \frac{u_*^3}{h_+} , \quad (2.53)$$

$$U(d) = U_{CL} , \quad (2.54)$$

$$\frac{dk}{dy}(d) = 0 , \quad (2.55)$$

$$\frac{d\varepsilon}{dy}(d) = 0 . \quad (2.56)$$

We recall that the k - ε model requires that U , at $y = h_+$, satisfies the ‘‘logarithmic law of the wall’’ (1.52):

$$U(h_+) = u_* \left[\frac{1}{\kappa} \ln \left(\frac{u_* h_+}{\nu} \right) + C \right] . \quad (2.57)$$

(2.57) represents effectively a condition on U , but should be interpreted as an equation for the friction velocity u_* . Hence u_* , which appears in (2.51) and in (2.53), is determined by (2.57) and depends on the U -solution component to be computed. This guarantees that U has the appropriate logarithmic behaviour at $y = h_+$. In §2.4.1, for the particular case of Couette flow in the limit $h_+ \rightarrow 0$, we will give an expression of the solution u_* to (2.57) in terms of the Reynolds number, while in §2.6.2 we will illustrate how (2.57) is usually implemented in practical computations.

Remark 2.3.1. For the analytic solution to (2.48)-(2.56) that will be presented in §2.3.2, it should also be noted that k , at $y = h_+$, satisfies the law of the wall (1.66):

$$k(h_+) = C_\mu^{-1/2} u_*^2 . \quad (2.58)$$

2.3. Stationary turbulent Couette flow

This is also often an assumption about k in many treatments of turbulence. We will make this assumption at several points later and explain how, together with (2.57), it is implemented in turbulence computations.

2.3.1 A possible scaling

We now briefly consider the scaling of the independent and dependent variables which is used in [39] and explain why this is not relevant for our study. It is not difficult to see that the following scaling of the variables

$$\begin{aligned} y &= d \bar{y} , \\ U &= u_* \bar{U} , \quad k = u_*^2 \bar{k} , \quad \varepsilon = \frac{u_*^3}{d} \bar{\varepsilon} , \end{aligned} \tag{2.59}$$

makes the boundary value problem (2.48)-(2.56) independent of u_* , in fact we have:

Lemma 2.3.1. *The system of ODE's (2.48)-(2.50) is invariant under the transformation (2.59), whilst the boundary conditions (2.51)-(2.56) change into:*

$$\begin{aligned} \left(C_\mu \frac{\bar{k}^2}{\bar{\varepsilon}} \frac{d\bar{U}}{d\bar{y}} \right) (d \bar{h}_+) &= 1 , \quad \frac{d\bar{k}}{d\bar{y}} (d \bar{h}_+) = 0 , \quad \bar{\varepsilon} (d \bar{h}_+) = \frac{1}{\kappa} \frac{1}{\bar{h}_+} , \\ \bar{U}(1) &= \bar{U}_{\text{CL}} , \quad \frac{d\bar{k}}{d\bar{y}}(1) = 0 , \quad \frac{d\bar{\varepsilon}}{d\bar{y}}(1) = 0 . \end{aligned}$$

with $\bar{h}_+ := h_+/d$.

Lemma 2.3.1 then shows that the nondimensional variables $(\bar{U}, \bar{k}, \bar{\varepsilon})$ satisfy a boundary value problem which is independent of u_* . But, neither in the computation of the analytical solution below nor in the numerical experiments that we will perform on the 1D and 2D Couette flow, will we pursue the change of variables (2.59). This, in fact, is specific to the Couette flow and would give rise to a model problem which would not reflect some important features (related to the implementation of (2.57) and (2.58) discussed in §§2.6.2, 2.6.3) of the more complicated flows that we will tackle in the remainder of our study.

2.3.2 Analytical solution

We now present the analytical solution to the boundary value problem (2.48)-(2.56).

Lemma 2.3.2. *The system of ODE's (2.48)-(2.50), subject to the boundary conditions (2.51)-*

2.3. Stationary turbulent Couette flow

(2.56), is satisfied by the functions:

$$U(y) = U_{CL} + \frac{u_*}{\kappa} \ln \left| \tan \left[\frac{\pi}{4} - \frac{\varepsilon_{cl}}{u_*^3} \frac{\kappa}{2} (d - y) \right] \right|, \quad (2.60)$$

$$k(y) = C_\mu^{-1/2} u_*^2, \quad (2.61)$$

$$\varepsilon(y) = \frac{\varepsilon_{cl}}{\cos \left[\frac{\varepsilon_{cl}}{u_*^3} \kappa (d - y) \right]}, \quad (2.62)$$

provided the parameter ε_{cl} is chosen as to solve the nonlinear equation

$$\frac{\varepsilon_{cl}}{\cos \left[\frac{\varepsilon_{cl}}{u_*^3} \kappa (d - h_+) \right]} = \frac{1}{\kappa} \frac{u_*^3}{h_+}. \quad (2.63)$$

Proof. We first show that equation (2.49), together with the boundary conditions (2.52) and (2.55), admits the solution (2.61). This is done as follows. Suppose that equation (2.48) is satisfied together with the boundary condition (2.51), then its integration over the domain $[h_+, y]$ gives:

$$\left(C_\mu \frac{k^2}{\varepsilon} \frac{dU}{dy} \right) (y) = u_*^2, \quad \forall y \in [h_+, d]. \quad (2.64)$$

Rearranging (2.64) to obtain an expression for dU/dy and substituting it into (2.49) yields:

$$\begin{aligned} -\frac{d}{dy} \left(C_\mu \frac{k^2}{\varepsilon} \frac{dk}{dy} \right) &= C_\mu \frac{k^2}{\varepsilon} \frac{\varepsilon^2 u_*^4}{C_\mu^2 k^4} - \varepsilon \\ &= \left(\frac{C_\mu^{-1} u_*^4}{k^2} - 1 \right) \varepsilon. \end{aligned} \quad (2.65)$$

It is then easy to see that the constant function

$$k = C_\mu^{-1/2} u_*^2, \quad \forall y \in [h_+, d], \quad (2.66)$$

satisfies equation (2.65); since

$$-\frac{d}{dy} \left(C_\mu \frac{k^2}{\varepsilon} \frac{dk}{dy} \right) = 0 = \left(\frac{C_\mu^{-1} u_*^4}{k^2} - 1 \right) \varepsilon.$$

Moreover k given by (2.66) also satisfies the boundary conditions (2.52), (2.55).

Next we show that the function (2.62) satisfies the equation (2.50) and the boundary conditions (2.53) and (2.56). Due to (2.63), the function (2.62) clearly satisfies the boundary

2.3. Stationary turbulent Couette flow

condition (2.53). Differentiating we obtain:

$$\frac{d\varepsilon}{dy} = -\frac{\varepsilon_{cl}^2 \kappa}{u_*^3} \frac{\sin\left[\frac{\varepsilon_{cl} \kappa}{u_*^3} (d-y)\right]}{\left\{\cos\left[\frac{\varepsilon_{cl} \kappa}{u_*^3} (d-y)\right]\right\}^2} \quad (2.67)$$

and we see immediately that the boundary condition (2.56) is also satisfied. Now, given k from (2.61), ε from (2.62) and $d\varepsilon/dy$ from (2.67), we have:

$$\begin{aligned} \frac{C_\mu k^2}{\sigma_\varepsilon \varepsilon} \frac{d\varepsilon}{dy} &= \frac{u_*^4}{\sigma_\varepsilon \varepsilon} \frac{1}{dy} \frac{d\varepsilon}{dy} \\ &= -\frac{u_*}{\sigma_\varepsilon} \varepsilon_{cl} \kappa \tan\left[\frac{\varepsilon_{cl} \kappa}{u_*^3} (d-y)\right], \end{aligned}$$

and the left-hand side of (2.50) then becomes:

$$\begin{aligned} -\frac{d}{dy} \left(\frac{C_\mu k^2}{\sigma_\varepsilon \varepsilon} \frac{d\varepsilon}{dy} \right) &= -\frac{\kappa^2}{\sigma_\varepsilon u_*^2} \frac{\varepsilon_{cl}^2}{\left\{\cos\left[\frac{\varepsilon_{cl} \kappa}{u_*^3} (d-y)\right]\right\}^2} \\ &= -\frac{\kappa^2}{\sigma_\varepsilon u_*^2} \varepsilon^2. \end{aligned} \quad (2.68)$$

Using k from (2.61), dU/dy from (2.64) and the definition of κ in (2.18), the right-hand side of (2.50) can be expressed as:

$$\begin{aligned} C_\mu C_{\varepsilon 1} k \left(\frac{dU}{dy} \right)^2 - C_{\varepsilon 2} \frac{\varepsilon^2}{k} &= \frac{C_\mu^{1/2} C_{\varepsilon 1}}{u_*^2} \varepsilon^2 - \frac{C_\mu^{1/2} C_{\varepsilon 2}}{u_*^2} \varepsilon^2 \\ &= -\frac{\kappa^2}{\sigma_\varepsilon u_*^2} \varepsilon^2, \end{aligned}$$

the same as (2.68). This shows that (2.62) satisfies the equation (2.50).

Finally we prove that the function (2.60) solves equation (2.48) subject to the boundary conditions (2.51) and (2.54). The velocity profile (2.60) clearly satisfies the boundary conditions (2.54). Using (2.61) and (2.62), differentiation of (2.60) yields:

$$\begin{aligned} \frac{dU}{dy} &= \frac{\varepsilon_{cl}}{u_*^2} \frac{1}{\cos\left[\frac{\varepsilon_{cl} \kappa}{u_*^3} (d-y)\right]} \\ &= \frac{u_*^2}{C_\mu k^2} \varepsilon, \end{aligned} \quad (2.69)$$

2.4. Couette flow in the limit $h_+ \rightarrow 0$

rearranging the terms in (2.69), we get:

$$C_\mu \frac{k^2}{\varepsilon} \frac{dU}{dy} = u_*^2 ,$$

it is then clear that both the boundary condition (2.51) and the equation (2.48) are satisfied. \square

Corollary 2.3.3. $(\varepsilon_{\text{cl}}, u_*)$ is a solution to the system of transcendental equations:

$$\frac{\varepsilon_{\text{cl}}}{\cos\left[\frac{\varepsilon_{\text{cl}}}{u_*^3} \kappa (d - h_+)\right]} = \frac{1}{\kappa} \frac{u_*^3}{h_+} \quad (2.70)$$

$$U_{\text{CL}} + \frac{u_*}{\kappa} \ln \left| \tan \left[\frac{\pi}{4} - \frac{\varepsilon_{\text{cl}} \kappa}{u_*^3} (d - h_+) \right] \right| = u_* \left[\frac{1}{\kappa} \ln \left(\frac{u_* h_+}{\nu} \right) + C \right]. \quad (2.71)$$

Proof. Equation (2.70) is simply (2.53) which was imposed above. Equation (2.71) follows from (2.57), by substituting for $U(h_+)$ its expression obtainable from (2.60). \square

We also have that, due to (2.71), the velocity profile (2.60) at the artificial wall has the correct logarithmic distribution prescribed by the k - ε model, and that k , in (2.61), obviously satisfies the law of the wall (2.58).

In [39], Henry and Reynolds proved that the profiles (2.60), (2.61) and (2.62) are the unique solution to the boundary value problem defined by (2.48)-(2.50) together with (2.51)-(2.56).

2.4 Couette flow in the limit $h_+ \rightarrow 0$

We now study the behaviour of the solution (2.60)-(2.62) in the limit as $h_+ \rightarrow 0$ (recall that h_+ is the distance between the artificial and physical wall).

The parameter h_+ can be regarded as the main parameter of the problem, and depends on the Reynold's number Re . In fact, according to the prescriptions of the k - ε model, as Re is increased, h_+ should be decreased in order for the equations to provide a good model of the turbulent flow close to the physical wall. For instance, if $Re = 10^7$, then a rough estimate of h_+ would be $h_+ \cong O(10^{-4})$. This then implies, through the boundary condition (2.53), that, as $h_+ \rightarrow 0$, ε blows up at the artificial wall. It also implies that dU/dy will blow up at $y = h_+$ as $h_+ \rightarrow 0$; to see this use the laws of the wall (2.53) and (2.58), respectively for ε and k , in (2.51) and rearrange the terms to obtain:

$$\frac{dU}{dy}(h_+) = \frac{u_*^2}{C_\mu (k(h_+))^2} \varepsilon(h_+) = \frac{u_*}{\kappa} \frac{1}{h_+} . \quad (2.72)$$

This situation is shown in Figure 2.2 and in Figure 2.3, where, as h_+ varies from 10^{-2} to 10^{-3} , a substantial change can be observed in the slope of U (Figure 2.2) and in the value of ε (Figure 2.3), in a neighbourhood of $y = h_+$. The behaviour discussed is not exclusive to Couette flow, but it is common to every turbulent flow described by the k - ε model, since

2.4. Couette flow in the limit $h_+ \rightarrow 0$

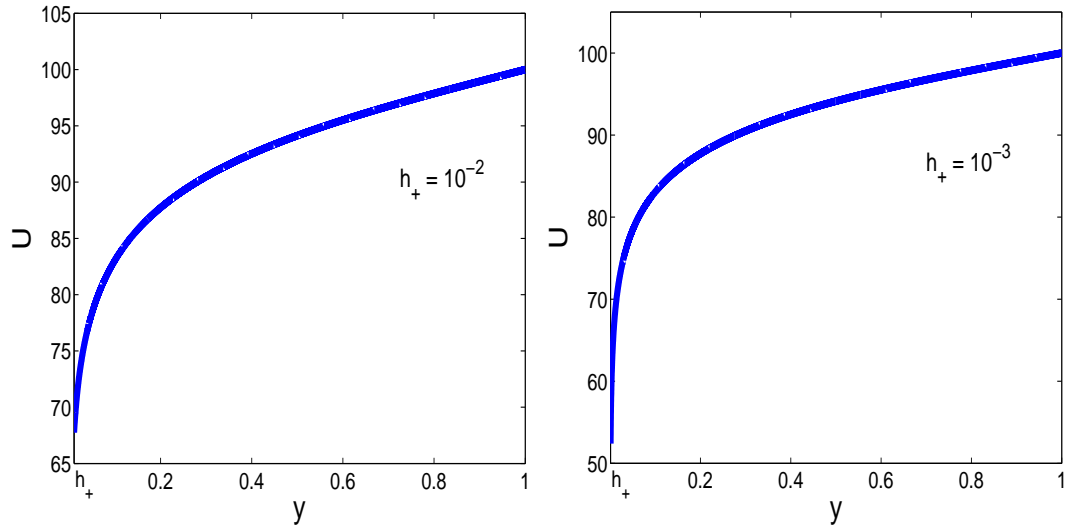


Figure 2.2: Profiles across the channel of the longitudinal component U of the mean velocity \mathbf{u} , corresponding to $h_+ = 10^{-2}$ (left) and $h_+ = 10^{-3}$ (right).

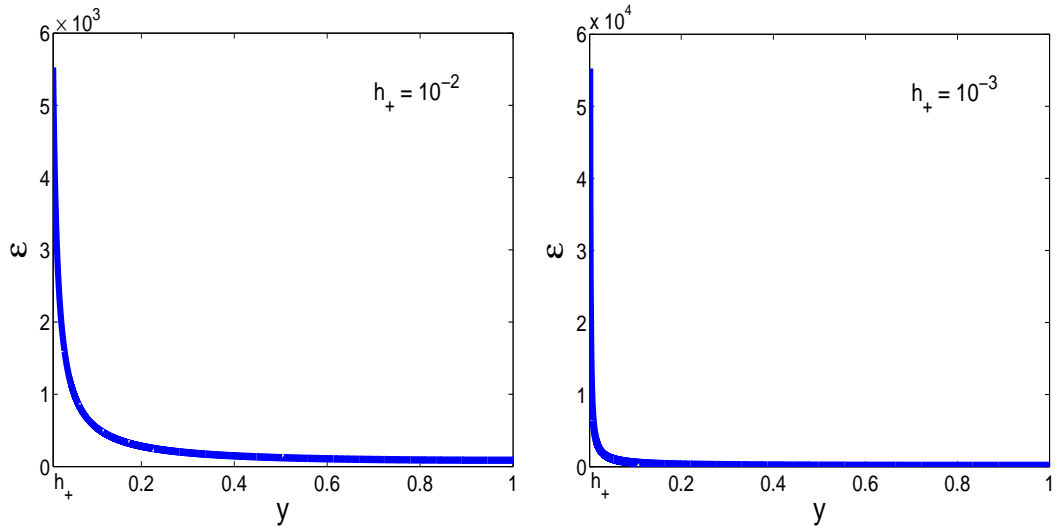


Figure 2.3: Profiles across the channel of the dissipation rate, corresponding to $h_+ = 10^{-2}$ (left) and $h_+ = 10^{-3}$ (right).

it is due to the boundary conditions (2.53) and (2.51) which are determined by the modelling procedure and are not affected by the specific characteristics of the flow under investigation.

Another feature common to turbulent flows described by the k - ε model, that we now explain in the context of Couette flow, is the fact that near h_+ source terms dominate diffusion terms in the transport equations (2.49), (2.50), as $h_+ \rightarrow 0$. To see this, first consider (2.49) and recall that the diffusion coefficient in (2.49) is

$$\mathcal{D}_k(y) := C_\mu \frac{(k(y))^2}{\varepsilon(y)},$$

while production and destruction of k are respectively given by:

2.4. Couette flow in the limit $h_+ \rightarrow 0$

$$\mathcal{P}_k(y) := C_\mu \frac{(k(y))^2}{\varepsilon(y)} \left(\frac{dU}{dy}(y) \right)^2, \quad \mathcal{S}_k(y) := \varepsilon(y).$$

Therefore, using (2.53), (2.58) and (2.72), at $y = h_+$ we have:

$$\frac{\mathcal{D}_k(h_+)}{\mathcal{P}_k(h_+)} = \frac{\kappa^2}{u_*^2} h_+^2 \rightarrow 0, \quad \frac{\mathcal{D}_k(h_+)}{\mathcal{S}_k(h_+)} = \frac{\kappa^2}{u_*^2} h_+^2 \rightarrow 0, \quad \text{as } h_+ \rightarrow 0. \quad (2.73)$$

Similarly, from (2.50) we have that the amount of diffusion relative to production and destruction of ε at the artificial wall is given respectively by:

$$\frac{\mathcal{D}_\varepsilon(h_+)}{\mathcal{P}_\varepsilon(h_+)} = \frac{1}{\sigma_\varepsilon C_\mu^{1/2} C_{\varepsilon 1}} \frac{\kappa^3}{u_*^3} h_+^3 \rightarrow 0, \quad \text{as } h_+ \rightarrow 0, \quad (2.74)$$

and

$$\frac{\mathcal{D}_\varepsilon(h_+)}{\mathcal{S}_\varepsilon(h_+)} = \frac{1}{\sigma_\varepsilon C_\mu^{1/2} C_{\varepsilon 2}} \frac{\kappa^3}{u_*^3} h_+^3 \rightarrow 0, \quad \text{as } h_+ \rightarrow 0. \quad (2.75)$$

The results (2.73), (2.74) and (2.75) can be extended to the case of Poiseuille flow, using (2.94)-(2.102), below.

This characteristic behaviour at the artificial wall will be exploited in §5.1 in order to derive a simplified equations which describes k in a small neighbourhood of $y = h_+$.

In the case of Couette flow, we now determine the behaviour of U , k and ε in the limit as $h_+ \rightarrow 0$.

Lemma 2.4.1. *At the leading order in $h_+ \rightarrow 0$, the system of ODE's (2.48)-(2.50) with boundary conditions (2.51)-(2.56), is satisfied by the functions:*

$$U(y) = U_{\text{CL}} + \frac{u_*}{\kappa} \ln \left[\tan \left(\frac{\pi y}{4d} \right) \right], \quad (2.76)$$

$$k(y) = C_\mu^{-1/2} u_*^2, \quad (2.77)$$

$$\varepsilon(y) = \frac{\pi}{2\kappa} \frac{u_*^3/d}{\sin \left(\frac{\pi y}{2d} \right)}, \quad (2.78)$$

with u_* and U_{cl} linked by the equation

$$U_{\text{CL}} = u_* \left[\frac{1}{\kappa} \ln \left(\frac{4 u_* d}{\pi \nu} \right) + C \right]. \quad (2.79)$$

Proof. We first show that, at the leading order in $h_+ \rightarrow 0$, equation (2.70) yields:

$$\varepsilon_{\text{cl}} = \frac{\pi}{2} \frac{1}{\kappa} \frac{u_*^3}{d}. \quad (2.80)$$

The profile (2.78) can then be obtained by substituting for ε_{cl} in (2.62), its expression in (2.80).

2.4. Couette flow in the limit $h_+ \rightarrow 0$

In order to obtain (2.80), take the inverse of both sides of (2.70), use a trigonometric identity for $\cos[\varepsilon_{\text{cl}} m(d - h_+)/u_*^3]$ and Taylor expansion in powers of h_+ , to get:

$$\frac{1}{\varepsilon_{\text{cl}}} \left[\cos\left(\kappa \frac{\varepsilon_{\text{cl}} d}{u_*^3}\right) \right] + \frac{\kappa}{u_*^3} \left[\sin\left(\kappa \frac{\varepsilon_{\text{cl}} d}{u_*^3}\right) \right] h_+ + o(h_+) = \frac{\kappa}{u_*^3} h_+ , \quad \text{as } h_+ \rightarrow 0 . \quad (2.81)$$

For (2.81) to hold we must have

$$\begin{cases} \cos\left(\kappa \frac{\varepsilon_{\text{cl}} d}{u_*^3}\right) = 0 \\ \frac{\kappa}{u_*^3} \sin\left(\kappa \frac{\varepsilon_{\text{cl}} d}{u_*^3}\right) = \frac{\kappa}{u_*^3} , \end{cases}$$

and this yields

$$\kappa \frac{\varepsilon_{\text{cl}} d}{u_*^3} = \frac{\pi}{2} , \quad (2.82)$$

from which (2.80) follows

Next we derive (2.76) and (2.79). Using (2.80) in (2.60), we get the profile of U at the leading order in $h_+ \rightarrow 0$:

$$U(y) = U_{\text{CL}} + \frac{u_*}{\kappa} \ln \left[\tan \left(\frac{\pi y}{4 d} \right) \right] . \quad (2.83)$$

This, according to the prescriptions of the k - ε model, must obey the ‘‘law of the wall’’ (2.57). Therefore substituting for $U(h_+)$ in the right-hand side of (2.57) its expression obtainable from (2.83), we get:

$$U_{\text{CL}} + \frac{u_*}{\kappa} \ln \left[\tan \left(\frac{\pi h_+}{4 d} \right) \right] = u_* \left[\frac{1}{\kappa} \ln \left(\frac{u_* h_+}{\nu} \right) + C \right] . \quad (2.84)$$

(Note that (2.84) can also be obtained directly from (2.71) using (2.80)).

Writing the Taylor expansion of the left-hand side of (2.84) in powers of h_+ and neglecting the higher order terms, we have:

$$U_{\text{CL}} + \frac{u_*}{\kappa} \ln \left(\frac{\pi h_+}{4 d} \right) = u_* \left[\frac{1}{\kappa} \ln \left(\frac{u_* h_+}{\nu} \right) + C \right] ,$$

from which (2.79) follows. (2.76) can finally be derived substituting U_{CL} from (2.79) into (2.83). \square

2.4.1 Computation of u_*

In this section, through a fixed point iteration, we derive an expression for u_* in terms of the Reynolds number Re , which shows that u_* grows as Re is increased. This expression for u_* , together with (2.80), will also be used in practical computation as initial guess for Newton’s

2.4. Couette flow in the limit $h_+ \rightarrow 0$

method for the system of transcendental equations (2.70)-(2.71). Recall that

$$Re = \frac{U_{CL} d}{\nu} ,$$

(see (2.23)). We consider the limit $Re \rightarrow \infty$.

Multiplying both sides of (2.79) by $\kappa d/\nu$, and introducing the new variable:

$$R_* := \frac{u_* d}{\nu} , \quad (2.85)$$

we obtain:

$$\kappa Re = R_* \left[\ln \left(\frac{4}{\pi} R_* \right) + \kappa C \right] ,$$

which is rearranged as

$$\kappa Re = R_* \ln(BR_*) , \quad (2.86)$$

with $B := (4/\pi) \exp(\kappa C)$. Multiplying both sides of (2.86) by B and then taking the logarithm we have:

$$\ln(B\kappa Re) = \ln(BR_*) + \ln(\ln(BR_*)) ,$$

and this is finally written as:

$$v + \ln v = u , \quad (2.87)$$

with $u := \ln(B\kappa Re) \gg 1$ known and $v := \ln(BR_*)$ unknown. Before giving, in Lemma 2.4.2 below, an expansion of the solution to (2.87) in terms of u (to which an expansion of u_* in terms of Re will correspond), we observe that (2.87) has a unique solution. In fact, the function $g : (0, +\infty) \rightarrow \mathbb{R}$ defined by

$$g(v) = v + \ln v - u .$$

is continuous and strictly increasing on $(0, +\infty)$, and also

$$\lim_{v \rightarrow 0^+} g(v) = -\infty , \quad \lim_{v \rightarrow +\infty} g(v) = +\infty .$$

Therefore there exists only one point $v_* \in (0, +\infty)$ where g vanishes, i.e. the solution of the equation (2.87) is unique.

The following Lemma is motivated by the observation that when $u \gg 1$ the only possible consistent balance of the terms in (2.87) is $v = O(u)$.

Lemma 2.4.2. *If $u > 1$ is a given number such that:*

$$u - \ln u > 1 , \quad (2.88)$$

2.4. Couette flow in the limit $h_+ \rightarrow 0$

then the sequence

$$\begin{cases} v_0 = u \\ v_{n+1} = u - \ln v_n \end{cases} \quad (2.89)$$

converges and its limit is the solution v_* of (2.87).

Proof. It can be easily verified by induction that

$$1 < v_n \leq u . \quad (2.90)$$

Consider now the subsequences $c_n = v_{2n}$ and $d_n = v_{2n+1}$ for all $n \in \mathbb{N}$. Then we have

$$\begin{cases} c_0 = u \\ c_{n+1} = u - \ln(u - \ln c_n) \end{cases} \quad (2.91)$$

and

$$\begin{cases} d_0 = u - \ln u \\ d_{n+1} = u - \ln(u - \ln d_n) . \end{cases} \quad (2.92)$$

We now prove by induction that the subsequence $\{c_n\}$ is strictly decreasing. First we show that $c_1 < c_0$. To see this consider that from (2.88) it follows that $\ln(u - \ln u) > 0$ and therefore:

$$\begin{aligned} c_1 &= u - \ln(u - \ln c_0) \\ &= u - \ln(u - \ln u) \\ &< u = c_0 . \end{aligned}$$

We now assume that $c_n < c_{n-1}$ and show that this implies $c_{n+1} < c_n$. We have:

$$\begin{aligned} c_n < c_{n-1} &\Rightarrow u - \ln c_n > u - \ln c_{n-1} \\ &\Rightarrow c_{n+1} = u - \ln(u - \ln c_n) < u - \ln(u - \ln c_{n-1}) = c_n . \end{aligned}$$

This then proves that $c_{n+1} < c_n$ for all $n \in \mathbb{N}$. Similarly it can be shown that the subsequence $\{d_n\}$ is strictly increasing. Therefore, due to (2.90), there exist c_* , $d_* \in [1, u]$ such that, as $n \rightarrow \infty$,

$$c_n \rightarrow c_* , \quad d_n \rightarrow d_* .$$

2.5. Stationary turbulent Poiseuille flow

From (2.91) and (2.92), it follows that

$$c_* = u - \ln(u - \ln c_*) , \quad d_* = u - \ln(u - \ln d_*) ,$$

that is c_* and d_* are zeros of the function

$$f(v) = v + \ln(u - \ln v) - u$$

in the interval $[1, u]$. But the function f is continuous and strictly increasing in $[1, u]$ and such that:

$$f(1) = -(u - \ln u - 1) < 0 , \quad f(u) = \ln(u - \ln u) > 0 ,$$

(remember that $u - \ln u > 1$), therefore there exists a unique point $v_* \in [1, u]$ where f vanishes. This implies $c_* = v_* = d_*$. The convergence of (2.91) and (2.92) to v_* implies the convergence of the sequence (2.89) to v_* and this, in turn, implies that

$$v_* = u - \ln v_* ,$$

i.e. v_* solves (2.87). □

We observe that in the limit we are considering, $u \gg 1$ (for $Re \rightarrow +\infty$), the condition (2.88) is certainly satisfied. Now, using the fact that:

$$\frac{\ln(\ln(B\kappa Re))}{\ln(B\kappa Re)} \ll 1 ,$$

we give the approximate solution to (2.86) corresponding to the term v_2 of the sequence (2.89):

$$R_* = \frac{\kappa Re}{\ln(B\kappa Re)} \left[1 + \frac{\ln(\ln(B\kappa Re))}{\ln(B\kappa Re)} + \dots \right] , \quad (2.93)$$

from which u_* can be obtained using the relation (2.85). u_* from (2.93) and ε_{cl} from (2.80) represent an extremely effective initial guess for Newton's method applied to the system (2.70)-(2.71).

2.5 Stationary turbulent Poiseuille flow

We now discuss the system of equations and the boundary conditions which define stationary turbulent Poiseuille flow in a straight channel and explain how its solution will be computed numerically. The Poiseuille flow is driven by the pressure difference between the inlet and the outlet of the channel and is characterized by no relative motion of the walls of the channel. Therefore the equations and the boundary conditions describing it can be obtained respectively from (2.39)-(2.41) and (2.42)-(2.47), setting $\mathcal{G} = \mathcal{G}_0 > 0$ in (2.39) and $\alpha = 1$ in (2.45). This

2.6. Weak formulation of the problem

gives the following system of ODE's:

$$-\frac{d}{dy} \left(C_\mu \frac{k^2}{\varepsilon} \frac{dU}{dy} \right) = \mathcal{G}_0 , \quad (2.94)$$

$$-\frac{d}{dy} \left(C_\mu \frac{k^2}{\varepsilon} \frac{dk}{dy} \right) = C_\mu \frac{k^2}{\varepsilon} \left(\frac{dU}{dy} \right)^2 - \varepsilon , \quad (2.95)$$

$$-\frac{d}{dy} \left(\frac{C_\mu k^2}{\sigma_\varepsilon \varepsilon} \frac{d\varepsilon}{dy} \right) = C_\mu C_{\varepsilon 1} k \left(\frac{dU}{dy} \right)^2 - C_{\varepsilon 2} \frac{\varepsilon^2}{k} , \quad (2.96)$$

subject to the boundary conditions:

$$\left(C_\mu \frac{k^2}{\varepsilon} \frac{dU}{dy} \right) (h_+) = u_*^2 , \quad (2.97)$$

$$\frac{dk}{dy}(h_+) = 0 , \quad (2.98)$$

$$\varepsilon(h_+) = \frac{1}{\kappa} \frac{u_*^3}{h_+} , \quad (2.99)$$

$$\frac{dU}{dy}(d) = 0 , \quad (2.100)$$

$$\frac{dk}{dy}(d) = 0 , \quad (2.101)$$

$$\frac{d\varepsilon}{dy}(d) = 0 . \quad (2.102)$$

As far as we are aware, the analytical solution to this problem above is not available. However a numerical solution to the turbulent Poiseuille flow can be computed numerically using continuation from the Couette case, as we now explain. We know that, in the case $\mathcal{G} = 0$ and $\alpha = 0$ (this choice of the parameters identifies the turbulent Couette flow), the system (2.39)-(2.41), with boundary conditions (2.42)-(2.47), has the unique solution (2.60)-(2.62). This can then be used as starting point of a continuation process based on two homotopy transformations, one on the parameter \mathcal{G} , from $\mathcal{G} = 0$ to $\mathcal{G} = \mathcal{G}_0$, and one on the parameter α , from $\alpha = 0$ to $\alpha = 1$. The final step of the continuation method, for $\mathcal{G} = \mathcal{G}_0$ and $\alpha = 1$, will then produce a solution to the Poiseuille flow, corresponding to a pressure drop between the inlet and the outlet of the channel given by $p_{\text{in}} - p_{\text{out}} = L \mathcal{G}_0$.

2.6 Weak formulation of the problem

We now derive the specific weak form of the RANS and k - ε equations, whose finite element discretisation, presented in §2.7, will be used throughout our 2D numerical experiments. We will also discuss the implementation of the law of the wall (2.14) typical of turbulence modelling.

2.6. Weak formulation of the problem

2.6.1 Weak form of the RANS

We will recast into the weak form the following expression of the RANS equations (2.1):

$$\begin{cases} \mathbf{u} \cdot \nabla \mathbf{u} - \nabla \nu_T \cdot (\nabla \mathbf{u})^T - \nabla \cdot (\nu_T \nabla \mathbf{u}) + \nabla p = \mathbf{0} \\ \nabla \cdot \mathbf{u} = 0, \end{cases} \quad (2.103)$$

where $\nu_T := C_\mu k^2 / \varepsilon$ (see (2.3)).

In order to obtain the first equation in (2.103) from the averaged linear momentum balance equation in (2.1), we express the divergence of $\boldsymbol{\sigma}$, which is defined in (2.2), as follows:

$$\begin{aligned} \nabla \cdot \boldsymbol{\sigma} &= \nabla \cdot (\nu_T \nabla \mathbf{u}) + \nabla \nu_T \cdot (\nabla \mathbf{u})^T + \nu_T \nabla \cdot (\nabla \mathbf{u})^T - \nabla p \\ &= \nabla \cdot (\nu_T \nabla \mathbf{u}) + \nabla \nu_T \cdot (\nabla \mathbf{u})^T - \nabla p, \end{aligned} \quad (2.104)$$

where we have used:

$$\nabla \cdot (\nabla \mathbf{u})^T = \nabla (\nabla \cdot \mathbf{u}) \quad (2.105)$$

$$= \mathbf{0}, \quad (2.106)$$

with (2.105) a vector identity and (2.106) a consequence of the averaged continuity equation. Then substituting (2.104) into the right-hand side of the first equation in (2.1) and rearranging the terms yield the result.

We now determine the weak form of (2.103) subject to the boundary conditions specified in §2.1. We take the scalar product of the first equation in (2.103) with a generic sufficiently smooth, vector-valued test function \mathbf{w} , whose function class will be defined later, and integrate all over the space $\Omega = [0, L] \times [h_+, d]$:

$$\begin{aligned} &\int_{\Omega} [\mathbf{u} \cdot \nabla \mathbf{u} - \nabla \nu_T \cdot (\nabla \mathbf{u})^T] \cdot \mathbf{w} \, d\Omega - \\ &- \int_{\Omega} [\nabla \cdot (\nu_T \nabla \mathbf{u})] \cdot \mathbf{w} \, d\Omega + \int_{\Omega} \nabla p \cdot \mathbf{w} \, d\Omega = 0. \end{aligned} \quad (2.107)$$

Integrating by parts the last two integrals of (2.107), and using the divergence theorem, we obtain:

$$\begin{aligned} &\int_{\Omega} [\mathbf{u} \cdot \nabla \mathbf{u} - \nabla \nu_T \cdot (\nabla \mathbf{u})^T] \cdot \mathbf{w} \, d\Omega + \int_{\Omega} \nu_T \nabla \mathbf{u} : (\nabla \mathbf{w})^T \, d\Omega - \\ &- \int_{\Omega} p \nabla \cdot \mathbf{w} \, d\Omega + \int_{\Gamma} [\mathbf{n} \cdot (p \mathbf{I} - \nu_T \nabla \mathbf{u})] \cdot \mathbf{w} \, d\Gamma = 0 \end{aligned} \quad (2.108)$$

2.6. Weak formulation of the problem

where $\Gamma = \Gamma_{\text{in}} \cup \Gamma_{\text{cl}} \cup \Gamma_{\text{out}} \cup \Gamma_{\text{w}}$ is the boundary of Ω and \mathbf{n} is the outward normal to the boundary. The boundary term in (2.108) can then be expressed as a sum of four different integrals each corresponding to one of the edges of Γ , given by

$$\int_{\Gamma_{\text{in}}} [\mathbf{n} \cdot (p\mathbf{I} - \nu_T \nabla \mathbf{u})] \cdot \mathbf{w} \, d\Gamma = \int_{\Gamma_{\text{in}}} \left[- \left(p - \nu_T \frac{\partial U}{\partial x} \right) w_1 + \nu_T \frac{\partial V}{\partial x} w_2 \right] d\Gamma \quad , \quad (2.109)$$

$$\int_{\Gamma_{\text{out}}} [\mathbf{n} \cdot (p\mathbf{I} - \nu_T \nabla \mathbf{u})] \cdot \mathbf{w} \, d\Gamma = \int_{\Gamma_{\text{out}}} \left[\left(p - \nu_T \frac{\partial U}{\partial x} \right) w_1 - \nu_T \frac{\partial V}{\partial x} w_2 \right] d\Gamma \quad , \quad (2.110)$$

$$\int_{\Gamma_{\text{cl}}} [\mathbf{n} \cdot (p\mathbf{I} - \nu_T \nabla \mathbf{u})] \cdot \mathbf{w} \, d\Gamma = \int_{\Gamma_{\text{cl}}} \left[-\nu_T \frac{\partial U}{\partial y} w_1 + \left(p - \nu_T \frac{\partial V}{\partial y} \right) w_2 \right] d\Gamma \quad , \quad (2.111)$$

$$\int_{\Gamma_{\text{w}}} [\mathbf{n} \cdot (p\mathbf{I} - \nu_T \nabla \mathbf{u})] \cdot \mathbf{w} \, d\Gamma = \int_{\Gamma_{\text{w}}} \left[\nu_T \frac{\partial U}{\partial y} w_1 - \left(p - \nu_T \frac{\partial V}{\partial y} \right) w_2 \right] d\Gamma \quad . \quad (2.112)$$

From (2.109) and (2.110), it becomes clear that (2.6)-(2.7) and (2.10)-(2.11) are the natural boundary conditions for the specific weak form of the RANS considered.

Now we specify the space where we will seek the solution \mathbf{u} and where the test function \mathbf{w} is defined. Let $H^1(\Omega)$ be the Sobolev space of square integrable functions whose first derivatives are also square integrable over Ω and let $\mathbf{H}^1(\Omega) := H^1(\Omega) \times H^1(\Omega)$. In the case of turbulent Couette flow, we seek the velocity field \mathbf{u} in the space

$$\mathbf{H}_{EC}^1(\Omega) = \{ \mathbf{v} \in \mathbf{H}^1(\Omega) : \mathbf{v} = (U_{\text{cl}}, 0) \text{ on } \Gamma_{\text{cl}} \text{ and } v_2 = 0 \text{ on } \Gamma_{\text{w}} \} \quad ,$$

and, correspondingly, we require that the test function \mathbf{w} is in

$$\mathbf{H}_{0C}^1(\Omega) = \{ \mathbf{v} \in \mathbf{H}^1(\Omega) : \mathbf{v} = \mathbf{0} \text{ on } \Gamma_{\text{cl}} \text{ and } v_2 = 0 \text{ on } \Gamma_{\text{w}} \} \quad .$$

In the case of the turbulent Poiseuille flow, we seek the velocity field in

$$\mathbf{H}_{0P}^1(\Omega) = \{ \mathbf{v} \in \mathbf{H}^1(\Omega) : v_2 = 0 \text{ on } \Gamma_{\text{cl}} \cup \Gamma_{\text{w}} \} \quad .$$

and require that $\mathbf{w} \in \mathbf{H}_{0P}^1(\Omega)$.

Then, using the boundary conditions (2.6)-(2.7) and (2.10)-(2.11), respectively in (2.109) and (2.110), we obtain:

$$\int_{\Gamma_{\text{in}}} [\mathbf{n} \cdot (p\mathbf{I} - \nu_T \nabla \mathbf{u})] \cdot \mathbf{w} \, d\Gamma = - \int_{\Gamma_{\text{in}}} p_{\text{in}} w_1 \, d\Gamma \quad ,$$

$$\int_{\Gamma_{\text{out}}} [\mathbf{n} \cdot (p\mathbf{I} - \nu_T \nabla \mathbf{u})] \cdot \mathbf{w} \, d\Gamma = \int_{\Gamma_{\text{out}}} p_{\text{out}} w_1 \, d\Gamma \quad ,$$

2.6. Weak formulation of the problem

($p_{\text{in}}=0=p_{\text{out}}$ for turbulent Couette flow). We also have:

$$\int_{\Gamma_{\text{cl}}} [\mathbf{n} \cdot (p\mathbf{I} - \nu_T \nabla \mathbf{u})] \cdot \mathbf{w} \, d\Gamma = 0 \quad ,$$

which, in the case of Couette flow, follows from (2.111) requiring that $\mathbf{w} \in \mathbf{H}_{0C}^1$, while, for Poiseuille flow, it ensues from (2.111) imposing both the boundary condition (2.19) with $\alpha = 1$ and $w_2 = 0$ on Γ_{cl} .

Finally due to the boundary condition (2.14) and the fact that, both for Couette and Poiseuille flow, $w_2 = 0$ on Γ_w , from (2.112) we get:

$$\begin{aligned} \int_{\Gamma_w} [\mathbf{n} \cdot (p\mathbf{I} - \nu_T \nabla \mathbf{u})] \cdot \mathbf{w} \, d\Gamma &= \int_{\Gamma_w} \nu_T \frac{\partial U}{\partial y} w_1 \, d\Gamma \\ &= \int_{\Gamma_w} u_*^2 w_1 \, d\Gamma \quad . \end{aligned} \quad (2.113)$$

But the parameter u_* can usually be determined only through measurements in the flow being studied, therefore, in practical computations of turbulent flows, a specific implementation of the boundary term (2.113) is needed. This is discussed in §2.6.2 below.

Using the above results in (2.108), we then get an expression for the weak form of the RANS, valid for both Couette and Poiseuille flow in straight channels:

$$\begin{aligned} a(\mathbf{u}, p, k, \varepsilon, \mathbf{w}) &:= \int_{\Omega} [\mathbf{u} \cdot \nabla \mathbf{u} - \nabla \nu_T \cdot (\nabla \mathbf{u})^T] \cdot \mathbf{w} \, d\Omega - \int_{\Omega} p \nabla \cdot \mathbf{w} \, d\Omega + \\ &+ \int_{\Omega} \nu_T \nabla \mathbf{u} : (\nabla \mathbf{w})^T \, d\Omega + \int_{\Gamma_w} u_*^2 w_1 \, d\Gamma - \int_{\Gamma_{\text{in}}} p_{\text{in}} w_1 \, d\Gamma + \int_{\Gamma_{\text{out}}} p_{\text{out}} w_1 \, d\Gamma = 0 \quad . \end{aligned} \quad (2.114)$$

In order to obtain the weak form of the averaged continuity equation (the second equation in (2.103)) we multiply it by a suitable test function ψ (that is related to the pressure p) and integrate all over the space Ω to obtain:

$$b(\mathbf{u}, \psi) = \int_{\Omega} \psi \nabla \cdot \mathbf{u} \, d\Omega = 0 \quad . \quad (2.115)$$

In both cases of Couette and Poiseuille flow, we seek the pressure p in $L_2(\Omega)$, the space of square integrable function over the domain Ω , and require that $\psi \in L_2(\Omega)$.

2.6.2 Implementation of the law of the wall for the stress

Since, as noticed above, the value of the parameter u_* can usually be known only by measurement, it is customary in turbulence modelling to implement u_* implicitly in (2.113), as now explain.

2.6. Weak formulation of the problem

From the previous section it is clear that the occurrence of u_* in (2.113), arises from the boundary condition (2.14):

$$\left(\nu_{\Gamma} \frac{dU}{dy} \right) (h_+) = u_*^2, \quad y = h_+, \quad (2.116)$$

the common strategy is then to determine u_* in (2.116) by using some combination of the wall law for U :

$$U(x, h_+) = u_*(x) \left[\frac{1}{\kappa} \ln \left(\frac{u_*(x) h_+}{\nu} \right) + C \right] \quad x \in \Gamma_w, \quad (2.117)$$

and the wall law for k :

$$k(x, h_+) = C_{\mu}^{-1/2} u_*^2(x) \quad x \in \Gamma_w. \quad (2.118)$$

There are clearly several ways which (2.117) and (2.118) can both be used to eliminate u_* and each would in effect imply a boundary condition relating U and k . We will proceed as follows: from (2.118) we get

$$u_*(x) = C_{\mu}^{1/4} (k(x, h_+))^{1/2}, \quad (2.119)$$

and substituting (2.119) into the logarithmic term of (2.117) we can obtain the following expression for u_* :

$$u_*(x) = \frac{U(x, h_+)}{\frac{1}{\kappa} \ln \left[\frac{C_{\mu}^{1/4} (k(x, h_+))^{1/2} h_+}{\nu} \right] + C}. \quad (2.120)$$

Now we use both (2.119) and (2.120) to eliminate u_* from the right-hand side of (2.116). More precisely, we replace the Neumann boundary condition (2.116) with the (nonlinear) ‘‘Robin boundary condition’’:

$$\nu_{\Gamma} \frac{\partial U}{\partial y} = \frac{\kappa C_{\mu}^{1/4} k^{1/2} U}{\ln \left[(C_{\mu}^{1/4} k^{1/2} h_+) / \nu \right] + \kappa C}, \quad y = h_+, \quad (2.121)$$

and consequently we have:

$$\begin{aligned} \int_{\Gamma_w} [\mathbf{n} \cdot (p\mathbf{I} - \nu_{\Gamma} \nabla \mathbf{u})] \cdot \mathbf{w} \, d\sigma &= \int_{\Gamma_w} \nu_{\Gamma} \frac{\partial U}{\partial y} w_1 \, d\sigma \\ &= \int_{\Gamma_w} \frac{\kappa C_{\mu}^{1/4} k^{1/2} U}{\ln \left[(C_{\mu}^{1/4} k^{1/2} h_+) / \nu \right] + \kappa C} w_1 \, d\sigma. \end{aligned} \quad (2.122)$$

2.6. Weak formulation of the problem

Finally, (2.114) becomes:

$$\begin{aligned}
a(\mathbf{u}, p, k, \varepsilon, \mathbf{w}) := & \int_{\Omega} [\mathbf{u} \cdot \nabla \mathbf{u} - \nabla \nu_T \cdot (\nabla \mathbf{u})^T] \cdot \mathbf{w} \, d\tau - \int_{\Omega} p \nabla \cdot \mathbf{w} \, d\tau + \\
& + \int_{\Omega} \nu_T \nabla \mathbf{u} : (\nabla \mathbf{w})^T \, d\tau + \int_{\Gamma_w} \frac{\kappa C_{\mu}^{1/4} k^{1/2} U}{\ln \left[(C_{\mu}^{1/4} k^{1/2} h_+) / \nu \right] + \kappa C} w_1 \, d\sigma - \\
& - \int_{\Gamma_{in}} p_{in} w_1 \, d\sigma + \int_{\Gamma_{out}} p_{out} w_1 \, d\sigma = 0 . \quad (2.123)
\end{aligned}$$

This combination of (2.119) and (2.120) for eliminating the unknown u_* to obtain (2.121), is typical of the ‘‘ad hoc’’ procedures common in turbulence modelling and requires further analysis.

In the following we give a simplified expression for (2.123) in the case of 1D turbulent Couette and Poiseuille flows. For such flows (see §2.2) we have

$$\mathbf{u} = \mathbf{u}(y) = (U(y), 0)^T, \quad k = k(y), \quad \varepsilon = \varepsilon(y), \quad (2.124)$$

and

$$\nabla p = (-\mathcal{G}, 0)^T, \quad \nu_T := C_{\mu} \frac{(k(y))^2}{\varepsilon(y)} = \nu_T(y). \quad (2.125)$$

Then, using (2.124) and (2.125) and the fact that now $\mathbf{w} = \mathbf{w}(y)$, it is not difficult to verify that:

$$\int_{\Omega} [\mathbf{u} \cdot \nabla \mathbf{u} - \nabla \nu_T \cdot (\nabla \mathbf{u})^T] \cdot \mathbf{w} \, d\tau + \int_{\Omega} \nu_T \nabla \mathbf{u} : (\nabla \mathbf{w})^T \, d\tau = \int_{h_+}^1 \nu_T(y) \frac{dU}{dy} \frac{dw_1}{dy} \, dy$$

and that:

$$\begin{aligned}
- \int_{\Omega} p \nabla \cdot \mathbf{w} \, d\tau - \int_{\Gamma_{in}} p_{in} w_1 \, d\sigma + \int_{\Gamma_{out}} p_{out} w_1 \, d\sigma &= \int_{\Omega} \nabla p \cdot \mathbf{w} \\
&= -\mathcal{G} \int_{h_+}^1 w_1(y) \, dy .
\end{aligned}$$

Now, we recall that the boundary integral

$$\int_{\Gamma_w} \frac{\kappa C_{\mu}^{1/4} k^{1/2} U}{\ln \left[(C_{\mu}^{1/4} k^{1/2} h_+) / \nu \right]} w_1 \, d\sigma ,$$

in (2.123), derives from the application of the divergence theorem to

$$\int_{\Omega} \nabla \cdot (\nu_T \nabla \mathbf{u} \cdot \mathbf{w}) \, d\tau , \quad (2.126)$$

2.6. Weak formulation of the problem

as in (2.107)-(2.108) and from the discussion which follows from there. In the 1D case we obtain

$$\begin{aligned} \int_{\Omega} \nabla \cdot (\nu_T \nabla \mathbf{u} \cdot \mathbf{w}) d\tau &= \int_{h_+}^1 \frac{d}{dy} \left(\nu_T \frac{dU}{dy} w_1(y) \right) dy \\ &= \left[\nu_T \frac{dU}{dy} w_1(y) \right]_{h_+}^1 = u_*^2 w_1(h_+) , \end{aligned} \quad (2.127)$$

where (2.127) follows from the boundary condition (2.42). In the case of Couette flow, from the fact that $w_1(1) = 0$ (due to the Dirichlet boundary condition $U(1) = U_{CL}$ which follows from (2.45) with $\alpha = 0$). In the case of Poiseuille flow, from the boundary condition $(dU/dy)(1) = 0$, as in (2.45) with $\alpha = 1$. Therefore we obtain:

$$a(U, k, \varepsilon, w_1) = \int_{h_+}^1 \nu_T \frac{dU}{dy} \frac{dw_1}{dy} dy - \mathcal{G} \int_{h_+}^1 w_1(y) dy + u_*^2 w_1(h_+) = 0 , \quad (2.128)$$

and, by eliminating u_*^2 as discussed at the beginning of this section (note that (2.119), (2.120) and (2.121) are valid also in 1D with the exception that all quantities involved are now independent of x), (2.128) can finally be expressed as

$$\begin{aligned} a(U, k, \varepsilon, w_1) &= \int_{h_+}^1 \nu_T \frac{dU}{dy} \frac{dw_1}{dy} dy - \mathcal{G} \int_{h_+}^1 w_1(y) dy + \\ &+ \frac{\kappa C_\mu^{1/4} (k(h_+))^{1/2} U(h_+)}{\ln \left[(C_\mu^{1/4} (k(h_+))^{1/2} h_+) / \nu \right]} w_1(h_+) = 0 . \end{aligned} \quad (2.129)$$

2.6.3 Weak form of the k - ε equations

In order to derive the weak form of the turbulence model equations, we multiply the transport equation for k and for ε in (2.4), respectively by the first and the second component of the test function $\mathbf{z} = (z_1, z_2)$, whose space of definition will be introduced subsequently, and integrate over the domain Ω . Integrating by parts the diffusion term of both equations and then using the divergence theorem, we obtain

$$\begin{aligned} &\int_{\Omega} (\mathbf{u} \cdot \nabla k) z_1 d\tau + \int_{\Omega} C_\mu \frac{k^2}{\varepsilon} \nabla k \cdot \nabla z_1 d\tau - \\ &- \int_{\Omega} C_\mu \frac{k^2}{\varepsilon} S(\mathbf{u}) z_1 d\tau + \int_{\Omega} \varepsilon z_1 d\tau - \int_{\Gamma} C_\mu \frac{k^2}{\varepsilon} (\nabla k \cdot \mathbf{n}) z_1 d\sigma = 0 \end{aligned} \quad (2.130)$$

2.6. Weak formulation of the problem

and

$$\begin{aligned} & \int_{\Omega} (\mathbf{u} \cdot \nabla \varepsilon) z_2 \, d\tau + \int_{\Omega} \frac{C_{\mu} k^2}{\sigma_{\varepsilon} \varepsilon} \nabla \varepsilon \cdot \nabla z_2 \, d\tau + \int_{\Omega} C_{\varepsilon 2} \frac{\varepsilon^2}{k} z_2 \, d\tau \\ & - \int_{\Omega} C_{\mu} C_{\varepsilon 1} k S(\mathbf{u}) z_2 \, d\tau - \int_{\Gamma} \frac{C_{\mu} k^2}{\sigma_{\varepsilon} \varepsilon} (\nabla \varepsilon \cdot \mathbf{n}) z_2 \, d\sigma = 0 . \end{aligned} \quad (2.131)$$

The solution (k, ε) to (2.130)-(2.131) is sought in the space $\mathbf{H}^1(\Omega) = H^1(\Omega) \times H^1(\Omega)$, and must satisfy the boundary conditions (2.8)-(2.9), (2.12)-(2.13), (2.16), (2.21)-(2.22), together with the following particular implementation of the law of the wall (2.17):

$$\varepsilon(x, h_+) - \frac{C_{\mu}^{3/4} (k(x, h_+))^{3/2}}{\kappa h_+} = 0, \quad x \in \Gamma_w, \quad (2.132)$$

which can be obtained from (2.17) using (2.119) to eliminate u_* . We also require that the test function \mathbf{z} is in $\mathbf{H}_{0T}^1(\Omega) = \{\mathbf{v} \in \mathbf{H}^1(\Omega) : v_2 = 0 \text{ on } \Gamma_w\}$.

The condition (2.132) is again obtained by an ‘‘ad hoc’’ elimination of u_* , analogous to (2.121).

Like in §2.6.1, the boundary term in (2.130) can be expressed as a sum of four integrals each corresponding to one of the sections of the boundary Γ , and, due to the rectangular geometry of the channel, we have that

$$\begin{aligned} & \int_{\Gamma_{\text{out}}} C_{\mu} \frac{k^2}{\varepsilon} (\nabla k \cdot \mathbf{n}) z_1 \, d\sigma = \int_{\Gamma_{\text{out}}} C_{\mu} \frac{k^2}{\varepsilon} \frac{\partial k}{\partial x} z_1 \, d\sigma, \\ & \int_{\Gamma_{\text{cl}}} C_{\mu} \frac{k^2}{\varepsilon} (\nabla k \cdot \mathbf{n}) z_1 \, d\sigma = \int_{\Gamma_{\text{cl}}} C_{\mu} \frac{k^2}{\varepsilon} \frac{\partial k}{\partial y} z_1 \, d\sigma, \end{aligned}$$

and similarly for the integrals on Γ_{in} and Γ_w . Therefore imposing (2.8), (2.12), (2.16) and (2.21), all four boundary integrals vanish and from (2.130) we get the weak form of the transport equation for k :

$$\begin{aligned} c(\mathbf{u}, k, \varepsilon, \mathbf{z}) & := \int_{\Omega} (\mathbf{u} \cdot \nabla k) z_1 \, d\tau + \int_{\Omega} C_{\mu} \frac{k^2}{\varepsilon} \nabla k \cdot \nabla z_1 \, d\tau - \\ & - \int_{\Omega} C_{\mu} \frac{k^2}{\varepsilon} S(\mathbf{u}) z_1 \, d\tau + \int_{\Omega} \varepsilon z_1 \, d\tau = 0 \end{aligned} \quad (2.133)$$

The same treatment of the boundary term in (2.131), and the boundary conditions (2.9), (2.13), (2.22), together with the requirement that $z_2 = 0$ on Γ_w , yields the weak form of the

2.6. Weak formulation of the problem

ε -transport equation:

$$\begin{aligned} d(\mathbf{u}, k, \varepsilon, \mathbf{z}) := & \int_{\Omega} (\mathbf{u} \cdot \nabla \varepsilon) z_2 \, d\tau + \int_{\Omega} \frac{C_{\mu}}{\sigma_{\varepsilon}} \frac{k^2}{\varepsilon} \nabla \varepsilon \cdot \nabla z_2 \, d\tau + \\ & + \int_{\Omega} C_{\varepsilon 2} \frac{\varepsilon^2}{k} z_2 \, d\tau - \int_{\Omega} C_{\mu} C_{\varepsilon 1} k S(\mathbf{u}) z_2 \, d\tau = 0 \end{aligned} \quad (2.134)$$

The statement of the weak form of the full problem is then: find $\mathbf{u} \in \mathbf{H}_{EC}^1(\Omega)$ (respectively $\mathbf{H}_{0p}^1(\Omega)$), $p \in L_2(\Omega)$ and $(k, \varepsilon) \in \mathbf{H}^1(\Omega)$ satisfying (2.132) such that

$$\begin{cases} a(\mathbf{u}, p, k, \varepsilon, \mathbf{w}) = 0 \\ b(\mathbf{u}, \psi) = 0 \\ c(\mathbf{u}, k, \varepsilon, \mathbf{z}) = 0 \\ d(\mathbf{u}, k, \varepsilon, \mathbf{z}) = 0 \end{cases} \quad (2.135)$$

for all $\mathbf{w} \in \mathbf{H}_{0C}^1(\Omega)$ (respectively $\mathbf{H}_{0p}^1(\Omega)$), all $\psi \in L_2(\Omega)$ and all $\mathbf{z} \in \mathbf{H}_{0T}^1(\Omega)$.

Finally we specify the weak forms (2.133) and (2.134) in the special case of 1D turbulent Couette and Poiseuille flows. In the one-dimensional setting we have:

$$\mathbf{u} = \mathbf{u}(y) = (U(y), 0)^T, \quad k = k(y), \quad \varepsilon = \varepsilon(y),$$

and $S(\mathbf{u})$, defined in (2.5), is given by:

$$S(\mathbf{u}) = \nabla \mathbf{u} : [\nabla \mathbf{u} + (\nabla \mathbf{u})^T] = \left(\frac{dU}{dy}(y) \right)^2.$$

It is then easy to verify that (2.133) and (2.134) can be expressed respectively as

$$\begin{aligned} c(U, k, \varepsilon, z_1) = & \int_{h_+}^1 C_{\mu} \frac{(k(y))^2}{\varepsilon(y)} \frac{dk}{dy} \frac{dz_1}{dy} \, dy - \\ & - \int_{h_+}^1 C_{\mu} \frac{(k(y))^2}{\varepsilon(y)} \left(\frac{dU}{dy}(y) \right)^2 z_1(y) \, dy + \int_{h_+}^1 \varepsilon(y) z_1(y) \, dy = 0 \end{aligned} \quad (2.136)$$

and as

$$\begin{aligned} d(U, k, \varepsilon, z_2) = & \int_{h_+}^1 \frac{C_{\mu}}{\sigma_{\varepsilon}} \frac{(k(y))^2}{\varepsilon(y)} \frac{d\varepsilon}{dy} \frac{z_2}{dy} \, dy - \\ & - \int_{h_+}^1 C_{\mu} C_{\varepsilon 1} k(y) \left(\frac{dU}{dy}(y) \right)^2 z_2(y) \, dy + \int_{h_+}^1 C_{\varepsilon 2} \frac{(\varepsilon(y))^2}{k(y)} z_2(y) \, dy = 0. \end{aligned} \quad (2.137)$$

We finally observe that in the one-dimensional case, (2.132) becomes:

2.7. Galerkin Finite Element Method equations

$$\varepsilon(h_+) - \frac{C_\mu^{3/4} (k(h_+))^{3/2}}{\kappa h_+} = 0 . \quad (2.138)$$

2.7 Galerkin Finite Element Method equations

We now consider the finite element approximation of the weak problem (2.135) and of the algebraic constraint (2.132). We seek a solution $(\mathbf{u}^h, p^h, k^h, \varepsilon^h)$ in the appropriate finite dimensional subspaces of those spaces in which $(\mathbf{u}, p, k, \varepsilon)$ above reside, so defining them as conforming approximation spaces.

Suppose Ω has been discretised via a mesh of convex quadrilateral finite elements, defined by a bilinear map from the unit quadrilateral. We shall approximate \mathbf{u} and (k, ε) in the same approximation space \mathbf{V}^h constructed of vector valued functions whose components are polynomial in form over each element of the discretisation and continuous between elements, this ensures that $\mathbf{V}^h \subset \mathbf{H}^1(\Omega)$. An approximation space S^h for the pressure p is chosen to be of functions which are polynomial in form over each element of the discretisation, but which do not have to be continuous between elements, in fact we only require $S^h \subset L_2(\Omega)$. We require \mathbf{V}^h, S^h to be a stable pair for the Stokes system in the Babuska-Brezzi sense, see [7].

In the case of Couette flow we can define the trial space \mathbf{V}_{EC}^h in which we seek an approximation \mathbf{u}^h to \mathbf{u} as follows:

$$\begin{aligned} \mathbf{V}_{0C}^h &:= \mathbf{V}^h \cap \mathbf{H}_{0C}^1 \\ \mathbf{V}_{EC}^h &:= (\hat{U}, 0) \oplus \mathbf{V}_{0C}^h , \end{aligned}$$

where $\hat{U} \in H^1(\Omega)$ is a function given by the extension on Ω of the Dirichlet data $U = U_{cl}$ on Γ_{cl} (in practice, \hat{U} is not needed in the interior of Ω , in fact only its nodal values on Γ_{cl} are needed, see below). For Poiseuille flow, we seek an approximation \mathbf{u}^h to \mathbf{u} in the space:

$$\mathbf{V}_{0P}^h := \mathbf{V}^h \cap \mathbf{H}_{0P}^1 .$$

Finally (k^h, ε^h) , approximation to (k, ε) , is sought in the trial space:

$$\mathbf{V}_{k-\varepsilon}^h := \mathbf{V}^h \cap \mathbf{H}^1(\Omega) ,$$

and must satisfy the ‘‘nodal law’’ (corresponding to (2.132)):

$$\varepsilon^h(x_i, h_+) - \frac{C_\mu^{3/4} (k^h(x_i, h_+))^{3/2}}{\kappa h_+} = 0 , \quad i \in \mathcal{N}_w , \quad (2.139)$$

with \mathcal{N}_w the set of indexes of the nodes on the boundary Γ_w which are ε -freedom.

The Galerkin approximation to the weak form stated in §2.6.3 is then given by: find $\mathbf{u}^h \in \mathbf{V}_{EC}^h$ (respectively \mathbf{V}_{0P}^h), $p^h \in S^h$ and $(k^h, \varepsilon^h) \in \mathbf{V}_{k-\varepsilon}^h$ satisfying (2.139) such that

2.7. Galerkin Finite Element Method equations

$$\begin{cases} a(\mathbf{u}^h, p^h, k^h, \varepsilon^h, \mathbf{w}^h) = 0 \\ b(\mathbf{u}^h, \psi^h) = 0 \\ c(\mathbf{u}^h, k^h, \varepsilon^h, \mathbf{z}^h) = 0 \\ d(\mathbf{u}^h, k^h, \varepsilon^h, \mathbf{z}^h) = 0 \end{cases} \quad (2.140)$$

for all $\mathbf{w}^h \in \mathbf{V}_{0C}^h$ (respectively \mathbf{V}_{0P}^h), all $\psi^h \in S^h$ and all $\mathbf{z}^h \in \mathbf{V}_{0k-\varepsilon}^h := \mathbf{V}^h \cap \mathbf{H}_{0T}^1(\Omega)$.

We now introduce specific bases for the above finite dimensional subspaces and derive the nonlinear finite element. Let

$$\{\phi_{1j_1} = (\phi_{j_1}, 0)^T, \phi_{2j_2} = (0, \phi_{j_2})^T\}, \quad j_1 \in \mathcal{N}_1, \quad j_2 \in \mathcal{N}_2$$

denote a basis for \mathbf{V}_{0C}^h (respectively \mathbf{V}_{0P}^h), with \mathcal{N}_1 the set of indexes of the nodes which are U -freedoms and correspondingly \mathcal{N}_2 . In the case of Couette flow, for example, \mathcal{N}_1 comprises the indexes of the nodes in $\Omega \setminus \Gamma_{cl}$ and \mathcal{N}_2 the indexes of the nodes in $\Omega \setminus \{\Gamma_w \cup \Gamma_{cl}\}$. Let

$$\{\psi_l\}, \quad l \in \mathcal{N}_p$$

and

$$\{\phi_{kj} = (\phi_j, 0)^T, \phi_{\varepsilon j} = (0, \phi_j)^T\} \quad j \in \mathcal{N}_{k-\varepsilon}$$

denote basis sets for S^h and $\mathbf{V}_{k-\varepsilon}^h$, with \mathcal{N}_p and $\mathcal{N}_{k-\varepsilon}$ the sets of indexes of the nodes which are pressure freedoms and k - ε -freedoms respectively. Then, the Galerkin formulation above is equivalent to: find $\mathbf{u}^h \in \mathbf{V}_{EC}^h$ (respectively \mathbf{V}_{0P}^h), $p^h \in S^h$ and $(k^h, \varepsilon^h) \in \mathbf{V}_{k-\varepsilon}^h$ satisfying (2.139) such that

$$\begin{cases} a(\mathbf{u}^h, p^h, k^h, \varepsilon^h, \phi_{\alpha j_\alpha}) = 0, \quad \alpha = 1, 2, \quad j_\alpha \in \mathcal{N}_\alpha \\ b(\mathbf{u}^h, \psi_l) = 0, \quad l \in \mathcal{N}_p \\ c(\mathbf{u}^h, k^h, \varepsilon^h, \phi_j) = 0, \quad j \in \mathcal{N}_{k-\varepsilon} \\ d(\mathbf{u}^h, k^h, \varepsilon^h, \phi_j) = 0, \quad j \in \mathcal{N}_{k-\varepsilon} \setminus \mathcal{N}_w \end{cases} \quad (2.141)$$

Finally, expanding the approximate solution $(\mathbf{u}^h, p^h, k^h, \varepsilon^h)$ via a linear combination of the basis functions and substituting the expansions into (2.139) and (2.141) yields the nonlinear finite element system:

$$\mathbf{F}(\mathbf{U}, \mathbf{V}, \mathbf{P}, \mathbf{k}, \varepsilon) = \begin{bmatrix} \mathbf{F}_U(\mathbf{U}, \mathbf{V}, \mathbf{P}, \mathbf{k}, \varepsilon) \\ \mathbf{F}_V(\mathbf{U}, \mathbf{V}, \mathbf{P}, \mathbf{k}, \varepsilon) \\ \mathbf{F}_P(\mathbf{U}, \mathbf{V}) \\ \mathbf{F}_k(\mathbf{U}, \mathbf{V}, \mathbf{k}, \varepsilon) \\ \mathbf{F}_{NL}(\mathbf{k}, \varepsilon) \\ \mathbf{F}_\varepsilon(\mathbf{U}, \mathbf{V}, \mathbf{k}, \varepsilon) \end{bmatrix} = \mathbf{0}, \quad (2.142)$$

2.7. Galerkin Finite Element Method equations

where \mathbf{U} is a vector of U -velocity freedoms and similarly $\mathbf{V}, \mathbf{P}, \mathbf{k}, \varepsilon$.

As example, we now give an expression for the components of \mathbf{F} , in (2.142), corresponding to the discretised k - ε equations (an expression for the discretised RANS equations can be obtained by adapting to the case we are considering the formulae for the discretised Navier-Stokes equations given in [7]). First, define

$$\nu_{\text{T}}^h := C_{\mu} \frac{(k^h)^2}{\varepsilon^h} = C_{\mu} \frac{(\boldsymbol{\phi} \cdot \mathbf{k})^2}{\boldsymbol{\phi} \cdot \boldsymbol{\varepsilon}}, \quad (2.143)$$

(in (2.143) $\boldsymbol{\phi}$ is a vector of basis functions ϕ_j , while in the following ϕ_1 is a vector of basis functions ϕ_{j_1} and similarly ϕ_2), we have that the “nodal law” vector $\mathbf{F}_{\text{NL}}(\mathbf{k}, \boldsymbol{\varepsilon})$ has entries:

$$(\mathbf{F}_{\text{NL}})_i = \varepsilon_i - \frac{C_{\mu}^{3/4} k_i^{3/2}}{\kappa h_+}, \quad i \in \Gamma_{\text{w}}$$

while the components $\mathbf{F}_{\mathbf{k}}(\mathbf{U}, \mathbf{V}, \mathbf{k}, \boldsymbol{\varepsilon})$ and $\mathbf{F}_{\boldsymbol{\varepsilon}}(\mathbf{U}, \mathbf{V}, \mathbf{k}, \boldsymbol{\varepsilon})$ can be expressed respectively as

$$\begin{aligned} \mathbf{F}_{\mathbf{k}}(\mathbf{U}, \mathbf{V}, \mathbf{k}, \boldsymbol{\varepsilon}) &= C(\mathbf{U}, \mathbf{V})\mathbf{k} + D(\mathbf{k}, \boldsymbol{\varepsilon})\mathbf{k} + K(\mathbf{U}, \mathbf{V}, \mathbf{k}, \boldsymbol{\varepsilon}) \begin{pmatrix} \mathbf{k} \\ \boldsymbol{\varepsilon} \end{pmatrix}, \\ \mathbf{F}_{\boldsymbol{\varepsilon}}(\mathbf{U}, \mathbf{V}, \mathbf{k}, \boldsymbol{\varepsilon}) &= C(\mathbf{U}, \mathbf{V})\boldsymbol{\varepsilon} + \frac{1}{\sigma_{\varepsilon}} D(\mathbf{k}, \boldsymbol{\varepsilon})\boldsymbol{\varepsilon} + T(\mathbf{U}, \mathbf{V}, \mathbf{k}, \boldsymbol{\varepsilon}) \begin{pmatrix} \mathbf{k} \\ \boldsymbol{\varepsilon} \end{pmatrix}, \end{aligned}$$

with

$$C(\mathbf{U}, \mathbf{V}) := \int_{\Omega} \boldsymbol{\phi} (\hat{U} + \phi_1 \cdot \mathbf{U}, \phi_2 \cdot \mathbf{V})^{\text{T}} \cdot \nabla \boldsymbol{\phi},$$

$$D(\mathbf{k}, \boldsymbol{\varepsilon}) := \int_{\Omega} \nu_{\text{T}}^h (\nabla \boldsymbol{\phi})^{\text{T}} \cdot \nabla \boldsymbol{\phi},$$

$$K(\mathbf{U}, \mathbf{V}, \mathbf{k}, \boldsymbol{\varepsilon}) := \begin{bmatrix} - \int_{\Omega} C_{\mu} \frac{\boldsymbol{\phi} \cdot \mathbf{k}}{\boldsymbol{\phi} \cdot \boldsymbol{\varepsilon}} S(\mathbf{U}, \mathbf{V}) \boldsymbol{\phi} \boldsymbol{\phi} d\tau & \int_{\Omega} \boldsymbol{\phi} \boldsymbol{\phi} d\tau \end{bmatrix}$$

and

$$T(\mathbf{U}, \mathbf{V}, \mathbf{k}, \boldsymbol{\varepsilon}) := \begin{bmatrix} - \int_{\Omega} C_{\mu} C_{\varepsilon 1} S(\mathbf{U}, \mathbf{V}) \boldsymbol{\phi} \boldsymbol{\phi} d\tau & \int_{\Omega} C_{\varepsilon 2} \frac{\boldsymbol{\phi} \cdot \boldsymbol{\varepsilon}}{\boldsymbol{\phi} \cdot \mathbf{k}} \boldsymbol{\phi} \boldsymbol{\phi} \end{bmatrix}.$$

In our 2D numerical experiments we will discretise the domain Ω via a mesh of quadrilaterals and approximate each component of the velocity field \mathbf{u} and the turbulence variables k, ε by a continuous piecewise biquadratic polynomial. The pressure field, instead, will be approximated by a discontinuous piecewise linear polynomial. This is often called the Q_2P_{-1} finite element method, see [7].

The nonlinear finite element system (2.142) will be solved by Newton’s method (see §4.1 for a description of the properties of the algorithm). At each Newton iteration, the entries of the Jacobian of the nonlinear system will be computed using the 3×3 points Gauss-Jacobi quadrature rule applied element wise, and the Jacobian will then be inverted using Gauss elimination

2.7. Galerkin Finite Element Method equations

with pivoting.

When solving the $1D$ version of the Couette and Poiseuille flow we will use a numerical procedure corresponding to the one described above. Therefore, U , k and ε will be approximated by continuous piecewise quadratic polynomials, and we will use Newton's method to solve the nonlinear finite element system. The Jacobian of the finite element system, whose entries will be computed using the 3 points Gauss-Jacobi quadrature rule, will then be inverted by Gauss elimination with pivoting.

Chapter 3

The finite element mesh

Basing our considerations on the properties of the boundary value problems describing the turbulent Couette and Poiseuille flows, we now tackle the issue of identifying a mesh appropriate for the discretisation of the RANS and k - ε equations.

The numerical computation of the solution to the k - ε model is certainly complicated by the highly nonlinear form of the equations. However, the main source of difficulties in devising an effective numerical scheme can be considered to be the behaviour of ε near the artificial wall. At the wall itself ε is prescribed by the boundary condition (2.17):

$$\varepsilon(h_+) = \frac{1}{\kappa} \frac{u_*^3}{h_+} . \quad (3.1)$$

We recall that, as the Reynold's number is increased, h_+ , in (3.1), must be reduced in order for the turbulence model to provide a satisfactory description of the properties of the flow near to the physical wall. For example, $h_+ \sim O(10^{-4})$ when $Re \sim O(10^7)$. Therefore, as $h_+ \rightarrow 0$ (for $Re \rightarrow +\infty$), the profile of ε at the artificial wall becomes very steep and blows up with order $1/h_+$:

$$\varepsilon(h_+) \sim \frac{1}{h_+} \quad \text{as } h_+ \rightarrow 0 . \quad (3.2)$$

If this behaviour is not appropriately captured by the numerical scheme employed for solving the equations, then the solution process is likely to fail. In order for the numerical method to be accurate and practical, it is therefore crucial to discretise the equations on a grid where profiles with the property (3.2) can be resolved with a minimum number of discretisation points.

We will show in §3.6 that a uniform mesh or a locally uniformly refined mesh is inadequate for our purposes, and so here we will describe mesh generation techniques based on the equidistribution principle. We shall identify an equidistributed h_+ -dependent mesh which is optimal (in a sense that will become clear in what follows) for the problem under investigation.

Not only is the mesh we propose very satisfactory from the point of view of the accuracy of the numerical results and of the practicality of their computation, but it also improves drastically the robustness of Newton's method for the nonlinear finite element system, as it will be shown later in Chapter 5.

3.1. Equidistributed meshes

This chapter is organized as follows. After a brief overview of the general properties of equidistributed meshes in §3.1, we discuss in §3.2 the classical estimate of the finite element error in terms of the error in best approximation, and in §3.3 the approach of Carey and Dinh [41] for generating effective equidistributed meshes. In §3.4, we present our solution, based on [41], to the problem of devising an appropriate mesh for the discretisation of the k - ε model, and we will assess the quality of the mesh we propose, by estimating the error in the interpolation of functions with the property (3.2), see §§3.4, 3.5. In §3.6, we then illustrate the inadequacy of uniform meshes for tackling the problem we are faced with, and finally, in §3.7, we give numerical evidence of the accuracy and practicality that can be attained by approximating the k - ε model with the mesh we have identified.

3.1 Equidistributed meshes

We now illustrate how equidistributed meshes are generated, their applications and properties. An extensive literature is available on this subject, see for example [42] and the books [43], [44].

The use of equidistributed meshes has been largely exploited in numerical schemes for solving both boundary value problems (BVP's) and initial-boundary value problems (in the latter case the equidistribution technique is referred to as the moving mesh method). Assume that a one-dimensional BVP has been discretised over the domain $[a, b]$, using the mesh

$$\Pi : a = x_1 < x_2 < \dots < x_N < x_{N+1} = b . \quad (3.3)$$

Then, by definition, Π is called an *equidistributed mesh* with respect to a given strictly positive *monitor function* M if it has the property:

$$\int_{x_i}^{x_{i+1}} M(x) dx = C , \quad i = 1, \dots, N \quad (3.4)$$

with C independent of i .

The function M , which will give the “ideal” mesh for the problem under investigation, is hard to identify and is usually chosen in such a way to reflect some expected properties of the solution to the BVP itself. It may even be a function of the solution u of the differential equation being solved. Typically, M is selected so that the grid points cluster in those regions where the solution has the largest gradient. Since the choice of M depends on the behaviour of the solution which is to be computed, in practice equidistributed meshes are usually determined adaptively. That is, once a solution has been obtained on a preliminary grid, the mesh points are redistributed so that (3.4) is satisfied with the monitor function M corresponding to the preliminary solution. The solution is then recomputed on the new grid. This procedure may then be iterated.

In order to understand the process of equidistribution more precisely, we now give a variational formulation of the problem of generating a 1D equidistributed mesh and show that

3.1. Equidistributed meshes

this has a unique solution. Let x be the spatial coordinate in the physical domain $\Omega_p = [a, b]$, where the function $u : \Omega_p \rightarrow \mathbb{R}$ is defined. Let us introduce a one-to-one smooth coordinate transformation from the computational domain $\Omega_c = [0, 1]$ to the physical domain Ω_p :

$$x = x(\xi) , \quad \xi \in \Omega_c = [0, 1] \tag{3.5}$$

$$x(0) = a , \quad x(1) = b ,$$

where ξ denotes the spatial coordinate in the computational domain Ω_c , and is the inverse of the transformation (3.5):

$$\xi = \xi(x) , \quad x \in \Omega_p = [a, b] \tag{3.6}$$

$$\xi(a) = 0 , \quad \xi(b) = 1 .$$

The usual approach to the process of equidistribution is to consider the mesh on Ω_p with property (3.4), the image of a uniform discretisation of Ω_c through the appropriate transformation (3.5). The lemma below specifies which property the inverse mapping $\xi = \xi(x)$ must have, in order for the mesh $x_i = x((i - 1)/N)$, $i = 1, 2, \dots, N + 1$, to satisfy (3.4).

Lemma 3.1.1. *Let M be a strictly positive valued function which is integrable and continuously differentiable over the domain Ω_p . Then there exists a unique minimizer $\xi = \xi(x)$ of the functional*

$$I(\xi) = \frac{1}{2} \int_a^b \frac{\xi_x^2}{M(x)} dx , \tag{3.7}$$

over the space $S = \{\eta \in C^2[a, b] : \eta(a) = 0, \eta(b) = 1\}$. Moreover the minimizer ξ has an inverse $x = x(\xi)$, and the mesh $x_i := x((i - 1)/N)$, $i = 1, 2, \dots, N + 1$, has the property (3.4).

Proof. In order to prove that (3.7) has a unique minimizer, suppose ξ is an extremal for I , then it must satisfy the Euler-Lagrange equation for all $x \in [a, b]$, i.e.,

$$\frac{d}{dx} \left[\frac{\partial}{\partial \xi_x} \left(\frac{1}{2} \frac{\xi_x^2}{M(x)} \right) \right] - \frac{\partial}{\partial \xi} \left(\frac{1}{2} \frac{\xi_x^2}{M(x)} \right) = 0 ,$$

and this reduces to

$$\frac{d}{dx} \left(\frac{1}{M(x)} \xi_x \right) = 0 , \tag{3.8}$$

which has the solution

$$\frac{1}{M(x)} \xi_x = \text{constant} . \tag{3.9}$$

Because of the boundary conditions in (3.6) the only extremal ξ for I is therefore

$$\xi(x) = \frac{\int_a^x M(\bar{x}) d\bar{x}}{\int_a^b M(\bar{x}) d\bar{x}} . \tag{3.10}$$

3.1. Equidistributed meshes

It can now be easily checked that for all $x \in [a, b]$ the function

$$f(x, \xi, \xi_x) := \frac{1}{2} \frac{\xi_x^2}{M(x)}$$

is convex for all (ξ, ξ_x) in the convex set $\mathbb{R}^+ \times \mathbb{R}^+$, this then implies that the extremal (3.10) minimizes I (see Theorem 10.7.1 and Theorem 10.7.2 p. 259 of [45]).

The existence of $x = x(\xi)$, the inverse of ξ , follows from the fact that ξ is monotonic increasing, as can be deduced from (3.10) recalling that M is strictly positive.

We finally obtain (3.4). From (3.10) we have that:

$$\int_{x_i}^{x_{i+1}} M(x) dx = (\xi(x_{i+1}) - \xi(x_i)) \int_a^b M(x) dx \quad (3.11)$$

and since $\xi(x_i) = \xi(x((i-1)/N)) = (i-1)/N$, the right-hand side of (3.11) is

$$\frac{1}{N} \int_a^b M(x) dx ,$$

a constant independent of i . The result then follows. \square

We observe that the functional (3.7) may be seen as a weighted H^1 -seminorm of ξ , and can then be interpreted as a weighted measure of the global roughness of the mapping ξ . In this sense, the equidistribution technique gives the smoothest point distribution attainable.

Now we obtain the conventional 1D *equidistribution principle*, see (3.12)-(3.13) below.

Corollary 3.1.2. *Since $M \in C^1(\Omega_p)$ is strictly positive and $\xi \in C^2(\Omega_p)$ is invertible, it follows that (3.8) and (3.9) are respectively equivalent to:*

$$\frac{d}{d\xi} [M(x(\xi)) x_\xi] = 0 , \quad (3.12)$$

and

$$M(x(\xi)) x_\xi = \text{constant} . \quad (3.13)$$

Proof. Performing the differentiation in (3.8) and rearranging the terms we get

$$\xi_{xx} = \frac{M_x}{M} \xi_x . \quad (3.14)$$

Using the chain rule and the fact that $\xi_x(x) = (x_\xi(\xi))^{-1}$ we obtain

$$M_x(x(\xi)) \xi_x(x(\xi)) = \left\{ \frac{d}{d\xi} [M(x(\xi))] \right\} \frac{1}{x_\xi^2} ,$$

$$\xi_{xx}(x(\xi)) = -\frac{1}{(x_\xi)^3} x_{\xi\xi} .$$

3.1. Equidistributed meshes

Substituting the last two expressions into (3.14), and rearranging the terms we have:

$$-Mx_{\xi\xi} = \left[\frac{d}{d\xi} M(x(\xi)) \right] x_{\xi} ,$$

from which (3.12) clearly follows. (3.13) is then obtained by integrating (3.12). \square

Next we give an expression for the mesh size in the physical domain Ω_p .

Corollary 3.1.3. *The length of the i -th subinterval $h_i = x_{i+1} - x_i$ of the equidistributed mesh defined above can be expressed as*

$$h_i = \frac{1}{N} \frac{1}{\xi_x(x_i)} \left(1 + O\left(\frac{1}{N}\right) \right) . \quad (3.15)$$

Proof. From (3.10) we have that:

$$\xi_x = \frac{M(x)}{\int_a^b M(\bar{x}) d\bar{x}} , \quad (3.16)$$

from which we get

$$x_{\xi} = \frac{\int_a^b M(\bar{x}) d\bar{x}}{M(x(\xi))} .$$

The result (3.15) is then obtained by integrating the last equation and using (3.16):

$$\begin{aligned} h_i = x(i/N) - x((i-1)/N) &= \int_a^b M(\bar{x}) d\bar{x} \int_{(i-1)/N}^{i/N} \frac{1}{M(x(\xi))} d\xi \\ &= \int_a^b M(\bar{x}) d\bar{x} \frac{1}{N} \frac{1}{M(x(i/N))} \left(1 + O\left(\frac{1}{N}\right) \right) \\ &= \frac{1}{N} \frac{\int_a^b M(\bar{x}) d\bar{x}}{M(x(i/N))} \left(1 + O\left(\frac{1}{N}\right) \right) \\ &= \frac{1}{N} \frac{1}{\xi_x(x_i)} \left(1 + O\left(\frac{1}{N}\right) \right) . \quad \square \end{aligned}$$

In the following, we will refer to the mapping ξ from the physical to the computational domain, given by (3.10), as the *grading function*.

Finally, we simply mention the two-dimensional formulation of the above variational approach for mesh generation, originally inspired by the work of Winslow [46], Brackbill and Saltzman [47] and Brackbill [48]. A 2D equidistributed mesh is provided by the minimizer of a functional of the form

$$I(\xi, \eta) = \frac{1}{2} \int_{\Omega_p} [(\nabla \xi)^T G_1^{-1} \nabla \xi + (\nabla \eta)^T G_2^{-1} \nabla \eta] dx dy \quad (3.17)$$

3.2. The finite element error

where $\xi = \xi(x, y)$, $\eta = \eta(x, y)$ is the mapping between the physical domain and the computational domain, and $G_1 = G_1(x, y)$ and $G_2 = G_2(x, y)$ are symmetric positive definite matrices, called the *monitor functions*. The functional (3.17) represents a natural extension of (3.7) to two-dimensional problems.

The choice of 2D monitor functions based on estimates of the error in the interpolant of the solution to a certain boundary value problem (as it is possible to do in the 1D case, see §3.3) is investigated in [49] and [50].

3.2 The finite element error

In this section we briefly discuss the standard finite element error estimates arising in the approximation of elliptic BVP's; these estimates represent the rationale behind the approach to mesh generation which will be presented in §§3.3, 3.4. In the following we will describe the bounds on the finite element error only in general terms, the details can be found, for example, in [51].

Let us introduce the space $H_0^1(\Omega) := \{v \in H^1(\Omega) : v = 0 \text{ on } \partial\Omega\}$, with $\Omega \subset \mathbb{R}^d$ ($d = 1, 2$), and consider the variational problem

$$\text{find } u \in H_0^1(\Omega) \text{ such that } a(u, v) = F(v), \quad \forall v \in H_0^1(\Omega), \quad (3.18)$$

where $a(\cdot, \cdot)$ is a bounded, symmetric, coercive, bilinear form on $H^1(\Omega)$ and $F(\cdot)$ is a bounded, linear functional on $H^1(\Omega)$. (3.18) can be interpreted as the weak formulation of some elliptic linear BVP for the function u satisfying homogeneous Dirichlet boundary conditions on $\partial\Omega$ (this last assumption is not crucial for the results that will be discussed in the following). The Galerkin finite element approximation to (3.18) is the following: given a discretisation of Ω and a finite-dimensional subspace $V^h \subset H_0^1(\Omega)$, consisting of functions which are polynomial in form over each element of the discretisation, find $u^h \in V^h$ such that

$$a(u^h, v^h) = F(v^h), \quad \forall v^h \in V^h.$$

One powerful aspect of the Galerkin method for (3.18) is that in the energy norm $\|\cdot\|_E$, defined as

$$\|v\|_E := \sqrt{a(v, v)}, \quad \forall v \in H^1(\Omega), \quad (3.19)$$

the error in the approximation u^h to u is optimal, in the following sense:

$$\|u - u^h\|_E \leq \min_{v^h \in V^h} \|u - v^h\|_E. \quad (3.20)$$

By a ‘‘duality’’ argument, it is also possible to estimate $\|u - u^h\|_{L_2(\Omega)}$ as follows:

$$\|u - u^h\|_{L_2(\Omega)} \leq \|u - u^h\|_E \inf_{z^h \in V^h} \|w - z^h\|_E, \quad (3.21)$$

3.2. The finite element error

where w is the solution to the dual problem corresponding to (3.18):

$$\text{find } w \in H_0^1(\Omega) \text{ such that } a(w, v) = (u - u_h, v), \quad \forall v \in H_0^1(\Omega)$$

with

$$(u - u_h, v) := \int_{\Omega} (u - u_h)v \, d\Omega .$$

Then, under suitable regularity assumptions, by exploiting the regularity of w and by appropriately choosing $z^h \in V^h$, it is possible to obtain from (3.21) the following bound:

$$\|u - u^h\|_{L_2(\Omega)} \leq C h \|u - u^h\|_E, \quad (3.22)$$

where h is the diameter of the mesh. Combining (3.20) and (3.22) gives:

$$\|u - u^h\|_{L_2(\Omega)} \leq C h \min_{v^h \in V^h} \|u - v^h\|_E. \quad (3.23)$$

Finally, from the boundness of the bilinear form $a(\cdot, \cdot)$, it follows that:

$$\|u - v^h\|_E = \sqrt{a(u - v^h, u - v^h)} \leq C' \|u - v^h\|_{H^1(\Omega)}, \quad \forall v^h \in V^h,$$

and using this in (3.20) and (3.23), yields:

$$\|u - u^h\|_E \leq C' \min_{v^h \in V^h} \|u - v^h\|_{H^1(\Omega)}, \quad (3.24)$$

$$\|u - u^h\|_{L_2(\Omega)} \leq \tilde{C} h \min_{v^h \in V^h} \|u - v^h\|_{H^1(\Omega)}. \quad (3.25)$$

A practical way to estimate the left-hand sides of (3.24)-(3.25) is to chose v^h as the finite element interpolant of u , denoted in the following by $\mathcal{I}^h u$, and this gives:

$$\|u - u^h\|_E \leq \sqrt{C_1} \|u - \mathcal{I}^h u\|_{H^1(\Omega)}, \quad (3.26)$$

$$\|u - u^h\|_{L_2(\Omega)} \leq \tilde{C} h \|u - \mathcal{I}^h u\|_{H^1(\Omega)}, \quad (3.27)$$

and then to bound the $H^1(\Omega)$ -norm of the interpolation error. By the Poincaré inequality:

$$\|v\|_{H^1(\Omega)} \leq \tilde{C}_1 |v|_{H^1(\Omega)}, \quad \forall v \in H_0^1(\Omega),$$

where

$$|v|_{H^1(\Omega)} := \left(\int_{\Omega} \|\nabla v\|_2^2 \, d\Omega \right)^{1/2}$$

is the $H^1(\Omega)$ -seminorm of $v \in H_0^1(\Omega)$. Then from (3.27) we get:

$$\|u - u^h\|_{L_2(\Omega)} \leq \hat{C} h |u - \mathcal{I}^h u|_{H^1(\Omega)}, \quad (3.28)$$

3.3. Optimal monitor functions

and a similar result follows from (3.26) (note that $(u - \mathcal{I}^h u) \in H_0^1(\Omega)$).

Error estimates corresponding to (3.24)-(3.25), and therefore to (3.26)-(3.28), also hold in the case of general linear elliptic BVP's for which the corresponding bilinear form $a(\cdot, \cdot)$ is neither symmetric nor coercive and in the case of nonlinear elliptic BVP's. They are derived using the strategy outlined above. That is, a ‘‘duality’’ argument gives the bound

$$\|u - u^h\|_{L^2(\Omega)} \leq Ch \|u - u^h\|_{H^1(\Omega)}, \quad (3.29)$$

which corresponds to (3.22), and an optimal $H^1(\Omega)$ estimate, corresponding to (3.20) (or (3.24)), can also be established:

$$\|u - u^h\|_{H^1(\Omega)} \leq C \inf_{v^h \in V^h} \|u - v^h\|_{H^1(\Omega)}. \quad (3.30)$$

Then combining (3.29) and (3.30) gives:

$$\|u - u^h\|_{L^2(\Omega)} \leq \tilde{C} h \inf_{v^h \in V^h} \|u - v^h\|_{H^1(\Omega)},$$

the result equivalent to (3.23) (or (3.25)).

The bounds (3.26)-(3.28) then suggest that a numerical scheme designed to constrain the error in the interpolant of the solution will also keep under control the accuracy of the finite element solution. This consideration is at the basis of the work of Carey and Dinh [41] which is discussed in the next section.

3.3 Optimal monitor functions

We now discuss the choice of monitor function proposed by Carey and Dinh [41]. This choice is motivated by the control of the error in the interpolant of the solution to a certain boundary value problem. The rationale behind this choice lies in the fact that, as shown in §3.2, the interpolation error often represents an estimate from above of the error in a finite element approximation to a differential equation. The argument of Carey and Dinh is outlined below.

Assume that the mesh Π in (3.3) satisfies the property (3.4), for some monitor function M . Let $h_i := x_{i+1} - x_i$ be the size of the i -th subinterval $\tau_i := [x_i, x_{i+1}]$. In this section and throughout the rest of this chapter, we will denote by $\pi_h^k u$ a *piecewise k -th degree polynomial interpolant* of the function u at the nodal points of Π . $\pi_h^k u$ is a polynomial of degree k on each interval τ_i and is not necessarily continuous across subinterval boundaries. Let $m \geq 0$ and let $|v|_{m, [a, b]}$ denote the $H^m([a, b])$ -seminorm of a function v over the interval $[a, b]$:

$$|v|_{m, [a, b]} := \left\{ \int_a^b (D^m v)^2 dx \right\}^{1/2}. \quad (3.31)$$

(Note that if $m = 0$, then (3.31) is just $\|v\|_{L_2([a, b])}$, the L_2 -norm of v on the interval $[a, b]$). Finally, let $e_h := u - \pi_h^k u$ be the interpolation error.

The problem tackled by Carey and Dinh [41] is to determine the monitor function M which

3.3. Optimal monitor functions

gives the sharpest upper bound on $|e_h|_{m,[a,b]}$ with respect to variations in the mesh coordinates. This is now discussed.

The main inequality given in [41], obtained by expanding the error e_h and its derivatives on τ_i in a Fourier series and using Parseval's identity, is

$$|e_h|_{m,[a,b]}^2 \leq \sum_{i=1}^N \left(\frac{h_i}{\pi}\right)^{2(k+1-m)} \int_{\tau_i} (D^{k+1}u)^2 dx , \quad (3.32)$$

for $k > m$ (we recall that k is the degree of the polynomial approximation on τ_i). The midpoint quadrature rule is then used to obtain an expression for each of the integrals on the right-hand side of (3.32):

$$\int_{\tau_i} (D^{k+1}u)^2 dx = h_i \left[(D^{k+1}u)(x_{i+1/2}) \right]^2 (1 + O(h_i)) \quad (3.33)$$

and also for

$$\int_{\tau_i} \xi' dx = h_i \xi'(x_{i+1/2})(1 + O(h_i)) . \quad (3.34)$$

(3.34) is combined with

$$\int_{\tau_i} \xi' dx = \xi(x_{i+1}) - \xi(x_i) = \frac{1}{N} \quad (3.35)$$

(we recall that $\xi(x_i) = (i-1)/N$, as noticed in the proof of Lemma 3.1.1), in order to derive the following expression for the length h_i of the interval τ_i :

$$h_i = \frac{1}{N \xi_x(x_{i+1/2})} (1 + O(h_i)) . \quad (3.36)$$

Expressions (3.33) and (3.36) are then substituted into (3.32) to get:

$$|e_h|_{m,[a,b]}^2 \leq \frac{1}{(\pi N)^{2(k+1-m)}} \sum_{i=1}^N \frac{[(D^{k+1}u)(x_{i+1/2})]^2}{[\xi'(x_{i+1/2})]^{2(k+1-m)}} h_i (1 + O(h_i)) . \quad (3.37)$$

Finally, interpreting the sum on the right-hand side of (3.37) as a Riemann sum and neglecting higher order terms, the following result is obtained:

$$|e_h|_{m,[a,b]}^2 \leq \frac{1}{(\pi N)^{2(k+1-m)}} \int_a^b \frac{(D^{k+1}u)^2}{(\xi')^{2(k+1-m)}} dx . \quad (3.38)$$

We now show that there exists a unique monitor function M which minimizes the asymptotic constant in (3.38):

$$\frac{1}{\pi^{2(k+1-m)}} \int_a^b \frac{(D^{k+1}u)^2}{(\xi')^{2(k+1-m)}} dx , \quad (3.39)$$

with respect to variations in the grid points. Note that the monitor function M appears in (3.39)

3.3. Optimal monitor functions

through ξ' , in fact:

$$\xi'(x) = \frac{M(x)}{\int_a^b M(\bar{x}) d\bar{x}} ,$$

(see (3.10)). The monitor function minimizing (3.39) will be called *optimal monitor function* and the corresponding equidistributed mesh will be the *optimal mesh*.

First we observe that (3.39) is minimal with respect to variations in the grid points if and only if the functional

$$J(\xi) = \int_a^b \frac{(D^{k+1}u)^2}{(\xi')^{2(k+1-m)}} dx \quad (3.40)$$

is minimal. The monitor function which minimizes (3.40) is next determined.

Lemma 3.3.1. *The optimal monitor function which minimizes the functional (3.40) over all admissible choices of the mesh is:*

$$M = \left(D^{k+1}u \right)^{2/[2(k+1-m)+1]} . \quad (3.41)$$

Proof. First we show that the only extremal for the functional (3.40) in the space $S = \{\eta \in C^2[a, b] : \eta(a) = 0, \eta(b) = 1\}$ is

$$\xi(x) = \frac{\int_a^x [(D^{k+1}u)(\bar{x})]^{2/[2(k+1-m)+1]} d\bar{x}}{\int_a^b [(D^{k+1}u)(\bar{x})]^{2/[2(k+1-m)+1]} d\bar{x}} . \quad (3.42)$$

This is the grading function corresponding to the monitor function (3.41), as it can be deduced from comparing (3.10) with (3.42). Then we prove that (3.42) minimizes J and the result follows.

To see that (3.42) is the extremal for (3.40) in the space S , consider the Euler-Lagrange equation for J (cf (3.8)):

$$\frac{d}{dx} \left(\frac{(D^{k+1}u)^2}{(\xi')^{2(k+1-m)+1}} \right) = 0 .$$

This is equivalent to

$$\frac{(D^{k+1}u)^2}{(\xi')^{2(k+1-m)+1}} = \text{constant} . \quad (3.43)$$

Then, integration of (3.43), using the boundary the boundary conditions imposed in the space S , yields the solution (3.42).

We finally have to show that the extremal (3.42) minimizes J . This follows from the fact that, for all $x \in [a, b]$, the function

$$f(x, \xi, \xi') := \frac{(D^{k+1}u)^2}{(\xi')^{2(k+1-m)}}$$

is convex for all (ξ, ξ') in the convex set $\mathbb{R}^+ \times \mathbb{R}^+$, as it can be easily checked (see Theorem

3.4. Monitor functions for specific classes of functions

10.7.1 and Theorem 10.7.2 p. 259 of [45]). \square

3.4 Monitor functions for specific classes of functions

We now discuss the properties of the equidistributed h_+ -dependent mesh, that we have identified for discretising the equations (2.39)-(2.41) over the domain $[h_+, d]$ (from now on it will be assumed that $d=1$).

As said at the beginning of this Chapter, the mesh should be chosen so that, in the limit $h_+ \rightarrow 0$, the profile of ε at the artificial wall:

$$\varepsilon(h_+) = \frac{1}{\kappa} \frac{u_*^3}{h_+}, \quad (3.44)$$

is captured as accurately as possible by the numerical scheme, using a number of discretisation points which does not make the computation impractical.

We will show that the grid which meets the previous requirements and noticeably improves the robustness of Newton's method for the nonlinear finite element system (as it will be discussed later in Chapter 5), is the equidistributed mesh with respect to the monitor function given in Lemma 3.3.1, applied to a particular class of functions f , designed to contain the function $\varepsilon(y)$ (given in (2.62) and in (2.78), for $h_+ \rightarrow 0$) as a particular case.

As mentioned above, the variable ε is expected to vary smoothly faraway from the artificial wall and resemble closely the function $f(y) = C/y$, with $C = u_*^3/\kappa$, in a neighbourhood of $y = h_+$, due to the boundary condition (3.44). Rather than considering ε directly, we will consider a class of functions which includes ε . So, for given real number $p > 0$ and integer $n \geq 0$, and for $f \in C^n([h_+, 1])$, we define the seminorm:

$$|f|_{n,p,[h_+,1]} := \|y^{n+p}(D^n f)(y)\|_{\infty,[h_+,1]},$$

and, in Corollary 3.4.2, we will determine a monitor function which minimizes, over all admissible choices of the mesh, the bound on $|e_h|_{m,[a,b]} := |f - \pi_h^k f|_{m,[a,b]}$ (where $\pi_h^k f$ is the piecewise k -th degree polynomial interpolant of f) that will be derived in Theorem 3.4.1 for all f in the space

$$V_{k+1,p,h_+} = \left\{ f \in C^{k+1}([h_+, 1]) : |f|_{k+1,p,[h_+,1]} < +\infty \text{ as } h_+ \rightarrow 0 \right\}. \quad (3.45)$$

Note that when $p=1$, the set (3.45) contains functions f whose $k+1$ derivative blows up like y^{k+2} , which coincides with the expected behaviour of ε . Moreover, we observe that for all $p > 0$, the function $g(y) := \ln(y)$ lies in the space V_{k+1,p,h_+} . This is relevant to our study because, as seen in (2.57),

$$U(h_+) = u_* \left[\frac{1}{\kappa} \ln \left(\frac{u_* h_+}{\nu} \right) + C \right],$$

3.4. Monitor functions for specific classes of functions

then we expect $U(y)$ to blow up logarithmically as $y = h_+ \rightarrow 0$.

We will also show that on the mesh we propose, the interpolation error for the functions $f \in V_{k+1,p,h_+}$ deteriorates very mildly when $h_+ \rightarrow 0$, which suggests that, in this limit, not many mesh points will be needed to resolve the profile (3.44).

Theorem 3.4.1. *Let $f \in V_{k+1,p,h_+}$ and let $\{y_i\}$, $i = 1, \dots, N + 1$, be a mesh on the interval $[h_+, 1]$ equidistributed with respect to a monitor function M . Then*

$$|e_h|_{m,[a,b]}^2 \leq \frac{|f|_{k+1,p,[h_+,1]}^2}{\left[\prod_{j=0}^k (p+j)\right]^2} \frac{1}{(\pi N)^{2(k+1-m)}} \int_{h_+}^1 \frac{[D^{k+1}(1/y^p)]^2}{[\xi']^{2(k+1-m)}} dy \quad (3.46)$$

Proof. We start with the upper bound for the $H^m([h_+, 1])$ seminorm of the interpolation error (3.32) given in [41]:

$$|e_h|_{m,[a,b]}^2 \leq \sum_{i=1}^N \left(\frac{h_i}{\pi}\right)^{2(k+1-m)} \int_{\tau_i} (D^{k+1}f)^2 dy, \quad (3.47)$$

where $\tau_i := [y_i, y_{i+1}]$. Multiplying and dividing the integrand in (3.47) by $y^{2(k+1+p)}$ we have:

$$\begin{aligned} |e_h|_{m,[a,b]}^2 &\leq \sum_{i=1}^N \left(\frac{h_i}{\pi}\right)^{2(k+1-m)} \int_{\tau_i} |y^{k+1+p} (D^{k+1}f)|^2 \left(\frac{1}{y^{k+1+p}}\right)^2 dy \\ &= C \sum_{i=1}^N \left(\frac{h_i}{\pi}\right)^{2(k+1-m)} \int_{\tau_i} |y^{k+1+p} (D^{k+1}f)|^2 \left[D^{k+1}\left(\frac{1}{y^p}\right)\right]^2 dy, \end{aligned} \quad (3.48)$$

where C is a constant which depends on p and k . Now, since

$$\sup_{\tau_i} |y^{k+1+p} D^{k+1}f| \leq |f|_{k+1,p,[h_+,1]},$$

from (3.48) we get:

$$|e_h|_{m,[a,b]}^2 \leq \frac{|f|_{k+1,p,[h_+,1]}^2}{\left[\prod_{j=0}^k (p+j)\right]^2} \sum_{i=1}^N \left(\frac{h_i}{\pi}\right)^{2(k+1-m)} \int_{\tau_i} \left[D^{k+1}\left(\frac{1}{y^p}\right)\right]^2 dy. \quad (3.49)$$

The sum in the right hand side of (3.49) is the same as the sum in the right hand side of (3.32) with $u = 1/y^p$, therefore, the same argument as in [41], which leads to (3.38), will then give the result (3.46). \square

Following the same strategy as Carey and Dinh [41], we now determine the monitor function which minimizes the integral

$$\int_{h_+}^1 \frac{[D^{k+1}(1/y^p)]^2}{[\xi']^{2(k+1-m)}} dy, \quad (3.50)$$

in the asymptotic constant in (3.46).

3.4. Monitor functions for specific classes of functions

Corollary 3.4.2. *The monitor function which minimizes (3.50) is the optimal monitor function for a piecewise k -th degree polynomial interpolation of $u(y) = 1/y^p$:*

$$M(y) = \left[D^{k+1} \left(\frac{1}{y^p} \right) \right]^{2/[2(k+1-m)+1]} . \quad (3.51)$$

Proof. The asymptotic constant in (3.46) is minimal if and only if the functional

$$K(\xi) = \int_{h_+}^1 \frac{[D^{k+1}(1/y^p)]^2}{[\xi']^{2(k+1-m)}} dy$$

is minimal. This is the same as (3.40) with $u = 1/y^p$. The result then follows from Lemma 3.3.1. \square

It is now convenient to introduce the notation:

$$r := 2(k+1-m) + 1 , \quad q := 2(m+p) - 1 . \quad (3.52)$$

We then obtain an expression for the grading function ξ corresponding to the monitor function (3.51).

Corollary 3.4.3. *The grading function corresponding to the monitor function (3.51) is given by*

$$\xi(y) = \frac{1 - (y/h_+)^{-q/r}}{1 - h_+^{q/r}} , \quad \text{for } (m, p) \neq (0, 1/2) , \quad (3.53)$$

and

$$\xi(y) = \frac{\ln(y/h_+)}{\ln(1/h_+)} , \quad \text{for } (m, p) = (0, 1/2) . \quad (3.54)$$

Proof. Substituting M from (3.51) into (3.10), we get:

$$\xi(y) = \frac{\int_{h_+}^y [D^{k+1}(1/s^p)]^{2/r} ds}{\int_{h_+}^1 [D^{k+1}(1/s^p)]^{2/r} ds} , \quad (3.55)$$

and, by computing the $(k+1)$ derivative of $1/s^p$ and by using the expressions for q and r in (3.52), from (3.55) we obtain

$$\xi(y) = \frac{\int_{h_+}^y s^{-(q/r+1)} ds}{\int_{h_+}^1 s^{-(q/r+1)} ds} . \quad (3.56)$$

It is then not difficult to check that, provided

$$\frac{q}{r} + 1 \neq 1 , \quad \text{i.e., } q \neq 0 , \quad \text{i.e., } m + p \neq \frac{1}{2} , \quad (3.57)$$

the computation of the integrals in (3.56) yields the expression for ξ in (3.53). As far as the

3.4. Monitor functions for specific classes of functions

condition (3.57) is concerned, it should be noted that

$$m + p \neq \frac{1}{2} \quad \Leftrightarrow \quad (m, p) \neq (0, 1/2) ,$$

since $m \in \mathbb{N}$ and we are considering $p > 0$.

If $q/r + 1 = 1$, i.e. $(m, p) = (0, 1/2)$, then note that:

$$\int_{h_+}^y s^{-(q/r+1)} ds = \ln \left(\frac{y}{h_+} \right) , \quad (3.58)$$

hence (3.54) follows from (3.56). \square

In the following, for the sake of clarity of the exposition, we will assume that $(m, p) \neq (0, 1/2)$. We will, then, avoid considering the approximation in the L_2 norm of functions $f \in V_{k+1,1/2,h_+}$. We recall that we are mostly interested in the properties of the piecewise polynomial interpolant of $f \in V_{k+1,1,h_+}$.

We now determine the mesh points which equidistribute the monitor function (3.51) and then, using in (3.46) the expression (3.53) for the grading function ξ , we will determine the explicit dependence on h_+ of the upper bound on the error in the interpolation of $f \in V_{k+1,p,h_+}$. Note that the equidistributed mesh with respect to the monitor function (3.51) will be the optimal mesh for a piecewise k -th degree polynomial interpolation of $u(y) = 1/y^p$ (in the sense of §3.3).

Lemma 3.4.4. *The mesh generated by (3.53), which equidistributes the monitor function (3.51), is:*

$$y_i = h_+ \left[1 - \frac{i-1}{N} \left(1 - h_+^{q/r} \right) \right]^{-r/q} \quad i = 1, 2, \dots, N+1 , \quad (3.59)$$

Proof. As discussed in §3.1, in the computational domain $\Omega_c = [0, 1]$, the mesh is uniform:

$$\xi_{i+1} - \xi_i = \frac{1}{N} , \quad (3.60)$$

but, since $\xi_1 = \xi(h_+) = 0$, from (3.60) we get:

$$\xi_i = \xi(y_i) = \frac{i-1}{N} , \quad i = 1, 2, \dots, N+1 .$$

Therefore, the grid points $\{y_i\}$ in the physical domain $\Omega_p = [h_+, 1]$ are given by the solution of the scalar equation:

$$\xi(y_i) - \frac{i-1}{N} = 0 . \quad (3.61)$$

Then (3.59) follows from solving (3.61) for y_i with ξ given in (3.53). \square

We now briefly discuss how the distributions of grid points (3.59) can be equivalently obtained from the 1D equidistribution principle (3.13). From (3.51), computing the $(k+1)$ -th derivative of y^{-p} and using the definitions of r and q in (3.52), we can express the monitor function as:

3.4. Monitor functions for specific classes of functions

$$M(y) = \left[(-1)^{k+1} \prod_{j=0}^k (p+j) \right]^{2/r} y^{-(q/r+1)}. \quad (3.62)$$

Substituting (3.62) into (3.13) (with y instead of x) and using the chain rule, we have, for $q \neq 0$ (i.e. $(m, p) \neq (0, 1/2)$),

$$(y(\xi))^{-(q/r+1)} \frac{dy}{d\xi}(\xi) = -\frac{r}{q} \frac{d}{d\xi} \left[(y(\xi))^{-q/r} \right] = \text{constant},$$

which yields the following ordinary differential equations for the coordinate transformation $y=y(\xi)$ from the computational domain to the physical domain:

$$\frac{d}{d\xi} \left[(y(\xi))^{-q/r} \right] = \text{constant}.$$

This has the solution

$$y(\xi) = h_+ \left[1 - \xi \left(1 - h_+^{q/r} \right) \right]^{-r/q}, \quad (3.63)$$

which satisfies $y(0) = h_+$, $y(1) = 1$. Finally, evaluating (3.63) at the points $\xi_i = (i-1)/N$ yields (3.59).

In §3.5, we will discuss in detail the distribution of mesh points (3.59) which minimizes the $L_2([h_+, 1])$ norm of the error in a piecewise quadratic approximation of $f(y) = 1/y$. We first establish a general estimate to show how the right-hand side of (3.46) depends on h_+ .

Lemma 3.4.5. *Let $(m, p) \neq (0, 1/2)$ and $f \in V_{k+1,p,h_+}$, then on the mesh (3.59), we have*

$$|e_h|_{m,[h_+,1]} \leq \frac{|f|_{k+1,p,[h_+,1]}}{\pi^{k+1-m}} \left(\frac{r}{q} \right)^{r/2} \left(1 - h_+^{q/r} \right)^{r/2} \frac{h_+^{-q/2}}{N^{k+1-m}}. \quad (3.64)$$

Proof. Using also (3.55), from which we get an expression for $\xi'(y)$, it is not difficult to see that the integral on the right-hand side of (3.46) (with $2(k+1-m)$ replaced by $r-1$, see (3.52)) can be expressed as follows:

$$\begin{aligned} \int_{h_+}^1 \frac{[D^{k+1}(1/y^p)]^2}{[\xi'(y)]^{r-1}} dy &= \left\{ \int_{h_+}^1 [D^{k+1}(1/s^p)]^{2/r} ds \right\}^{r-1} \int_{h_+}^1 \frac{[D^{k+1}(1/y^p)]^2}{[D^{k+1}(1/y^p)]^{2-2/r}} \\ &= \left\{ \int_{h_+}^1 [D^{k+1}(1/y^p)]^{2/r} dy \right\}^r \\ &= \left(\prod_{j=0}^k (p+j) \right)^2 \left(\int_{h_+}^1 y^{-(q/r+1)} dy \right)^r. \end{aligned} \quad (3.65)$$

Since by assumption $(m, p) \neq (0, 1/2)$, we have that $q \neq 0$ and the integral in (3.65) yields:

$$\left(\int_{h_+}^1 s^{-2(k+1+p)/r} ds \right)^r = \left(\frac{r}{q} \right)^r \left(1 - h_+^{q/r} \right)^r h_+^{-q},$$

3.4. Monitor functions for specific classes of functions

which is substituted back into (3.65), to obtain:

$$\int_{h_+}^1 \frac{[D^{k+1}(1/y^p)]^2}{[\xi'(y)]^{r-1}} dy = \left(\prod_{j=0}^k (p+j) \right)^2 \left(\frac{r}{q} \right)^r \left(1 - h_+^{q/r} \right)^r h_+^{-q}. \quad (3.66)$$

The result then follows from substituting the expression (3.66) into (3.46). \square

We now analyse the behaviour of the bound (3.64) as $h_+ \rightarrow 0$. For simplicity, we study the dependence of the error on h_+ , N and f only.

Theorem 3.4.6. *Let the assumptions of Lemma 3.4.5 hold. Suppose*

$$\text{either } m \geq 1 \quad \text{or} \quad p > 1/2. \quad (3.67)$$

Then there exists a constant C_1 , which does not blow up as $h_+ \rightarrow 0$, such that

$$|e_h|_{m,[h_+,1]} \leq C_1 h_+^{-(m+p)+1/2} \frac{|f|_{k+1,p,[h_+,1]}}{N^{k+1-m}}. \quad (3.68)$$

If

$$m = 0 \quad \text{and} \quad p < 1/2, \quad (3.69)$$

then

$$\|e_h\|_{L_2([h_+,1])} \leq C_2 \frac{|f|_{k+1,p,[h_+,1]}}{N^{k+1}} \quad (3.70)$$

with asymptotic constant C_2 bounded as $h_+ \rightarrow 0$.

Proof. Assume that (3.67) holds. Then, recalling the definition of r and q in (3.52):

$$r := 2(k+1-m) + 1, \quad q := 2(m+p) - 1, \quad (3.71)$$

we observe that $r > 0$, since $k > m$, and that

$$m \geq 1 \quad \Rightarrow \quad q = 2 \left(m - \frac{1}{2} \right) + 2p \geq 1 + 2p > 1 \quad \forall p > 0,$$

and similarly

$$p > \frac{1}{2} \quad \Rightarrow \quad q = 2m + 2 \left(p - \frac{1}{2} \right) > 2m \geq 0 \quad \forall m \geq 0.$$

Hence (3.68) follows from observing that, using the definition of q in (3.71), (3.64) can be written as

$$|e_h|_{m,[h_+,1]} \leq C_1 h_+^{-(m+p)+1/2} \frac{|f|_{k+1,p,[h_+,1]}}{N^{k+1-m}},$$

with constant

$$C_1 := \frac{\left(1 - h_+^{q/r} \right)^{r/2}}{\pi^{k+1-m}} \left(\frac{r}{q} \right)^{r/2}, \quad (3.72)$$

3.5. A particular case

which is bounded as $h_+ \rightarrow 0$, since, in this limit, $h_+^{q/r} \rightarrow 0$ due to the fact that $q/r > 0$.

Assume now that (3.69) holds. We observe that

$$m = 0 \quad \text{and} \quad p < 1/2 \quad \Rightarrow \quad q = 2 \left(p - \frac{1}{2} \right) < 0 ,$$

moreover, by setting $m=0$ in (3.64), we get:

$$\|e\|_{L_2([h_+,1])} \leq \frac{|f|_{k+1,p,[h_+,1]}}{\pi^{k+1}} \left(\frac{r}{q} \right)^{r/2} \left(1 - h_+^{q/r} \right)^{r/2} \frac{h_+^{-q/2}}{N^{k+1}} . \quad (3.73)$$

The result (3.70) then follows from rearranging the right-hand side of (3.73) as:

$$\|e\|_{L_2([h_+,1])} \leq C_2 \frac{|f|_{k+1,p,[h_+,1]}}{N^{k+1}} , \quad (3.74)$$

with constant

$$\begin{aligned} C_2 &:= \left(\frac{r}{q} \right)^{r/2} \left(1 - h_+^{q/r} \right)^{r/2} \frac{h_+^{-q/2}}{\pi^{k+1}} \\ &= \frac{1}{\pi^{k+1}} \left[-r \frac{\left(1 - h_+^{-q/r} \right)}{q} \right]^{r/2} , \end{aligned} \quad (3.75)$$

and noticing that $h_+^{-q/r} \rightarrow 0$ as $h_+ \rightarrow 0$, since $-q/r > 0$. □

Observation 3.4.1. It is clear, respectively from (3.68) and (3.70), that, as $h_+ \rightarrow 0$, the bound on the $H^m([h_+, 1])$ seminorm of the interpolation error blows up proportionally to $h_+^{-(m+p)+1/2}$ in the regime of the parameters (3.67), while is independent of h_+ when $m=0$ and $p < 1/2$. Moreover, we notice that, by increasing the degree k of the polynomial interpolation, it is possible to obtain a better approximation to $f \in V_{k+1,p,h_+}$ because of the very mild dependence on k of the asymptotic constants C_1 and C_2 , respectively in (3.72) and (3.75). Note that in (3.68), changes in the value of k will not affect the order of blow-up of the asymptotic constant. We finally observe that for $p > 1/2$, the $L_2([h_+, 1])$ norm ($m=0$) of the interpolation error shows the mildest deterioration as $h_+ \rightarrow 0$, namely of order $h_+^{-p+1/2}$, as it follows from (3.68) by setting $m=0$.

3.5 A particular case

We now discuss the above results in the case of the particular function $f(y) = 1/y$, focusing, specifically, on its piecewise quadratic interpolation. This choice is motivated by the fact that in a neighbourhood of $y = h_+$, as $h_+ \rightarrow 0$, the asymptotic behaviour in the direction orthogonal to the artificial wall of the variable ε , in the k - ε system (2.4), is expected to be represented well by the profile $1/y$, and by the fact that in the particular finite element method, in this thesis

3.5. A particular case

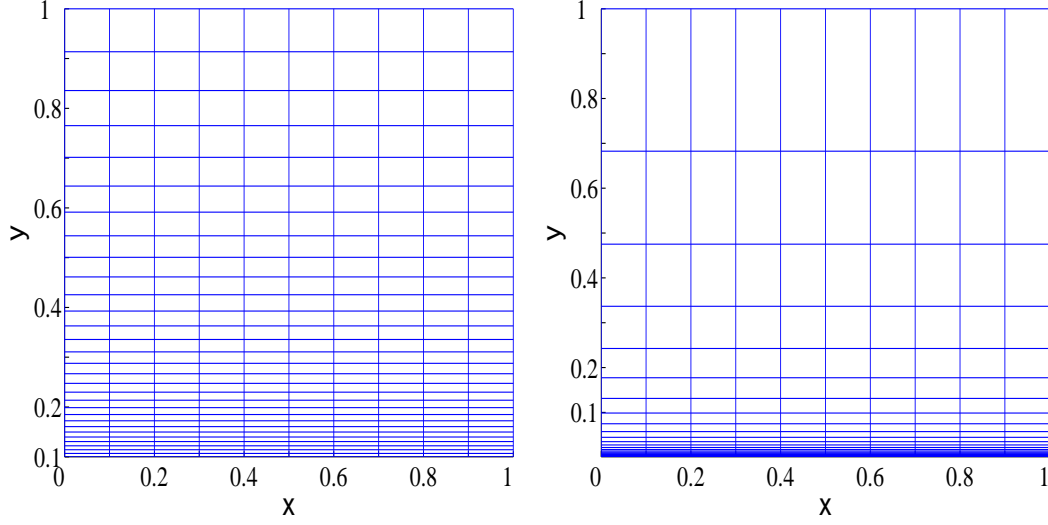


Figure 3.1: Discretisation of the channel for $h_+ = 10^{-1}$ (left) and $h_+ = 10^{-3}$ (right), with a mesh given by the tensor product between a uniform mesh in the x -direction and the equidistributed mesh (3.76) with $N = 30$ in the y -direction.

ε will be approximated using piecewise quadratic polynomial basis functions. This study will then provide us with some insights into the properties of our finite element discretisation.

Let us consider the optimal distribution of mesh points (in the sense of §3.3) for a piecewise quadratic interpolation of $f(y) = 1/y$ over the interval $[h_+, 1]$, when the interpolation error is measured in the $L_2([h_+, 1])$ norm. Then, $k = 2$, $p = 1$ and $m = 0$ and from (3.52), $r = 7$ and $q = 1$, and (3.59) gives:

$$y_i = h_+ \left(1 - \frac{i-1}{N} \left(1 - h_+^{1/7} \right) \right)^{-7} \quad i = 1, 2, \dots, N+1. \quad (3.76)$$

This mesh in the y -direction is combined with a uniform mesh in the x -direction and plotted in Figure 3.1.

In this case Theorem 3.4.6 yields

$$\|e\|_{L_2([h_+, 1])} \leq C_1 h_+^{-1/2} \frac{|f|_{3,1,[h_+, 1]}}{N^3}, \quad (3.77)$$

(for $f(y) = 1/y$, we have $|f|_{3,1,[h_+, 1]} = 1$).

To illustrate (3.77), in Table 3.1, for a sequence of decreasing values of h_+ , we compute the piecewise quadratic interpolant of $f(y) = 1/y$ at the points y_i , $(y_i + y_{i+1})/2$ and y_{i+1} of the mesh (3.76) (with fixed $N = 62$ and $N = 124$) and then measure its error in the norm $L_2([h_+, 1])$.

Table 3.1 indicates the $O(h_+^{-1/2})$ blow up predicted by the theoretical result (3.77). It also shows the effectiveness of the mesh (3.76) in approximating the profile $1/y$. In fact, for only 64 elements the relative error in the piecewise quadratic interpolation of $f(y) = 1/y$, when $h_+ = 10^{-13}$, is very small of order 10^{-4} , that is

3.5. A particular case

h_+	$N=64$		$N=128$	
	$\ e_h\ _{L_2([h_+,1])}$	EOBU	$\ e_h\ _{L_2([h_+,1])}$	EOBU
10^{-4}	4.005×10^{-3}		5.004×10^{-4}	
10^{-5}	1.784×10^{-2}	0.649	2.223×10^{-3}	0.649
10^{-6}	7.083×10^{-2}	0.599	8.847×10^{-3}	0.599
10^{-7}	2.616×10^{-1}	0.567	3.267×10^{-2}	0.567
10^{-8}	9.218×10^{-1}	0.547	1.150×10^{-1}	0.547
10^{-9}	3.145	0.533	3.923×10^{-1}	0.533
10^{-10}	10.50	0.523	1.309	0.523
10^{-11}	34.52	0.517	4.30	0.516
10^{-12}	112.3	0.512	13.97	0.512
10^{-13}	363.5	0.509	45.1	0.508

Table 3.1: Dependence on $h_+ \rightarrow 0$ of the L_2 -norm of the error in the piecewise quadratic interpolation of $f(y) = 1/y$ at the nodes (3.76) and estimated order of blow-up (EOBU).

$$\frac{\|e\|_{L_2([10^{-13},1])}}{\|1/y\|_{L_2([10^{-13},1])}} = 1.15 \times 10^{-4} .$$

The final result of this section is about the fine structure of the mesh (3.59) near the wall $y = h_+$. Let $\bar{h}_+ \ll 1$ be a fixed value of the coordinate of the artificial wall and consider the following two sets of nodes of the grid (3.59):

$$\tilde{\mathcal{N}}_w := \{i \in \mathbb{N} \mid y_i = O(h_+) \text{ as } h_+ \rightarrow \bar{h}_+\} ,$$

$$\tilde{\mathcal{N}}_{cl} := \{i \in \mathbb{N} \mid y_i = O(1) \text{ as } h_+ \rightarrow \bar{h}_+\} .$$

Let N be sufficiently large, then from (3.59) it is not difficult to see that:

$$i \text{ s.t. } \frac{i-1}{N} \ll 1 \Rightarrow i \in \tilde{\mathcal{N}}_w ,$$

and that

$$i \text{ s.t. } \frac{i-1}{N} \approx 1 \Rightarrow i \in \tilde{\mathcal{N}}_{cl} .$$

We will prove, in particular, that

3.5. A particular case

$$i \in \tilde{\mathcal{N}}_w \Rightarrow \frac{h_i}{y_i} = O\left(\frac{1}{N}\right),$$

which shows that if N is sufficiently large, then the number of elements in a neighbourhood of \bar{h}_+ , is sufficient to resolve accurately the boundary layer of width $O(\bar{h}_+)$, as it can be seen from considering, for example, that $h_i/y_i = O(1/N)$ implies

$$\frac{h_1}{\bar{h}_+} = O\left(\frac{1}{N}\right), \quad \frac{h_2}{\bar{h}_+} = O\left(\frac{1}{N}\right) + \text{h.o.t.} .$$

We have:

Lemma 3.5.1. *Let $\bar{h}_+ \ll 1$ and let $h_+ \rightarrow \bar{h}_+$, then the mesh (3.59) is such that*

$$i \in \tilde{\mathcal{N}}_w \Rightarrow \frac{h_i}{y_i} = O\left(\frac{1}{N}\right), \quad (3.78)$$

and

$$i \in \tilde{\mathcal{N}}_{cl} \Rightarrow \frac{h_i}{y_i} = O\left(\frac{h_+^{-q_1/r}}{N}\right). \quad (3.79)$$

Proof. The relation between the mesh size h_i and the grid point y_i can be derived from (3.15), which, neglecting the higher order terms, gives:

$$h_i = \frac{1}{N} \frac{1}{\xi'(y_i)}. \quad (3.80)$$

The derivative of the grading function can be obtained from (3.53):

$$\xi'(y) = \frac{q_1}{r} \frac{y^{-1-q_1/r}}{h_+^{-q_1/r} - 1},$$

and by evaluating the last expression at $y = y_i$, substituting the result into (3.80) and rearranging the terms we get:

$$\frac{h_i}{y_i} = \frac{r}{q_1} \frac{1}{N} \left[\left(\frac{y_i}{h_+}\right)^{q/r} - y_i^{q/r} \right]. \quad (3.81)$$

If $i \in \tilde{\mathcal{N}}_w$, then:

$$\left(\frac{y_i}{h_+}\right)^{q/r} = O(1) \quad \text{and} \quad y_i^{q/r} = O\left(h_+^{q/r}\right) \ll 1, \quad \text{as } h_+ \rightarrow \bar{h}_+ \ll 1$$

and the result (3.78) follows from (3.81). In the case when $i \in \tilde{\mathcal{N}}_{cl}$, we can get the result (3.79) rearranging (3.81) as

$$\frac{h_i}{y_i} = \frac{r}{q_1} \frac{h_+^{-q/r}}{N} \left[y_i^{q/r} - (y_i h_+)^{q/r} \right]$$

and observing that if $i \in \tilde{\mathcal{N}}_{cl}$, then

$$y_i^{q/r} = O(1) \quad \text{and} \quad (y_i h_+)^{q/r} = O(h_+^{q/r}) \ll 1, \quad \text{as } h_+ \rightarrow \bar{h}_+ \ll 1. \quad \square$$

3.6. Close-up of the approximation of $f(y) = 1/y$

Note that the blow-up in h_i/y_i for $i \in \tilde{\mathcal{N}}_{\text{cl}}$, as $h_+ \rightarrow \bar{h}_+$, (see (3.79)), is very mild when the error in a piecewise quadratic interpolation of $1/y$ is measured in the $L_2([h_+, 1])$ norm, in fact in this case we have $q/r = 1/7$ (from (3.52) with $k = 2$ and $m = 0$). This is important in later sections.

3.6 Close-up of the approximation of $f(y) = 1/y$

In this section we pursue further the study of the properties of the interpolant of $f(y) = 1/y$ over the interval $[h_+, 1]$, with $h_+ \rightarrow 0$, which was started in §3.5. Our investigation aims at highlighting the difficulties posed by the approximation of the variable ε in the k - ε system (2.4) and at showing how beneficial the use of the mesh (3.76) is. For this purpose, first, through a Taylor expansion, we will derive an expression for the $L_2([h_+, 1])$ -norm of the error in a continuous piecewise quadratic interpolation of $1/y$ on a fairly general mesh, we will then study the behaviour of the error on uniform discretisations of the interval $[h_+, 1]$ and compare it with the properties of (3.77) (see §3.6.1). Finally, in §3.6.2, we will briefly describe an alternative derivation for (3.76) and (3.77).

Let $\{y_i\}$, $i = 1, 2, \dots, N + 1$, define a mesh of N intervals over the domain $[h_+, 1]$, with $y_1 = h_+$, $y_{N+1} = 1$ and let $h_i = y_{i+1} - y_i$ denote the length of the interval τ_i , $i = 1, 2, \dots, N$. Let $\pi_h^2 f$ be a piecewise quadratic interpolant of $f(y) = 1/y$ at the nodes y_i . We now give an expression for the $L_2([h_+, 1])$ norm of the interpolation error $e_h := f - \pi_h^2 f$.

We have:

$$\|e_h\|_{L_2([h_+, 1])}^2 = \int_{h_+}^1 |f - \pi_h^2 f|^2 dy ,$$

which can be written as:

$$\|e_h\|_{L_2([h_+, 1])}^2 = \sum_{i=1}^N E_i^2 , \quad (3.82)$$

where

$$E_i^2 := \int_{\tau_i} |f - \pi_h^2 f|^2 dy \quad (3.83)$$

is the square of the L_2 -norm of the local interpolation error.

Define:

$$g(s) = f(y_i + sh_i) , \quad s \in [0, 1]$$

and let

$$\tilde{g}(s) = (\pi_h^2 f)(y_i + sh_i) , \quad s \in [0, 1] , \quad i = 1, \dots, N$$

be the continuous piecewise quadratic polynomial interpolant of $f = 1/y$ at the points y_i ,

3.6. Close-up of the approximation of $f(y) = 1/y$

$(y_i + y_{i+1})/2$ and y_{i+1} of τ_i . Then an easy calculation shows that for all $s \in [0, 1]$:

$$\tilde{g}(s) = \frac{1-s}{y_i} + \frac{s}{y_{i+1}} - \frac{2h_i^2}{y_{i+1}y_i(y_i + y_{i+1})}s(1-s), \quad i = 1, \dots, N. \quad (3.84)$$

(3.83) can then be written as:

$$E_i^2 = \int_0^1 \left\{ \frac{1}{y_i + sh_i} - \left[\frac{1-s}{y_i} + \frac{s}{y_{i+1}} - \frac{2h_i^2}{y_{i+1}y_i(y_i + y_{i+1})}s(1-s) \right] \right\}^2 h_i ds,$$

and introducing the parameter $\alpha_i := h_i/y_i$, the last expression can be rearranged in the following form:

$$E_i^2 = \frac{\alpha_i}{y_i} \int_0^1 \left[\frac{1}{1 + \alpha_i s} - (1-s) - \frac{s}{1 + \alpha_i} + \frac{2\alpha_i^2 s(1-s)}{(1 + \alpha_i)(2 + \alpha_i)} \right]^2 ds. \quad (3.85)$$

We will consider meshes with the property:

$$\alpha_i := \frac{h_i}{y_i} \ll 1, \quad (3.86)$$

which, as discussed in §3.5, guarantees that the number of elements in a neighbourhood of h_+ is sufficient to resolve accurately the boundary layer. For N large enough, (3.86) is also met by the optimal mesh for a piecewise quadratic interpolation of $1/y$ (3.76), compare with (3.78) and (3.79) with $q_1 = 1$ and $r = 7$ (corresponding to $k = 2$ and $m = 0$). We have:

Lemma 3.6.1. *Under the condition (3.86),*

$$\|e_h\|_{L_2([h_+, 1])} = \sqrt{\frac{1}{840} \sum_{i=1}^N \frac{1}{y_i} (\alpha_i^7 + O(\alpha_i^8))}. \quad (3.87)$$

Proof. If (3.86) holds, then the Taylor expansion of (3.85) in powers of α_i yields:

$$E_i^2 = \frac{1}{y_i} \left(\frac{\alpha_i^7}{840} + O(\alpha_i^8) \right).$$

The result (3.87) then follows from substituting the last expression into (3.82) and taking the square root. \square

In §3.6.1, (3.87) will be used to derive an expression for the interpolation error on uniform discretisations of $[h_+, 1]$, while in §3.6.2 from its minimisation with respect to variations in the grid points we will reobtain (3.76) and (3.77).

3.6. Close-up of the approximation of $f(y) = 1/y$

3.6.1 Uniform mesh

Now, let the domain $[h_+, 1]$ be partitioned with the uniform mesh:

$$y_i = h_+ + (i - 1) \frac{1 - h_+}{N}, \quad i = 1, 2, \dots, N + 1 \quad (3.88)$$

satisfying the condition:

$$\frac{h}{y_1} = \frac{h}{h_+} = \frac{1 - h_+}{N h_+} \ll 1, \quad (3.89)$$

which, in the case of a uniform discretisation, is obviously equivalent to (3.86), since $\alpha_i = h/y_i \leq h/y_1$ for all $i = 1, 2, \dots, N$. We have:

Lemma 3.6.2. *If the interval $[h_+, 1]$ is discretised using the uniform mesh (3.88) with property (3.89), then the $L_2([h_+, 1])$ -norm of the interpolation error (3.87) can be approximately expressed as:*

$$\|e_h\|_{L_2([h_+, 1])} \approx \sqrt{\frac{(1 - h_+)^7 (1 - h_+^7) h_+^{-7/2}}{5880 N^3}}. \quad (3.90)$$

Proof. Taking the square of (3.87) and using the expression $h = (1 - h_+)/N$ and the fact that $h/y_i \leq h/y_1 = h/h_+$, we have:

$$\begin{aligned} \|e_h\|_{L_2([h_+, 1])}^2 &= \frac{1}{840} \sum_{i=1}^N \frac{h^7}{y_i^8} \left(1 + O\left(\frac{h}{y_i}\right)\right) \\ &= \frac{(1 - h_+)^7}{840} \sum_{i=1}^N \frac{1}{y_i^8} \frac{1}{N^7} \left(1 + O\left(\frac{h}{y_i}\right)\right) \\ &= \frac{1}{N^6} \frac{(1 - h_+)^7}{840} \sum_{i=1}^N \frac{1}{y_i^8} \frac{1}{N} \left(1 + O\left(\frac{1}{N h_+}\right)\right). \end{aligned} \quad (3.91)$$

Interpreting the sum on the right-hand side of the last expression as a Riemann sum and neglecting higher order terms we obtain:

$$\|e_h\|_{L_2([h_+, 1])}^2 \approx \frac{1}{N^6} \frac{(1 - h_+)^7}{840} \int_{h_+}^1 \frac{1}{s^8} ds,$$

and therefore

$$\|e_h\|_{L_2([h_+, 1])}^2 \approx \frac{(1 - h_+)^7 (1 - h_+^7) h_+^{-7}}{5880 N^6}.$$

The result (3.90) then follows from taking the square root of the last expression. \square

At the end of this section we will illustrate, through numerical experiments, that the estimate (3.90) correctly describes the behaviour of the interpolation error, by showing that the constant

3.6. Close-up of the approximation of $f(y) = 1/y$

$$c(h_+) := \sqrt{\frac{(1-h_+)^7(1-h_+^7)}{5880}} \frac{1}{h_+^{7/2}}, \quad (3.92)$$

in (3.90), represents a very good estimate of the actual asymptotic constant. First, we make two observations that follow obviously from (3.90):

Corollary 3.6.3. *Consider the limit $h_+ \rightarrow 0$, then on the uniform mesh (3.88) with property (3.89) the continuous piecewise quadratic interpolant (3.84) of $f(y) = 1/y$ will converge to f in the $L_2([h_+, 1])$ -norm if and only if $N \rightarrow \infty$ at least with order $h_+^{-(7/6+\delta)}$.*

Corollary 3.6.4. *Let the domain $[h_+, 1]$ be subdivided into a uniform mesh with property (3.89). Then the $L_2([h_+, 1])$ -norm of the error in the continuous piecewise quadratic interpolant (3.84) of $f(y) = 1/y$ is smaller than a given tolerance τ :*

$$\|e_h\|_{L_2([h_+, 1])} \leq \tau, \quad ,$$

if and only if

$$N \geq \left[\frac{(1-h_+)^7(1-h_+^7)}{5880} \right]^{1/6} \frac{h_+^{-7/6}}{\tau^{1/3}} \quad (3.93)$$

We now compare the results above with the behaviour of the interpolation error on the optimal mesh (3.76). As already seen in §3.5, on the mesh (3.76), an upper bound for the square of the $L_2([h_+, 1])$ -norm of the error for a piecewise quadratic interpolation of $f(y) = 1/y$, is given by (3.77) with $|f|_{3,1,[h_+, 1]} = 1$:

$$\|e\|_{L_2([h_+, 1])}^2 \leq \frac{7^7}{\pi^6} \frac{1}{N^6 h_+}. \quad (3.94)$$

From (3.94), we have that, in the limit $h_+ \rightarrow 0$, the piecewise quadratic approximation of $f(y) = 1/y$ on the optimal mesh will converge to f if

$$N \sim h_+^{-(\frac{1}{6}+\delta)}.$$

This certainly represents a big improvement on the condition

$$N \sim h_+^{-(\frac{7}{6}+\delta)}$$

required for convergence on the uniform mesh.

When the optimal mesh (3.76) is used, then the number of mesh points needed for the interpolation error (3.77), with $k=2$, to be less than a given tolerance τ is bounded from below by:

$$N \geq \left(\frac{7^{7/2}}{\tau} \right)^{1/3} h_+^{-1/6}. \quad (3.95)$$

Again, (3.95) is a considerable improvement on (3.93).

3.6. Close-up of the approximation of $f(y) = 1/y$

$$\Lambda := \left(| N^3 \|e_h\|_{L_2([h_+,1])} - c(h_+) | \right) / c(h_+)$$

	$h_+ = 10^{-1}$ $c(h_+) = 28.5$	$h_+ = 10^{-2}$ $c(h_+) = 125,903$	$h_+ = 10^{-3}$ $c(h_+) = 410,951,477$
h/h_+	Λ	Λ	Λ
2.25	6.7×10^{-1}	6.8×10^{-1}	6.8×10^{-1}
1.125	3.9×10^{-1}	4.2×10^{-1}	4.2×10^{-1}
5.6×10^{-1}	1.4×10^{-1}	1.8×10^{-1}	1.8×10^{-1}
2.8×10^{-1}	9.8×10^{-3}	5.6×10^{-2}	6.0×10^{-2}
1.4×10^{-1}	3.6×10^{-2}	1.2×10^{-2}	1.6×10^{-2}
7.0×10^{-2}	5.0×10^{-2}	7.8×10^{-4}	3.8×10^{-3}
3.5×10^{-2}	5.7×10^{-2}	6.6×10^{-3}	7.0×10^{-3}

Table 3.2: Numerical illustration of the accuracy of the asymptotic constant (3.92).

Now we discuss how well the constant (3.92) approximates the actual asymptotic constant. In order to estimate the closeness of the two constants, we have computed $\|e_h\|_{L_2([h_+,1])}$ on a sequence of uniform meshes characterised by decreasing values of the ratio h/h_+ , with $h_+ = 10^{-1}, 10^{-2}, 10^{-3}$, (recall that for $h/h_+ \ll 1$ we expect $\|e_h\|_{L_2([h_+,1])}$ to have the expression (3.91)) and for each grid we have calculated the quantity:

$$\Lambda := \left| \frac{N^3 \|e_h\|_{L_2([h_+,1])} - c(h_+)}{c(h_+)} \right| .$$

The results, given in Table 3.2, show that $c(h_+)$ represents a very good approximation to the actual asymptotic constant even for relatively big values of the parameter h/h_+ . In fact, for $h/h_+ = 1.4 \times 10^{-1}$ we have that $\Lambda = O(10^{-2})$ for all values of h_+ considered.

3.6.2 Alternative derivation of the optimal mesh for approximating $f(y) = 1/y$

In this subsection we return to the case $m = 0, p = 1, k = 2$ and describe an alternative derivation for (3.76), which shows that it can be obtained by requiring that the error identity (3.87) be minimized with respect to variations in the mesh points. This is consistent with the fact that (3.87) is an expression for the interpolation error valid on grids satisfying the condition (3.86), which is a property of the mesh (3.76), as shown in Lemma 3.5.1.

Corollary 3.6.5. *The interpolation error (3.87) is minimal with respect to variations in the grid points on the mesh (3.76):*

$$y_i = h_+ \left(1 - \frac{i-1}{N} \left(1 - h_+^{1/7} \right) \right)^{-7} \quad i = 1, 2, \dots, N+1, \quad (3.96)$$

3.6. Close-up of the approximation of $f(y) = 1/y$

where it has the approximate expression

$$\|e\|_{L_2([h_+,1])} \approx \frac{7^{7/2}}{\sqrt{840}} \left(1 - h_+^{1/7}\right)^{7/2} \frac{h_+^{-1/2}}{N^3} . \quad (3.97)$$

Proof. Let the mesh $\Pi : h_+ = y_1 < y_2 < \dots < y_{N+1} = 1$, have the property (3.86) and be the image of a uniform mesh of the domain $[0, 1]$ through a mapping g in the space

$$S = \{\eta \in C^2([0, 1]) : \eta(0) = h_+, \eta(1) = 1\} .$$

Let $\Delta t := t_{i+1} - t_i = 1/N$ be the size of the uniform grid of $[0, 1]$, then, using Taylor expansion, we have that:

$$\begin{aligned} h_i &= y_{i+1} - y_i = g(t_{i+1}) - g(t_i) \\ &= \frac{1}{N} g'(t_i) \left(1 + O\left(\frac{1}{N}\right)\right) , \end{aligned}$$

and also, for all $n \in \mathbb{N}$,

$$\begin{aligned} \alpha_i^n &= \left(\frac{h_i}{y_i}\right)^n = \left[\frac{1}{N} \frac{g'(t_i)}{g(t_i)} \left(1 + O\left(\frac{1}{N}\right)\right)\right]^n \\ &= \frac{1}{N^n} \left(\frac{g'(t_i)}{g(t_i)}\right)^n \left(1 + O\left(\frac{1}{N}\right)\right) . \end{aligned}$$

Therefore (3.87) can be written as

$$\begin{aligned} \|e\|_{L_2([h_+,1])}^2 &= \frac{1}{840} \sum_{i=1}^N \frac{1}{y_i} (\alpha_i^7 + O(\alpha_i^8)) \\ &= \frac{1}{840} \sum_{i=1}^N \frac{(g'(t_j))^7}{(g(t_j))^8} \frac{1}{N^7} \left(1 + O\left(\frac{1}{N}\right)\right) \\ &\approx \frac{1}{840} \frac{1}{N^6} \int_0^1 \frac{(g'(t))^7}{(g(t))^8} dt . \end{aligned} \quad (3.98)$$

Hence $\|e_h\|_{L_2([h_+,1])}$ is minimal with respect to variations in the mesh points if and only if the functional:

$$I(g, g') := \int_0^1 \frac{(g'(t))^7}{(g(t))^8} dt \quad (3.99)$$

is minimal. Since the functional I does not depend explicitly on the independent variable t , it can be shown that a first order differential equation for its extremals is given by:

$$(g'(t))^7 = \text{const } (g(t))^8 ,$$

3.7. Numerical tests for the accuracy and practicality of the mesh

(see Theorem 2.3.1 p. 38 of [45]). This has the solution

$$g(t) = h_+ \left(1 - t \left(1 - h_+^{1/7} \right) \right)^{-7}, \quad (3.100)$$

which satisfies $g(0) = 0$, $g(1) = 1$. It can be proved that (3.100) is a weak minimizer of the functional (3.99) (see Theorem 10.5.1 p. 242 of [45]). The mapping (3.100) generates the mesh (3.96) and by substituting it into (3.98), we finally obtain:

$$\|e\|_{L_2([h_+,1])}^2 \approx \frac{7^7}{840} \left(1 - h_+^{1/7} \right)^7 \frac{h_+^{-1}}{N^6},$$

from which (3.97) follows. □

3.7 Numerical tests for the accuracy and practicality of the mesh

We now assess the practical utility of the equidistributed mesh (3.76), especially for small values of h_+ . We will pursue this comparing the solution to the 1D Couette flow (2.48)-(2.56) obtained on the mesh (3.76) with the solution computed on uniform and “ad hoc” exponentially graded meshes (the properties of the latter family of meshes will be discussed in §3.7.2 below). Numerical experiments will be carried out also for the 2D Couette flow, presented in §2.1. In this case we will consider the tensor product of meshes obtained by using (3.76) in the y -direction and a uniform mesh in the x -direction.

We recall that in 2D, each component of the velocity field $\mathbf{u} := (U, V)$ and the turbulence variables k, ε will be approximated by continuous piecewise biquadratic polynomials while the pressure p will be approximated by a discontinuous piecewise linear polynomial. Correspondingly, in 1D we will approximate U and (k, ε) using continuous piecewise quadratic polynomials. Both in 1D and in 2D the nonlinear finite element system will be solved by Newton’s method (see §4.1 for a description of the algorithm), this will be initialized by the finite element interpolant of the analytical solution (which is available for Couette flow).

In our numerical experiments the Reynolds number will be equal to 10^7 , therefore considering values of h_+ as small as 10^{-4} will make sense from the point of view of turbulence modelling.

3.7.1 Equidistributed mesh vs. uniform mesh

We now compare the numerical solutions to the Couette flow computed on the equidistributed mesh (3.76):

$$y_i = h_+ \left(1 - \frac{i-1}{N} \left(1 - h_+^{1/7} \right) \right)^{-7}, \quad i = 1, 2, \dots, N+1 \quad (3.101)$$

and on the uniform mesh:

$$y_i = h_+ + (i-1) \frac{1-h_+}{N}, \quad i = 1, 2, \dots, N+1 \quad (3.102)$$

3.7. Numerical tests for the accuracy and practicality of the mesh

Below we present the relative error in the solution to the 1D turbulent Couette flow obtained on the meshes above with $N = 16$ and $N = 128$, for a sequence of decreasing values of h_+ .

		MESH (16 ELEMENTS)		MESH (128 ELEMENTS)	
h_+	RELATIVE ERROR	EQUIDISTR.	UNIFORM	EQUIDISTR.	UNIFORM
10^{-1}	$\ U^h - U^*\ _2 / \ U^*\ _2$	9.52×10^{-7}	1.54×10^{-5}	2.35×10^{-10}	4.50×10^{-9}
	$\ k^h - k^*\ _2 / \ k^*\ _2$	9.80×10^{-6}	5.20×10^{-4}	2.39×10^{-9}	1.65×10^{-7}
	$\ \varepsilon^h - \varepsilon^*\ _2 / \ \varepsilon^*\ _2$	1.79×10^{-5}	9.89×10^{-4}	4.34×10^{-9}	2.42×10^{-7}
10^{-2}	$\ U^h - U^*\ _2 / \ U^*\ _2$	2.59×10^{-5}	1.39×10^{-2}	6.46×10^{-9}	5.93×10^{-5}
	$\ k^h - k^*\ _2 / \ k^*\ _2$	1.24×10^{-4}	1.50×10^{-1}	3.23×10^{-8}	1.19×10^{-3}
	$\ \varepsilon^h - \varepsilon^*\ _2 / \ \varepsilon^*\ _2$	1.14×10^{-4}	5.11×10^{-1}	2.74×10^{-8}	2.91×10^{-3}
10^{-3}	$\ U^h - U^*\ _2 / \ U^*\ _2$	2.34×10^{-4}	∞	5.87×10^{-8}	9.52×10^{-3}
	$\ k^h - k^*\ _2 / \ k^*\ _2$	7.77×10^{-4}	∞	2.29×10^{-7}	1.21×10^{-1}
	$\ \varepsilon^h - \varepsilon^*\ _2 / \ \varepsilon^*\ _2$	1.76×10^{-4}	∞	4.52×10^{-8}	5.83×10^{-1}
10^{-4}	$\ U^h - U^*\ _2 / \ U^*\ _2$	1.60×10^{-3}	∞	3.80×10^{-7}	∞
	$\ k^h - k^*\ _2 / \ k^*\ _2$	4.02×10^{-3}	∞	1.27×10^{-6}	∞
	$\ \varepsilon^h - \varepsilon^*\ _2 / \ \varepsilon^*\ _2$	3.40×10^{-3}	∞	7.57×10^{-7}	∞

Table 3.3: Relative error in the numerical solution of the 1D Couette flow for a sequence of decreasing values of h_+ , obtained on the equidistributed mesh (3.101), with 16 and 128 elements, and on the corresponding uniform grid. (∞ indicates that Newton's method has failed to converge).

From the results given in Table 3.3 it is clear that the equidistributed mesh (3.101) is by far superior to the uniform mesh (3.102), where the solution deteriorates much more dramatically as h_+ is reduced. On the equidistributed mesh, in particular, it is possible to achieve a satisfactory accuracy even for a fairly small number of elements. In fact, on the mesh (3.101) with just 16 elements, when $h_+ = 10^{-2}$ the relative error both in k and in ε is $O(10^{-4})$ and is $O(10^{-5})$ in U , and when $h_+ = 10^{-4}$ the error in each solution component is also small, $O(10^{-3})$. On the corresponding uniform mesh Newton's method fails to converge already for $h_+ = 10^{-3}$ and when convergence is attained, for $h_+ = 10^{-1}$ and $h_+ = 10^{-2}$, the solution is respectively two and three order of magnitudes less accurate than the one obtained on the equidistributed mesh.

When the number of elements is equal to 128, Newton's method attains convergence on the mesh (3.102) when $h_+ = 10^{-3}$, but the relative errors in the solution components k and ε are big approximately equal to 0.1 and 0.6 respectively. On the corresponding equidistributed mesh the relative error both in k and in ε is $O(10^{-8})$. Also for $h_+ = 10^{-2}$, the solution for k and ε is five order of magnitudes more accurate on the equidistributed mesh than on the

3.7. Numerical tests for the accuracy and practicality of the mesh

uniform mesh.

		MESH (20 × 16 ELEMENTS)		MESH (20 × 128 ELEMENTS)	
h_+	RELATIVE ERROR	EQUIDISTR.	UNIFORM	EQUIDISTR.	UNIFORM
10^{-1}	$\ U^h - U^*\ _2 / \ U^*\ _2$	3.88×10^{-6}	2.40×10^{-5}	2.53×10^{-8}	4.94×10^{-8}
	$\ k^h - k^*\ _2 / \ k^*\ _2$	7.28×10^{-6}	4.95×10^{-4}	1.63×10^{-7}	1.57×10^{-8}
	$\ \varepsilon^h - \varepsilon^*\ _2 / \ \varepsilon^*\ _2$	8.53×10^{-5}	1.76×10^{-3}	1.92×10^{-7}	4.30×10^{-6}
10^{-2}	$\ U^h - U^*\ _2 / \ U^*\ _2$	5.05×10^{-5}	1.15×10^{-2}	1.08×10^{-7}	6.06×10^{-5}
	$\ k^h - k^*\ _2 / \ k^*\ _2$	1.54×10^{-4}	1.40×10^{-1}	1.43×10^{-7}	1.18×10^{-3}
	$\ \varepsilon^h - \varepsilon^*\ _2 / \ \varepsilon^*\ _2$	5.18×10^{-4}	4.01×10^{-1}	1.13×10^{-6}	4.03×10^{-3}
10^{-3}	$\ U^h - U^*\ _2 / \ U^*\ _2$	2.96×10^{-4}	∞	6.36×10^{-7}	9.13×10^{-3}
	$\ k^h - k^*\ _2 / \ k^*\ _2$	1.43×10^{-3}	∞	3.17×10^{-7}	1.20×10^{-1}
	$\ \varepsilon^h - \varepsilon^*\ _2 / \ \varepsilon^*\ _2$	8.65×10^{-4}	∞	5.12×10^{-6}	5.67×10^{-1}
10^{-4}	$\ U^h - U^*\ _2 / \ U^*\ _2$	1.38×10^{-3}	∞	3.30×10^{-6}	∞
	$\ k^h - k^*\ _2 / \ k^*\ _2$	8.50×10^{-3}	∞	7.91×10^{-6}	∞
	$\ \varepsilon^h - \varepsilon^*\ _2 / \ \varepsilon^*\ _2$	3.26×10^{-3}	∞	6.47×10^{-6}	∞

Table 3.4: Relative error in the numerical solution of the 2D Couette flow at the outlet of the channel for a sequence of decreasing values of h_+ . (∞ indicates that Newton's method has failed to converge).

In Table 3.4 we give the relative errors in the U -, k -, ε -solution components of the 2D Couette flow at the outlet of the channel. We compare the results obtained on uniform meshes with those arising on meshes given by the combination of a uniform mesh in the x -direction with the mesh (3.102) in the y -direction.

The errors $\|V^h - V^*\|_2$, $\|p^h - p^*\|_2$ do not appear in Table 3.4, because, if Newton's method attains convergence, they are very small, of order machine epsilon, independently of the mesh.

The qualitative observations made earlier in the case of the 1D turbulent Couette flow hold true for the 2D formulation of the problem. Similarly to the 1D results, the use of the equidistributed mesh (3.101) in the y -direction gives a satisfactorily accurate solution for small values of h_+ , even in the case of a small number of elements. On the contrary, for a uniform discretisation of the channel with 20×16 elements Newton's method does not converge already when $h_+ = 10^{-3}$. On the uniform mesh with 20×128 elements, Newton's method does attain convergence for $h_+ = 10^{-3}$, but, similarly to the 1D case, the quality of the solution is much worse than in the case when the mesh (3.101) is used in the y -direction. Already for $h_+ = 10^{-2}$ the accuracy of the k - and ε -solution components is approximately three order of magnitudes worse on the uniform mesh.

3.7. Numerical tests for the accuracy and practicality of the mesh

It should also be noted that Table 3.3 and Table 3.4 clearly indicate that in the case of a uniform mesh the convergence of Newton's method depends on h_+ and the algorithm becomes more robust, with respect to small values of h_+ , as the number of elements is increased. On the other hand, when the equidistributed mesh is used the convergence of Newton's method does not appear to depend on h_+ and the algorithm seems to be equally robust with respect to small values of h_+ when 16 or 126 elements are used. We will investigate and explain this behaviour in Chapter 5.

3.7.2 Equidistributed mesh vs. exponentially graded mesh

The performances of the equidistributed mesh (3.101) are now compared with those of an exponentially graded mesh, whose features are described below. Exponentially graded meshes are implemented in the industrial finite element code ENTWIFE.

Properties of exponentially graded meshes

The mesh $h_+ = y_1 < y_2 < \dots < y_{N+1} = 1$ is said to be *exponentially graded* if the ratio of the sizes of its adjacent elements does not vary throughout the domain. Hence, if $h_i := y_{i+1} - y_i$ denotes the size of the i -th element, we must have:

$$\alpha := \frac{h_{i+1}}{h_i} = \text{constant} \quad i = 1, 2, \dots, N \quad (3.103)$$

and α is independent of i . From (3.103) it is easy to obtain:

$$h_{i+1} = \alpha^i h_1, \quad i = 1, 2, \dots, N \quad (3.104)$$

which shows that the grid is exponentially expanding towards one of the two end points of the domain. Now, combining (3.104) with the fact that

$$y_1 = h_+, \quad y_i = h_+ + \sum_{j=1}^{i-1} h_j \quad i = 2, 3, \dots, N+1,$$

it is not difficult to see that the nodes of an equidistributed mesh are distributed according to the rule:

$$y_i = h_+ + \frac{\alpha^{i-1} - 1}{\alpha - 1} h_1 \quad i = 1, 2, \dots, N+1. \quad (3.105)$$

The size of the first element h_1 is related to α , N and the size of the domain, through the formula:

$$h_1 = \frac{\alpha - 1}{\alpha^N - 1} (1 - h_+), \quad (3.106)$$

which can be obtained by using (3.104) in $\sum_{i=1}^N h_i = 1 - h_+$ (or equivalently imposing that $y_{N+1} = 1$ in (3.105)). Substituting (3.106) into (3.105), we finally get:

3.7. Numerical tests for the accuracy and practicality of the mesh

$$y_i = h_+ + \frac{\alpha^{i-1} - 1}{\alpha^N - 1}(1 - h_+), \quad i = 1, 2, \dots, N + 1. \quad (3.107)$$

In our numerical experiments, we have determined the distribution of mesh points (3.107) by prescribing directly α and N , another possibility could be to assign the values of h_+ and N and then to compute α from (3.106). For given number of elements and h_+ , the value of α has been chosen “ad hoc” to minimize $\|\varepsilon^h - \varepsilon^*\|_2$. In more general situations, when the analytical solution to the problem being solved is not available, identifying the appropriate value of α is not an easy task and in Table 3.7 we will show that even a small perturbation to α can cause Newton’s method to diverge.

		MESH (16 ELEMENTS)		MESH (128 ELEMENTS)	
h_+	RELATIVE ERROR	EQUIDISTR.	EXPONENTIAL	EQUIDISTR.	EXPONENTIAL
10^{-1}	$\ U^h - U^*\ _2 / \ U^*\ _2$	9.52×10^{-7}	9.29×10^{-7}	2.35×10^{-10}	2.46×10^{-10}
	$\ k^h - k^*\ _2 / \ k^*\ _2$	9.80×10^{-6}	9.47×10^{-6}	2.39×10^{-9}	2.33×10^{-9}
	$\ \varepsilon^h - \varepsilon^*\ _2 / \ \varepsilon^*\ _2$	1.79×10^{-5}	1.85×10^{-5}	4.34×10^{-9}	4.44×10^{-9}
10^{-2}	$\ U^h - U^*\ _2 / \ U^*\ _2$	2.59×10^{-5}	2.87×10^{-5}	6.46×10^{-9}	6.81×10^{-9}
	$\ k^h - k^*\ _2 / \ k^*\ _2$	1.24×10^{-4}	1.18×10^{-4}	3.23×10^{-8}	2.93×10^{-8}
	$\ \varepsilon^h - \varepsilon^*\ _2 / \ \varepsilon^*\ _2$	1.14×10^{-4}	1.30×10^{-4}	2.74×10^{-8}	3.28×10^{-8}
10^{-3}	$\ U^h - U^*\ _2 / \ U^*\ _2$	2.34×10^{-4}	1.88×10^{-4}	5.87×10^{-8}	5.15×10^{-8}
	$\ k^h - k^*\ _2 / \ k^*\ _2$	7.77×10^{-4}	5.27×10^{-4}	2.29×10^{-7}	1.56×10^{-7}
	$\ \varepsilon^h - \varepsilon^*\ _2 / \ \varepsilon^*\ _2$	1.76×10^{-4}	2.49×10^{-4}	4.52×10^{-8}	6.69×10^{-8}
10^{-4}	$\ U^h - U^*\ _2 / \ U^*\ _2$	1.60×10^{-3}	4.37×10^{-4}	3.80×10^{-7}	1.16×10^{-7}
	$\ k^h - k^*\ _2 / \ k^*\ _2$	4.02×10^{-3}	1.11×10^{-3}	1.27×10^{-6}	3.29×10^{-7}
	$\ \varepsilon^h - \varepsilon^*\ _2 / \ \varepsilon^*\ _2$	3.40×10^{-3}	4.93×10^{-4}	7.57×10^{-7}	1.37×10^{-7}

Table 3.5: Relative error in the numerical solution of the 1D Couette flow for a sequence of decreasing values of h_+ , obtained on the equidistributed mesh (3.101), with 16 and 128 elements, and on the corresponding exponentially graded mesh (3.105), with α chosen to minimize $\|\varepsilon^h - \varepsilon^*\|$.

In Table 3.5 we present the relative error in the solution to the 1D turbulent Couette flow obtained on the meshes (3.101) and (3.105) with 16 and 128 elements, for increasingly smaller values of h_+ .

The numerical experiments show that the solution on the equidistributed mesh is of the same quality as the solution on the “ad hoc” exponentially graded mesh. The only appreciable difference between the two solutions occurs for $h_+ = 10^{-4}$ and $N = 16$, when the relative error in ε on the mesh (3.105) is nearly one order of magnitude smaller than on the mesh (3.101).

3.7. Numerical tests for the accuracy and practicality of the mesh

When $N = 126$ the relative errors are very small on both meshes for all values of h_+ and no important differences can be noticed.

		MESH (20 × 16 ELEMENTS)		MESH (20 × 64 ELEMENTS)	
h_+	RELATIVE ERROR	EQUIDISTR.	EXPONENTIAL	EQUIDISTR.	EXPONENTIAL
10^{-1}	$\ U^h - U^*\ _2 / \ U^*\ _2$	3.88×10^{-6}	4.36×10^{-6}	6.64×10^{-8}	5.71×10^{-8}
	$\ k^h - k^*\ _2 / \ k^*\ _2$	7.28×10^{-6}	7.38×10^{-6}	1.49×10^{-7}	1.45×10^{-7}
	$\ \varepsilon^h - \varepsilon^*\ _2 / \ \varepsilon^*\ _2$	8.53×10^{-5}	9.04×10^{-5}	1.36×10^{-6}	1.32×10^{-6}
10^{-2}	$\ U^h - U^*\ _2 / \ U^*\ _2$	5.05×10^{-5}	3.14×10^{-5}	8.08×10^{-7}	5.85×10^{-7}
	$\ k^h - k^*\ _2 / \ k^*\ _2$	1.54×10^{-4}	7.23×10^{-5}	7.18×10^{-7}	4.07×10^{-7}
	$\ \varepsilon^h - \varepsilon^*\ _2 / \ \varepsilon^*\ _2$	5.18×10^{-4}	5.78×10^{-4}	8.39×10^{-6}	9.55×10^{-6}
10^{-3}	$\ U^h - U^*\ _2 / \ U^*\ _2$	2.96×10^{-4}	9.54×10^{-5}	4.74×10^{-6}	1.15×10^{-6}
	$\ k^h - k^*\ _2 / \ k^*\ _2$	1.43×10^{-3}	2.85×10^{-4}	7.42×10^{-6}	5.27×10^{-6}
	$\ \varepsilon^h - \varepsilon^*\ _2 / \ \varepsilon^*\ _2$	8.65×10^{-4}	1.08×10^{-3}	1.38×10^{-5}	1.81×10^{-5}
10^{-4}	$\ U^h - U^*\ _2 / \ U^*\ _2$	1.38×10^{-3}	2.95×10^{-4}	2.02×10^{-5}	8.04×10^{-6}
	$\ k^h - k^*\ _2 / \ k^*\ _2$	8.50×10^{-3}	1.65×10^{-3}	5.06×10^{-5}	2.77×10^{-5}
	$\ \varepsilon^h - \varepsilon^*\ _2 / \ \varepsilon^*\ _2$	3.26×10^{-3}	3.11×10^{-4}	4.08×10^{-5}	4.85×10^{-5}

Table 3.6: Relative error in the numerical solution of the 2D Couette flow at the outlet of the channel for a sequence of decreasing values of h_+ .

The relative errors in U , k and ε obtained at the outlet of the channel, in the 2D formulation of the Couette flow, are given in Table 3.6. Similarly to before, the channel has been discretised using the grids given by the tensor product of a uniform mesh in the x -direction (with 20 elements) respectively with the mesh (3.101) and (3.105) in the y -direction, for $N = 16$ and $N = 64$.

The 2D numerical experiments confirm the results obtained in the 1D version of the Couette flow. There is no significant difference between the solutions obtained on the two grids a part from the case $h_+ = 10^{-4}$, $N = 16$, when the relative error on the mesh exponentially graded in the y -direction is one order of magnitude lower. This difference, anyway, already disappears when $N = 64$.

Finally, in Table 3.7, we investigate the sensitivity to α (see (3.105)) of the results obtained on the exponentially graded mesh (we recall that, for given h_+ and N , the values of the relative errors presented in Table 3.5 and in Table 3.6, were obtained on meshes for which α was chosen “ad hoc” to minimize $\|\varepsilon^h - \varepsilon^*\|_2$). This will be done by assessing the quality of the solution to the Couette flow on “non optimal” exponentially graded meshes, generated by perturbing the “optimal” values of α in the 1D meshes used to produce the results given in Table 3.5. More

3.7. Numerical tests for the accuracy and practicality of the mesh

		MESH (16 ELEMENTS)		MESH (128 ELEMENTS)	
h_+	RELATIVE ERROR	EQUIDISTR.	EXPONENTIAL (NON OPTIMAL)	EQUIDISTR.	EXPONENTIAL (NON OPTIMAL)
10^{-1}	$\ U^h - U^*\ _2 / \ U^*\ _2$	9.52×10^{-7}	2.90×10^{-4}	2.35×10^{-10}	∞
	$\ k^h - k^*\ _2 / \ k^*\ _2$	9.80×10^{-6}	1.48×10^{-3}	2.39×10^{-9}	∞
	$\ \varepsilon^h - \varepsilon^*\ _2 / \ \varepsilon^*\ _2$	1.79×10^{-5}	2.02×10^{-3}	4.34×10^{-9}	∞
10^{-2}	$\ U^h - U^*\ _2 / \ U^*\ _2$	2.59×10^{-5}	1.97×10^{-3}	6.46×10^{-9}	∞
	$\ k^h - k^*\ _2 / \ k^*\ _2$	1.24×10^{-4}	3.72×10^{-3}	3.23×10^{-8}	∞
	$\ \varepsilon^h - \varepsilon^*\ _2 / \ \varepsilon^*\ _2$	1.14×10^{-4}	2.05×10^{-3}	2.74×10^{-8}	∞
10^{-3}	$\ U^h - U^*\ _2 / \ U^*\ _2$	2.34×10^{-4}	6.17×10^{-3}	5.87×10^{-8}	∞
	$\ k^h - k^*\ _2 / \ k^*\ _2$	7.77×10^{-4}	8.17×10^{-3}	2.29×10^{-7}	∞
	$\ \varepsilon^h - \varepsilon^*\ _2 / \ \varepsilon^*\ _2$	1.76×10^{-4}	5.78×10^{-3}	4.52×10^{-8}	∞
10^{-4}	$\ U^h - U^*\ _2 / \ U^*\ _2$	1.60×10^{-3}	1.11×10^{-2}	3.80×10^{-7}	∞
	$\ k^h - k^*\ _2 / \ k^*\ _2$	4.02×10^{-3}	1.71×10^{-2}	1.27×10^{-6}	∞
	$\ \varepsilon^h - \varepsilon^*\ _2 / \ \varepsilon^*\ _2$	3.40×10^{-3}	2.18×10^{-2}	7.57×10^{-7}	∞

Table 3.7: Relative error in the numerical solution of the 1D Couette flow for a sequence of decreasing values of h_+ , obtained on the equidistributed mesh (3.101), with 16 and 128 elements, and on the corresponding “non optimal” exponentially graded mesh

specifically, the values of α will be doubled when $N = 16$ and will be changed into $(5/4)\alpha$ for $N = 128$. The results presented in Table 3.7 show a clear deterioration in the quality of the solution on the “non optimal” exponentially graded mesh. In fact, for $N = 16$ the relative errors on the exponential mesh are now much bigger than on the corresponding equidistributed mesh, especially for $h_+ = 10^{-1}, 10^{-2}$ (compare with Table 3.7), and, even more dramatically, when $N = 128$, a perturbation to α as small as $\alpha/4$, prevents Newton’s method from converging for all values of h_+ considered. Such a high sensitivity to α clearly represents a big obstacle to the successful use of exponentially graded meshes in practical computations of the k - ε model. The equidistributed grid, instead, does not require any parameter to be tuned as h_+ varies and has also a mathematical certainty which is useful to us later when considering the robustness of Newton’s method.

Chapter 4

Affine invariant properties of Newton's method

In this chapter we discuss some abstract results on the convergence theory for Newton's iterative method which will be exploited in Chapter 5, where the properties of the iterative scheme applied to the k - ε model will be investigated.

There are two possible approaches to the convergence analysis of Newton's method: "the local theory" and the "semilocal theory". Both provide sufficient conditions for convergence. In the local theory the existence of a solution to the nonlinear operator equation is assumed and also the initial guess is assumed to be sufficiently close to this solution. The semilocal theory, instead, requires only that some conditions hold at the initial guess and these then guarantee both the existence of a solution and the convergence of the method to it. The literature on Newton's method is extremely vast, a detailed treatment of the local theory can be found in [52], [53] and [54], while the semilocal theory is illustrated in [55], [56], [57] and [58]. The relation between the two theories is investigated in [59].

In this chapter and the next, we will base our study on the local convergence theory. The local theory, in fact, allows a more intuitive picture of the problem under investigation and, as will be shown in the following, describes the key feature of Newton's method in practical applications: the quadratic reduction in the error at each iteration. The Newton-Kantorovich theorem, which is at the heart of the semilocal theory, cannot predict the same quadratic reduction in the error due to the weaker assumptions it relies on.

This chapter initially deals with an overview of the local convergence analysis of Newton's method (§4.1), whose invariance under affine covariant and affine contravariant transformations of the underlying nonlinear operator equation is discussed in §4.2 and §4.3 respectively (both transformations will be needed in the analysis of Newton's method for the k - ε model in Chapter 5). In §4.4 it will be shown that the classical local convergence theory lacks the affine invariant properties that the method itself has and, in §4.5, we will propose a possible way to overcome this difficulty when an affine covariant and an affine contravariant transformation are considered simultaneously.

In [58], the invariance of Newton's method under four affine transformations has been

4.1. Local convergence theory of Newton's method

investigated and four different convergence theories, each reflecting one of the affine invariant properties of the iterative scheme, have been proposed in the framework of the semilocal theory. (Note that the theory we refer to as semilocal is called in [58] “local” in order to distinguish it from the “global” theory of Newton’s method, where no conditions on the initial guess are required, but additional “global structure” of the nonlinear operator is assumed). However in [58] the case when affine covariant and contravariant transformations are applied at the same time is not covered. It turns out that such combination is beneficial in the analysis of the k - ε system. As far as we are aware, there is no convergence theory for Newton’s method which is at the same time invariant under covariant and contravariant transformation.

In the following sections the abstract study of the convergence properties of Newton’s method will be carried out in Banach spaces. In Chapter 5, the practical applications of this study will be discussed in the particular case of \mathbb{R}^n .

4.1 Local convergence theory of Newton's method

Throughout this chapter, we will consider a nonlinear operator equation of the form

$$F(x) = 0 \tag{4.1}$$

where $F : D \subset X \rightarrow Y$ is a nonlinear mapping, defined on a open convex domain D of a Banach space X with values in a Banach space Y . (In the following, $\|\cdot\|$ will denote both the norm on X and on Y and also the corresponding operator norm for bounded linear operators from X to Y . It should be clear from the context which norm is being used).

The main computational tool to solve systems like (4.1) with a solution x^* is *Newton's method*:

$$x^{k+1} = x^k - F'(x^k)^{-1}F(x^k) \quad k = 0, 1, \dots \tag{4.2}$$

which, under appropriate conditions (that will be examined below), produces a sequence $\{x^k\}_{k=0}^{\infty}$ converging to x^* . In (4.2) $F'(x^k)$ denotes the Fréchet derivative of the nonlinear operator F at the point x^k . At each step of Newton’s method the linear equation

$$F(x^k) + F'(x^k)s^k = 0 \tag{4.3}$$

must be solved for s^k , and the new approximation to x^* is given by

$$x^{k+1} = x^k + s^k .$$

This iterative scheme is based on a linearisation of the equation (4.1) at the current iterate x^k . A way to show this is to consider the equation satisfied by the error $h := x^* - x^k$. If the operator F is differentiable, we have

4.1. Local convergence theory of Newton's method

$$\begin{aligned} 0 &= F(x^*) = F(x^k + h) \\ &= F(x^k) + F'(x^k)h + \zeta , \end{aligned} \quad (4.4)$$

where, if F is sufficiently smooth, $\|\zeta\| = o(\|h\|)$. (In fact if F' is Lipschitz continuous in a neighbourhood of x^k , then, as it can be seen from Lemma 4.1.1 (a), $\|\zeta\| = O(\|h\|^2)$). The result (4.4) suggests that, under appropriate conditions on F' , $\{x^k\}$ may converge quadratically to x^* (see Theorem 4.1.2). Then, comparing (4.4) with (4.3), it becomes clear that (4.3) is a linearisation procedure for the operator F around x^k .

We finally observe that (4.2) can be interpreted as a fixed point iteration:

$$x^{k+1} = H(x^k) ,$$

with the fixed point map H given by the Newton iteration operator:

$$H(x) = x - F(x)^{-1}F(x) . \quad (4.5)$$

Some properties of the operator H will be exploited in the convergence analysis of Newton's method below.

If V is a subset of the Banach space X , then, in what follows, we will write $G \in \text{Lip}_\gamma(V)$ if the mapping G is Lipschitz continuous with constant γ in the set V :

$$\|G(y) - G(x)\| \leq \gamma\|y - x\| \quad \forall x, y \in V ,$$

while $B(\bar{x}, r)$ will denote the open ball of radius r centered at \bar{x} :

$$B(\bar{x}, r) = \{x \in X \mid \|x - \bar{x}\| < r\} .$$

We now state, without giving the proof, a Lemma which will be needed in Theorem 4.1.2, where we will present sufficient conditions for the local convergence of Newton's method. (The proof of (a) in Lemma 4.1.1 can be found in [55], p. 73, while (b) is a consequence of the Banach perturbation lemma, see [60], pp. 266-267.).

Lemma 4.1.1. *Let $F : D \subset X \rightarrow Y$ be continuously differentiable in $B(\bar{x}, r) \subset D$. Assume*

- (i) $F' \in \text{Lip}_\gamma(B(\bar{x}, r))$,
- (ii) $F'(\bar{x})$ is nonsingular, with $\|F'(\bar{x})^{-1}\| \leq \beta$.

Then

$$(a) \quad \|F(y) - F(x) - F'(x)(y - x)\| \leq \frac{\gamma}{2}\|y - x\|^2 \quad \forall x, y \in B(\bar{x}, r) ,$$

4.1. Local convergence theory of Newton's method

(b) $F'(x)$ is nonsingular and

$$\|F'(x)^{-1}\| \leq \frac{\beta}{1 - \beta\gamma\|x - \bar{x}\|} \quad \forall x \in B(\bar{x}, \bar{\delta}),$$

$$\text{with } \bar{\delta} = \min \left\{ r, \frac{1}{\beta\gamma} \right\}.$$

The theorem below establishes sufficient conditions for Newton's method to converge quadratically to a solution of (4.1).

Theorem 4.1.2. *Suppose there exists $x^* \in D$ such that $F(x^*) = 0$, and suppose the conditions of Lemma 4.1.1 are satisfied at $\bar{x} = x^*$. Set $\delta = \min \{r, 2/(3\beta\gamma)\} \leq \bar{\delta}$, with $\bar{\delta}$ defined in Lemma 4.1.1. Then, provided the starting guess x^0 satisfies $x^0 \in B(x^*, \delta)$, we have:*

(A) *the sequence $\{x^k\}$ of Newton iterates generated by (4.2) is well defined, remains in $B(x^*, \delta)$ and converges to x^* ,*

(B) *the rate of convergence of $\{x^k\}$ to x^* is q -quadratic, i.e. there exists $K > 0$ such that:*

$$\|x^{k+1} - x^*\| < K\|x^k - x^*\|^2, \quad (4.6)$$

$$\text{and } K = \frac{3}{2}\beta\gamma,$$

(C) *the following error estimate holds*

$$\|x^{k+1} - x^*\| \leq \frac{2}{3\beta\gamma} \left(\frac{3}{2}\beta\gamma\|x^0 - x^*\| \right)^{2^{k+1}}, \quad k = 1, 2, \dots \quad (4.7)$$

In Theorem 4.1.2, the radius δ of the ball $B(x^*, \delta)$, represents an estimate from below of the actual ball of convergence of Newton's method. The symbol ε is often used instead of δ , but we use δ here since, in this thesis, ε indicates the dissipation of mean turbulent kinetic energy, as described in other chapters.

The above estimate of δ , was obtained by Rheinbodt in [61]. The following proof of Theorem 4.1.2 uses some of the arguments of Rheinbodt [61] and some of the arguments of Dennis and Schnabel [53], whose proof yields an estimate for δ which is slightly smaller than the one given in [61].

Proof of Theorem 4.1.2 We will first prove the following two statements:

(i) $F'(x)^{-1}$ is well defined for all $x \in B(x^*, \delta)$, and

$$\|F'(x)^{-1}\| \leq \frac{\beta}{1 - \beta\gamma\|x - x^*\|} < 3\beta \quad \forall x \in B(x^*, \delta) \quad (4.8)$$

(ii) the Newton iteration operator (4.5):

$$H(x) = x - F'(x)^{-1}F(x)$$

4.1. Local convergence theory of Newton's method

is well defined for all $x \in B(x^*, \delta)$ and satisfies

$$\|H(x) - x^*\| \leq \alpha \|x - x^*\| < \|x - x^*\| \quad \forall x \in B(x^*, \delta) \quad (4.9)$$

with

$$\alpha = \frac{1}{2} \frac{\beta\gamma \|x - x^*\|}{1 - \beta\gamma \|x - x^*\|} < 1 .$$

We prove (i). The nonsingularity of $F'(x)$ in $B(x^*, \delta)$ and the first inequality in (4.8) are implied by Lemma 4.1.1 (b). The second inequality in (4.8) follows from the observation that

$$1 - \beta\gamma \|x - x^*\| > 1 - \beta\gamma\delta \geq 1 - \frac{2}{3} = \frac{1}{3} .$$

We next prove (ii). The Newton iteration operator H is well defined for $x \in B(x^*, \delta)$, since, from (i), $F'(x)$ is nonsingular in $B(x^*, \delta)$. (4.9) is now shown. Let $x \in B(x^*, \delta)$, using also Lemma 4.1.1, we get:

$$\begin{aligned} \|H(x) - x^*\| &= \|x - F'(x)^{-1}F(x) - x^*\| \\ &= \|x - x^* - F'(x)^{-1}(F(x) - F(x^*))\| \\ &= \|F'(x)^{-1}[F(x^*) - F(x) - F'(x)(x^* - x)]\| \\ &\leq \|F'(x)^{-1}\| \|F(x^*) - F(x) - F'(x)(x^* - x)\| \\ &\leq \frac{1}{2} \frac{\beta\gamma}{1 - \beta\gamma \|x - x^*\|} \|x - x^*\|^2 \\ &= \frac{1}{2} \frac{\beta\gamma \|x - x^*\|}{1 - \beta\gamma \|x - x^*\|} \|x - x^*\| \\ &= \alpha \|x - x^*\| . \end{aligned} \quad (4.10)$$

To show that $\alpha < 1$, use the second inequality in (4.8) and the definition of δ , to obtain

$$\begin{aligned} \alpha &= \frac{1}{2} \frac{\beta}{1 - \beta\gamma \|x - x^*\|} \gamma \|x - x^*\| \\ &< \frac{3}{2} \beta\gamma \|x - x^*\| \\ &< \frac{3}{2} \beta\gamma\delta \leq 1 . \end{aligned}$$

4.1. Local convergence theory of Newton's method

From (ii), it follows that if $x^0 \in B(x^*, \delta)$ then x^1 is well defined. Moreover by (4.9),

$$\|x^1 - x^*\| = \|H(x^0) - x^*\| < \|x^0 - x^*\| < \delta ,$$

so $x^1 \in B(x^*, \delta)$. It then follows by induction that x^k is well defined and that $x^k \in B(x^*, \delta)$ for all $k \geq 1$.

We now show the convergence of the Newton iterates to x^* . Since $x^k \in B(x^*, \delta)$ for all k , we can use (4.10) and the second inequality in (4.8) to obtain:

$$\begin{aligned} \|x^{k+1} - x^*\| &= \|H(x^k) - x^*\| \\ &\leq \frac{1}{2} \frac{\beta\gamma}{1 - \beta\gamma\|x^k - x^*\|} \|x^k - x^*\|^2 \\ &< \frac{3}{2} \beta\gamma \|x^k - x^*\|^2 , \end{aligned} \tag{4.11}$$

and this gives:

$$\begin{aligned} \|x^{k+1} - x^*\| &< \frac{3}{2} \beta\gamma \|x^k - x^*\|^2 \\ &< \left(\frac{3}{2} \beta\gamma\right)^3 \|x^{k-1} - x^*\|^4 \\ &< \dots < \left(\frac{3}{2} \beta\gamma\right)^{2^{k+1}-1} \|x^0 - x^*\|^{2^{k+1}} \\ &= \frac{2}{3\beta\gamma} \left(\frac{3}{2} \beta\gamma \|x^0 - x^*\|\right)^{2^{k+1}} . \end{aligned} \tag{4.12}$$

The convergence of $\{x^k\}$ to x^* then follows from (4.12), since, using the definition of δ , we have:

$$\frac{3}{2} \beta\gamma \|x^0 - x^*\| < \frac{3}{2} \beta\gamma \delta \leq 1 .$$

Finally, the q-quadratic rate of convergence (4.6) and the error bound (4.7) are shown respectively in (4.11) and (4.12). \square

4.1.1 Termination of the iteration

In the practical computations whose outcomes are presented throughout this thesis, we have terminated Newton's iteration when the change in the iterate x^n is smaller than a given threshold τ :

$$\|x^{n+1} - x^n\| \leq \tau .$$

This criterion is motivated by the following result:

4.2. Affine covariant transformation

Lemma 4.1.3. *Let the assumptions of Theorem 4.1.2 hold, then:*

$$\|x^n - x^*\| = \|x^{n+1} - x^n\| + O(\|x^n - x^*\|^2) . \quad (4.13)$$

This shows that, near the solution x^* , $(x^{n+1} - x^n)$ is essentially of the same size as $(x^n - x^*)$. We now prove (4.13).

Proof of Lemma 4.1.3 We have that

$$\begin{aligned} x^{n+1} - x^n &= (x^* - x^n) + x^{n+1} - x^* \\ &= (x^* - x^n) + x^n - F'(x^n)^{-1}F(x^n) - x^* \\ &= (x^* - x^n) - F'(x^n)^{-1}[F(x^*) + F(x^n) + F'(x^n)(x^* - x^n)] , \end{aligned} \quad (4.14)$$

and from (4.14), using also Lemma 4.1.1 (a) and (4.8), we get:

$$\|x^{n+1} - x^n\| - \frac{3}{2}\beta\gamma\|x^n - x^*\|^2 \leq \|x^n - x^*\| \leq \|x^{n+1} - x^n\| + \frac{3}{2}\beta\gamma\|x^n - x^*\|^2$$

from which (4.13) follows. □

4.2 Affine covariant transformation

We now investigate the properties of Newton's method for the nonlinear operator equation (4.1):

$$F(x) = 0 , \quad (4.15)$$

when the mapping $F: D \subset X \rightarrow Y$ undergoes the affine transformation

$$F \rightarrow G := AF , \quad (4.16)$$

where A denotes a one-to-one bounded linear map from the Banach space Y onto the Banach space Z . Without loss of generality, we now assume that F is differentiable all over its domain D .

Under the transformation (4.16), the nonlinear equation (4.15) transforms into:

$$G(x) = AF(x) = 0 , \quad (4.17)$$

our aim is then to determine the relation between the Newton's sequence for (4.15) and the Newton's sequence for (4.17).

Transformations such as (4.16) occur very often in practical computations. In fact, for example, the operation of replacing some of the equations in (4.15) each with its linear combination with the remaining ones or of multiplying them by constant factors can be expressed in the form (4.16).

4.2. Affine covariant transformation

The following invariance property is called *affine covariance*.

Proposition 4.2.1. (*Affine covariant invariance of Newton's method*) Let $\{x^k\}$ and $\{\tilde{x}^k\}$ be respectively the Newton's iterates for the system (4.15) and the transformed system (4.17). Provided $x^0 = \tilde{x}^0$, then

$$x^k = \tilde{x}^k \quad k = 0, 1, 2, \dots$$

Proof. From the chain rule and the fact that the Fréchet derivative of a linear operator is the linear operator itself, it follows that the Fréchet derivative in D of the nonlinear mapping G is

$$G'(x) = AF'(x) \ , \quad x \in D \ . \quad (4.18)$$

In particular (4.18) shows that $G'(x)$ is invertible at all points in D where $F'(x)$ is invertible. The result then follows from the observations above and the invertibility of A . In fact, Newton's method applied to the system (4.15) gives:

$$\begin{aligned} x^{k+1} &= x^k - F'(x^k)^{-1}F(x^k) \\ &= x^k - F'(x^k)^{-1}A^{-1}AF(x^k) \\ &= x^k - (AF'(x^k))^{-1}(AF(x^k)) \\ &= x^k - G'(x^k)^{-1}G(x^k) \ . \end{aligned} \quad (4.19)$$

If $x^0 = \tilde{x}^0$, from (4.19) we get

$$\begin{aligned} x^1 &= x^0 - G'(x^0)^{-1}G(x^0) \\ &= \tilde{x}^0 - G'(\tilde{x}^0)^{-1}G(\tilde{x}^0) = \tilde{x}^1 \ , \end{aligned}$$

it is then easy to prove by induction that $x^k = \tilde{x}^k$ for all $k \geq 0$. □

We conclude this section by asking whether the theory for Newton's method actually reflects the affine covariance property of the algorithm. That is does the theory guarantee the same convergence properties to the iterates $\{x^k\}$ and $\{\tilde{x}^k\}$ if $x^0 = \tilde{x}^0$? It is immediately obvious that this may well not be the case when the standard convergence theorem, presented in §4.1, is considered. In fact, the standard norm used when the system (4.15) is solved by Newton's method will be replaced by a *weighted norm* when Newton's algorithm is applied to

4.3. Affine contravariant transformation

system (4.17):

$$\|F(x)\| \rightarrow \|AF(x)\| = \|G(x)\| , \quad (4.20)$$

$$\|F'(x)\| \rightarrow \|AF'(x)\| = \|G'(x)\| , \quad (4.21)$$

and, from a computational point of view, the change of norm (4.20) may entail a change in the criterion for the termination of the iterations which is usually based on the size of the residual. The change of norm (4.21) may affect, instead, the estimates of the Lipschitz constant of the Fréchet derivative and of the bound on its inverse. This can then lead to an estimate of the size of the convergence ball of Newton's method applied to system (4.15) which does not agree with the predictions of the theory for Newton's algorithm applied to the transformed system (4.17). (This will be first shown in an abstract form in §4.4, and then illustrated by a simple example in Chapter 5).

A local convergence theory which is invariant under the transformation (4.16) can indeed be obtained telescoping the assumptions (i) and (ii) of Lemma 4.1.1, with $\bar{x} = x^*$, into the following "affine covariant Lipschitz condition":

$$\|F'(x^*)^{-1}(F'(y) - F'(x))\| \leq \omega_* \|y - x\| \quad \forall x, y \in B(x^*, r) .$$

This was done by Bader [62], as reported in [58], see p. 48 and p. 105. An affine covariant version of the semilocal theory is discussed in detail in [58].

4.3 Affine contravariant transformation

We now study the behaviour of Newton's method applied to the nonlinear operator equation (4.1):

$$F(x) = 0 , \quad (4.22)$$

when the domain space D of the mapping $F : D \subset X \rightarrow Y$ is affinely transformed according to the rule:

$$x \rightarrow \tilde{x} := B^{-1}x , \quad x \in D \quad (4.23)$$

where B is a one-to-one bounded linear map from \tilde{D} , a convex subset of the Banach space W , onto D . Equation (4.22) is then accordingly transformed into:

$$G(\tilde{x}) = F(B\tilde{x}) = 0 , \quad (4.24)$$

with $G : \tilde{D} \subset W \rightarrow Y$

In contrast to the covariant transformation in §4.2 (where the system is transformed), here it is the solution which is transformed. In practical computations, transformations like (4.24)

4.3. Affine contravariant transformation

occur when the variables are nondimensionalised or their unit of measurement is changed.

The relation between the Newton's iterates for (4.22) and the Newton's iterates for (4.24) is next determined. The property expressed by the following proposition is called *affine contravariance*.

Proposition 4.3.1. (*Affine contravariant invariance of Newton's method*) *Let the domain space D of the nonlinear operator F be transformed according to (4.23) and let $\{x^k\}$ and $\{\tilde{x}^k\}$ be respectively the Newton's iterates for the system (4.22) and the transformed system (4.24). Provided $\tilde{x}^0 = B^{-1}x^0$, the Newton's iterates $\{x^k\}$ will transform analogously, i.e.:*

$$\tilde{x}^k = B^{-1}x^k \quad k = 0, 1, 2, \dots \quad (4.25)$$

Proof. Similarly to the proof of Proposition 4.2.1, the chain rule and the fact that B is a linear operator give the following expression for the Fréchet derivative in \tilde{D} of G :

$$G'(\tilde{x}) = F'(B\tilde{x})B, \quad \tilde{x} \in \tilde{D}. \quad (4.26)$$

$G'(\tilde{x})$ is then invertible at all points $\tilde{x} = B^{-1}x$ corresponding to those points $x \in D$ where $F'(x)$ is invertible. These observations are used below in showing (4.25).

Newton's method applied to (4.22) gives:

$$x^{k+1} = x^k - F'(x^k)^{-1}F(x^k),$$

and multiplication of both sides of the last expression by B^{-1} yields:

$$B^{-1}x^{k+1} = B^{-1}x^k - B^{-1}F'(x^k)^{-1}F(x^k). \quad (4.27)$$

If $\tilde{x}^0 = B^{-1}x^0$, from (4.27) we get

$$\begin{aligned} B^{-1}x^1 &= B^{-1}x^0 - B^{-1}F'(x^0)^{-1}F(x^0) \\ &= \tilde{x}^0 - B^{-1}F'(B\tilde{x}^0)^{-1}F(B\tilde{x}^0) \\ &= \tilde{x}^0 - G'(\tilde{x}^0)^{-1}G(\tilde{x}^0) = \tilde{x}^1. \end{aligned}$$

It can then be easily proved, by induction, that:

$$\tilde{x}^k = B^{-1}x^k \quad \forall k \geq 0. \quad \square$$

Proposition 4.3.1 shows that, provided $\tilde{x}^0 = B^{-1}x^0$, the sequence $\{\tilde{x}^k\}$ converges to \tilde{x}^* solution of (4.24), if and only if the sequence $\{x^k\}$ converges to $x^* = B\tilde{x}^*$ (which is the solution of (4.22)). It is important to observe that when switching from Newton's method applied to (4.22), to Newton's method applied to (4.24), the standard norms will correspondingly change

4.4. Discrepancy between the theory for Newton's method and its affine properties

into *weighted norms*:

$$\|x^k - x^*\| \rightarrow \|B^{-1}(x^k - x^*)\| = \|\tilde{x}^k - \tilde{x}^*\| \quad (4.28)$$

$$\|F'(x)\| \rightarrow \|F'(B\tilde{x})B\| = \|G'(\tilde{x})\| . \quad (4.29)$$

As already noticed in §4.2, the standard convergence theory may then lead to conclusions about the iterates $\{x^k\}$ which substantially differ from its predictions about the iterates $\{\tilde{x}^k\}$. This is explained in more detail in the next section.

4.4 Discrepancy between the theory for Newton's method and its affine properties

We now investigate the effect of applying both covariant and contravariant transformations to the nonlinear operator equation:

$$F(x) = 0 , \quad (4.30)$$

with $F : D \subset X \rightarrow Y$ and solution x^* . Such double transformations are crucial in the k - ε system in Chapter 5. Thus, if A and B are the operators defined respectively in §4.2 and §4.3, we shall consider the nonlinear equation:

$$G(\tilde{x}) = AF(B\tilde{x}) = 0 , \quad (4.31)$$

with $G : \tilde{D} \subset W \rightarrow Z$ and solution $\tilde{x}^* = B^{-1}x^*$, resulting from the concurrent application of the affine transformations

$$F \rightarrow G := AF , \quad x \in D \rightarrow \tilde{x} := B^{-1}x \in \tilde{D} . \quad (4.32)$$

Let $\{x^k\}$ and $\{\tilde{x}^k\}$ be respectively the Newton's iterates for (4.30) and for (4.31), then the following corollary is an obvious consequence of Proposition 4.2.1 and Proposition 4.3.1.

Corollary 4.4.1. *If $x^0 = B\tilde{x}^0$, then the sequence $\{\tilde{x}^k\}$ converges to \tilde{x}^* if and only if the sequence $\{x^k\}$ converges to $x^* = B\tilde{x}^*$.*

However the result of Corollary 4.4.1 is not sufficiently reflected in the convergence theory presented in §4.1. In fact, in the following we will show that if $B(x^*, \delta)$ and $B(\tilde{x}^*, \tilde{\delta})$ are respectively the convergence balls of the iterates $\{x^k\}$ and $\{\tilde{x}^k\}$ predicted by Theorem 4.1.2, then it may be possible that

$$\tilde{x}^0 \in B(\tilde{x}^*, \tilde{\delta}) \quad \text{but} \quad x^0 \notin B(x^*, \delta) , \quad \text{where} \quad x^0 = B\tilde{x}^0 . \quad (4.33)$$

In this case Theorem 4.1.2 would guarantee that $\tilde{x}^k \rightarrow \tilde{x}^*$, but would not guarantee that $x^k \rightarrow x^*$. A practical realisation of (4.33) will follow in Chapter 5.

4.4. Discrepancy between the theory for Newton's method and its affine properties

We now explain this in more detail. Let the operator G satisfy the assumptions of Theorem 4.1.2:

$$G' \in \text{Lip}_{\tilde{\gamma}}(B(\tilde{x}^*, \tilde{r})) \quad \text{and} \quad \|G'(\tilde{x}^*)^{-1}\| \leq \tilde{\beta}. \quad (4.34)$$

It then follows from Theorem 4.1.2 that for all starting guesses $\tilde{x}^0 \in B(\tilde{x}^*, \tilde{\delta})$, with

$$\tilde{\delta} \leq \frac{2}{3\tilde{\beta}\tilde{\gamma}}, \quad (4.35)$$

the Newton's iterates \tilde{x}^k for (4.31) are well defined, remain in $B(\tilde{x}^*, \tilde{\delta})$ and converge quadratically to \tilde{x}^* . We now show that the transformed initial guess $x^0 = B\tilde{x}^0$ lies in a ball centred on x^* , $B(x^*, \delta')$, which, under certain conditions (that will be examined below), has the property: $B(x^*, \delta) \subset B(x^*, \delta')$. Hence, it may happen that $x^0 \notin B(x^*, \delta)$ and therefore the convergence of $\{x^k\}$ is not guaranteed by Theorem 4.1.2.

Lemma 4.4.2. *If $x^0 = B\tilde{x}^0$, and $\tilde{x}^0 \in B(\tilde{x}^*, \tilde{\delta})$ then*

$$x^0 \in B(x^*, \delta') \quad \text{with} \quad \delta' = \frac{2\|B\|}{3\tilde{\beta}\tilde{\gamma}} \quad (4.36)$$

Proof. We have

$$\|x^0 - x^*\| = \|B(\tilde{x}^0 - \tilde{x}^*)\| \leq \|B\|\|\tilde{x}^0 - \tilde{x}^*\| < \|B\|\tilde{\delta} \leq \frac{2\|B\|}{3\tilde{\beta}\tilde{\gamma}}. \quad \square$$

We now estimate δ , the lower bound on the radius of the convergence ball of the iterates $\{x^k\}$ predicted by Theorem 4.1.2, in terms of the parameters of the problem under investigation and then determine under which conditions $\delta' > \delta$.

We will need the lemma below, which is proved at the end of this section.

Lemma 4.4.3. *Let the nonlinear operators F and G and their domains D and \tilde{D} be related as in (4.32) and let G have the properties (4.34). Then*

$$F' \in \text{Lip}_{\gamma}(B(x^*, r)) \quad \text{with} \quad \gamma = \|A^{-1}\|\|B^{-1}\|^2\tilde{\gamma} \quad \text{and} \quad r = \frac{\tilde{r}}{\|B^{-1}\|} \quad (4.37)$$

and

$$\|F'(x^*)^{-1}\| \leq \beta \quad \text{with} \quad \beta = \|A\|\|B\|\tilde{\beta}. \quad (4.38)$$

Let $\kappa(A) := \|A\|\|A^{-1}\| \geq 1$ be the condition number of the operator A , and similarly $\kappa(B)$, we have

Theorem 4.4.4. *Let the operators F and G and their respective domains D and \tilde{D} be related as in (4.32) and let G satisfy the assumptions of Theorem 4.1.2. Then the lower bound δ for the radius of the convergence ball of the iterates $\{x^k\}$ predicted by Theorem 4.1.2 for (4.30) is bounded above by:*

$$\delta \leq \frac{1}{\kappa(A)\kappa(B)\|B^{-1}\|} \frac{2}{3\tilde{\beta}\tilde{\gamma}}. \quad (4.39)$$

4.4. Discrepancy between the theory for Newton's method and its affine properties

Proof. The result follows from using the expressions for γ and β , respectively in (4.37) and (4.38), in the upper bound for δ predicted by Theorem 4.1.2 applied to the nonlinear operator F :

$$\delta \leq \frac{2}{3\beta\gamma} .$$

□

The inequality (4.39) allows the possibility that a particular choice of either A or B can make δ arbitrarily small. In particular, if either $\kappa(A) > 1$ or $\kappa(B) > 1$, then it might be possible that the initial guess x^0 is not in the convergence ball $B(x^*, \delta)$, in fact we have that $\delta' > \delta$ as it is shown below using (4.36) and (4.39):

$$\frac{\delta'}{\delta} \geq \frac{2\|B\|}{3\tilde{\beta}\tilde{\gamma}} \left(\frac{1}{\kappa(A)\kappa(B)\|B^{-1}\|} \frac{2}{3\tilde{\beta}\tilde{\gamma}} \right)^{-1} = \kappa(A)(\kappa(B))^2 > 1 .$$

We finally prove Lemma 4.4.3.

Proof of Lemma 4.4.3. (4.37) is next shown. To obtain this, let $x = B\tilde{x}$, $y = B\tilde{y} \in B(x^*, \tilde{r}/\|B^{-1}\|)$, then it is easy to verify that $\tilde{x}, \tilde{y} \in B(\tilde{x}^*, \tilde{r})$, the ball of \tilde{x}^* where $G'(\tilde{x})$ is Lipschitz continuous.

We have

$$\begin{aligned} \|F'(y) - F'(x)\| &= \|A^{-1}(G'(\tilde{y}) - G'(\tilde{x}))B^{-1}\| \\ &\leq \|A^{-1}\| \|B^{-1}\| \|G'(\tilde{y}) - G'(\tilde{x})\| \\ &\leq \|A^{-1}\| \|B^{-1}\| \tilde{\gamma} \|\tilde{y} - \tilde{x}\| \\ &= \|A^{-1}\| \|B^{-1}\| \tilde{\gamma} \|B^{-1}(y - x)\| \\ &\leq \|A^{-1}\| \|B^{-1}\|^2 \tilde{\gamma} \|y - x\| . \end{aligned}$$

Therefore, the Lipschitz constant γ of $F'(x)$ in $B(x^*, \tilde{r}/\|B^{-1}\|)$ is such that

$$\gamma \leq \|A^{-1}\| \|B^{-1}\|^2 \tilde{\gamma} , \tag{4.40}$$

but, due to the optimality of the bounds used in the proof above (for the problem that will be examined in §5.1, it can be shown indeed that there exist x, y such that $\|F'(y) - F'(x)\| = \|A^{-1}\| \|B^{-1}\|^2 \tilde{\gamma} \|y - x\|$), it follows that

$$\gamma = \|A^{-1}\| \|B^{-1}\|^2 \tilde{\gamma} ,$$

and this value of γ cannot be bettered.

We next show (4.38). This is done as follows:

4.5. A weighted norm

$$\begin{aligned}
\|F'(x^*)^{-1}\| &= \|BG'(\tilde{x}^*)^{-1}A\| \\
&\leq \|A\| \|B\| \|G'(\tilde{x}^*)^{-1}\| \\
&\leq \|A\| \|B\| \tilde{\beta}.
\end{aligned}$$

Thus

$$\beta \leq \|A\| \|B\| \tilde{\beta}, \quad (4.41)$$

and the result follows from the use of optimal bounds. In §5.1.2, it will be shown that, for the model problem we will be considering, $\|F'(x^*)^{-1}\| = \|A\| \|B\| \tilde{\beta}$, so that in general the estimate (4.41) cannot be improved. \square

4.5 A weighted norm

We now discuss a possible way to overcome the lack of invariance of the standard convergence theory for Newton's method, which we have described in §4.4.

We will show that there exists a weighted norm where the iterates x^k , generated by Newton's method applied to the "unscaled" problem (4.30), have all the properties exhibited in the standard norm by the iterates \tilde{x}^k for the "scaled" problem (4.31). (The practical utility of the weighted norm will be investigated in detail in Chapter 5).

In particular, we have in mind the situation when the original unscaled problem is a system of nonlinear equations in \mathbb{R}^n depends on a "bad" parameter μ and the transformations (4.32), with matrices $A, B \in \mathbb{R}^n \times \mathbb{R}^n$ both different from the identity and possibly dependent on μ , is sought so that either the scaled system or its Jacobian do not depend critically on μ . The conclusions of the standard convergence theory for Newton's method applied to the scaled system (4.31) will then be robust with respect to variations in μ and so its predictions about Newton's iterates for the unscaled system (4.30) should also be.

We recall that from the study presented in §§4.2, 4.3, it follows that if $x^0 = B\tilde{x}^0$ then $x^k = B\tilde{x}^k$ for all $k \geq 1$. Therefore if we consider the following weighted norm (which, hereafter, will be called the B -norm):

$$\|\cdot\|_B := \|B^{-1}(\cdot)\|, \quad (4.42)$$

for the iterates x^k , with $\|\cdot\|$ any standard norm on the space where the linear operator B is defined, the identity

$$\|x^k - x^*\|_B = \|\tilde{x}^k - \tilde{x}^*\| \quad (4.43)$$

4.5. A weighted norm

holds, and the following main property ensues:

- (i) the sequence $\{\tilde{x}^k\}$ converges to \tilde{x}^* , in the standard norm, if and only if the sequence $\{x^k\}$ converges to x^* , in the B -norm.

That is, the actual radius of the ball of convergence of the iterates x^k measured in the B -norm is the same as the actual radius of the ball of convergence of the iterates \tilde{x}^k measured in the standard norm and there is a one-to-one correspondence between the points in the two balls. As far as the predictions of Theorem 4.1.2 are concerned, (4.43) clearly implies that

- (ii) The radius of the quadratic convergence ball of the iterates x^k measured in the B -norm, is the same as the radius of the quadratic convergence ball of the iterates \tilde{x}^k measured in the standard norm:

$$\|\tilde{x}^{k+1} - \tilde{x}^*\| \leq K\|\tilde{x}^k - \tilde{x}^*\|^2 \iff \|x^{k+1} - x^*\|_B \leq K\|x^k - x^*\|_B^2 .$$

- (iii) The same error estimate holds for the iterates x^k and for the iterates \tilde{x}^k , respectively in the standard and in the B -norm:

$$\|\tilde{x}^k - \tilde{x}^*\| \leq \phi_k \iff \|x^k - x^*\|_B \leq \phi_k ,$$

with

$$\phi_k = \frac{1}{K}(K\|\tilde{x}^0 - \tilde{x}^*\|)^{2^k} = \frac{1}{K}(K\|x^0 - x^*\|_B)^{2^k} .$$

The Newton convergence theory applied to the scaled problem (4.31), using the standard norm $\|\cdot\|$, will then yield results about the behaviour of the iterates \tilde{x}^k , which will also hold for the iterates x^k in the weighted norm $\|\cdot\|_B$.

Chapter 5

Iterative procedures for the discretised k - ε model

The focus of this chapter is on the analysis of the convergence properties of Newton's method for the systems arising from the discretisation of the coupled RANS and k - ε equations and of the k - ε equations only. We will prove that if the problem which is being solved by Newton's method is well posed as $h_+ \rightarrow 0$ and the mesh is appropriately chosen (see condition (5.78)), then, in a specific weighted norm, the lower estimate for the convergence ball of the algorithm, provided by Theorem 4.1.2, does not shrink to zero as $h_+ \rightarrow 0$. This will be done by exploiting the invariance of Newton's method under a combination of affine covariant and affine contravariant transformations of the underlying nonlinear system (see §§4.4, 4.5). We will also show that the most commonly used iterative scheme based on the decoupling of the RANS from the k - ε equations, which is implemented in the industrial code FEAT (Finite Element Analysis Toolbox), does not have the same robustness as Newton's method, in fact, we will see, its performances drastically worsen in the limit $h_+ \rightarrow 0$.

This chapter is organized as follows. In §5.1, we will initially carry out a detailed study of the properties of Newton's method applied to the 2×2 algebraic system of equations provided by the diffusionless k -equation evaluated at $y = h_+$ combined with the law of the wall (2.44) for ε . Despite its simplicity, this reduced problem encapsulates some of the key features of the k - ε model at $y = h_+$, for $h_+ \rightarrow 0$, such as the blow-up of ε and the predominance of source terms over diffusion (see §2.4), and will turn out to be particularly enlightening for the behaviour of Newton's method for the full finite element system. This will be discussed in §5.2, where, by pursuing the same strategy adopted in §5.1, we will show that the choice of a graded mesh is essential for guaranteeing the robustness of Newton's method with respect to $h_+ \rightarrow 0$, both when the scheme is applied to the coupled discretised RANS and k - ε equations and when it is used for solving the discretised k - ε equations only with given velocity field. In §5.3, we will consider the iterative method based on the decoupling of the RANS from the k - ε equations, which we will refer to as inner-outer iteration. Through numerical experiments, we will show that the performances of the inner-outer iteration dramatically deteriorates as $h_+ \rightarrow 0$, even on the equidistributed mesh (3.101) on which Newton's method performs robustly. We will

5.1. Newton's method for a model reduced 2×2 problem

explain this by proving that the inner-outer iteration applied to the 3×3 algebraic system of equations obtained by combining the 2×2 system of §5.1 with the law of the wall for U has a convergence ball with zero radius.

Our study then shows that Newton's method should be the method of choice for solving the discretised RANS and k - ε equations, and that its approximations (such is the inner-outer iteration, see the beginning of §5.3) should be considered very carefully.

5.1 Newton's method for a model reduced 2×2 problem

We now investigate in detail the properties of Newton's method for a special 2×2 algebraic system of equations derived by restricting the k - ε system to the artificial wall, and neglecting diffusion. This study will show the practical utility of the abstract theory of Chapter 4 and provide us with some insight into the behaviour of Newton's algorithm for the discretised full k - ε system to be considered later.

Neglecting the second order term in (2.40) yields the diffusionless k -equation, over the domain $[h_+, 1]$:

$$-C_\mu \left(\frac{dU}{dy} \right)^2 \frac{k^2}{\varepsilon} + \varepsilon = 0 . \quad (5.1)$$

In (5.1), dU/dy has the property:

$$\frac{dU}{dy}(h_+) = \frac{1}{C_\mu} \frac{\varepsilon(h_+)}{(k(h_+))^2} u_*^2 = \frac{u_*}{\kappa} \frac{1}{h_+} ,$$

which follows from (2.42), rearranging the terms and using the laws of the wall (2.44) and (2.58), respectively for ε and k .

Evaluating (5.1) at $y = h_+$ gives an approximate relation between k and ε at h_+ :

$$-\alpha^2 \frac{k(h_+)^2}{\varepsilon(h_+)} + \varepsilon(h_+) = 0 , \quad (5.2)$$

where

$$\alpha := C_\mu^{1/2} \frac{dU}{dy}(h_+) = \frac{C_\mu^{1/2} u_*}{\kappa} \frac{1}{h_+} . \quad (5.3)$$

As observed in §2.4, there exists a neighbourhood of $y = h_+$ where diffusion is much smaller than production and dissipation, and so, in this region, equation (5.2) can be considered a first order approximation to (2.40). In the case of turbulent Couette flow the diffusive term in the k -transport equation (2.40) is exactly zero, since production and dissipation of turbulent kinetic energy perfectly balance each other, and the solution of (2.40) is $k = C_\mu^{-1/2} u_*^2 = \text{const}$, see §2.3.

The behaviour of ε at the artificial wall is prescribed by the law of the wall (2.44). As typical of turbulence modelling, this has been implemented as the nonlinear Dirichlet boundary condition :

5.1. Newton's method for a model reduced 2×2 problem

$$\varepsilon(h_+) = \frac{C_\mu^{3/4} (k(h_+))^{3/2}}{\kappa h_+}, \quad (5.4)$$

see (2.44), (2.58).

Equations (5.2) and (5.4) form a nonlinear system for $k(h_+)$ and $\varepsilon(h_+)$, which we express as

$$F(x) := \begin{bmatrix} -\alpha^2 \frac{k_+^2}{\varepsilon_+} + \varepsilon_+ \\ \varepsilon_+ - \eta \alpha k_+^{3/2} \end{bmatrix} = 0, \quad (5.5)$$

where $F : \mathbb{R}^+ \times \mathbb{R}^+ \rightarrow \mathbb{R}^2$, $k_+ := k(h_+)$, $\varepsilon_+ := \varepsilon(h_+)$, $x := (k_+, \varepsilon_+)^T$,

$$\eta := \frac{C_\mu^{1/4}}{u_*} = O(1), \quad \text{as } h_+ \rightarrow 0, \quad (5.6)$$

and α is given in (5.3). The solution to (5.5) is

$$x^* = \left(\frac{1}{\eta^2}, \frac{\alpha}{\eta^2} \right)^T = \left(\frac{u_*^2}{\sqrt{C_\mu}}, \frac{u_*^3}{\kappa h_+} \right), \quad (5.7)$$

We are interested in investigating the robustness of nonlinear solvers for (5.5) as $h_+ \rightarrow 0$, since this is of direct relevance to the behaviour of practical solvers for turbulence models. Note that the coefficient α appearing in both equations of (5.5), and defined in (5.3), depends on h_+ , and blows up with $O(1/h_+)$ as $h_+ \rightarrow 0$. In the $L_\infty([h_+, 1])$ -norm, the solution (5.7) also blows up with $O(1/h_+)$, in fact

$$\|x^*\|_\infty = \frac{u_*^3}{\kappa h_+}, \quad \text{as } h_+ \rightarrow 0.$$

We will study the convergence properties of Newton's method under affine transformations of the system (5.5). In particular we consider the scaled version of (5.5):

$$G(\tilde{x}) := D_E F(D_V \tilde{x}), \quad (5.8)$$

where

$$D_E := \frac{1}{\alpha} \begin{bmatrix} 1 & 0 \\ 0 & 1 \end{bmatrix}, \quad D_V := \begin{bmatrix} 1 & 0 \\ 0 & \alpha \end{bmatrix}, \quad (5.9)$$

and

$$\tilde{x} := (\tilde{k}_+, \tilde{\varepsilon}_+)^T = D_V^{-1} x = \left(k_+, \frac{\varepsilon_+}{\alpha} \right)^T.$$

The scaling (5.8) is chosen to ensure that the transformed system does not depend on the

5.1. Newton's method for a model reduced 2×2 problem

large parameter α , equivalently the small parameter h_+ . It is easy to see that (5.8) is

$$G(\tilde{x}) = \begin{bmatrix} -\frac{\tilde{k}_+^2}{\tilde{\varepsilon}_+} + \tilde{\varepsilon}_+ \\ \tilde{\varepsilon}_+ - \eta \tilde{k}_+^{3/2} \end{bmatrix} = 0, \quad (5.10)$$

and it has solution

$$\tilde{x}^* = D_V^{-1} x^* = \left(\frac{1}{\eta^2}, \frac{1}{\eta^2} \right)^T = \left(\frac{u_*^2}{\sqrt{C_\mu}}, \frac{u_*^2}{\sqrt{C_\mu}} \right). \quad (5.11)$$

Note that $\|\tilde{x}^*\|_\infty = 1/\eta^2 = O(1)$ as $h_+ \rightarrow 0$, and (5.10) no longer depends on the large parameter α .

We will be mainly interested in comparing the lower estimates for the radii of the convergence balls predicted by Theorem 4.1.2 for Newton's method applied to (5.5) and to (5.10), especially their behaviour as $h_+ \rightarrow 0$. We will say that Newton's method converges *robustly* if the lower bound for the radius of its ball of convergence, predicted by Theorem 4.1.2, does not become arbitrarily small as $h_+ \rightarrow 0$.

The rest of this section is organized as follows. In §5.1.1 we will prove the following theorem:

Theorem 5.1.1. *In the weighted L_∞ norm induced by D_V , the iterates $\{x^k\}$, generated by Newton's method applied to the unscaled system (5.5), converge robustly to x^* as $h_+ \rightarrow 0$.*

In §5.1.2 we will show:

Theorem 5.1.2. *The predicted lower bound for the radius of the convergence ball of Newton's method for the unscaled system (5.5), measured in the standard L_∞ norm, becomes arbitrarily small as $h_+ \rightarrow 0$.*

We will also give an example of a family of initial guesses for which Theorem 4.1.2 will guarantee the convergence of Newton's method in the weighted norm induced by D_V , but will not guarantee the convergence of the method if the standard norm is used.

In the following we will consider \mathbb{R}^2 equipped with the infinity norm $\|\cdot\|_\infty$, and with the weighted norm $\|\cdot\|_{D_V^{-1}}$ defined by:

$$\|y\|_{D_V^{-1}} = \|D_V^{-1}y\|, \quad y \in \mathbb{R}^2. \quad (5.12)$$

5.1.1 Convergence analysis in the weighted norm

Let $B_{D_V}(x^*, \tilde{\delta})$ be the lower bound on the ball of convergence of the Newton's iterates $\{x^k\}$ for the system (5.5) predicted by Theorem 4.1.2, with radius $\tilde{\delta}$ measured in the weighted norm induced by D_V :

$$B_{D_V}(x^*, \tilde{\delta}) := \left\{ x \in \mathbb{R}^2 \mid \|x - x^*\|_{D_V^{-1}} < \tilde{\delta} \right\}. \quad (5.13)$$

5.1. Newton's method for a model reduced 2×2 problem

Then, from §4.5, we have that

$$B(\tilde{x}^*, \tilde{\delta}) := \left\{ \tilde{x} = D_V^{-1}x, x \in \mathbb{R}^2 \mid \|\tilde{x} - \tilde{x}^*\|_\infty < \tilde{\delta} \right\} \quad (5.14)$$

is the ball of convergence of the iterates $\{\tilde{x}^k\}$ for the system (5.10) predicted by Theorem 4.1.2, and

$$x \in B_{D_V}(x^*, \tilde{\delta}) \Leftrightarrow \tilde{x} \in B(\tilde{x}^*, \tilde{\delta}) .$$

Thus, in order to prove Theorem 5.1.1, we will show that the upper bound on $\tilde{\delta}$ given by Theorem 4.1.2 applied to the scaled mapping G in (5.8) is unaffected by the limit $h_+ \rightarrow 0$. That is, we will prove that there exist two strictly positive constants \tilde{c}_1, \tilde{c}_2 independent of h_+ such that;

$$\tilde{c}_1 \leq \frac{2}{3\tilde{\beta}\tilde{\gamma}} \leq \tilde{c}_2 \quad \text{as } h_+ \rightarrow 0 , \quad (5.15)$$

where $\tilde{\beta}$ and $\tilde{\gamma}$ are as described in Theorem 4.1.2 applied to G . We recall that $\tilde{\beta}$ is the upper bound on $\|G'(\tilde{x}^*)^{-1}\|$ and $\tilde{\gamma}$ is the Lipschitz constant of G' .

The result (5.15) can be easily deduced considering that both the coefficients multiplying the unknowns of the system (5.10) and its solution \tilde{x}^* (see (5.11)) are independent of h_+ , thus neither $\tilde{\beta}$ nor $\tilde{\gamma}$ can depend on h_+ . However, in the following proof of Theorem 5.1.1 we will give precise estimates of $\tilde{\beta}$ and $\tilde{\gamma}$, since these will be needed later to show the tightness of the bounds (4.40) and (4.41).

Proof of Theorem 5.1.1. We will prove that

$$(I) \quad \tilde{\beta} = \frac{7}{2}$$

(II) there exist two strictly positive constants \tilde{d}_1, \tilde{d}_2 independent of h_+ such that

$$\tilde{d}_1 \leq \tilde{\gamma} \leq \tilde{d}_2 . \quad (5.16)$$

(5.15) will then follow from (I) and (II), with $\tilde{c}_1 = 4/(21\tilde{d}_2)$ and $\tilde{c}_2 = 4/(21\tilde{d}_1)$.

Proof of (I) We have that the Fréchet derivative of G , represented by the Jacobian matrix

$$J_G(\tilde{x}) = \begin{bmatrix} -2\frac{\tilde{k}_+}{\tilde{\varepsilon}_+} & \left(\frac{\tilde{k}_+}{\tilde{\varepsilon}_+}\right)^2 + 1 \\ -\frac{3}{2}\eta\tilde{k}_+^{1/2} & 1 \end{bmatrix} ,$$

is nonsingular at $\tilde{x}^* = (1/\eta^2, 1/\eta^2)^T$ solution to $G(\tilde{x}) = 0$ (see (5.11)), in fact

$$J_G(\tilde{x}^*) = \begin{bmatrix} -2 & 2 \\ -\frac{3}{2} & 1 \end{bmatrix}$$

5.1. Newton's method for a model reduced 2×2 problem

and thus $\det(J_G(\tilde{x}^*)) = 1$. $J_G(\tilde{x}^*)^{-1}$ is then given by:

$$J_G(\tilde{x}^*)^{-1} = \begin{bmatrix} 1 & -2 \\ \frac{3}{2} & -2 \end{bmatrix},$$

and we have:

$$\|J_G(\tilde{x}^*)^{-1}\|_\infty = \max\left\{3, \frac{7}{2}\right\} = \frac{7}{2} =: \tilde{\beta}. \quad (5.17)$$

Proof of (II) We will first show that there exist two vectors \tilde{v} and \tilde{w} such that:

$$\frac{\|J_G(\tilde{w}) - J_G(\tilde{v})\|}{\|\tilde{w} - \tilde{v}\|} = \tilde{d}_1 \quad (5.18)$$

with \tilde{d}_1 independent of h_+ . This, by definition of the Lipschitz constant $\tilde{\gamma}$:

$$\tilde{\gamma} := \sup_{\tilde{x} \neq \tilde{y}} \frac{\|J_G(\tilde{y}) - J_G(\tilde{x})\|}{\|\tilde{y} - \tilde{x}\|}, \quad (5.19)$$

will imply that:

$$\tilde{\gamma} \geq \tilde{d}_1. \quad (5.20)$$

Then we will determine \tilde{d}_2 independent of h_+ such that

$$\tilde{\gamma} \leq \tilde{d}_2, \quad (5.21)$$

and (5.16) will derive from (5.20) and (5.21).

Let $\tilde{x} = (\tilde{x}_1, \tilde{x}_2)^\top$ and $\tilde{y} = (\tilde{y}_1, \tilde{y}_2)^\top$, from

$$J_G(\tilde{y}) - J_G(\tilde{x}) = \begin{bmatrix} -2 \left(\frac{\tilde{y}_1}{\tilde{y}_2} - \frac{\tilde{x}_1}{\tilde{x}_2} \right) & \left(\frac{\tilde{y}_1}{\tilde{y}_2} \right)^2 - \left(\frac{\tilde{x}_1}{\tilde{x}_2} \right)^2 \\ -\frac{3}{2} \eta (\tilde{y}_1^{1/2} - \tilde{x}_1^{1/2}) & 0 \end{bmatrix},$$

we get

$$\begin{aligned} \|J_G(\tilde{y}) - J_G(\tilde{x})\|_\infty &= \\ &= \max \left\{ \left| \frac{\tilde{y}_1}{\tilde{y}_2} - \frac{\tilde{x}_1}{\tilde{x}_2} \right| \left(2 + \left| \frac{\tilde{y}_1}{\tilde{y}_2} + \frac{\tilde{x}_1}{\tilde{x}_2} \right| \right), \frac{3}{2} \eta \frac{|\tilde{y}_1 - \tilde{x}_1|}{|\tilde{y}_1^{1/2} + \tilde{x}_1^{1/2}|} \right\}. \end{aligned} \quad (5.22)$$

In order to prove (5.18), consider \tilde{x} and \tilde{y} in a neighbourhood of $\tilde{x}^* = (1/\eta^2, 1/\eta^2)^\top$, as

5.1. Newton's method for a model reduced 2×2 problem

specified below:

$$\tilde{x} = \tilde{v} := \left(\frac{1}{\eta^2}, \frac{1}{\tilde{\mu}} \frac{1}{\eta^2} \right)^T, \quad \tilde{y} = \tilde{w} := \left(\frac{1}{\eta^2}, \frac{1}{\tilde{\zeta}} \frac{1}{\eta^2} \right)^T, \quad (5.23)$$

with $\tilde{\mu}, \tilde{\zeta} \in \mathbb{R}^+$ and $\tilde{\mu} \neq \tilde{\zeta}$. We have that:

$$\|\tilde{w} - \tilde{v}\|_\infty = \frac{|\tilde{\zeta} - \tilde{\mu}|}{\tilde{\mu}\tilde{\zeta}} \frac{1}{\eta^2},$$

and that:

$$\|J_G(\tilde{w}) - J_G(\tilde{v})\|_\infty = |\tilde{\zeta} - \tilde{\mu}| \left(2 + (\tilde{\zeta} + \tilde{\mu}) \right),$$

therefore:

$$\frac{\|J_G(\tilde{w}) - J_G(\tilde{v})\|_\infty}{\|\tilde{w} - \tilde{v}\|_\infty} = \tilde{\mu}\tilde{\zeta} \left(2 + (\tilde{\zeta} + \tilde{\mu}) \right) \eta^2. \quad (5.24)$$

If \tilde{v} and \tilde{w} are sufficiently close to \tilde{x}^* , then $\tilde{\mu}$ and $\tilde{\zeta}$ are independent of h_+ and since η does not depend on h_+ either (see its definition in (5.6)), (5.24) proves (5.18). (5.20) then follows.

We now show (5.21). Using $|\tilde{y}_i - \tilde{x}_i| \leq \|\tilde{y} - \tilde{x}\|_\infty$, $i = 1, 2$, and

$$\begin{aligned} \left| \frac{\tilde{y}_1}{\tilde{y}_2} - \frac{\tilde{x}_1}{\tilde{x}_2} \right| &= \left| \frac{\tilde{x}_2(\tilde{y}_1 - \tilde{x}_1) - \tilde{x}_1(\tilde{y}_2 - \tilde{x}_2)}{\tilde{x}_2\tilde{y}_2} \right| \\ &\leq \left(\frac{1}{|\tilde{y}_2|} + \left| \frac{\tilde{x}_1}{\tilde{x}_2\tilde{y}_2} \right| \right) \|\tilde{y} - \tilde{x}\|_\infty, \end{aligned}$$

in the right-hand side of (5.22) and rearranging the terms we obtain:

$$\frac{\|J_G(\tilde{y}) - J_G(\tilde{x})\|_\infty}{\|\tilde{y} - \tilde{x}\|_\infty} \leq \tilde{M}(\tilde{x}, \tilde{y}), \quad (5.25)$$

with

$$\tilde{M}(\tilde{x}, \tilde{y}) := \max \left\{ \frac{1}{|\tilde{y}_2|} \left(1 + \left| \frac{\tilde{x}_1}{\tilde{x}_2} \right| \right) \left(2 + \left| \frac{\tilde{y}_1}{\tilde{y}_2} + \frac{\tilde{x}_1}{\tilde{x}_2} \right| \right), \frac{3}{2} \eta \frac{1}{|\tilde{y}_1^{1/2} + \tilde{x}_1^{1/2}|} \right\}. \quad (5.26)$$

Therefore, by definition of $\tilde{\gamma}$ (see (5.19)), from (5.25) we deduce:

$$\tilde{\gamma} \leq \sup_{\tilde{x} \neq \tilde{y}} \tilde{M}(\tilde{x}, \tilde{y}). \quad (5.27)$$

But, from the fact that x^* does not depend on h_+ , it follows that there exists a neighbourhood of x^* where \tilde{x} and \tilde{y} are independent of h_+ and so is $\sup_{\tilde{x} \neq \tilde{y}} \tilde{M}(\tilde{x}, \tilde{y})$. We can then conclude that (5.27) implies (5.21). \square

5.1. Newton's method for a model reduced 2×2 problem

5.1.2 Convergence analysis in the standard norm

Let $B(x^*, \delta)$ be the lower bound on the ball of convergence of the Newton's iterates $\{x^k\}$ for (5.5) predicted by Theorem 4.1.2, with radius δ measured in the infinity norm $\|\cdot\|_\infty$:

$$B(x^*, \delta) = \{x \in \mathbb{R}^2 \mid \|x - x^*\|_\infty < \delta\} . \quad (5.28)$$

Similarly to §5.1.1, to prove Theorem 5.1.2 we will show that the upper bound on δ given by Theorem 4.1.2 applied to the unscaled mapping F in (5.5), becomes arbitrarily small as $h_+ \rightarrow 0$. That is, we will prove that:

$$\frac{2}{3\beta\gamma} = O(h_+) \quad \text{as } h_+ \rightarrow 0 , \quad (5.29)$$

with β and γ as in Theorem 4.1.2 applied to F .

Thus, the predicted lower bound for the radius of the convergence ball for Newton's method shrinks to 0 as $h_+ \rightarrow 0$.

First, from (5.3), we recall that:

$$\alpha = \frac{C_\mu^{1/2} u_*}{\kappa} \frac{1}{h_+} . \quad (5.30)$$

Proof of Theorem 5.1.2 We will show:

$$(I) \quad \beta = \frac{7}{2}$$

$$(II) \quad \gamma = O\left(\frac{1}{h_+}\right) \quad \text{as } h_+ \rightarrow 0 .$$

(I) and (II) will then imply (5.29).

To obtain (I), we observe that the Jacobian matrix $J_F(x)$, given by

$$J_F(x) = \begin{bmatrix} -2\alpha^2 \frac{k_+}{\varepsilon_+} & \alpha^2 \left(\frac{k_+}{\varepsilon_+}\right)^2 + 1 \\ -\frac{3}{2}\sigma k_+^{1/2} & 1 \end{bmatrix} ,$$

is nonsingular at $x^* = (1/\eta^2, \alpha/\eta^2)^T$, since $\det(J_F(x^*)) = \alpha > 0$, as it follows from

$$J_F(x^*) = \begin{bmatrix} -2\alpha & 2 \\ -\frac{3}{2}\alpha & 1 \end{bmatrix} .$$

5.1. Newton's method for a model reduced 2×2 problem

We then have

$$J_F(x^*)^{-1} = \begin{bmatrix} \frac{1}{\alpha} & -\frac{2}{\alpha} \\ \frac{3}{2} & -2 \end{bmatrix},$$

from which we get:

$$\|J_F(x^*)^{-1}\|_\infty = \max \left\{ \frac{3}{\alpha}, \frac{7}{2} \right\} = \max \left\{ \frac{3\kappa}{C_\mu^{1/2}} \frac{h_+}{u_*}, \frac{7}{2} \right\} = \frac{7}{2} =: \beta, \quad (5.31)$$

for h_+ sufficiently small.

We next prove (II). The proof is organized as now explained. We first show that there exist two vectors v and w such that:

$$\frac{\|J_F(w) - J_F(v)\|_\infty}{\|w - v\|_\infty} = O\left(\frac{1}{h_+}\right) \quad \text{as } h_+ \rightarrow 0, \quad (5.32)$$

and from the definition of γ (see §4.1), we have that

$$\gamma \geq \sup_{x \neq y} \frac{\|J_F(w) - J_F(v)\|}{\|w - v\|} = O\left(\frac{1}{h_+}\right). \quad (5.33)$$

We will also show that

$$\gamma \leq O\left(\frac{1}{h_+}\right) \quad \text{as } h_+ \rightarrow 0, \quad (5.34)$$

and hence (II) follows.

Let $x = (x_1, x_2)^\top$ and $y = (y_1, y_2)^\top$, from

$$J_F(y) - J_F(x) = \begin{bmatrix} -2\alpha^2 \left(\frac{y_1}{y_2} - \frac{x_1}{x_2} \right) & \alpha^2 \left(\left(\frac{y_1}{y_2} \right)^2 - \left(\frac{x_1}{x_2} \right)^2 \right) \\ -\frac{3}{2}\sigma(y_1^{1/2} - x_1^{1/2}) & 0 \end{bmatrix},$$

we obtain:

$$\|J_F(y) - J_F(x)\|_\infty = \alpha M_1(x, y), \quad (5.35)$$

with

$$M_1(x, y) := \max \left\{ \alpha \left| \frac{y_1}{y_2} - \frac{x_1}{x_2} \right| \left(2 + \left| \frac{y_1}{y_2} + \frac{x_1}{x_2} \right| \right), \frac{3}{2}\eta \frac{|y_1 - x_1|}{|y_1^{1/2} + x_1^{1/2}|} \right\}. \quad (5.36)$$

We now show that (5.33) holds. To prove this, we will determine v, w in a neighbourhood of x^* with the property:

5.1. Newton's method for a model reduced 2×2 problem

(i) there exist two strictly positive constants c_1, c_2 independent of h_+ such that:

$$c_1 \leq \frac{M_1(v, w)}{\|w - v\|_\infty} \leq c_2 \quad \text{as } h_+ \rightarrow 0. \quad (5.37)$$

Then, using (5.37) and (5.30) in

$$\frac{\|J_F(w) - J_F(v)\|_\infty}{\|w - v\|_\infty} = \alpha \frac{M_1(v, w)}{\|w - v\|_\infty},$$

which can be obtained from (5.35), will yield (5.32) and (5.33) will follow.

Let

$$v := \left(\mu \frac{1}{\eta^2}, \frac{\alpha}{\eta^2} \right)^T, \quad w := \left(\zeta \frac{1}{\eta^2}, \frac{\alpha}{\eta^2} \right)^T$$

with $\zeta, \mu \in \mathbb{R}^+$ and $\mu \neq \zeta$, we have:

$$\|w - v\|_\infty = \frac{|\zeta - \mu|}{\eta^2},$$

and, using (5.30),

$$\begin{aligned} M_1(v, w) &= \max \left\{ |\zeta - \mu| \left(2 + \frac{1}{\alpha} |\zeta + \mu| \right), \frac{3}{2} \frac{|\zeta - \mu|}{\zeta^{1/2} + \mu^{1/2}} \right\} \\ &= \max \left\{ 2 |\zeta - \mu|, \frac{3}{2} \frac{|\zeta - \mu|}{\zeta^{1/2} + \mu^{1/2}} \right\} \quad \text{as } h_+ \rightarrow 0. \end{aligned}$$

Hence:

$$\frac{M_1(v, w)}{\|w - v\|_\infty} = \eta^2 \max \left\{ 2, \frac{3}{2} \frac{1}{\zeta^{1/2} + \mu^{1/2}} \right\} \quad \text{as } h_+ \rightarrow 0,$$

which proves (5.37), since $\eta = O(1)$ as $h_+ \rightarrow 0$ and ζ and μ are fixed numbers. (5.32) and (5.33) then follow.

We now prove (5.34). Using the same technique as in (5.25), (5.35)-(5.36) yield:

$$\|J_F(y) - J_F(x)\|_\infty \leq \alpha M_2(x, y) \|y - x\|_\infty,$$

with

$$M_2(x, y) := \max \left\{ \frac{\alpha}{|y_2|} \left(1 + \left| \frac{x_1}{x_2} \right| \right) \left(2 + \left| \frac{y_1}{y_2} + \frac{x_1}{x_2} \right| \right), \frac{3}{2} \eta \frac{1}{|y_1^{1/2} + x_1^{1/2}|} \right\}, \quad (5.38)$$

therefore, by definition of γ , we have:

$$\gamma \leq \alpha \sup_{x \neq y} M_2(x, y). \quad (5.39)$$

5.1. Newton's method for a model reduced 2×2 problem

We now show that there exists a neighbourhood of x^* , where

$$d_1 \leq M_2(x, y) \leq d_2 \quad \text{as } h_+ \rightarrow 0, \quad (5.40)$$

with d_1 and d_2 strictly positive constants independent of h_+ , (5.34) will then follow from (5.39), (5.30) and (5.40).

In order to prove (5.40), consider the change of variable:

$$x = (x_1, x_2)^T = D_V \tilde{x} = (\tilde{x}_1, \alpha \tilde{x}_2)^T, \quad y = (y_1, y_2)^T = D_V \tilde{y} = (\tilde{y}_1, \alpha \tilde{y}_2)^T, \quad (5.41)$$

then $M_2(x, y)$, in (5.38), transforms into

$$\begin{aligned} \tilde{M}_2(\tilde{x}, \tilde{y}) &:= M_2(x(\tilde{x}), y(\tilde{y})) \\ &= \max \left\{ \frac{1}{|\tilde{y}_2|} \left(1 + \frac{1}{\alpha} \left| \frac{\tilde{x}_1}{\tilde{x}_2} \right| \right) \left(2 + \frac{1}{\alpha} \left| \frac{\tilde{y}_1}{\tilde{y}_2} + \frac{\tilde{x}_1}{\tilde{x}_2} \right| \right), \frac{3}{2} \eta \frac{1}{|\tilde{y}_1^{1/2} + \tilde{x}_1^{1/2}|} \right\} \end{aligned} \quad (5.42)$$

If \tilde{x} and \tilde{y} are sufficiently close to \tilde{x}^* , then they are independent of h_+ , since \tilde{x}^* is so, and using (5.30) we have:

$$\frac{1}{\alpha} \left| \frac{\tilde{x}_1}{\tilde{x}_2} \right| \rightarrow 0, \quad \frac{1}{\alpha} \left| \frac{\tilde{y}_1}{\tilde{y}_2} + \frac{\tilde{x}_1}{\tilde{x}_2} \right| \rightarrow 0 \quad \text{as } h_+ \rightarrow 0,$$

hence, in the limit $h_+ \rightarrow 0$,

$$\tilde{M}_2(\tilde{x}, \tilde{y}) = \max \left\{ \frac{2}{|\tilde{y}_2|}, \frac{3}{2} \eta \frac{1}{|\tilde{y}_1^{1/2} + \tilde{x}_1^{1/2}|} \right\}.$$

Therefore there exists a neighbourhood of \tilde{x}^* , where:

$$\tilde{b}_1 \leq \tilde{M}_2(\tilde{x}, \tilde{y}) \leq \tilde{b}_2 \quad \text{as } h_+ \rightarrow 0,$$

with \tilde{b}_1 and \tilde{b}_2 strictly positive constants independent of h_+ , and this, in turn, implies the existence of a neighbourhood of x^* where (5.40) holds. \square

Observation 5.1.1. In this case, the bound (4.41) is achieved. This follows because $A = D_E$ and $B = D_V$, and from (5.9), we have

$$\|D_E\|_\infty = \frac{1}{\alpha}, \quad \|D_V\|_\infty = \alpha, \quad \text{as } h_+ \rightarrow 0. \quad (5.43)$$

Thus, recalling from (5.17) and (5.31) that $\tilde{\beta} = 7/2 = \beta$, we have:

$$\beta = \frac{7}{2} = \frac{1}{\alpha} \alpha \tilde{\beta} = \|D_E\|_\infty \|D_V\|_\infty \tilde{\beta}.$$

Observation 5.1.2. As a proof of the practical usefulness of the abstract formulation of §4.4

5.1. Newton's method for a model reduced 2×2 problem

we now show that (5.29) can also be obtained using the result (4.39), which, in our case, takes the expression:

$$\delta \leq \frac{2}{3\beta\gamma} = \frac{1}{\kappa(D_E)\kappa(D_V)\|D_V^{-1}\|} \frac{2}{3\tilde{\beta}\tilde{\gamma}} . \quad (5.44)$$

From the definitions of D_E and D_V in (5.9), we get

$$\|D_E^{-1}\|_\infty = \alpha , \quad \|D_V^{-1}\|_\infty = 1 , \quad \text{as } h_+ \rightarrow 0 ,$$

and using (5.43) we have:

$$\kappa(D_E) = 1 , \quad \kappa(D_V) = \alpha .$$

(5.44) finally yields:

$$\delta \leq \frac{1}{\alpha} \frac{2}{3\tilde{\beta}\tilde{\gamma}} = O(h_+) \quad \text{as } h_+ \rightarrow 0 ,$$

using (5.30) and the fact that both $\tilde{\beta}$ and $\tilde{\gamma}$ are independent of h_+ , as proved in §5.1.1.

The next example shows that the striking difference in the results of Theorems 5.1.1 and 5.1.2. is a consequence of the fact that the standard convergence theory for Newton's method lacks the affine invariant properties of the algorithm. This has already been investigated in abstract terms in §4.4. In the following example, it will be illustrated by discussing a practical situation when Theorem 4.1.2 guarantees the convergence of the Newton's sequence $\{\tilde{x}^k\}$ for (5.10) but does not ensure the convergence of the sequence $\{x^k\}$ for (5.5), even though the initial guesses are related by:

$$x^0 = D_V \tilde{x}^0 . \quad (5.45)$$

We recall that if (5.45) holds then $\{\tilde{x}^k\}$ converges to \tilde{x}^* if and only if $\{x^k\}$ converges to x^* , see Corollary 4.4.1.

Example 5.1.1. Let $\xi \in (0, \tilde{\delta})$, let $\rho := 1 + \eta^2(\tilde{\delta} - \xi)$ and let

$$\tilde{x}^0 := \rho \tilde{x}^* = \rho \left(\frac{1}{\eta^2}, \frac{1}{\eta^2} \right)^T$$

be the initial guess for the iterates $\{\tilde{x}^k\}$. It is easy to check that \tilde{x}^0 is in $B(\tilde{x}^*, \tilde{\delta})$, the ball of quadratic convergence of Newton's method applied to (5.10) (see (5.14)). In fact we have:

$$\|\tilde{x}^0 - \tilde{x}^*\|_\infty = |\rho - 1| \|\tilde{x}^*\|_\infty = \tilde{\delta} - \xi < \tilde{\delta} ,$$

hence Theorem 4.1.2 ensures the convergence of the Newton's sequence $\{\tilde{x}^k\}$ for the system

5.1. Newton's method for a model reduced 2×2 problem

(5.10). Consider now the transformed starting guess x^0 for the iterates $\{x^k\}$:

$$x^0 = D_V \tilde{x}^0 = \rho x^* = \rho \left(\frac{1}{\eta^2}, \frac{\alpha}{\eta^2} \right)^T,$$

we have that

$$\|x^0 - x^*\|_\infty = (\tilde{\delta} - \xi)\alpha = O\left(\frac{1}{h_+}\right) \quad \text{as } h_+ \rightarrow 0.$$

Therefore, for h_+ sufficiently small, x^0 is not in $B(x^*, \delta)$, the ball of quadratic convergence of Newton's method applied to (5.5) (see (5.28)), because $\delta \leq O(h_+)$ as $h_+ \rightarrow 0$ (see §5.1.2). Then Theorem 4.1.2 does not guarantee the convergence of the Newton's sequence $\{x^k\}$ for the system (5.5). But we know $\{x^k\}$ does converge to x^* from Corollary 4.4.1.

5.1.3 Practical properties of Newton's method

We now show that the weighted L_∞ norm induced by D_V , defined in (5.12), with D_V given in (5.9), is not merely a useful tool for overcoming a failure of the standard convergence theory of Newton's method applied to system (5.5), but is also essential for explaining the size of the errors in Newton's iterates as the iteration proceeds.

Let

$$x^{n+1} = x^n - F'(x^n)^{-1} F(x^n) \tag{5.46}$$

be the Newton's iterates for the system (5.5):

$$F(x) := \begin{bmatrix} -\alpha^2 \frac{k_+^2}{\varepsilon_+} + \varepsilon_+ \\ \varepsilon_+ - \eta \alpha k_+^{3/2} \end{bmatrix} = 0, \tag{5.47}$$

with $x^n := (k_+^n, \varepsilon_+^n)^T$ and

$$F'(x^n)^{-1} = \frac{1}{\det(F'(x^n))} \begin{bmatrix} 1 & -\alpha^2 \left(\frac{k_+^n}{\varepsilon_+^n} \right)^2 - 1 \\ \frac{3}{2} \eta \alpha (k_+^n)^{1/2} & -2\alpha^2 \frac{k_+^n}{\varepsilon_+^n} \end{bmatrix}, \tag{5.48}$$

where

$$\det(F'(x^n)) = -2\alpha^2 \frac{k_+^n}{\varepsilon_+^n} + \frac{3}{2} \eta \alpha (k_+^n)^{1/2} \left[\alpha^2 \left(\frac{k_+^n}{\varepsilon_+^n} \right)^2 + 1 \right],$$

and let us recall that the solution to (5.47) is

$$x^* = (k_+^*, \varepsilon_+^*)^T = \left(\frac{1}{\eta^2}, \frac{\alpha}{\eta^2} \right)^T. \tag{5.49}$$

5.1. Newton's method for a model reduced 2×2 problem

In what follows, we will first try to get some insight into the practical aspects of Newton's method for (5.47), by analyzing qualitatively the behaviour of the iterates (5.46) in the weighted L_∞ norm (see Observation 5.1.3 and Observation 5.1.4). The preliminary qualitative observations will then be formalized (see Lemma 5.1.3, Proposition 5.1.5 and Proposition 5.1.6) and finally illustrated by numerical experiments (see Table 5.1 and Table 5.2).

Observation 5.1.3. Consider the condition that the iterates $\{x^n\}$ all lie in $B_{D_V}(x^*, \tilde{\delta})$, the ball of convergence predicted by Theorem 4.1.2, with centre in x^* and radius $\tilde{\delta}$ measured in the weighted L_∞ norm (see (5.13)):

$$\|x^n - x^*\|_{D_V^{-1}} = \|D_V^{-1}(x^n - x^*)\|_\infty = \max \left\{ |k_+^n - k_+^*|, \frac{1}{\alpha} |\varepsilon_+^n - \varepsilon_+^*| \right\} < \tilde{\delta}. \quad (5.50)$$

For $n=0$ this yields:

$$\|x^0 - x^*\|_{D_V^{-1}} = \max \left\{ |k_+^0 - k_+^*|, \frac{1}{\alpha} |\varepsilon_+^0 - \varepsilon_+^*| \right\} < \tilde{\delta},$$

this suggests that if $h_+ \ll 1$ (correspondingly $\alpha \gg 1$), then ε_+^0 can be much less accurate than k_+^0 without preventing Newton's method from converging, provided the following scaling proportionality holds

$$|\varepsilon_+^0 - \varepsilon_+^*| = \alpha |k_+^0 - k_+^*| \quad (5.51)$$

and k_+^0 is sufficiently close to k_+^* . Moreover, observing from (5.49) that

$$\varepsilon_+^* = \alpha k_+^*, \quad (5.52)$$

we can expect the iterates $\{x^n = (k_+^n, \varepsilon_+^n)^T\}$ to satisfy asymptotically the relation:

$$\varepsilon_+^n \sim \alpha k_+^n, \quad (5.53)$$

and therefore also:

$$|\varepsilon_+^n - \varepsilon_+^*| \sim \alpha |k_+^n - k_+^*|, \quad (5.54)$$

where the right-hand side can be obtained from the left-hand side using (5.52) and (5.53). Note that the properties (5.53)-(5.54) are consistent with the condition that $x^n \in B_{D_V}(x^*, \tilde{\delta})$, see (5.50).

Thus for the rest of this subsection we shall assume that the components of the initial guess $x^0 = (k_+^0, \varepsilon_+^0)^T$ are related by:

$$\varepsilon_+^0 = \alpha k_+^0. \quad (5.55)$$

From this we will show that

- i) $x^n \in B_{D_V}(x^*, \tilde{\delta})$ for all $n = 0, 1, \dots$, provided k_+^0 is sufficiently accurate (see Lemma 5.1.3)
- ii) the sequence $\{x^n\}$ satisfies (5.53)-(5.54) (see Lemma 5.1.4 and Proposition 5.1.5).

5.1. Newton's method for a model reduced 2×2 problem

iii) the accuracy of the iterates x^n increases as $h_+ \rightarrow 0$ (see Proposition 5.1.6).

The relation (5.54) will finally be illustrated numerically in Table 5.1 and Table 5.2. Finally, note that (5.55), combined with (5.52), implies (5.51):

$$|\varepsilon_+^0 - \varepsilon_+^*| = \alpha |k_+^0 - k_+^*| \gg |k_+^0 - k_+^*|, \quad \text{for } h_+ \ll 1.$$

Lemma 5.1.3. *Let $x^0 = (k_+^0, \varepsilon_+^0)$ have the property (5.55) and let*

$$|k_+^0 - k_+^*| < \tilde{\delta}, \quad (5.56)$$

then $x^n \in B_{D_V}(x^*, \tilde{\delta})$.

Proof. As noticed above, (5.55) yields:

$$|\varepsilon_+^0 - \varepsilon_+^*| = \alpha |k_+^0 - k_+^*|,$$

using this and (5.56), we get

$$\begin{aligned} \|x^0 - x^*\|_{D_V^{-1}} &= \|D_V^{-1}(x^0 - x^*)\|_\infty \\ &= \max \left\{ |k_+^0 - k_+^*|, \frac{1}{\alpha} |\varepsilon_+^0 - \varepsilon_+^*| \right\} = |k_+^0 - k_+^*| < \tilde{\delta}, \end{aligned}$$

i.e. $x^0 \in B_{D_V}(x^*, \tilde{\delta})$. It is then a property on Newton's method that $x^n \in B_{D_V}(x^*, \tilde{\delta})$ for all n , see Theorem 4.1.2. \square

We now show that the Newton's iterates have the properties (5.53)-(5.54).

Lemma 5.1.4. *Provided the starting guess $x^0 = (k_+^0, \varepsilon_+^0)^\top$ satisfies (5.55), we have that the components of the iterates $x^n = (k_+^n, \varepsilon_+^n)^\top$ are such that*

$$\varepsilon_+^n = \alpha k_+^n, \quad \forall n = 0, 1, 2, \dots \quad (5.57)$$

Proof. The proof is by induction on n . (5.57) is obviously true for $n = 0$ as a result of the choice of x^0 . Assume that the components of the n -th iterate x^n satisfy (5.57), then, using this assumption, we get the following expression for $w^n := (s^n, t^n)^\top$, the Newton's correction to x^n ,

$$w^n = \begin{bmatrix} s^n \\ t^n \end{bmatrix} := -F'(x^n)^{-1}F(x^n) = \frac{-2}{\det(J_F(x^n))} \begin{bmatrix} \varepsilon_+^n - \eta(k_+^n)^{3/2} \\ \alpha(\varepsilon_+^n - \eta(k_+^n)^{3/2}) \end{bmatrix},$$

which shows that

$$t^n = \alpha s^n. \quad (5.58)$$

5.1. Newton's method for a model reduced 2×2 problem

Therefore we obtain:

$$\varepsilon_+^{n+1} = \varepsilon_+^n + t^n = \alpha (k_+^n + s^n) = \alpha k_+^{n+1},$$

we then conclude that (5.57) holds for every n . \square

Proposition 5.1.5. *If the starting guess $x^0 = (k_+^0, \varepsilon_+^0)^T$ satisfies (5.55), then*

$$|\varepsilon_+^n - \varepsilon_+^*| = \alpha |k_+^n - k_+^*| \quad \forall n = 0, 1, 2, \dots \quad (5.59)$$

Proof. (5.59) follows from (5.57) and the fact $\varepsilon_+^* = \alpha k_+^*$ (see (5.49)):

$$|\varepsilon_+^n - \varepsilon_+^*| = |\alpha k_+^n - \alpha k_+^*| = \alpha |k_+^n - k_+^*| \quad \forall n = 0, 1, 2, \dots \quad \square$$

We now discuss the prediction of Theorem 4.1.2 about the q-quadratic convergence of Newton's iterates $\{x^n\}$ for (5.47).

Observation 5.1.4. In the weighted L_∞ norm, the q-quadratic convergence of the sequence $\{x^n\}$ is expressed by:

$$\frac{\|x^{n+1} - x^*\|_{D_V^{-1}}}{\|x^n - x^*\|_{D_V^{-1}}^2} < \tilde{K} := \frac{3}{2} \tilde{\beta} \tilde{\gamma}, \quad (5.60)$$

see (4.6). Note that the asymptotic constant \tilde{K} is independent of h_+ , because both $\tilde{\beta}$ and $\tilde{\gamma}$ do not depend on h_+ , as it was shown in the proof of Theorem 5.1.1 (numerical illustration of the h_+ -independence of \tilde{K} will be given in Table 5.1 and Table 5.2). On the other hand, in the standard L_∞ norm we have:

$$\frac{\|x^{n+1} - x^*\|_\infty}{\|x^n - x^*\|_\infty^2} < K := \frac{3}{2} \beta \gamma = O\left(\frac{1}{h_+}\right), \quad \text{as } h_+ \rightarrow 0 \quad (5.61)$$

as follows from the fact that

$$\beta = \frac{7}{2}, \quad \gamma = O\left(\frac{1}{h_+}\right), \quad \text{as } h_+ \rightarrow 0,$$

(see the proof of Theorem 5.1.2). However, in Proposition 5.1.6 below, exploiting the h_+ -independence of \tilde{K} , we will show instead that the rate of convergence in the L_∞ norm is correctly described by

$$\frac{\|x^{n+1} - x^*\|_\infty}{\|x^n - x^*\|_\infty^2} < O(h_+), \quad \text{as } h_+ \rightarrow 0$$

(numerical illustration of this will be given in Table 5.1 and Table 5.2). Therefore, the L_∞ estimate of the Lipschitz constant γ , which determines the proportionality of K to $1/h_+$ in (5.61), proves again to be misleading. In fact we obtain the startling result that Newton's method becomes *more* robust as $h_+ \rightarrow 0$. This phenomenon is also observed in the full k - ε system, see Table 5.9.

5.1. Newton's method for a model reduced 2×2 problem

Proposition 5.1.6. *If the initial guess x^0 satisfies (5.55), then*

$$\frac{\|x^{n+1} - x^*\|_\infty}{\|x^n - x^*\|_\infty^2} < C h_+, \quad \forall n = 0, 1, 2, \dots \quad (5.62)$$

with constant C independent of h_+ .

Proof. By (5.59) and the fact that $\alpha \gg 1$ we have:

$$\begin{aligned} \|x^n - x^*\|_\infty &= \max \left\{ |k_+^n - k_+^*|, |\varepsilon_+^n - \varepsilon_+^*| \right\} \\ &= \max \left\{ |k_+^n - k_+^*|, \alpha |k_+^n - k_+^*| \right\} \\ &= \alpha |k_+^n - k_+^*|, \end{aligned}$$

therefore:

$$\frac{\|x^{n+1} - x^*\|_\infty}{\|x^n - x^*\|_\infty^2} = \frac{1}{\alpha} \frac{|k_+^{n+1} - k_+^*|}{|k_+^n - k_+^*|^2}. \quad (5.63)$$

But, using (5.59), we also get:

$$\begin{aligned} \|x^n - x^*\|_{D_V^{-1}} &= \max \left\{ |k_+^n - k_+^*|, \frac{1}{\alpha} |\varepsilon_+^n - \varepsilon_+^*| \right\} \\ &= \max \left\{ |k_+^n - k_+^*|, |k_+^n - k_+^*| \right\} \\ &= |k_+^n - k_+^*|. \end{aligned} \quad (5.64)$$

Finally, combining (5.64) with (5.63) we obtain:

$$\frac{\|x^{n+1} - x^*\|_\infty}{\|x^n - x^*\|_\infty^2} = \frac{1}{\alpha} \frac{\|x^{n+1} - x^*\|_{D_V^{-1}}}{\|x^n - x^*\|_{D_V^{-1}}^2} < \tilde{K} \frac{1}{\alpha},$$

from which the result follows using the definition of α in (5.3) and the fact that \tilde{K} is independent of h_+ . \square

We now discuss the computational experiments that we have performed as illustration to the results presented throughout this subsection.

The robust convergence of Newton's method for (5.47) with respect to $h_+ \rightarrow 0$ (see Theorem 5.1.1), has been checked numerically by showing that the actual ball of convergence of Newton's method does not shrink as $h_+ \rightarrow 0$. For this purpose, we have considered a sequence of decreasing values of h_+ , $\{h_+ = 10^{-1}, 10^{-2}, 10^{-3}, 10^{-4}\}$, and, for each h_+ , the following family of initial guesses for Newton's method:

$$x_{i,j}^0 = x^* + \rho_i v_j \quad (5.65)$$

where x^* is the solution to (5.47), given in (5.49), $\{\rho_i\}$ is an increasing sequence of positive numbers and $\{v_j\}$ is a sequence random vectors uniformly distributed over the interval $[0, 1]$. The experiment then consists in prescribing ρ_i and in initializing Newton's method with N

5.2. Robustness of Newton's method for the discretised 1D turbulence equations

different initial guesses $x_{i,j}^0$, $j = 1, \dots, N$ corresponding to N different random vectors v_j . If the algorithm successfully converges for all initial guesses $x_{i,j}^0$, then ρ_i is replaced by ρ_{i+1} and N other initial guesses $x_{i+1,j}^0$ are considered as before, and so on. The value $\rho_{\bar{n}}$ for which Newton's method fails to converge will then represent an estimate of the upper bound on the radius of the actual ball of convergence. This experiment has proved Newton's method for (5.47) to converge robustly because decreasing the value of h_+ from 10^{-1} to 10^{-4} has not determined a corresponding decrease in $\rho_{\bar{n}}$. Due to the simplicity of the system (5.47), it has not been possible to identify a finite value of $\rho_{\bar{n}}$ for which Newton's algorithm failed, in fact in this case it seems $\rho_{\bar{n}} = \infty$.

Clear numerical illustration of Proposition 5.1.5, Proposition 5.1.6 and of the h_+ -independence of \tilde{K} in (5.60) is given in Table 5.1 and in Table 5.2.

The results presented in Table 5.1 have been obtained by starting Newton's method with $x^0 = (k_+^0, \varepsilon_+^0)^T$ satisfying (5.55):

$$\varepsilon_+^0 = \alpha k_+^0,$$

and choosing $k_+^0 = 428.2$. They show that (5.59) is satisfied by every iterate, as predicted by Proposition 5.1.5, and confirm (5.62) together with the h_+ -independence of \tilde{K} . (Several other values of k_+^0 have been used, always yielding similar results). In order to show experimentally that (5.59) is an asymptotic property of the Newton's sequence $\{x^n\}$, we have considered initial guesses as in (5.65):

$$x^0 = x^* + \rho w$$

where ρ is a number and w is a random vector uniformly distributed over the interval $[0, 1]$. In Table 5.2, we present the results corresponding to $\rho = 500$ and $w = (0.69318, 0.650106)^T$. These illustrate once more (5.62) and the h_+ -independence of \tilde{K} , and show that (in our experiments at least) the iterates x^n do satisfy asymptotically (5.59), even if the initial guess assumption (5.55) is not satisfied.

5.2 Robustness of Newton's method for the discretised 1D turbulence equations

After having analyzed in detail the model 2×2 system (5.5), we now turn to the analysis of Newton's method for the system arising from the discretisation of the full 1D turbulent Couette and Poiseuille flows. Initially, we will briefly derive the finite element approximation to the 1D weak forms presented in §2.6, then we will devote §5.2.1 and §5.2.2 to studying the properties of Newton's method for the discrete RANS and k - ε equations and for the k - ε equations only. (In the latter case the velocity field will be assumed to be known exactly in the boundary value problem (2.39)-(2.47)). In both cases we will apply a combination of affine covariant and contravariant transformations, and identify a condition on the size of the mesh such that, in a

5.2. Robustness of Newton's method for the discretised 1D turbulence equations

$$\varepsilon_+^0 = \alpha k_+^0, \quad k_+^0 = 428.2$$

		$h_+ = 10^{-1}, \alpha = 1.99 \times 10$			$h_+ = 10^{-2}, \alpha = 1.99 \times 10^2$		
n	$\frac{\ x^n - x^*\ _\infty}{\ x^{n-1} - x^*\ _\infty^2}$	$\frac{\ x^n - x^*\ _{D_V^{-1}}}{\ x^{n-1} - x^*\ _{D_V^{-1}}^2}$	$\frac{ \varepsilon_+^n - \varepsilon_+^* }{ k_+^n - k_+^* }$	$\frac{\ x^n - x^*\ _\infty}{\ x^{n-1} - x^*\ _\infty^2}$	$\frac{\ x^n - x^*\ _{D_V^{-1}}}{\ x^{n-1} - x^*\ _{D_V^{-1}}^2}$	$\frac{ \varepsilon_+^n - \varepsilon_+^* }{ k_+^n - k_+^* }$	
0			1.99×10			1.99×10^2	
1	4.35×10^{-5}	8.69×10^{-4}	1.99×10	4.35×10^{-6}	8.69×10^{-4}	1.99×10^2	
2	1.18×10^{-4}	2.35×10^{-3}	1.99×10	1.18×10^{-5}	2.36×10^{-3}	1.99×10^2	
3	2.96×10^{-4}	5.91×10^{-3}	1.99×10	2.96×10^{-5}	5.91×10^{-3}	1.99×10^2	
4	6.50×10^{-4}	1.30×10^{-2}	1.99×10	6.50×10^{-5}	1.30×10^{-2}	1.99×10^2	
5	1.11×10^{-3}	2.21×10^{-2}	1.99×10	1.11×10^{-4}	2.21×10^{-2}	1.99×10^2	
6	1.34×10^{-3}	2.67×10^{-2}	1.99×10	1.34×10^{-4}	2.67×10^{-2}	1.99×10^2	
7	1.36×10^{-3}	2.71×10^{-2}	1.99×10	1.36×10^{-4}	2.72×10^{-2}	1.99×10^2	

		$h_+ = 10^{-3}, \alpha = 1.99 \times 10^3$			$h_+ = 10^{-4}, \alpha = 1.99 \times 10^4$		
n	$\frac{\ x^n - x^*\ _\infty}{\ x^{n-1} - x^*\ _\infty^2}$	$\frac{\ x^n - x^*\ _{D_V^{-1}}}{\ x^{n-1} - x^*\ _{D_V^{-1}}^2}$	$\frac{ \varepsilon_+^n - \varepsilon_+^* }{ k_+^n - k_+^* }$	$\frac{\ x^n - x^*\ _\infty}{\ x^{n-1} - x^*\ _\infty^2}$	$\frac{\ x^n - x^*\ _{D_V^{-1}}}{\ x^{n-1} - x^*\ _{D_V^{-1}}^2}$	$\frac{ \varepsilon_+^n - \varepsilon_+^* }{ k_+^n - k_+^* }$	
0			1.99×10^3			1.99×10^4	
1	4.35×10^{-7}	8.69×10^{-4}	1.99×10^3	4.35×10^{-8}	8.68×10^{-4}	1.99×10^4	
2	1.18×10^{-6}	2.35×10^{-3}	1.99×10^3	1.18×10^{-7}	2.35×10^{-3}	1.99×10^4	
3	2.96×10^{-6}	5.91×10^{-3}	1.99×10^3	2.96×10^{-7}	5.91×10^{-3}	1.99×10^4	
4	6.49×10^{-6}	1.30×10^{-2}	1.99×10^3	6.50×10^{-7}	1.30×10^{-2}	1.99×10^4	
5	1.11×10^{-5}	2.21×10^{-2}	1.99×10^3	1.11×10^{-6}	2.21×10^{-2}	1.99×10^4	
6	1.33×10^{-5}	2.67×10^{-2}	1.99×10^3	1.34×10^{-6}	2.67×10^{-2}	1.99×10^4	
7	1.36×10^{-5}	2.71×10^{-2}	1.99×10^3	1.36×10^{-6}	2.71×10^{-2}	1.99×10^4	

Table 5.1: Rates of convergence of Newton's sequence for (5.47) and proportionality between the errors in each component of the iterate $x^n = (k_+^n, \varepsilon_+^n)^T$ when Newton's method is initialized with $x^0 = (k_+^0, \varepsilon_+^0)^T$ such that $\varepsilon_+^0 = \alpha k_+^0$, $k_+^0 = 428.2$.

suitable neighbourhood of the true solution, the Jacobian of the transformed system remains bounded with bounded inverse as $h_+ \rightarrow 0$. This, together with the affine invariant properties of Newton's method discussed in §§4.4, 4.5, will then be exploited to show the robust convergence of Newton's method for the untransformed original system. We will give numerical illustration

5.2. Robustness of Newton's method for the discretised 1D turbulence equations

$$x^0 = x^* + \rho w, \quad \rho = 500, \quad w = (0.69318, 0.650106)^T$$

		$h_+ = 10^{-1}, \alpha = 1.99 \times 10$			$h_+ = 10^{-2}, \alpha = 1.99 \times 10^2$		
n	$\frac{\ x^n - x^*\ _\infty}{\ x^{n-1} - x^*\ _\infty^2}$	$\frac{\ x^n - x^*\ _{D_V^{-1}}}{\ x^{n-1} - x^*\ _{D_V^{-1}}^2}$	$\frac{ \varepsilon_+^n - \varepsilon_+^* }{ k_+^n - k_+^* }$	$\frac{\ x^n - x^*\ _\infty}{\ x^{n-1} - x^*\ _\infty^2}$	$\frac{\ x^n - x^*\ _{D_V^{-1}}}{\ x^{n-1} - x^*\ _{D_V^{-1}}^2}$	$\frac{ \varepsilon_+^n - \varepsilon_+^* }{ k_+^n - k_+^* }$	
0			9.38×10^{-1}			9.38×10^{-1}	
1	8.54×10^{-4}	8.54×10^{-4}	4.87×10^{-1}	1.28×10^{-2}	8.39×10^{-4}	1.52×10	
2	1.06×10^{-2}	2.14×10^{-3}	4.96	1.13×10^{-3}	1.93×10^{-3}	1.36×10^2	
3	1.32×10^{-2}	1.62×10^{-2}	1.25×10^2	4.36×10^{-4}	4.01×10^{-2}	5.45×10^2	
4	2.60×10^{-3}	5.19×10^{-2}	2.95×10	2.23×10^{-4}	4.46×10^{-2}	2.80×10^2	
5	3.54×10^{-4}	9.42×10^{-3}	1.50×10	5.89×10^{-5}	1.52×10^{-2}	1.55×10^2	
6	2.10×10^{-3}	2.47×10^{-2}	1.91×10	1.84×10^{-4}	2.28×10^{-2}	1.93×10^2	
7	1.48×10^{-3}	2.71×10^{-2}	1.99×10	1.45×10^{-4}	2.70×10^{-2}	1.99×10^2	
8				1.36×10^{-4}	2.72×10^{-2}	1.99×10^2	
		$h_+ = 10^{-3}, \alpha = 1.99 \times 10^3$			$h_+ = 10^{-4}, \alpha = 1.99 \times 10^4$		
n	$\frac{\ x^n - x^*\ _\infty}{\ x^{n-1} - x^*\ _\infty^2}$	$\frac{\ x^n - x^*\ _{D_V^{-1}}}{\ x^{n-1} - x^*\ _{D_V^{-1}}^2}$	$\frac{ \varepsilon_+^n - \varepsilon_+^* }{ k_+^n - k_+^* }$	$\frac{\ x^n - x^*\ _\infty}{\ x^{n-1} - x^*\ _\infty^2}$	$\frac{\ x^n - x^*\ _{D_V^{-1}}}{\ x^{n-1} - x^*\ _{D_V^{-1}}^2}$	$\frac{ \varepsilon_+^n - \varepsilon_+^* }{ k_+^n - k_+^* }$	
0			9.38×10^{-1}			9.38×10^{-1}	
1	1.45×10^{-1}	8.37×10^{-4}	1.73×10^2	1.47	8.37×10^{-4}	1.75×10^3	
2	9.30×10^{-5}	1.91×10^{-3}	1.46×10^3	9.13×10^{-6}	1.91×10^{-3}	1.47×10^4	
3	4.08×10^{-5}	4.34×10^{-2}	5.28×10^3	4.06×10^{-6}	4.38×10^{-2}	5.26×10^4	
4	2.23×10^{-5}	4.46×10^{-2}	2.78×10^3	2.23×10^{-6}	4.46×10^{-2}	2.78×10^4	
5	6.36×10^{-6}	1.65×10^{-2}	1.54×10^3	6.41×10^{-7}	1.66×10^{-2}	1.55×10^4	
6	1.79×10^{-5}	2.22×10^{-2}	1.93×10^3	1.78×10^{-6}	2.21×10^{-2}	1.93×10^4	
7	1.45×10^{-5}	2.69×10^{-2}	1.99×10^3	1.45×10^{-6}	2.69×10^{-2}	1.99×10^4	
8	1.36×10^{-5}	2.71×10^{-2}	1.99×10^3	1.36×10^{-6}	2.71×10^{-2}	1.99×10^4	

Table 5.2: Rates of convergence of Newton's sequence for (5.47) and proportionality between the errors in each component of the iterate $x^n = (k_+^n, \varepsilon_+^n)^T$ when Newton's method is initialized with $x^0 = x^* + \rho w$ where x^* is the solution to (5.47), $\rho = 500$ and $w = (0.69318, 0.650106)^T$

of the theoretical results for one- and two-dimensional flows.

We make the following assumption:

5.2. Robustness of Newton's method for the discretised 1D turbulence equations

Assumption 5.2.1. From now to the end of Chapter 5 we will restrict our analysis to the continuous piecewise linear finite element approximation of the 1D turbulent Couette flow (2.48)-(2.56).

It should be remarked that Assumption 5.2.1 has been made with the only purpose of presenting our arguments in the clearest possible way. In fact, the results on the robustness of Newton's method, which follow below, can be proved also for the 1D turbulent Poiseuille flow (2.94)-(2.102) and for continuous finite elements of any order.

Let the domain $[h_+, 1]$ be divided into N subintervals:

$$h_+ = y_1 < y_2 < \dots < y_N < y_{N+1} = 1$$

with the j^{th} subinterval $e_j := [y_j, y_{j+1}]$ having length h_j . We consider the discretisation on the mesh $\{y_i\}$ of (2.128) (with $\mathcal{G} = 0$), (2.136), (2.138) and (2.137), with u_* , in (2.128), supposed to be known. Even if u_* is regarded as known, we are still assuming that, at $y = h_+$, ε and k are related by (2.138). Let

$$U^h(y) = \sum_{j=1}^N U_j \phi_j(y) + U_{\text{CL}} \phi_{N+1}(y), \quad k^h(y) = \sum_{j=1}^{N+1} k_j \phi_j(y), \quad \varepsilon^h(y) = \sum_{j=1}^{N+1} \varepsilon_j \phi_j(y)$$

be the finite element approximations to U , k and ε respectively (where $\{\phi_j\}$ are the usual hat functions), and let

$$\mathbf{F}(\mathbf{x}) = \begin{bmatrix} \mathbf{F}_U(\mathbf{x}) \\ \mathbf{F}_k(\mathbf{x}) \\ \mathbf{F}_{\text{nl}}(\mathbf{x}) \\ \mathbf{F}_\varepsilon(\mathbf{x}) \end{bmatrix} = \mathbf{0} \quad (5.66)$$

be the nonlinear system arising from the discretisation of the equations considered. In (5.66) there are $3N + 2$ equations, and

$$\mathbf{x} := (\mathbf{U}^T, \mathbf{k}^T, \boldsymbol{\varepsilon}^T)^T := (U_1, \dots, U_N, k_1, \dots, k_{N+1}, \varepsilon_1, \dots, \varepsilon_{N+1})^T$$

is the vector of U -, k - and ε -freedoms, while

$$(\mathbf{F}_U(\mathbf{x}))_i := a(U^h, k^h, \varepsilon^h, \phi_i), \quad i = 1, \dots, N, \quad (5.67)$$

with the form a given by (2.128) with $\mathcal{G} = 0$,

$$(\mathbf{F}_k(\mathbf{x}))_i := c(U^h, k^h, \varepsilon^h, \phi_i), \quad i = 1, \dots, N + 1, \quad (5.68)$$

with c specified in (2.133),

$$\mathbf{F}_{\text{nl}}(\mathbf{x}) := \varepsilon_1 - \frac{C_\mu^{3/4} k_1^{3/2}}{\kappa h_+}, \quad (5.69)$$

5.2. Robustness of Newton's method for the discretised 1D turbulence equations

and

$$(\mathbf{F}_\varepsilon(\mathbf{x}))_i := d(U^h, k^h, \varepsilon^h, \phi_i), \quad i = 2, \dots, N+1, \quad (5.70)$$

where d is defined in (2.134).

5.2.1 Newton's method for the RANS and k - ε equations

The convergence properties of Newton's method for (5.66) are now studied in the limit as $h_+ \rightarrow 0$. Before presenting the details, we briefly indicate our strategy. Initially we will show that, under a certain condition on the mesh grading (see (5.78)), it is possible to design a combination of affine covariant and contravariant transformations of system (5.66), such that all constant terms in the transformed system are essentially independent of h_+ , in the sense that they do not blow up or become arbitrarily small in the limit as $h_+ \rightarrow 0$ (what we mean by "constant terms" will become clear in Lemma 5.2.2). This, together with the assumption that the problem is well posed as $h_+ \rightarrow 0$ (see (5.100)), will imply the robust convergence for the transformed system. The robustness of Newton's method for (5.66) will then follow from its affine covariant and contravariant properties (§§4.4, 4.5).

We now simultaneously perform an appropriate affine covariant and an affine contravariant transformation of the system (5.66). Let us define the diagonal matrix

$$B := \begin{pmatrix} I_N & & & & \\ & I_{N+1} & & & \\ & & 1/y_1 & & \\ & & & \ddots & \\ & & & & 1/y_{N+1} \end{pmatrix},$$

with I_N and I_{N+1} respectively the $N \times N$ and $(N+1) \times (N+1)$ identity matrices. Then introduce the following combination of affine covariant and affine contravariant transformations of (5.66):

$$\mathbf{G}(\tilde{\mathbf{x}}) := B^{-1} \mathbf{F}(B\tilde{\mathbf{x}}) = \begin{bmatrix} \mathbf{G}_U(\tilde{\mathbf{x}}) \\ \mathbf{G}_k(\tilde{\mathbf{x}}) \\ \mathbf{G}_{\text{nl}}(\tilde{\mathbf{x}}) \\ \mathbf{G}_\varepsilon(\tilde{\mathbf{x}}) \end{bmatrix} = \mathbf{0}, \quad (5.71)$$

where:

$$\begin{aligned} \tilde{\mathbf{x}} &= B^{-1} \mathbf{x} = B^{-1} (\mathbf{U}^T, \mathbf{k}^T, \varepsilon^T)^T =: (\mathbf{U}^T, \mathbf{k}^T, \tilde{\varepsilon}^T)^T = \\ &= (U_1, \dots, U_N, k_1, \dots, k_{N+1}, \tilde{\varepsilon}_1, \dots, \tilde{\varepsilon}_{N+1})^T. \end{aligned} \quad (5.72)$$

Note that the transformations (5.71)-(5.72) involve a scaling both of the equations corresponding to the ε -freedoms and of the nodal values of ε^h , while the equations corresponding to the U - and k -freedoms and the nodal values of U^h and k^h are kept unchanged (the action of B^{-1}

5.2. Robustness of Newton's method for the discretised 1D turbulence equations

on \mathbf{x} essentially corresponds to scaling the ε -component of \mathbf{x} by y). By defining

$$\tilde{\varepsilon}^h(y) := \sum_{j=1}^{N+1} \tilde{\varepsilon}_j \phi_j(y) ,$$

and the “scaling operator” S such that:

$$S(\tilde{\varepsilon}^h)(y) = \sum_{j=1}^{N+1} \frac{\tilde{\varepsilon}_j}{y_j} \phi_j(y) = \varepsilon^h(y) , \quad (5.73)$$

the components of $\mathbf{G}(\tilde{\mathbf{x}})$ in (5.71) can be expressed as:

$$(\mathbf{G}_U(\tilde{\mathbf{x}}))_i = a(U^h, k^h, S(\tilde{\varepsilon}^h), \phi_i) , \quad i = 1, \dots, N \quad (5.74)$$

$$(\mathbf{G}_k(\tilde{\mathbf{x}}))_i = c(U^h, k^h, S(\tilde{\varepsilon}^h), \phi_i) , \quad i = 1, \dots, N+1 \quad (5.75)$$

$$\mathbf{G}_{\text{nl}}(\tilde{\mathbf{x}}) = \tilde{\varepsilon}_1 - \frac{C_\mu^{3/4}}{\kappa} k_1^{3/2} , \quad (5.76)$$

$$(\mathbf{G}_\varepsilon(\tilde{\mathbf{x}}))_i = y_i d(U^h, k^h, S(\tilde{\varepsilon}^h), \phi_i) , \quad i = 2, \dots, N+1 . \quad (5.77)$$

To see the benefits of the chosen scaling, consider, in particular, the following result:

Lemma 5.2.1. *The coefficients in the scaled “nodal law” $\mathbf{G}_{\text{nl}}(\tilde{\mathbf{x}})$ in (5.71) are independent of h_+ (see (5.76)).*

Proof. Recall that from (5.72) we have $\tilde{\varepsilon}_1 = y_1 \varepsilon_1$ with $y_1 = h_+$, hence, writing out the third component of (5.71), we have:

$$\begin{aligned} \mathbf{G}_{\text{nl}}(\tilde{\mathbf{x}}) &= y_1 \mathbf{F}_{\text{nl}}(B\tilde{\mathbf{x}}) \\ &= h_+ \left(\frac{\tilde{\varepsilon}_1}{h_+} - \frac{C_\mu^{3/4}}{\kappa} \frac{k_1^{3/2}}{h_+} \right) \\ &= \tilde{\varepsilon}_1 - \frac{C_\mu^{3/4}}{\kappa} k_1^{3/2} . \quad \square \end{aligned}$$

Indeed, we now show:

Lemma 5.2.2. *Assume that there exists a strictly positive constant C independent of h_+ such that*

$$\frac{h_j}{y_j} \leq C , \quad j = 1, 2, \dots, N \quad (5.78)$$

then $\mathbf{G}_U(\tilde{\mathbf{x}})$, $\mathbf{G}_k(\tilde{\mathbf{x}})$ and $\mathbf{G}_\varepsilon(\tilde{\mathbf{x}})$ (respectively first, second and fourth component of $\mathbf{G}(\tilde{\mathbf{x}})$ in (5.71)) are rational functions of $\tilde{\mathbf{x}}$ with coefficients which are bounded independently of h_+ as $h_+ \rightarrow 0$.

5.2. Robustness of Newton's method for the discretised 1D turbulence equations

We will show that the robust convergence of Newton's method for (5.71) is guaranteed by (5.78) together with the assumption that the original unscaled system is well posed for (see (5.100) and Observation 5.2.1) as $h_+ \rightarrow 0$. It should be noted that for a uniform mesh on the domain $[h_+, 1]$, with $h_+ \ll 1$, the number of elements needed to satisfy (5.78) is

$$N \gtrsim C h_+^{-1} . \quad (5.79)$$

Since in applications $h_+ = 10^{-3}$ or 10^{-4} , this can clearly make the computation unpractical (consider that N is the number of mesh points in one coordinate direction only). This observation then highlights the key role that graded meshes can have in assuring the robustness of Newton's method, by satisfying (5.78) with a small number of elements. In particular, Lemma 3.5.1 shows that the equidistributed mesh (3.59) readily meets the condition (5.78).

Below we will show that, for each $i = 2, \dots, N+1$, $(\mathbf{G}_\varepsilon(\tilde{\mathbf{x}}))_i$ (see (5.77)) is a rational function of $\tilde{\mathbf{x}}$ with coefficients which do not blow up or become arbitrarily small as $h_+ \rightarrow 0$. This will be done as now explained. First $(\mathbf{G}_\varepsilon(\tilde{\mathbf{x}}))_i$ will be expressed as a sum of integrals over the elements $e_j = [y_j, y_{j+1}]$ which contain the node y_i , then, through a special affine transformation, each element $e_j = [y_j, y_{j+1}]$ will be mapped onto the canonical interval $[-1, 1]$ and the corresponding elemental integral will be accordingly transformed. Finally, each transformed elemental integral will be shown to contain only rational functions of $\tilde{\mathbf{x}}$ which have coefficients bounded independently of $h_+ \rightarrow 0$. Applying exactly the same strategy to $(\mathbf{G}_U(\tilde{\mathbf{x}}))_i$ and $(\mathbf{G}_k(\tilde{\mathbf{x}}))_i$, respectively in (5.74) and (5.75), will yield the proof of Lemma 5.2.2.

Proof of Lemma 5.2.2 Expressing the form d in (5.77) (this is defined in (2.134)) in terms of the sum of the integrals over the elements e_j which contain the node y_i , we can write $(\mathbf{G}_\varepsilon(\tilde{\mathbf{x}}))_i$ as:

$$(\mathbf{G}_\varepsilon(\tilde{\mathbf{x}}))_i = \sum_{j: y_i \in e_j} y_i d^{e_j}(U^h, k^h, S(\tilde{\varepsilon}^h), \phi_i) , \quad i = 2, \dots, N+1 \quad (5.80)$$

with

$$\begin{aligned} y_i d^{e_j}(U^h, k^h, S(\tilde{\varepsilon}^h), \phi_i) = y_i \int_{e_j} \left\{ \frac{C_\mu}{\sigma_\varepsilon} \frac{(k^h)^2}{S(\tilde{\varepsilon}^h)} \frac{dS(\tilde{\varepsilon}^h)}{dy} \frac{d\phi_i}{dy} - \right. \\ \left. - C_{\varepsilon 1} C_\mu \left(\frac{dU^h}{dy} \right)^2 k^h \phi_i + C_{\varepsilon 2} \frac{(S(\tilde{\varepsilon}^h))^2}{k^h} \phi_i \right\} dy . \end{aligned} \quad (5.81)$$

The interval $e_j = [y_j, y_{j+1}]$ is then mapped onto the canonical interval $[-1, 1]$ by the affine transformation:

$$y = \frac{1}{2} y_j (1 - \eta) + \frac{1}{2} y_{j+1} (1 + \eta) , \quad \eta \in [-1, 1] , \quad (5.82)$$

and within each element e_j , U^h , k^h and $S(\tilde{\varepsilon}^h)$ are expressed in terms of the element basis

5.2. Robustness of Newton's method for the discretised 1D turbulence equations

functions $N_\alpha(\eta) = \phi_{j(\alpha)}(y(\eta))$ as shown below:

$$U^h(y(\eta)) = \sum_{\alpha=1}^2 U_{j(\alpha)} N_\alpha(\eta) =: \widehat{U}^h(\eta) , \quad (5.83)$$

$$k^h(y(\eta)) = \sum_{\alpha=1}^2 k_{j(\alpha)} N_\alpha(\eta) =: \widehat{k}^h(\eta) , \quad (5.84)$$

$$S(\widehat{\varepsilon}^h)(y(\eta)) = \sum_{\alpha=1}^2 \frac{\widehat{\varepsilon}_{j(\alpha)}}{y_{j(\alpha)}} N_\alpha(\eta) .$$

The index α refers to the local numbering of the vertices, and is such that $j(1) = j$, $j(2) = j+1$, with either $j = i$ or $j + 1 = i$. For reasons that will become clear below, we write $S(\widehat{\varepsilon}^h)(y(\eta))$ as follows:

$$S(\widehat{\varepsilon}^h)(y(\eta)) = \frac{1}{y_{j(1)}} \widehat{S}(\widehat{\varepsilon}^h)(\eta) , \quad (5.85)$$

where

$$\widehat{S}(\widehat{\varepsilon}^h)(\eta) := y_{j(1)} \sum_{\alpha=1}^2 \frac{\widehat{\varepsilon}_{j(\alpha)}}{y_{j(\alpha)}} N_\alpha(\eta) = \sum_{\alpha=1}^2 r_{j(\alpha)} \widehat{\varepsilon}_{j(\alpha)} N_\alpha(\eta) \quad (5.86)$$

with

$$r_{j(\alpha)} := \frac{y_{j(1)}}{y_{j(\alpha)}} . \quad (5.87)$$

Also, observing from (5.82) that

$$\frac{dy}{d\eta} = \frac{h_j}{2} , \quad (5.88)$$

we have:

$$\frac{d\phi_{j(\alpha)}}{dy}(y(\eta)) = \frac{2}{h_j} \frac{dN_\alpha}{d\eta}(\eta) , \quad (5.89)$$

while from (5.83) and (5.85) we get respectively:

$$\frac{dU}{dy}(y(\eta)) = \frac{2}{h_j} \frac{d\widehat{U}^h}{d\eta}(\eta) , \quad (5.90)$$

and

$$\frac{dS(\widehat{\varepsilon}^h)}{dy}(y(\eta)) = \frac{1}{y_{j(1)}} \frac{2}{h_j} \frac{d\widehat{S}(\widehat{\varepsilon}^h)}{d\eta}(\eta) . \quad (5.91)$$

Using (5.83)-(5.85) and (5.88)-(5.91) we can then express (5.81) as

$$\begin{aligned} y_i d^{ej}(\widehat{U}^h, \widehat{k}^h, \widehat{S}(\widehat{\varepsilon}^h), N_\alpha) &= \frac{y_i}{y_{j(1)}} \int_{[-1,1]} \left\{ \frac{2C_\mu}{\sigma_\varepsilon} \left(\frac{(\widehat{k}^h(\eta))^2}{\widehat{S}(\widehat{\varepsilon}^h)(\eta)} \right) \left(\frac{d\widehat{S}(\widehat{\varepsilon}^h)}{d\eta} \right) \frac{dN_\alpha}{d\eta} \frac{y_{j(1)}}{h_j} - \right. \\ &\quad \left. - 2C_{\varepsilon 1} C_\mu \left(\frac{d\widehat{U}^h}{d\eta} \right)^2 \widehat{k}^h(\eta) N_\alpha(\eta) \frac{y_{j(1)}}{h_j} + \frac{C_{\varepsilon 2}}{2} \frac{(\widehat{S}(\widehat{\varepsilon}^h)(\eta))^2}{\widehat{k}^h(\eta)} N_\alpha(\eta) \frac{h_j}{y_{j(1)}} \right\} d\eta . \end{aligned} \quad (5.92)$$

All constant terms in (5.92) are now shown to be bounded independently of $h_+ \rightarrow 0$. The

5.2. Robustness of Newton's method for the discretised 1D turbulence equations

terms in (5.92) which could exhibit a strong dependence on $h_+ \rightarrow 0$ are:

$$\frac{y_i}{y_{j(1)}} = \frac{y_i}{y_j}, \quad r_{j(\alpha)} = \frac{y_{j(1)}}{y_{j(\alpha)}} = \frac{y_j}{y_{j(\alpha)}}, \quad \frac{y_{j(1)}}{h_j} = \frac{y_j}{h_j}, \quad \frac{h_j}{y_{j(1)}} = \frac{h_j}{y_j}. \quad (5.93)$$

The first appears as a multiplicative constant outside the integral, the second is contained in the expressions for $\widehat{S}(\varepsilon^h)(\eta)$ and its derivative $d\widehat{S}(\varepsilon^h)/d\eta$ (see (5.86)), the third is both in the diffusion and in the source term and finally the last coefficient appears in the destruction term. For the first term in (5.93), it is not difficult to show that:

$$1 \leq \frac{y_i}{y_j} \leq 1 + C, \quad \text{for } j \text{ such that } y_i \in e_j. \quad (5.94)$$

To obtain (5.94), first recall that either $y_j = y_i$ or $y_{j+1} = y_i$, therefore:

$$\frac{y_i}{y_j} = \begin{cases} 1, & y_j = y_i \\ \frac{y_i}{y_{i-1}} = \frac{y_{i-1} + h_{i-1}}{y_{i-1}}, & y_{j+1} = y_i \end{cases} \quad (5.95)$$

then note that, for $y_{j+1} = y_i$, we have:

$$1 < \frac{y_{i-1} + h_{i-1}}{y_{i-1}} = 1 + \frac{h_{i-1}}{y_{i-1}} \leq 1 + C, \quad (5.96)$$

where we have used (5.78), finally (5.94) follows from (5.95) and (5.96). It is also easy to see that the second term in (5.93) can be bounded as follows:

$$\frac{1}{1+C} \leq r_{j(\alpha)} \leq 1, \quad \alpha = 1, 2. \quad (5.97)$$

For this consider that:

$$r_{j(\alpha)} = \frac{y_j}{y_{j(\alpha)}} = \begin{cases} 1, & \alpha = 1 \\ \frac{y_j}{y_{j+1}} = \frac{y_j}{y_j + h_j}, & \alpha = 2 \end{cases} \quad (5.98)$$

and for $\alpha=2$, by using also (5.78), it is not difficult to obtain:

$$\frac{1}{1+C} \leq \frac{y_j}{y_j + h_j} < 1, \quad (5.99)$$

hence (5.98) and (5.99) imply (5.97). The following lower bound for the third term in (5.93) is an obvious consequence of (5.78):

$$\frac{1}{C} \leq \frac{y_j}{h_j},$$

and the last term is bounded from above independently of $h_+ \rightarrow 0$ by assumption. This then shows that the integrand in (5.92) does not contain coefficients which blow up or tend to zero as $h_+ \rightarrow 0$, and this, together with the fact that the domain of integration is independent of h_+ , implies that none of the equations $(\mathbf{G}_\varepsilon(\tilde{\mathbf{x}}))_i, i=2, \dots, N+1$, in (5.77), contains terms which

5.2. Robustness of Newton's method for the discretised 1D turbulence equations

blow up or become arbitrarily small as $h_+ \rightarrow 0$. The same line of reasoning applied to (5.74) and (5.75) will yield the result. \square

Lemma 5.2.2 is now used to show that in a neighbourhood of the solution to (5.71), the entries of the Jacobian $\mathbf{G}'(\tilde{\mathbf{x}})$ are bounded independently of $h_+ \rightarrow 0$ (recall that the convergence of Newton's method depends on the properties of the Jacobian of the nonlinear system which is being solved, see Lemma 4.1.1 and Theorem 4.1.2). The result below clearly follows from Lemma 5.2.2.

Corollary 5.2.3. *Let the assumption of Lemma 5.2.2 hold. Then the solution $\tilde{\mathbf{x}}^*$ to (5.71) does not blow up or become arbitrarily small as $h_+ \rightarrow 0$.*

From Lemma 5.2.2 and Corollary 5.2.3, we then have

Lemma 5.2.4. *Let the assumption of Lemma 5.2.2 hold. Then there exist a neighbourhood of $\tilde{\mathbf{x}}^*$, $B(\tilde{\mathbf{x}}^*, \tilde{\sigma})$, such that for all $\tilde{\mathbf{y}} \in B(\tilde{\mathbf{x}}^*, \tilde{\sigma})$ the entries of the Jacobian of the system in (5.71),*

$$(\mathbf{G}'(\tilde{\mathbf{y}}))_{ij} := \frac{\partial G_i}{\partial \tilde{x}_j}(\tilde{\mathbf{y}}) ,$$

do not blow up or become arbitrarily small as $h_+ \rightarrow 0$.

Proof. The result follows from the fact that the entries of $\mathbf{G}(\tilde{\mathbf{x}})$ are rational functions of $\tilde{\mathbf{x}}$ with coefficients bounded independently of $h_+ \rightarrow 0$ (see Lemma 5.2.1 and Lemma 5.2.2) and the fact that if $\tilde{\mathbf{y}}$ is sufficiently close to $\tilde{\mathbf{x}}^*$, then $\|\tilde{\mathbf{y}}\|$ does not blow up or tend to 0 as $h_+ \rightarrow 0$ because so does $\|\tilde{\mathbf{x}}^*\|$ (Corollary 5.2.3). \square

We finally have:

Theorem 5.2.5. *Let the assumption of Lemma 5.2.2 hold, and suppose that there exists a strictly positive constant b independent of h_+ such that*

$$|\det(\mathbf{G}'(\tilde{\mathbf{x}}^*))| > b . \tag{5.100}$$

Then Newton's method for (5.71) is robust in the limit $h_+ \rightarrow 0$.

Observation 5.2.1. Note that (5.100) indicates that, as $h_+ \rightarrow 0$, the problem (5.71) is well posed for Newton's method to be used. It should also be remarked that (5.100) follows the assumption that the original unscaled problem (5.66) is well posed, i.e. that there exists a strictly positive constant b independent of h_+ such that

$$|\det(\mathbf{F}'(\mathbf{x}^*))| > b . \tag{5.101}$$

It is easy to see this, in fact from (5.71) we have $\mathbf{G}'(\tilde{\mathbf{x}}^*) = B^{-1}\mathbf{F}'(B\tilde{\mathbf{x}}^*)B$ and therefore $\det(\mathbf{G}'(\tilde{\mathbf{x}}^*)) = \det(\mathbf{F}'(\mathbf{x}^*))$. The validity of (5.101) (and therefore of (5.100)) has been verified computationally.

5.2. Robustness of Newton's method for the discretised 1D turbulence equations

Proof of Theorem 5.2.5 Theorem 4.1.2 predicts that Newton's sequence for (5.71) has ball of convergence $B(\tilde{\mathbf{x}}^*, \tilde{\delta})$ with radius $\tilde{\delta}$ such that:

$$\tilde{\delta} \leq \frac{2}{3\tilde{\beta}\tilde{\gamma}},$$

where $\tilde{\gamma}$ is the Lipschitz constant of the Jacobian $\mathbf{G}'(\tilde{\mathbf{x}})$:

$$\tilde{\gamma} := \sup_{\tilde{\mathbf{y}} \neq \tilde{\mathbf{z}}} \frac{\|\mathbf{G}'(\tilde{\mathbf{y}}) - \mathbf{G}'(\tilde{\mathbf{z}})\|}{\|\tilde{\mathbf{y}} - \tilde{\mathbf{z}}\|}$$

and $\tilde{\beta}$ the upper bound on the inverse of the Jacobian evaluated at the solution $\tilde{\mathbf{x}}^*$:

$$\tilde{\beta} \geq \|(\mathbf{G}'(\tilde{\mathbf{x}}^*))^{-1}\|.$$

From Lemma 5.2.4 it follows that for all $\tilde{\mathbf{y}}, \tilde{\mathbf{z}}$ in $B(\tilde{\mathbf{x}}^*, \tilde{\sigma})$, $\tilde{\gamma}$ is essentially independent of h_+ , moreover Lemma 5.2.4 and assumption (5.100) imply that β does not blow up or tend to 0 as $h_+ \rightarrow 0$. Therefore if $2/(3\tilde{\beta}\tilde{\gamma}) \leq \tilde{\sigma}$, then we set $\tilde{\delta} = 2/(3\tilde{\beta}\tilde{\gamma})$, otherwise if $\tilde{\sigma} < 2/(3\tilde{\beta}\tilde{\gamma})$, we choose $\tilde{\delta} = \tilde{\sigma}$ and the convergence of Newton's method for (5.71) will be robust with respect to $h_+ \rightarrow 0$ in $B(\tilde{\mathbf{x}}^*, \tilde{\delta})$. \square

Theorem 5.2.6. *Let the assumptions of Theorem 5.2.5 hold. Then Newton's method for (5.66) is robust as $h_+ \rightarrow 0$.*

Proof. From Corollary 4.4.1 (a) we have that Newton's method for (5.66) converges robustly as $h_+ \rightarrow 0$ for all $\mathbf{x}^0 = B\tilde{\mathbf{x}}^0$ with $\tilde{\mathbf{x}}^0 \in B(\tilde{\mathbf{x}}^*, \tilde{\delta})$. \square

Numerical experiments

We now give numerical evidence of the fact that, in the limit as $h_+ \rightarrow 0$, Newton's method for the discretised RANS and k - ε equations, converges robustly on meshes which satisfy (5.78) for sufficiently small values of the constant C .

The experiments we present below, involve the application of Newton's method to the non-linear systems arising from the continuous piecewise quadratic approximation of 1D turbulent Couette and Poiseuille flows (experiments for 2D flows will be discussed at the end of §5.2.2). We have chosen to use 1D quadratic elements for our experiments because quadratic elements are our favoured 2D elements. For both flows, the finite element system will be denoted by

$$\mathbf{F}(\mathbf{x}) = \begin{bmatrix} \mathbf{F}_U(\mathbf{x}) \\ \mathbf{F}_k(\mathbf{x}) \\ \mathbf{F}_{nl}(\mathbf{x}) \\ \mathbf{F}_\varepsilon(\mathbf{x}) \end{bmatrix} = \mathbf{0}, \quad (5.102)$$

and we note that if the interval $[h_+, 1]$ is subdivided into a mesh with N elements, then (5.102) will consist of $P = (6N + 2)$ equations in the case of Couette flow and of $P = 3(2N + 1)$

5.2. Robustness of Newton's method for the discretised 1D turbulence equations

equations for Poiseuille flow. In Table 5.4 and Table 5.5, we present the results when $N = 64$ and $N = 128$, for which we correspondingly have $P \approx 384$ and $P \approx 768$.

The practical robust convergence of Newton's method for (5.102) has been tested through an experiment of the same kind as the one described at the end of §5.1.3. That is, we consider the sequence $\{10^{-1}, 10^{-2}, 10^{-3}, 10^{-4}\}$ of decreasing values of h_+ , and, for each h_+ , the set of initial guesses:

$$\mathbf{x}_{ij}^0 = \mathbf{x}^* + \rho_i \mathbf{v}_{ij}, \quad i = 1, 2, \dots, j = 1, 2, \dots, P \quad (5.103)$$

where \mathbf{x}^* is the numerical solution to (5.102), $\{\rho_i\}$, $i = 1, 2, \dots$, is a strictly increasing sequence of positive numbers and $\{\mathbf{v}_{ij}\}$, $i = 1, 2, \dots, j = 1, 2, \dots, P$, is a sequence of vectors of the form:

$$\mathbf{v}_{ij} = \frac{\mathbf{w}_{ij}}{\|\mathbf{w}_{ij}\|_\infty},$$

with \mathbf{w}_{ij} a random vector whose P components are uniformly distributed over the interval $[0, 1]$. Newton's method is then initialized with $\mathbf{x}_{1j}^0 = \mathbf{x}^* + \rho_1 \mathbf{v}_{1j}$, $j = 1, 2, \dots, P$ and if the method attains convergence for all \mathbf{x}_{1j}^0 , the next family of starting guesses $\mathbf{x}_{2j}^0 = \mathbf{x}^* + \rho_2 \mathbf{v}_{2j}$ (with $\rho_2 > \rho_1$) is considered and so forth. This algorithm is schematized below:

Algorithm 5.2.1.

1. For $h_+ = 10^{-1}, 10^{-2}, 10^{-3}, 10^{-4}$
 - i. $i = 1, j = 0$
 - ii. While $j \leq P$
 - (a) $j = j + 1$
 - (b) Generate the vector \mathbf{v}_{ij}
 - (c) Solve the finite element system by Newton's method initialized with $\mathbf{x}^0 = \mathbf{x}^* + \rho_i \mathbf{v}_{ij}$
 - (d) If Newton's method fails to converge then exit
 - (e) If $j = P + 1$ then $i = i + 1, j = 0$

The value ρ_M for which there exists a vector \mathbf{v}_{Mj} such that Newton's method diverges, will represent an upper bound on the radius ρ of the actual ball of convergence of the method, and ρ will then be estimated as: $\rho_{M-1} \leq \rho < \rho_M$. (Algorithm 5.2.1 will also be used to test the robust convergence of Newton's method for the system arising from the discretisation of the 1D and 2D k - ε equations only, as discussed at the end of §5.2.2). We now show experimentally that if, for all $h_+ = 10^{-1}, 10^{-2}, 10^{-3}, 10^{-4}$, the mesh on $[h_+, 1]$ satisfies (5.78) with a sufficiently small constant C , then ρ does not become smaller and smaller as h_+ is reduced.

The experimental estimates of ρ are presented in Table 5.4, for Couette flow, and in Table 5.5, for Poiseuille flow. In the case of Couette flow (Table 5.4), we compare the behaviours of the convergence ball of Newton's method on three different type of meshes: the equidistributed

5.2. Robustness of Newton's method for the discretised 1D turbulence equations

MESH (64 ELEMENTS)

h_+		EQUIDISTR.	UNIFORM	EXPONENT.
10^{-1}	$\max_j \{h_j/y_j\}$	4.3×10^{-2}	1.4×10^{-1}	4.7×10^{-2}
10^{-2}	$\max_j \{h_j/y_j\}$	1.1×10^{-1}	1.5	9.9×10^{-2}
10^{-3}	$\max_j \{h_j/y_j\}$	2.0×10^{-1}	15.6	1.5×10^{-1}
10^{-4}	$\max_j \{h_j/y_j\}$	3.4×10^{-1}	156	2.0×10^{-1}

Table 5.3: Maximum value of the ratio h_j/y_j , $j=1, \dots, N$, (see (5.78)) on three discretisations of the domain $[h_+, 1]$, for a sequence of decreasing values of h_+ .

mesh (3.101), the uniform mesh and the exponentially graded mesh (3.107) (in this case we use the value of α which, for given h_+ and number of elements, minimizes the error $\|\varepsilon^h - \varepsilon^*\|_2$, as already done in the numerical experiments discussed in §3.7.2). For Poiseuille flow (Table 5.5), we compare the estimated values of ρ on the equidistributed and uniform meshes. For both flows we present the results in the cases of meshes with 64 and 128 elements.

For the sequence $\{h_+ = 10^{-1}, 10^{-2}, 10^{-3}, 10^{-4}\}$ and $N=64$, the constant C in (5.78) can be estimated as:

$$C = \begin{cases} 3.4 \times 10^{-1}, & \text{equidistributed mesh} \\ 156, & \text{uniform mesh} \\ 2.0 \times 10^{-1}, & \text{exponential mesh} \end{cases}$$

This follows from the data presented in Table 5.3, where, as h_+ varies from 10^{-1} to 10^{-4} , we specify the values of $\max_j \{h_j/y_j\}$ on the meshes considered with 64 elements, and from these we derive C as:

$$C = \max_{h_+} \{ \max_j \{h_j/y_j\} \},$$

(obviously, for $N=128$ smaller values of C are to be expected). On the equidistributed and exponentially graded meshes, the constant C is relatively small (even in this case of just 64 elements), and correspondingly the ball of convergence of Newton's method does not shrink as h_+ is reduced (in fact it slightly increases in size as h_+ becomes smaller), as can be clearly seen from Table 5.4 and Table 5.5. On the uniform mesh, as h_+ is reduced with N fixed, $\max_j \{h_j/y_j\}$ is essentially proportional to $1/h_+$ (see Table 5.3), hence C is much bigger than on the corresponding equidistributed and exponentially graded mesh. It then follows that the size of the ball of convergence depends on h_+ and it turns out that $\rho = 0$ for small values of h_+ , see Table 5.4 and Table 5.5.

5.2. Robustness of Newton's method for the discretised 1D turbulence equations

1D COUETTE FLOW $(\bar{\rho} := \rho/10^{-1})$

h_+	MESH (64 ELEMENTS)			MESH (128 ELEMENTS)		
	EQUIDISTR.	UNIFORM	EXPONENT.	EQUIDISTR.	UNIFORM	EXPONENT.
10^{-1}	$1.21 \leq \bar{\rho} < 1.26$	$1.16 \leq \bar{\rho} < 1.21$	$1.01 \leq \bar{\rho} < 1.06$	$0.61 \leq \bar{\rho} < 0.66$	$0.56 \leq \bar{\rho} < 0.61$	$0.56 \leq \bar{\rho} < 0.61$
10^{-2}	$2.06 \leq \bar{\rho} < 2.11$	$1.26 \leq \bar{\rho} < 1.31$	$1.51 \leq \bar{\rho} < 1.56$	$1.11 \leq \bar{\rho} < 1.16$	$0.66 \leq \bar{\rho} < 0.71$	$0.86 \leq \bar{\rho} < 0.91$
10^{-3}	$2.81 \leq \bar{\rho} < 2.86$	$\rho=0$	$1.76 \leq \bar{\rho} < 1.81$	$1.46 \leq \bar{\rho} < 1.51$	$0.66 \leq \bar{\rho} < 0.71$	$0.81 \leq \bar{\rho} < 0.86$
10^{-4}	$3.16 \leq \bar{\rho} < 3.21$	$\rho=0$	$1.91 \leq \bar{\rho} < 1.96$	$1.71 \leq \bar{\rho} < 1.76$	$\rho=0$	$1.36 \leq \bar{\rho} < 1.41$

Table 5.4: Experimental estimates of the radius ρ of the convergence ball of Newton's method for the 1D Couette flow ($\rho = 10^{-1}\bar{\rho}$). For a sequence of decreasing values of h_+ , three meshes on the domain $[h_+, 1]$ have been considered: the equidistributed mesh (3.101), the uniform mesh and the exponentially graded mesh (3.107).

1D POISEUILLE FLOW $(\bar{\rho} = \rho/10^{-1})$

h_+	MESH (64 ELEMENTS)		MESH (128 ELEMENTS)	
	EQUIDISTR.	UNIFORM	EQUIDISTR.	UNIFORM
10^{-1}	$1.61 \leq \bar{\rho} < 1.66$	$1.31 \leq \bar{\rho} < 1.36$	$0.86 \leq \bar{\rho} < 0.91$	$0.66 \leq \bar{\rho} < 0.71$
10^{-2}	$1.66 \leq \bar{\rho} < 2.71$	$1.41 \leq \bar{\rho} < 1.46$	$1.36 \leq \bar{\rho} < 1.41$	$0.76 \leq \bar{\rho} < 0.81$
10^{-3}	$2.76 \leq \bar{\rho} < 3.11$	$\rho=0$	$1.71 \leq \bar{\rho} < 1.76$	$0.76 \leq \bar{\rho} < 0.81$
10^{-4}	$3.66 \leq \bar{\rho} < 3.71$	$\rho=0$	$1.91 \leq \bar{\rho} < 1.96$	$\rho=0$

Table 5.5: Experimental estimates of the radius ρ of the convergence ball of Newton's method for the 1D Poiseuille flow ($\rho = 10^{-1}\bar{\rho}$). For a sequence of decreasing values of h_+ , the domain $[h_+, 1]$ has been discretised using the equidistributed mesh (3.101) and the uniform mesh.

5.2. Robustness of Newton's method for the discretised 1D turbulence equations

5.2.2 Newton's method for the k - ε equations

We now discuss the convergence properties of Newton's method for the discretised k - ε equations, assuming that the velocity field U is known exactly in the coupled system (2.48)-(2.50) and satisfies the boundary conditions (2.51) and (2.56). This section is organized along the lines of §5.2.1, and in our analysis we will use some observations already made there and at the beginning of §5.2. Hence, in what follows, we will not give a detailed account of those parts of our argument which simply represent an adaptation of what done before, but, we will rather try to highlight the characteristic aspects of the problem we are now tackling.

Let

$$\mathbf{F}(\mathbf{x}) = \begin{bmatrix} \mathbf{F}_k(\mathbf{x}) \\ \mathbf{F}_{\text{nl}}(\mathbf{x}) \\ \mathbf{F}_\varepsilon(\mathbf{x}) \end{bmatrix} = \mathbf{0} , \quad (5.104)$$

with $\mathbf{x} := (\mathbf{k}^\top, \boldsymbol{\varepsilon}^\top)^\top := (k_1, \dots, k_{N+1}, \varepsilon_1, \dots, \varepsilon_{N+1})^\top$, be the nonlinear system arising from the discretisation of (2.136), (2.138) and (2.137), with the derivative of the velocity field $(dU/dy)(y)$, in (2.136) and (2.137), assumed to be known exactly from U . As in §5.2.1, in order to show that Newton's method for (5.104) converges robustly with respect to $h_+ \rightarrow 0$, we will first design a special combination of affine covariant and affine contravariant transformations of (5.104) and prove that, under appropriate conditions on the size of the mesh and on $(dU/dy)(y)$, there exists a neighbourhood of the true solution where the Jacobian of the transformed system remains bounded with bounded inverse as $h_+ \rightarrow 0$. The robustness of Newton's method for (5.104) will then follow from its affine invariant properties.

In (5.104), we have that:

$$(\mathbf{F}_k(\mathbf{x}))_i = c(U, k^h, \varepsilon^h, \phi_i) , \quad i = 1, \dots, N + 1 , \quad (5.105)$$

$$\mathbf{F}_{\text{nl}}(\mathbf{x}) = \varepsilon_1 - \frac{C_\mu^{3/4} k_1^{3/2}}{\kappa h_+} , \quad (5.106)$$

and

$$(\mathbf{F}_\varepsilon(\mathbf{x}))_i = d(U, k^h, \varepsilon^h, \phi_i) \quad i = 2, \dots, N + 1 , \quad (5.107)$$

with the forms c and d defined respectively in (2.133) and (2.134). We now introduce the diagonal matrix

$$B := \begin{pmatrix} I_{N+1} & & & \\ & 1/y_1 & & \\ & & \ddots & \\ & & & 1/y_{N+1} \end{pmatrix} , \quad (5.108)$$

and the following combination of affine covariant and affine contravariant transformations of

5.2. Robustness of Newton's method for the discretised 1D turbulence equations

the system (5.104):

$$\mathbf{G}(\tilde{\mathbf{x}}) := B^{-1}\mathbf{F}(B\tilde{\mathbf{x}}) = \begin{bmatrix} \mathbf{G}_k(\tilde{\mathbf{x}}) \\ \mathbf{G}_{\text{nl}}(\tilde{\mathbf{x}}) \\ \mathbf{G}_\varepsilon(\tilde{\mathbf{x}}) \end{bmatrix} = \mathbf{0} , \quad (5.109)$$

with

$$\begin{aligned} \tilde{\mathbf{x}} &= B^{-1}\mathbf{x} = B^{-1}(\mathbf{k}^T, \boldsymbol{\varepsilon}^T)^T =: (\mathbf{k}^T, \tilde{\boldsymbol{\varepsilon}}^T)^T \\ &= (k_1, \dots, k_{N+1}, \tilde{\varepsilon}_1, \dots, \tilde{\varepsilon}_{N+1})^T . \end{aligned} \quad (5.110)$$

Similarly to (5.71)-(5.72), the transformations (5.109)-(5.110) involve a scaling both of the equations corresponding to the ε -freedoms and of the nodal values of ε^h , while the equations corresponding to the k -freedoms and the nodal values of k^h are kept unchanged.

The components of $\mathbf{G}(\tilde{\mathbf{x}})$ in (5.109) can then be expressed as:

$$(\mathbf{G}_k(\tilde{\mathbf{x}}))_i = c(U, k^h, S(\tilde{\varepsilon}^h), \phi_i) , \quad i = 1, \dots, N + 1 , \quad (5.111)$$

$$\mathbf{G}_{\text{nl}}(\tilde{\mathbf{x}}) = \tilde{\varepsilon}_1 - \frac{C_\mu^{3/4}}{\kappa} k_1^{3/2} , \quad (5.112)$$

$$(\mathbf{G}_\varepsilon(\tilde{\mathbf{x}}))_i = y_i d(U, k^h, S(\tilde{\varepsilon}^h), \phi_i) , \quad i = 2, \dots, N + 1 . \quad (5.113)$$

with $S(\tilde{\varepsilon}^h)$ defined in (5.73).

As before, no constant terms in the scaled ‘‘nodal law’’ (5.112) depend on h_+ , and we have:

Lemma 5.2.7. *Assume that there exist strictly positive constants C, C_1, C_2 independent of h_+ such that*

$$\frac{h_j}{y_j} \leq C , \quad j = 1, 2, \dots, N \quad (5.114)$$

and that

$$C_1 \leq \left| y_j \frac{dU}{dy}(y) \right| \leq C_2 , \quad y \in e_j = [y_j, y_{j+1}] , \quad j = 1, 2, \dots, N , \quad (5.115)$$

then $\mathbf{G}_k(\tilde{\mathbf{x}})$ and $\mathbf{G}_\varepsilon(\tilde{\mathbf{x}})$ (respectively first and third component of $\mathbf{G}(\tilde{\mathbf{x}})$ in (5.109)) are rational functions of $\tilde{\mathbf{x}}$ with coefficients which are bounded independently of h_+ as $h_+ \rightarrow 0$.

It should be remarked that (5.115) can be regarded as a very natural property of dU/dy . In fact dU/dy resembles closely the function $1/y$ in a neighbourhood of $y = h_+$ (this is due to the boundary condition (2.51) and is discussed in §2.4, see (2.72)), and can be expected to vary smoothly away from the artificial wall. Also to clarify the need for (5.115), we now prove that, for each $i = 2, \dots, N + 1$, $(\mathbf{G}_\varepsilon(\tilde{\mathbf{x}}))_i$ (see (5.113)) is a rational function of $\tilde{\mathbf{x}}$ with coefficients which do not blow up or become arbitrarily small as $h_+ \rightarrow 0$. This will be done following the pattern of the proof of Lemma 5.2.2: first (5.113) is expressed as a sum of integrals over the elements $e_j = [y_j, y_{j+1}]$ containing the node y_i , then each element e_j is mapped onto the canonical interval $[-1, 1]$ and finally the constant terms in the transformed elemental integrals

5.2. Robustness of Newton's method for the discretised 1D turbulence equations

are shown to be bounded independently of $h_+ \rightarrow 0$. The same strategy applied to (5.111) will yield the proof of Lemma 5.2.7.

Proof of Lemma 5.2.7. Simply by replacing U^h with U in (5.80) and (5.81), we get the following expression for (5.113) as a sum of elemental integrals:

$$(\mathbf{G}_\varepsilon(\tilde{\mathbf{x}}))_i = \sum_{j: y_i \in e_j} y_i d^{e_j}(U, k^h, S(\tilde{\varepsilon}^h), \phi_i) \quad (5.116)$$

with

$$\begin{aligned} y_i g_i^{e_j}(U, k^h, S(\tilde{\varepsilon}^h)) &= y_i \int_{e_j} \left\{ \frac{C_\mu (k^h)^2}{\sigma_\varepsilon S(\tilde{\varepsilon}^h)} \frac{dS(\tilde{\varepsilon}^h)}{dy} \frac{d\phi_i}{dy} - \right. \\ &\left. - C_{\varepsilon 1} C_\mu \left(\frac{dU}{dy} \right)^2 k^h \phi_i + C_{\varepsilon 2} \frac{(S(\tilde{\varepsilon}^h))^2}{k^h} \phi_i \right\} dy. \end{aligned} \quad (5.117)$$

(Recall that dU/dy in (5.117) is assumed to be known exactly from $U(y)$). The interval $e_j := [y_j, y_{j+1}]$ is now mapped onto the canonical interval $[-1, 1]$, through the affine transformation (5.82), and by using (5.84), (5.85), (5.88), (5.89), and (5.91), we have that (5.117) is transformed into:

$$\begin{aligned} y_i d^{e_j}(U, \hat{k}^h, \hat{S}(\tilde{\varepsilon}^h), N_\alpha) &= \frac{y_i}{y_{j(1)}} \int_{[-1,1]} \left\{ \frac{2C_\mu}{\sigma_\varepsilon} \left(\frac{(\hat{k}^h(\eta))^2}{\hat{S}(\tilde{\varepsilon}^h(\eta))} \right) \left(\frac{d\hat{S}(\tilde{\varepsilon}^h)}{d\eta} \right) \frac{dN_\alpha}{d\eta} \frac{y_{j(1)}}{h_j} - \right. \\ &\left. - \frac{C_{\varepsilon 1}}{2} C_\mu \left(\frac{dU}{dy}(y(\eta)) \right)^2 \hat{k}^h(\eta) N_\alpha(\eta) y_{j(1)} h_j + \frac{C_{\varepsilon 2}}{2} \frac{(\hat{S}(\tilde{\varepsilon}^h(\eta))^2}{\hat{k}^h(\eta)} N_\alpha(\eta) \frac{h_j}{y_{j(1)}} \right\} d\eta. \end{aligned} \quad (5.118)$$

By multiplying $(dU/dy)(y(\eta))$ in (5.118) by:

$$1 := \frac{y_{j(1)}}{y_{j(1)}},$$

(5.118) can be rearranged into:

$$\begin{aligned} y_i d^{e_j}(\hat{U}^h, \hat{k}^h, \hat{S}(\tilde{\varepsilon}^h), N_\alpha) &= \frac{y_i}{y_{j(1)}} \int_{[-1,1]} \left\{ \frac{2C_\mu}{\sigma_\varepsilon} \left(\frac{(\hat{k}^h(\eta))^2}{\hat{S}(\tilde{\varepsilon}^h(\eta))} \right) \left(\frac{d\hat{S}(\tilde{\varepsilon}^h)}{d\eta} \right) \frac{dN_\alpha}{d\eta} \frac{y_{j(1)}}{h_j} - \right. \\ &\left. - \frac{C_{\varepsilon 1}}{2} C_\mu \left(y_{j(1)} \frac{dU}{dy}(y(\eta)) \right)^2 \hat{k}^h(\eta) N_\alpha(\eta) \frac{h_j}{y_{j(1)}} + \frac{C_{\varepsilon 2}}{2} \frac{(\hat{S}(\tilde{\varepsilon}^h(\eta))^2}{\hat{k}^h(\eta)} N_\alpha(\eta) \frac{h_j}{y_{j(1)}} \right\} d\eta. \end{aligned} \quad (5.119)$$

The constant coefficients in (5.119) are now shown to be bounded independently of $h_+ \rightarrow 0$. In (5.119), in addition to the terms in (5.93), the only other coefficient which could have a strong dependence on h_+ is

$$y_{j(1)} \frac{dU}{dy}(y(\eta)) = y_j \frac{dU}{dy}(y(\eta)), \quad \eta \in [-1, 1],$$

but this is bounded because of (5.115). \square

5.2. Robustness of Newton's method for the discretised 1D turbulence equations

It is not difficult to see that under the assumption of Lemma 5.2.7, the results of Corollary 5.2.3 and Lemma 5.2.4 can also be obtained in the case we are investigating, therefore we have:

Theorem 5.2.8. *Let the assumption of Lemma 5.2.7 hold, and suppose that there exists a constant b independent of h_+ such that*

$$\det(\mathbf{G}'(\tilde{\mathbf{x}}^*)) > b . \quad (5.120)$$

Then Newton's method for (5.109) is robust with respect to $h_+ \rightarrow 0$.

The robustness of Newton's method for (5.104) follows from its affine covariant and contravariant properties as in Theorem 5.2.6.

Numerical experiments

Algorithm 5.2.1 has also been used to test the robust convergence of Newton's method for the finite element system (5.104). This has $P = 2(N + 1)$ equations in both cases of Couette and Poiseuille flow. It should also be remarked that in order to assemble (5.104), it is necessary to evaluate the derivative of the velocity field at the quadrature points (to see this observe that dU/dy appears in the expression (5.116)-(5.117) for $(\mathbf{G}_\varepsilon(\tilde{\mathbf{x}}))_i$). Both for Couette and Poiseuille flow, we have used the element-wise derivative of the U^h -solution component to the full finite element system (5.66), as (approximate) expression for dU/dy .

Similarly to before, for the sequence $\{10^{-1}, 10^{-2}, 10^{-3}, 10^{-4}\}$ of decreasing values of h_+ , the size of the convergence ball of Newton's method has been estimated on different discretisations of the domain $[h_+, 1]$. For Couette flow (see Table 5.6), we have considered the equidistributed mesh (3.101), the uniform mesh and the exponentially graded mesh (3.107) (again, α has been chosen ad "hoc" to minimize $\|\varepsilon^h - \varepsilon^*\|_2$). In the case of Poiseuille flow (see Table 5.7), we have used the equidistributed mesh (3.101) and the uniform mesh. From the numerical results it is clear that on the equidistributed and exponentially graded meshes, the size of the ball of convergence of Newton's method is independent of h_+ , while on the uniform mesh it shrinks to zero for small values of h_+ , see Table 5.6 and Table 5.7. As argued in §5.2.1, these results can be explained considering that, for all $h_+ = 10^{-1}, \dots, 10^{-4}$, the equidistributed and exponentially graded meshes, with 64 and 128 elements, can satisfy (5.114) for a sufficiently small constant C , while the uniform mesh cannot meet the same condition with the number of elements considered (see (5.79) for an estimate of the number of elements needed by the uniform mesh to satisfy (5.114)).

Comparing Table 5.4 and Table 5.5 with Table 5.6 and Table 5.7, it becomes clear that, when applied to the discretised k - ε equations with given velocity field, Newton's method has a bigger ball of convergence than when applied to the full U - k - ε system. This may suggest that an iterative scheme which exploits the decoupling between dynamical and model equations will perform better than Newton's method for the system of fully coupled equations. But, we will see in §5.3 that this is not the case and that Newton's method should be the method of choice for the RANS and k - ε equations.

5.3. An inner-outer iteration

Algorithm 5.2.1 has also been used to test the robustness of Newton’s method applied to the $2D$ k - ε equations for Couette flow, when the domain $[0, 1] \times [h_+, 1]$ is discretised through the tensor product of meshes obtained by using (3.101) and (3.107) in the y -direction and a uniform mesh in the x -direction, see Table 5.8. Similarly to the $1D$ case, the performances of Newton’s method on the equidistributed and exponentially graded meshes are far better than on the uniform mesh, where, for the number of elements considered, $\rho=0$ when $h_+ = 10^{-3}, 10^{-4}$. On all meshes the size of the ball of convergence appears to be particularly small and on the equidistributed and exponentially graded meshes with $h_+ = 10^{-2}, 10^{-3}, 10^{-4}$, it is slightly smaller is than when $h_+ = 10^{-1}$, but does not change significantly when h_+ is reduced from 10^{-3} to 10^{-4} .

Finally, we discuss the experimental results on the convergence of the Newton’s sequence $\{\mathbf{x}^n := ((\mathbf{k}^n)^T, (\boldsymbol{\varepsilon}^n)^T)^T\}$ for the discretised $1D$ k - ε equations. For different initial guesses of the form $\mathbf{x}^0 = \mathbf{x}^* + \rho \mathbf{v}$, as in (5.103), we have measured the rate of convergence of the sequence $\{\mathbf{x}^n\}$ both in the standard infinity-norm and in the weighted norm $\|\cdot\|_{B^{-1}} := \|B^{-1}(\cdot)\|_\infty$, with B defined in (5.108). As already noticed for the reduced 2×2 system (see Observation 5.1.4, Proposition 5.1.6, Table 5.1 and Table 5.2) we have observed that

$$\frac{\|\mathbf{x}^{n+1} - \mathbf{x}^*\|_\infty}{\|\mathbf{x}^n - \mathbf{x}^*\|_\infty^2} \leq O(h_+)$$

and that

$$\frac{\|\mathbf{x}^{n+1} - \mathbf{x}^*\|_{B^{-1}}}{\|\mathbf{x}^n - \mathbf{x}^*\|_{B^{-1}}^2} \leq K$$

with K independent of h_+ . In Table 5.9, for a specific vector \mathbf{v} , we present the result in the case of Couette flow when the equidistributed mesh with 32 elements is used and $\rho = 22$. We have also monitored the relation between the errors at the artificial wall and, as for the reduced 2×2 system, it turns out that:

$$\frac{|(\boldsymbol{\varepsilon}^n)_1 - (\boldsymbol{\varepsilon}^*)_1|}{|(\mathbf{k}^n)_1 - (\mathbf{k}^*)_1|} \leq O\left(\frac{1}{h_+}\right).$$

5.3 An inner-outer iteration

We now give experimental and analytical evidence for the assertion that Newton’s method for the system of fully coupled RANS and k - ε equations should be preferred to the commonly used iterative scheme based on the decoupling of the RANS equations from the k - ε system. The latter method is at the basic nonlinear solver implemented in the industrial finite element code FEAT and we will refer to it as “inner-outer iteration”.

This section is organized as follows. We will first explain how the inner-outer iteration can be interpreted as an approximation to Newton’s algorithm, then present the numerical experiments which show that its performances deteriorate dramatically as h_+ is decreased (§5.3.1). Finally we prove that the ball of convergence of the inner-outer iteration applied to a simple

5.3. An inner-outer iteration

1D COUETTE FLOW

h_+	MESH (64 ELEMENTS)			MESH (128 ELEMENTS)		
	EQUIDIST.	UNIFORM	EXPONENT.	EQUIDIST.	UNIFORM	EXPONENT.
10^{-1}	$25 \leq \rho < 26$	$27 \leq \rho < 28$	$24 \leq \rho < 25$	$23 \leq \rho < 24$	$25 \leq \rho < 26$	$24 \leq \rho < 25$
10^{-2}	$24 \leq \rho < 25$	$31 \leq \rho < 32$	$24 \leq \rho < 25$	$25 \leq \rho < 26$	$30 \leq \rho < 31$	$24 \leq \rho < 25$
10^{-3}	$24 \leq \rho < 25$	$\rho = 0$	$25 \leq \rho < 26$	$25 \leq \rho < 26$	$22 \leq \rho < 23$	$24 \leq \rho < 25$
10^{-4}	$25 \leq \rho < 26$	$\rho = 0$	$25 \leq \rho < 26$	$25 \leq \rho < 26$	$\rho = 0$	$24 \leq \rho < 25$

Table 5.6: Couette flow: experimental estimates of the radius ρ of the convergence ball of Newton's method applied to the discretised 1D k - ε equations, for a sequence of decreasing values of h_+ .

1D POISEUILLE FLOW

h_+	MESH (64 ELEMENTS)		MESH (128 ELEMENTS)	
	EQUIDIST.	UNIFORM	EQUIDIST.	UNIFORM
10^{-1}	$15 \leq \rho < 16$	$14 \leq \rho < 15$	$14 \leq \rho < 15$	$10 \leq \rho < 11$
10^{-2}	$14 \leq \rho < 15$	$15 \leq \rho < 16$	$16 \leq \rho < 17$	$13 \leq \rho < 14$
10^{-3}	$14 \leq \rho < 15$	$\rho = 0$	$14 \leq \rho < 15$	$13 \leq \rho < 14$
10^{-4}	$12 \leq \rho < 13$	$\rho = 0$	$13 \leq \rho < 14$	$\rho = 0$

Table 5.7: Poiseuille flow: experimental estimates of the radius ρ of the convergence ball of Newton's method applied to the discretised 1D k - ε equations, for a sequence of decreasing values of h_+ .

5.3. An inner-outer iteration

2D COUETTE FLOW $(\bar{\rho} := \rho/10^{-2})$

h_+	MESH (10×32 ELEMENTS)			MESH (10×64 ELEMENTS)		
	EQUIDIST.	UNIFORM	EXPONEN.	EQUIDIST.	UNIFORM	EXPONEN.
10^{-1}	$2.7 \leq \bar{\rho} < 2.9$	$3.7 \leq \bar{\rho} < 4.0$	$2.0 \leq \bar{\rho} < 2.1$	$2.5 \leq \bar{\rho} < 2.7$	$3.7 \leq \bar{\rho} < 4.0$	$2.9 \leq \bar{\rho} < 3.1$
10^{-2}	$2.0 \leq \bar{\rho} < 2.2$	$2.5 \leq \bar{\rho} < 2.7$	$1.6 \leq \bar{\rho} < 1.7$	$1.7 \leq \bar{\rho} < 1.9$	$3.7 \leq \bar{\rho} < 4.0$	$2.0 \leq \bar{\rho} < 2.1$
10^{-3}	$1.1 \leq \bar{\rho} < 1.2$	$\rho=0$	$1.2 \leq \bar{\rho} < 1.3$	$1.4 \leq \bar{\rho} < 1.5$	$\rho=0$	$2.0 \leq \bar{\rho} < 2.1$
10^{-4}	$1.2 \leq \bar{\rho} < 1.3$	$\rho=0$	$1.4 \leq \bar{\rho} < 1.5$	$1.1 \leq \bar{\rho} < 1.2$	$\rho=0$	$1.2 \leq \bar{\rho} < 1.3$

Table 5.8: Experimental estimates of the radius ρ of the convergence ball of Newton's method applied to the discretised 2D k - ε equations, for a sequence of decreasing values of h_+ .

model problem (obtained by restricting the RANS and k - ε equations to the artificial wall and neglecting diffusion) has null radius. (Below, we will initially use the notation introduced in §2.7).

We now describe the inner-outer iteration for the system (2.142). Given the initial guess $((\mathbf{U}^0)^T, (\mathbf{V}^0)^T, (\mathbf{P}^0)^T, (\mathbf{k}^0)^T, (\boldsymbol{\varepsilon}^0)^T)^T$, the inner-outer iteration consists of the following steps:

Algorithm 5.3.1.

Step 1

- i. Compute the discretised turbulent viscosity (see (2.143))

$$(\nu_t^h)^n = C_\mu \frac{(\boldsymbol{\phi} \cdot \mathbf{k}^n)^2}{\boldsymbol{\phi} \cdot \boldsymbol{\varepsilon}^n}.$$

- ii. Solve* the discretised dynamical equations

$$\begin{bmatrix} \mathbf{F}_U(\mathbf{U}^{n+1}, \mathbf{V}^{n+1}, \mathbf{P}^{n+1}, (\nu_t^h)^n) \\ \mathbf{F}_V(\mathbf{U}^{n+1}, \mathbf{V}^{n+1}, \mathbf{P}^{n+1}, (\nu_t^h)^n) \\ \mathbf{F}_P(\mathbf{U}^{n+1}, \mathbf{V}^{n+1}) \end{bmatrix} = \mathbf{0} \quad (5.121)$$

for $((\mathbf{U}^{n+1})^T, (\mathbf{V}^{n+1})^T, (\mathbf{P}^{n+1})^T)^T$.

Step 2

- i. Given $((\mathbf{U}^{n+1})^T, (\mathbf{V}^{n+1})^T)^T$ from Step 1, solve* the discretised turbulence model equations

$$\begin{bmatrix} \mathbf{F}_k(\mathbf{U}^{n+1}, \mathbf{V}^{n+1}, \mathbf{k}^{n+1}, \boldsymbol{\varepsilon}^{n+1}) \\ \mathbf{F}_{NL}(\mathbf{k}^{n+1}, \boldsymbol{\varepsilon}^{n+1}) \\ \mathbf{F}_\varepsilon(\mathbf{U}^{n+1}, \mathbf{V}^{n+1}, \mathbf{k}^{n+1}, \boldsymbol{\varepsilon}^{n+1}) \end{bmatrix} = \mathbf{0}$$

for \mathbf{k}^{n+1} and $\boldsymbol{\varepsilon}^{n+1}$.

5.3. An inner-outer iteration

$$\mathbf{x}^0 = \mathbf{x}^* + \rho \mathbf{v}, \quad \rho = 22$$

		$h_+ = 10^{-1}$			$h_+ = 10^{-2}$		
n	$\frac{\ \mathbf{x}^n - \mathbf{x}^*\ _\infty}{\ \mathbf{x}^{n-1} - \mathbf{x}^*\ _\infty^2}$	$\frac{\ \mathbf{x}^n - \mathbf{x}^*\ _{B^{-1}}}{\ \mathbf{x}^{n-1} - \mathbf{x}^*\ _{B^{-1}}^2}$	$\frac{ (\boldsymbol{\varepsilon}^n)_1 - (\boldsymbol{\varepsilon}^*)_1 }{ (\mathbf{k}^n)_1 - (\mathbf{k}^*)_1 }$	$\frac{\ \mathbf{x}^n - \mathbf{x}^*\ _\infty}{\ \mathbf{x}^{n-1} - \mathbf{x}^*\ _\infty^2}$	$\frac{\ \mathbf{x}^n - \mathbf{x}^*\ _{B^{-1}}}{\ \mathbf{x}^{n-1} - \mathbf{x}^*\ _{B^{-1}}^2}$	$\frac{ (\boldsymbol{\varepsilon}^n)_1 - (\boldsymbol{\varepsilon}^*)_1 }{ (\mathbf{k}^n)_1 - (\mathbf{k}^*)_1 }$	
0			1.12			1.12	
1	7.96×10^{-4}	8.41×10^{-3}	8.83×10	8.42×10^{-5}	9.77×10^{-3}	6.14×10^2	
2	9.04×10^{-4}	1.36×10^{-2}	2.97×10	9.69×10^{-5}	1.29×10^{-2}	2.95×10^2	
3	9.26×10^{-4}	1.61×10^{-2}	9.60	1.00×10^{-4}	1.59×10^{-2}	1.55×10^2	
4	8.60×10^{-4}	1.79×10^{-2}	3.10×10	8.98×10^{-5}	1.79×10^{-2}	1.82×10^2	
5	8.61×10^{-4}	1.81×10^{-2}	3.00×10	9.00×10^{-5}	1.81×10^{-2}	2.57×10^2	
6				9.00×10^{-5}	1.81×10^{-2}	2.56×10^2	

		$h_+ = 10^{-3}$			$h_+ = 10^{-4}$		
n	$\frac{\ \mathbf{x}^n - \mathbf{x}^*\ _\infty}{\ \mathbf{x}^{n-1} - \mathbf{x}^*\ _\infty^2}$	$\frac{\ \mathbf{x}^n - \mathbf{x}^*\ _{B^{-1}}}{\ \mathbf{x}^{n-1} - \mathbf{x}^*\ _{B^{-1}}^2}$	$\frac{ (\boldsymbol{\varepsilon}^n)_1 - (\boldsymbol{\varepsilon}^*)_1 }{ (\mathbf{k}^n)_1 - (\mathbf{k}^*)_1 }$	$\frac{\ \mathbf{x}^n - \mathbf{x}^*\ _\infty}{\ \mathbf{x}^{n-1} - \mathbf{x}^*\ _\infty^2}$	$\frac{\ \mathbf{x}^n - \mathbf{x}^*\ _{B^{-1}}}{\ \mathbf{x}^{n-1} - \mathbf{x}^*\ _{B^{-1}}^2}$	$\frac{ (\boldsymbol{\varepsilon}^n)_1 - (\boldsymbol{\varepsilon}^*)_1 }{ (\mathbf{k}^n)_1 - (\mathbf{k}^*)_1 }$	
0			1.12			1.12	
1	8.41×10^{-6}	1.05×10^{-2}	5.63×10^3	8.38×10^{-7}	1.11×10^{-2}	5.48×10^4	
2	9.82×10^{-6}	1.33×10^{-2}	2.94×10^3	9.86×10^{-7}	1.31×10^{-2}	2.94×10^4	
3	1.03×10^{-5}	1.56×10^{-2}	1.67×10^3	1.03×10^{-6}	1.56×10^{-2}	1.73×10^4	
4	9.01×10^{-6}	1.78×10^{-2}	1.78×10^3	9.01×10^{-7}	1.77×10^{-2}	1.78×10^4	
5	9.04×10^{-6}	1.81×10^{-2}	1.78×10^3	9.05×10^{-7}	1.80×10^{-2}	6.51×10^4	
6	9.04×10^{-6}	1.81×10^{-2}	3.07×10^3	9.05×10^{-7}	1.80×10^{-2}	3.28×10^4	

Table 5.9: 1D Couette flow: rates of convergence of Newton's sequence $\{\mathbf{x}^n := ((\mathbf{k}^n)^T, (\boldsymbol{\varepsilon}^n)^T)^T\}$ for (5.104) and proportionality between the errors at the artificial wall in each of the two components of the iterate \mathbf{x}^n .

Step 3

- i. Go back to *Step 1* unless

$$\|\mathbf{U}^{n+1} - \mathbf{U}^n, \mathbf{V}^{n+1} - \mathbf{V}^n, \mathbf{P}^{n+1} - \mathbf{P}^n, \mathbf{k}^{n+1} - \mathbf{k}^n, \boldsymbol{\varepsilon}^{n+1} - \boldsymbol{\varepsilon}^n\| < \tau$$

for some tolerance τ (i.e. overall convergence is achieved).

In the above, solve* indicates the application of Newton's method, and, in order to emphasize the fact that the turbulence variables appear in the RANS equations only through the eddy viscosity (see (2.103)), we have made $(\nu_t^h)^n$ an argument of \mathbf{F}_U (and of \mathbf{F}_V), see (5.121),

5.3. An inner-outer iteration

instead of writing $\mathbf{F}_{\mathbf{U}}(\mathbf{U}^{n+1}, \mathbf{V}^{n+1}, \mathbf{P}^{n+1}, \mathbf{k}^n, \varepsilon^n)$ (and similarly for $\mathbf{F}_{\mathbf{V}}$). This abuse of the notation will be repeated in the following.

The inner-outer iteration is widely used because it appears as a rather natural way to solve the finite element system (2.142); in fact the decoupling of dynamical and model equations makes the RANS equations with specified ν_t (see *Step 1* of the algorithm) formally identical to the Navier-Stokes equations for variable-viscosity laminar flows, and these flows have been successfully treated using what are now standard techniques. That is, the Navier-Stokes equations are discretised using the Galerkin finite element method and the resulting set of algebraic equations is tackled by means of Newton's method. After *Step 1*, it is then practical to discretise the turbulence model equations by the Galerkin finite element method, approximating the variables k and ε by the velocity basis functions which are already available, and this gives *Step 2* of the inner-outer iteration. From a computational point of view, the inner-outer iteration clearly presents the advantage of requiring the inversion of matrices which are sensibly smaller than those involved in Newton's method for the system of fully coupled equations. But, in the following two subsections, we will show that the method of choice for solving the discretised RANS and k - ε equations should really be Newton's method, or at least a better approximation of the full Newton method than the inner-outer iteration presented here.

We now briefly discuss how one step of the inner-outer iteration can be seen as an approximation to one step of Newton's method applied to the full finite element system (2.142). As seen in §4.1, Newton's method for improving a guess

$$\bar{\mathbf{x}} := (\bar{\mathbf{U}}^T, \bar{\mathbf{V}}^T, \bar{\mathbf{P}}^T, \bar{\mathbf{k}}^T, \bar{\varepsilon}^T)^T \quad (5.122)$$

to the solution $\mathbf{x}^* := ((\mathbf{U}^*)^T, (\mathbf{V}^*)^T, (\mathbf{P}^*)^T, (\mathbf{k}^*)^T, (\varepsilon^*)^T)^T$ of (2.142), requires that the linear system

$$\mathbf{F}'(\bar{\mathbf{x}})\bar{\mathbf{S}} = -\mathbf{F}(\bar{\mathbf{x}}) , \quad (5.123)$$

is solved for $\bar{\mathbf{S}}$, and the new approximation to \mathbf{x}^* is then given by the update:

$$\bar{\mathbf{z}} = \bar{\mathbf{x}} + \bar{\mathbf{S}} , \quad (5.124)$$

and satisfies:

$$\mathbf{F}'(\bar{\mathbf{x}})\bar{\mathbf{z}} = \mathbf{F}'(\bar{\mathbf{x}})\bar{\mathbf{x}} - \mathbf{F}(\bar{\mathbf{x}}) . \quad (5.125)$$

At any point \mathbf{x} , we have that the Jacobian matrix $\mathbf{F}'(\mathbf{x})$ (which appears in (5.123) and (5.125)

5.3. An inner-outer iteration

evaluated at $\mathbf{x} = \bar{\mathbf{x}}$) can be expressed as:

$$\mathbf{F}'(\mathbf{x}) = \begin{bmatrix} (\mathbf{F}_U)_U(\mathbf{x}) & (\mathbf{F}_U)_V(\mathbf{x}) & (\mathbf{F}_U)_P(\mathbf{x}) & (\mathbf{F}_U)_k(\mathbf{x}) & (\mathbf{F}_U)_\varepsilon(\mathbf{x}) \\ (\mathbf{F}_V)_U(\mathbf{x}) & (\mathbf{F}_V)_V(\mathbf{x}) & (\mathbf{F}_V)_P(\mathbf{x}) & (\mathbf{F}_V)_k(\mathbf{x}) & (\mathbf{F}_V)_\varepsilon(\mathbf{x}) \\ (\mathbf{F}_P)_U(\mathbf{x}) & (\mathbf{F}_P)_V(\mathbf{x}) & \mathbf{0} & \mathbf{0} & \mathbf{0} \\ (\mathbf{F}_k)_U(\mathbf{x}) & (\mathbf{F}_k)_V(\mathbf{x}) & \mathbf{0} & (\mathbf{F}_k)_k(\mathbf{x}) & (\mathbf{F}_k)_\varepsilon(\mathbf{x}) \\ \mathbf{0} & \mathbf{0} & \mathbf{0} & (\mathbf{F}_{nl})_k(\mathbf{x}) & (\mathbf{F}_{nl})_\varepsilon(\mathbf{x}) \\ (\mathbf{F}_\varepsilon)_U(\mathbf{x}) & (\mathbf{F}_\varepsilon)_V(\mathbf{x}) & \mathbf{0} & (\mathbf{F}_\varepsilon)_k(\mathbf{x}) & (\mathbf{F}_\varepsilon)_\varepsilon(\mathbf{x}) \end{bmatrix},$$

where, for example,

$$[(\mathbf{F}_U)_k(\mathbf{x})]_{ij} := \frac{\partial (\mathbf{F}_U)_i(\mathbf{x})}{\partial (\mathbf{k})_j},$$

and similarly the other terms. Now, note that if, at a first order approximation, the coupling between the dynamical and the turbulence variables is neglected, then $\mathbf{F}'(\mathbf{x})$ can correspondingly be approximated by:

$$\tilde{\mathbf{F}}'(\mathbf{x}) := \begin{bmatrix} (\mathbf{F}_U)_U(\mathbf{x}) & (\mathbf{F}_U)_V(\mathbf{x}) & (\mathbf{F}_U)_P(\mathbf{x}) & \mathbf{0} & \mathbf{0} \\ (\mathbf{F}_V)_U(\mathbf{x}) & (\mathbf{F}_V)_V(\mathbf{x}) & (\mathbf{F}_V)_P(\mathbf{x}) & \mathbf{0} & \mathbf{0} \\ (\mathbf{F}_P)_U(\mathbf{x}) & (\mathbf{F}_P)_V(\mathbf{x}) & \mathbf{0} & \mathbf{0} & \mathbf{0} \\ \mathbf{0} & \mathbf{0} & \mathbf{0} & (\mathbf{F}_k)_k(\mathbf{x}) & (\mathbf{F}_k)_\varepsilon(\mathbf{x}) \\ \mathbf{0} & \mathbf{0} & \mathbf{0} & (\mathbf{F}_{nl})_k(\mathbf{x}) & (\mathbf{F}_{nl})_\varepsilon(\mathbf{x}) \\ \mathbf{0} & \mathbf{0} & \mathbf{0} & (\mathbf{F}_\varepsilon)_k(\mathbf{x}) & (\mathbf{F}_\varepsilon)_\varepsilon(\mathbf{x}) \end{bmatrix} \quad (5.126)$$

$$=: \begin{bmatrix} & \mathbf{0} & \mathbf{0} \\ \tilde{\mathbf{F}}'_D(\mathbf{x}) & \mathbf{0} & \mathbf{0} \\ & \mathbf{0} & \mathbf{0} \\ \mathbf{0} & \mathbf{0} & \mathbf{0} \\ \mathbf{0} & \mathbf{0} & \mathbf{0} & \tilde{\mathbf{F}}'_M(\mathbf{x}) \\ \mathbf{0} & \mathbf{0} & \mathbf{0} & \end{bmatrix} \quad (5.127)$$

and this then makes it possible to approximate the full Newton's iteration (5.125) for $\bar{\mathbf{z}}$, by a sequence of Newton's steps for the dynamical variables only, followed by a sequence of Newton's steps for the turbulence variables alone, as now briefly explained. (In (5.127), $\tilde{\mathbf{F}}'_D(\mathbf{x})$ and $\tilde{\mathbf{F}}'_M(\mathbf{x})$ clearly represent the top left and bottom right block of (5.126), and are respectively due to the coupling between the dynamical variables only and between the turbulence model variables alone).

Once the approximation (5.126) is in place, the update to the dynamical part $(\bar{\mathbf{U}}^T, \bar{\mathbf{V}}^T, \bar{\mathbf{P}}^T)^T$ of the guess (5.122), is determined by the Newton's sequence $\{\tilde{\mathbf{z}}_D^i := ((\tilde{\mathbf{U}}^i)^T, (\tilde{\mathbf{V}}^i)^T, (\tilde{\mathbf{P}}^i)^T)^T\}$

5.3. An inner-outer iteration

such that:

$$\tilde{\mathbf{F}}'_D(\tilde{\mathbf{z}}_D^i, \bar{\nu}_t^h) \tilde{\mathbf{z}}_D^{i+1} = \tilde{\mathbf{F}}'_D(\tilde{\mathbf{z}}_D^i, \bar{\nu}_t^h) \tilde{\mathbf{z}}_D^i - \begin{bmatrix} \mathbf{F}_U(\tilde{\mathbf{z}}_D^i, \bar{\nu}_t^h) \\ \mathbf{F}_V(\tilde{\mathbf{z}}_D^i, \bar{\nu}_t^h) \\ \mathbf{F}_P(\tilde{\mathbf{z}}_D^i) \end{bmatrix}, \quad i = 0, 1, 2, \dots \quad (5.128)$$

with

$$\bar{\nu}_t^h = C_\mu \frac{(\phi \cdot \bar{\mathbf{k}})^2}{\phi \cdot \bar{\boldsymbol{\varepsilon}}},$$

and $\tilde{\mathbf{z}}_D^0 = (\bar{\mathbf{U}}^T, \bar{\mathbf{V}}^T, \bar{\mathbf{P}}^T)^T$. If $\tilde{\mathbf{W}} := (\tilde{\mathbf{U}}^T, \tilde{\mathbf{V}}^T)^T$ is the converged value of the sequence $\{\tilde{\mathbf{z}}_D^i\}$, then this new velocity field is substituted into the discretised k - ε equations, and these are solved by Newton's method in order to update the turbulence part $(\bar{\mathbf{k}}^T, \bar{\boldsymbol{\varepsilon}}^T)^T$ of the guess $\bar{\mathbf{x}}$. This yields the sequence $\{\tilde{\mathbf{z}}_M^i := ((\tilde{\mathbf{k}}^i)^T, (\tilde{\boldsymbol{\varepsilon}}^i)^T)^T\}$ such that:

$$\tilde{\mathbf{F}}'_M(\tilde{\mathbf{W}}, \tilde{\mathbf{z}}_M^i) \tilde{\mathbf{z}}_M^{i+1} = \tilde{\mathbf{F}}'_M(\tilde{\mathbf{W}}, \tilde{\mathbf{z}}_M^i) \tilde{\mathbf{z}}_M^i - \begin{bmatrix} \mathbf{F}_k(\tilde{\mathbf{W}}, \tilde{\mathbf{z}}_M^i) \\ \mathbf{F}_\varepsilon(\tilde{\mathbf{W}}, \tilde{\mathbf{z}}_M^i) \end{bmatrix}, \quad i = 0, 1, 2, \dots \quad (5.129)$$

with $\tilde{\mathbf{z}}_M^0 = (\bar{\mathbf{k}}^T, \bar{\boldsymbol{\varepsilon}}^T)^T$.

(5.128) and (5.129) clearly correspond to *Step 1* and *Step 2* of Algorithm 5.3.1 and give an update to (5.122) which can be interpreted as an approximation to (5.124).

5.3.1 Numerical experiments

We now experimentally assess the properties of the inner-outer iteration by applying it to the discretised 1D turbulent Couette flow and by comparing its performances with those of Newton's method.

We will consider the continuous piecewise quadratic approximation of (2.129) (with $\mathcal{G} = 0$), (2.136), (2.138) and (2.137), both on the equidistributed mesh (3.101) and on the exponentially graded mesh (3.107), and will denote by

$$\mathbf{F}(\mathbf{U}, \mathbf{k}, \boldsymbol{\varepsilon}) = \begin{bmatrix} \mathbf{F}_U(\mathbf{U}, \mathbf{k}, \boldsymbol{\varepsilon}) \\ \mathbf{F}_k(\mathbf{U}, \mathbf{k}, \boldsymbol{\varepsilon}) \\ \mathbf{F}_{nl}(\mathbf{U}, \mathbf{k}, \boldsymbol{\varepsilon}) \\ \mathbf{F}_\varepsilon(\mathbf{U}, \mathbf{k}, \boldsymbol{\varepsilon}) \end{bmatrix} = \mathbf{0}, \quad (5.130)$$

the resulting finite element system. Clearly, for the 1D case we are now considering with both $V = 0$ and $p = 0$, *Step 1* of the inner-outer iteration simply involves the solution of the system:

$$\mathbf{F}_U(\mathbf{U}^{n+1}, \mathbf{k}^n, \boldsymbol{\varepsilon}^n) = \mathbf{0}, \quad (5.131)$$

for \mathbf{U}^{n+1} , while the overall convergence criterion (see *Step 3* of Algorithm 5.3.1) becomes:

$$\|\mathbf{x}^{n+1} - \mathbf{x}^n\|_2 < \tau, \quad (5.132)$$

5.3. An inner-outer iteration

where

$$\mathbf{x}^n = ((\mathbf{U}^n)^T, (\mathbf{k}^n)^T, (\boldsymbol{\varepsilon}^n)^T)^T. \quad (5.133)$$

Even if (5.131) is linear in \mathbf{U}^{n+1} (to see this consider that (2.129) is linear in U), we will solve it by Newton's method, this will converge to the solution of (5.131) in just one iteration, independently of the initial guess.

In order to assess the convergence properties of the inner-outer iteration, we have performed a numerical experiment of the same kind as that illustrated in Algorithm 5.2.1, that is we have initialized the method with different guesses of the form:

$$\mathbf{x}^0 = \mathbf{x}^* + \rho \mathbf{v}$$

where ρ denotes a strictly positive number and the vector \mathbf{v} is of the form:

$$\mathbf{v} = \frac{\mathbf{w}}{\|\mathbf{w}\|_\infty}$$

with \mathbf{w} chosen so that its components are uniformly distributed over the interval $[0, 1]$. The numerical tests have clearly shown that the inner-outer iteration performs far worse than Newton's method. In fact, it turns out that, for the same initial guesses for which Newton's method converges quadratically to the solution of (5.130), the inner-outer iteration either converges very slowly, when $h_+ = 10^{-1}, 10^{-2}$, or fails to converge for $h_+ = 10^{-3}, 10^{-4}$. This is now discussed by examining experimental results concerning the convergence history of $\|\mathbf{x}^{n+1} - \mathbf{x}^n\|_2$ (on whose size the convergence criterion is based, see (5.132)) and of $\|\mathbf{F}(\mathbf{U}^n, \mathbf{k}^n, \boldsymbol{\varepsilon}^n)\|_2$. The results we will present below, obviously correspond also to a specific choice of the mesh (equidistributed or exponentially graded) and of the vector \mathbf{v} , but, we have observed that these two parameters do not significantly affect the quality of the experimental outcomes. Therefore, in the following, we will mainly emphasize the values of ρ and h_+ .

The convergence history of $\|\mathbf{x}^{n+1} - \mathbf{x}^n\|_2$ (with \mathbf{x}^n given in (5.133)) on the equidistributed mesh (3.101) with 64 elements, for $h_+ = 10^{-1}$ and $\rho = 0.12$, is represented in the top pictures of Figure 5.1. These plots clearly show that convergence to zero of the difference between two consecutive iterates is extremely slow, in fact after 13 iterations $\|\mathbf{x}^{n+1} - \mathbf{x}^n\|_2 = O(10^{-1})$ and it takes 35 iterations in order for $\|\mathbf{x}^{n+1} - \mathbf{x}^n\|_2 < \tau = 10^{-8}$ (for the same values of the parameters Newton's method meets the convergence criterion in 6 iterations, see also Table 5.4). The bottom plots of Figure 5.2 represent the convergence history of the residual $\|\mathbf{F}(\mathbf{U}^n, \mathbf{k}^n, \boldsymbol{\varepsilon}^n)\|_2$, this reduces considerably at the first iteration, but after 10 iterations is still $O(10^{-4})$. The performance of the inner-outer iteration worsens for $h_+ = 10^{-3}, 10^{-4}$. In fact, when $h_+ = 10^{-3}$ there are values of ρ for which Newton's method converges, but for which the inner-outer iteration fails, and more dramatically, when $h_+ = 10^{-4}$, the inner-outer iteration will always diverge no matter how small the value of ρ is. The top picture of Figure 5.2 shows the blow-up in $\|\mathbf{x}^{n+1} - \mathbf{x}^n\|_2$ when $\rho = 0.25$ and the domain $[h_+, 1]$, with $h_+ = 10^{-3}$, is discretised by the equidistributed mesh (3.101) with 64 elements. The bottom plots show the behaviour of the residual: this reduces at the first iteration and then increases, slowly but steadily (for

5.3. An inner-outer iteration

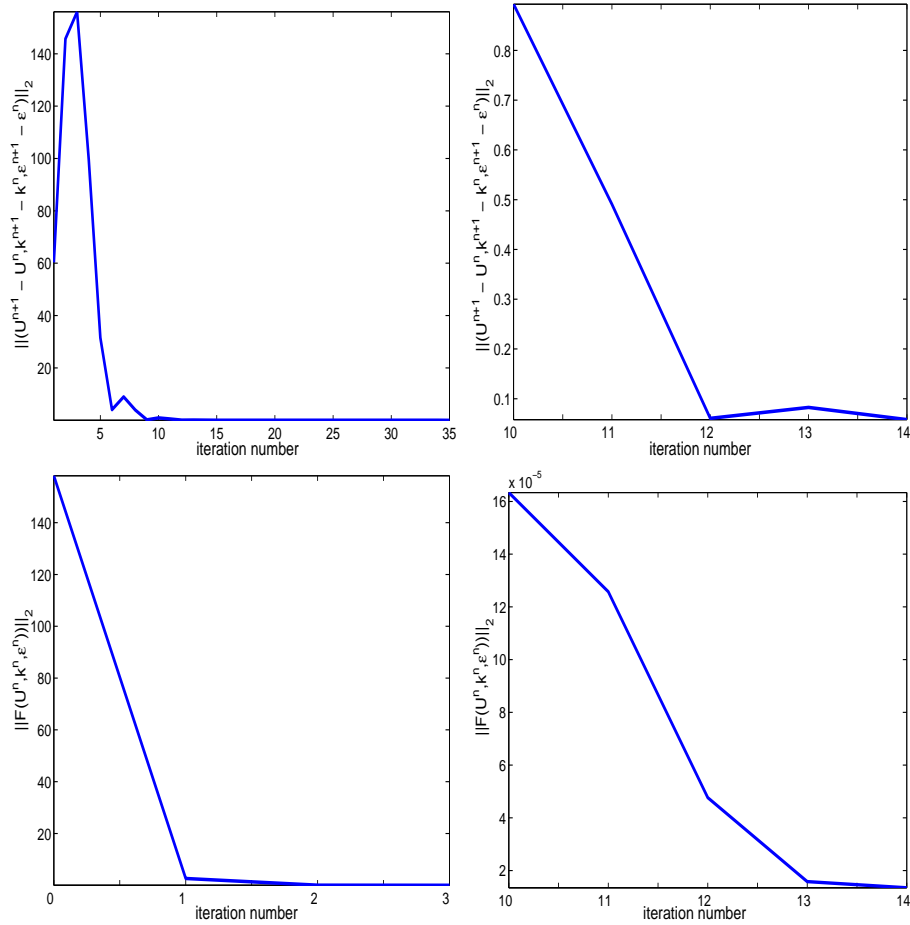


Figure 5.1: Convergence history of $\|U^{n+1} - U^n, k^{n+1} - k^n, \epsilon^{n+1} - \epsilon^n\|_2$ (top) and $\|F(U^n, k^n, \epsilon^n)\|_2$ (bottom), on the equidistributed mesh (3.101) with 64 elements when $h_+ = 10^{-1}$ and $\rho = 0.12$

$h_+ = 10^{-3}$ and $\rho = 0.25$ Newton's method attains convergence on the equidistributed mesh with 64 elements, as it can be seen from Table 5.4).

5.3.2 Convergence analysis for a model problem

In order to get some insight into the properties of the inner-outer iteration applied to the RANS and k - ϵ equations, we now study its convergence in the case of a special 3×3 algebraic system of equations derived by restricting the RANS and k - ϵ equations to the artificial wall, and neglecting diffusion. This simplified system reflects some of the key features of the full turbulence model at $y = h_+$, such as the predominance of source terms over diffusion in the transport equation for k and the blow up of dU/dy and ϵ , as discussed in §2.4. We will show that the solution to the reduced system is not a point of attraction for the iterates generated by the inner-outer algorithm. This, obviously, does not represent an explanation of the numerical results presented in §5.3.1, but, together with them, seriously challenges the efficacy of the inner-outer iteration for the turbulence model we are considering. By contrast Newton's method for this 3×3 system always converges (provided the initial guess is close enough to the true solution).

5.3. An inner-outer iteration

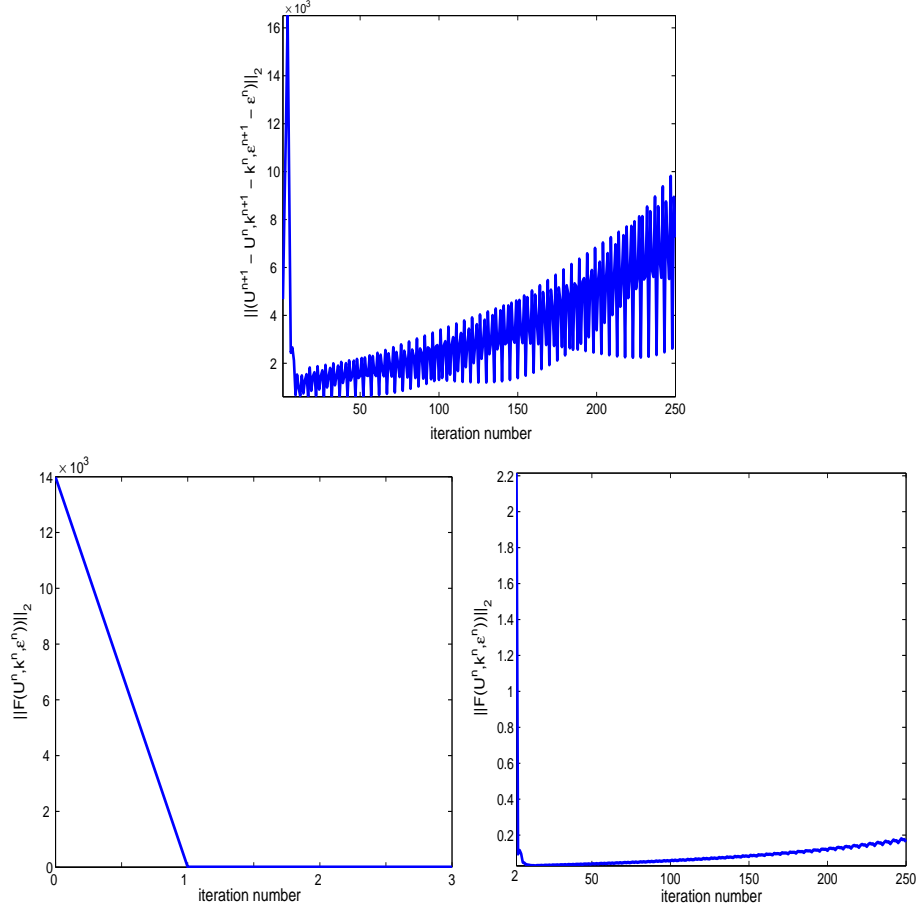


Figure 5.2: Convergence history of $\|U^{n+1} - U^n, k^{n+1} - k^n, \varepsilon^{n+1} - \varepsilon^n\|_2$ (top) and $\|F(U^n, k^n, \varepsilon^n)\|_2$ (bottom), on the equidistributed mesh (3.101) with 64 elements when $h_+ = 10^{-3}$ and $\rho = 0.25$

The diffusionless k -equation and the behaviour of ε at $y = h_+$ are given respectively in (5.2):

$$-C_\mu \left(\frac{dU}{dy}(h_+) \right)^2 \frac{(k(h_+))^2}{\varepsilon(h_+)} + \varepsilon(h_+) = 0, \quad (5.134)$$

and in (5.4):

$$\varepsilon(h_+) - \eta \alpha (k(h_+))^{3/2} = 0, \quad (5.135)$$

where

$$\alpha := \frac{C_\mu^{1/2} u_*}{\kappa} \frac{1}{h_+}, \quad \eta := \frac{C_\mu^{1/4}}{u_*}.$$

At $y = h_+$, the velocity field U must satisfy the boundary condition (2.42), which, using the above definition of η , can be expressed as:

$$C_\mu^{1/2} \frac{(k(h_+))^2}{\varepsilon(h_+)} \frac{dU}{dy}(h_+) = \frac{1}{\eta^2}. \quad (5.136)$$

We then consider the system of nonlinear equations (5.136), (5.134) and (5.135) for the

5.3. An inner-outer iteration

variables $\mathcal{G}_+ := (dU/dy)(h_+)$, $k_+ := k(h_+)$ and $\varepsilon_+ := \varepsilon(h_+)$:

$$\begin{cases} F_{\mathcal{G}_+}(\mathcal{G}_+, k_+, \varepsilon_+) := C_\mu^{1/2} \frac{k_+^2}{\varepsilon_+} \mathcal{G}_+ - \frac{1}{\eta^2} = 0 \\ F_{k_+}(\mathcal{G}_+, k_+, \varepsilon_+) := -C_\mu \mathcal{G}_+^2 \frac{k_+^2}{\varepsilon_+} + \varepsilon_+ = 0 \\ F_{\varepsilon_+}(k_+, \varepsilon_+) := \varepsilon_+ - \eta \alpha k_+^{3/2} = 0 \end{cases} \quad (5.137)$$

with solution

$$(\mathcal{G}_+^*, k_+^*, \varepsilon_+^*)^T = \left(\frac{\alpha}{C_\mu^{1/2}}, \frac{1}{\eta^2}, \frac{\alpha}{\eta^2} \right)^T, \quad (5.138)$$

and apply to it the inner-outer iteration. We have:

Lemma 5.3.1. *The inner-outer iteration applied to the system (5.137) produces the sequences:*

$$\mathcal{G}_+^{n+1} = \frac{1}{C_\mu^{1/2} \eta^2} \frac{\varepsilon_+^n}{(k_+^n)^2}, \quad (5.139)$$

$$k_+^{n+1} = \frac{1}{\eta^6 \alpha^2} \frac{(\varepsilon_+^n)^2}{(k_+^n)^4}, \quad (5.140)$$

$$\varepsilon_+^{n+1} = \frac{1}{\eta^8 \alpha^2} \frac{(\varepsilon_+^n)^3}{(k_+^n)^6}, \quad (5.141)$$

$n=0, 1, 2, \dots$

Proof. Solving the dynamical equation:

$$F_{\mathcal{G}_+}(\mathcal{G}_+^{n+1}, k_+^n, \varepsilon_+^n) := C_\mu^{1/2} \frac{(k_+^n)^2}{\varepsilon_+^n} \mathcal{G}_+^{n+1} - \frac{1}{\eta^2} = 0$$

for \mathcal{G}_+^{n+1} yields (5.139). It can then be easily verified that (5.140)-(5.141) is the solution to the equations:

$$\begin{cases} F_{k_+}(\mathcal{G}_+^{n+1}, k_+^{n+1}, \varepsilon_+^{n+1}) = 0 \\ F_{\varepsilon_+}(k_+^{n+1}, \varepsilon_+^{n+1}) = 0 \end{cases}$$

with \mathcal{G}_+^{n+1} given in (5.139). □

From (5.139)-(5.140)-(5.141), we observe that, for a given initial guess (k_+^0, ε_+^0) , the iteration (5.139) for the dynamical variable \mathcal{G}_+ is decoupled from the sequences (5.140)-(5.141) for the turbulence variables (k_+, ε_+) , and we express (5.140)-(5.141) in the form of the following fixed-point iteration

$$\begin{bmatrix} k_+^{n+1} \\ \varepsilon_+^{n+1} \end{bmatrix} = \mathbf{G} \left(\begin{bmatrix} k_+^n \\ \varepsilon_+^n \end{bmatrix} \right) := \begin{bmatrix} g_1(k_+^n, \varepsilon_+^n) \\ g_2(k_+^n, \varepsilon_+^n) \end{bmatrix} \quad (5.142)$$

5.3. An inner-outer iteration

with

$$\begin{bmatrix} g_1(t, s) \\ g_2(t, s) \end{bmatrix} := \begin{bmatrix} \frac{1}{\eta^6 \alpha^2} \frac{s^2}{t^4} \\ \frac{1}{\eta^8 \alpha^2} \frac{s^3}{t^6} \end{bmatrix}. \quad (5.143)$$

Clearly (see (5.138))

$$(k_+^*, \varepsilon_+^*)^T = (1/\eta^2, \alpha/\eta^2)^T \quad (5.144)$$

is the fixed point of (5.142).

We will then prove that (5.138) is not a point of attraction for (5.139)-(5.140)-(5.141), by showing that (5.144) is not a point of attraction for (5.142).

The following lemma indicates, in fact, that (5.144) may well not be a point of attraction of the iteration (5.142).

Lemma 5.3.2. *The spectral radius of $\mathbf{G}'(k_+^*, \varepsilon_+^*)$ is*

$$\rho(\mathbf{G}'(k_+^*, \varepsilon_+^*)) = 1.$$

Proof. The Jacobian of \mathbf{G} evaluated at the fixed point $(1/\eta^2, \alpha/\eta^2)^T$ is

$$\mathbf{G}'(k_+^*, \varepsilon_+^*) = \begin{pmatrix} -4 & \frac{2}{\alpha} \\ -6\alpha & 3 \end{pmatrix}. \quad (5.145)$$

The result then follows from the fact that the spectrum of (5.145) is $\sigma(\mathbf{G}'(k_+^*, \varepsilon_+^*)) = \{0, -1\}$, as it can be easily verified. \square

We now prove that there does not exist an open ball S of (5.144) such that for any $(k_+^0, \varepsilon_+^0)^T \in S$, the iterates $\{(k_+^n, \varepsilon_+^n)^T\}$ in (5.142) converge to (5.144).

We start with the following observation:

Lemma 5.3.3. *The sequence (5.142)-(5.143) may be written as:*

$$\begin{cases} k_+^1 = \frac{1}{\eta^6 \alpha^2} \frac{(\varepsilon_+^0)^2}{(k_+^0)^4} \\ k_+^{n+2} = \frac{1}{\eta^4} \frac{1}{k_+^{n+1}} \quad n = 0, 1, \dots \end{cases} \quad \begin{cases} \varepsilon_+^1 = \frac{1}{\eta^8 \alpha^2} \frac{(\varepsilon_+^0)^3}{(k_+^0)^6} \\ \varepsilon_+^{n+2} = \frac{\alpha^2}{\eta^4} \frac{1}{\varepsilon_+^{n+1}} \quad n = 0, 1, \dots \end{cases} \quad (5.146)$$

Proof. Using (5.140) and (5.141) we have:

$$\begin{aligned} k_+^{n+2} &= \frac{1}{\eta^6 \alpha^2} \frac{(\varepsilon_+^{n+1})^2}{(k_+^{n+1})^4} = \frac{1}{\eta^6 \alpha^2} \left[\frac{1}{\eta^8 \alpha^2} \frac{(\varepsilon_+^n)^3}{(k_+^n)^6} \right]^2 \left[\frac{1}{\eta^6 \alpha^2} \frac{(\varepsilon_+^n)^2}{(k_+^n)^4} \right]^{-4} \\ &= \eta^2 \alpha^2 \left[\frac{(\varepsilon_+^n)^2}{(k_+^n)^4} \right]^{-1} = \frac{1}{\eta^4} \frac{1}{k_+^{n+1}}, \end{aligned}$$

5.3. An inner-outer iteration

and similarly:

$$\begin{aligned}\varepsilon_+^{n+2} &= \frac{1}{\eta^8 \alpha^2} \frac{(\varepsilon_+^{n+1})^3}{(k_+^{n+1})^6} = \frac{1}{\eta^8 \alpha^2} \left[\frac{1}{\eta^8 \alpha^2} \frac{(\varepsilon_+^n)^3}{(k_+^n)^6} \right]^3 \left[\frac{1}{\eta^6 \alpha^2} \frac{(\varepsilon_+^n)^2}{(k_+^n)^4} \right]^{-6} \\ &= \eta^4 \alpha^4 \left[\frac{(\varepsilon_+^n)^3}{(k_+^n)^6} \right]^{-1} = \frac{\alpha^2}{\eta^4} \frac{1}{\varepsilon_+^{n+1}}.\end{aligned}$$

The result then follows. \square

We now give a necessary and sufficient condition for the convergence of the sequence $\{k_+^n\}$ in (5.146).

Lemma 5.3.4. *The sequence*

$$\begin{cases} k_+^1 &= \frac{1}{\eta^6 \alpha^2} \frac{(\varepsilon_+^0)^2}{(k_+^0)^4} \\ k_+^{n+2} &= \frac{1}{\eta^4} \frac{1}{k_+^{n+1}} \quad n = 0, 1, \dots \end{cases}$$

is convergent if and only if $\varepsilon_+^0 = \eta^2 \alpha (k_+^0)^2$. If the sequence converges, then its limit is $1/\eta^2$.

Proof. We will consider the subsequences $c^n := k_+^{2(n+1)}$ and $d^n := k_+^{2n+1}$, $n = 0, 1, 2, \dots$, and show that

$$c^n = \eta^2 \alpha^2 \frac{(k_+^0)^4}{(\varepsilon_+^0)^2} \quad \forall n = 0, 1, 2, \dots \quad (5.147)$$

and that

$$d^n = \frac{1}{\eta^6 \alpha^2} \frac{(\varepsilon_+^0)^2}{(k_+^0)^4} \quad \forall n = 0, 1, 2, \dots \quad (5.148)$$

The result will then follow by observing that

$$c^n = \frac{1}{\eta^2} = d^n \quad \forall n = 0, 1, 2, \dots \quad \Leftrightarrow \quad \varepsilon_+^0 = \eta^2 \alpha (k_+^0)^2,$$

therefore

$$k_+^n = \frac{1}{\eta^2} \quad \forall n = 1, 2, \dots \quad \Leftrightarrow \quad \varepsilon_+^0 = \eta^2 \alpha (k_+^0)^2,$$

whilst if $\varepsilon_+^0 \neq \eta^2 \alpha (k_+^0)^2$, then

$$c^n = \eta^2 \alpha^2 \frac{(k_+^0)^4}{(\varepsilon_+^0)^2} \neq \frac{1}{\eta^6 \alpha^2} \frac{(\varepsilon_+^0)^2}{(k_+^0)^4} = d^n,$$

and $\{k_+^n\}$ is not a convergent sequence.

We now show (5.147) by induction. We have:

$$c^0 = k_+^2 = \frac{1}{\eta^4} \frac{1}{k_+^1} = \eta^2 \alpha^2 \frac{(k_+^0)^4}{(\varepsilon_+^0)^2}.$$

5.3. An inner-outer iteration

We now assume that $c^n = \eta^2 \alpha^2 (k_+^0)^4 / (\varepsilon_+^0)^2$ and prove that this implies $c^{n+1} = \eta^2 \alpha^2 (k_+^0)^4 / (\varepsilon_+^0)^2$.

We have:

$$c^{n+1} = k_+^{2(n+1)+2} = \frac{1}{\eta^4} \frac{1}{k_+^{2(n+1)+1}} = k_+^{2(n+1)} = c^n = \eta^2 \alpha^2 \frac{(k_+^0)^4}{(\varepsilon_+^0)^2}.$$

This then proves (5.147). (5.148) can be similarly proved by induction. \square

A similar convergence result holds for the sequence $\{\varepsilon_+^n\}$ in (5.146):

Lemma 5.3.5. *The sequence*

$$\begin{cases} \varepsilon_+^1 &= \frac{1}{\eta^8 \alpha^2} \frac{(\varepsilon_+^0)^3}{(k_+^0)^6} \\ \varepsilon_+^{n+2} &= \frac{\alpha^2}{\eta^4} \frac{1}{\varepsilon_+^{n+1}} \end{cases}$$

is convergent if and only if $\varepsilon_+^0 = \eta^2 \alpha (k_+^0)^2$. If the sequence converges, then its limit is α / η^2 .

Proof. It is not difficult to prove by induction that the subsequence $a^n := \varepsilon_+^{2(n+1)}$ is such that:

$$a^n = \eta^4 \alpha^4 \frac{(k_+^0)^6}{(\varepsilon_+^0)^3} \quad \forall n = 0, 1, 2, \dots \quad (5.149)$$

and that the subsequence $b^n := \varepsilon_+^{2n+1}$ is such that:

$$b^n = \frac{1}{\eta^8 \alpha^2} \frac{(\varepsilon_+^0)^3}{(k_+^0)^6} \quad \forall n = 0, 1, 2, \dots \quad (5.150)$$

Similarly to the proof of Lemma 5.3.4, the result then follows from the fact that:

$$a^n = \frac{\alpha}{\eta^2} = b^n \quad \forall n = 0, 1, 2, \dots \quad \Leftrightarrow \quad \varepsilon_+^0 = \eta^2 \alpha (k_+^0)^2,$$

therefore:

$$\varepsilon_+^n = \frac{\alpha}{\eta^2} \quad \forall n = 1, 2, \dots \quad \Leftrightarrow \quad \varepsilon_+^0 = \eta^2 \alpha (k_+^0)^2,$$

whilst if $\varepsilon_+^0 \neq \eta^2 \alpha (k_+^0)^2$, then

$$a^n = \eta^4 \alpha^4 \frac{(k_+^0)^6}{(\varepsilon_+^0)^3} \neq \frac{1}{\eta^8 \alpha^2} \frac{(\varepsilon_+^0)^3}{(k_+^0)^6} = b^n$$

and the sequence $\{\varepsilon_+^n\}$ is not convergent. \square

We then have:

Theorem 5.3.6. *The fixed point (5.144) is not a point of attraction for the iteration (5.142)-(5.143).*

5.3. An inner-outer iteration

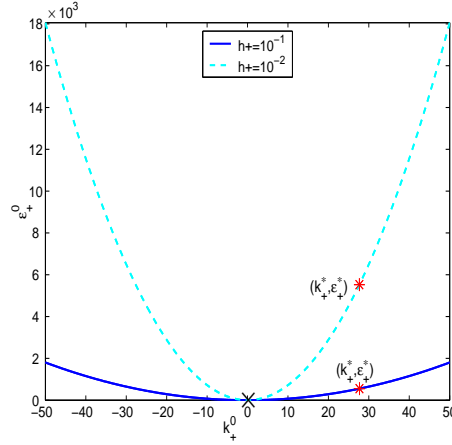


Figure 5.3: Curves in the (k_+^0, ε_+^0) plane representing the locus of initial guesses for which the sequence (5.151) converges to the fixed point (k_+^*, ε_+^*) (the point $(0, 0)$ is excluded), for $h_+ = 10^{-1}$ (continuous line) and $h_+ = 10^{-2}$ (dashed line).

Proof. From Lemmata 5.3.4, 5.3.5, we have that the iterates (5.142)-(5.143):

$$\begin{bmatrix} k_+^{n+1} \\ \varepsilon_+^{n+1} \end{bmatrix} = \begin{bmatrix} \frac{1}{\eta^6 \alpha^2} \frac{(\varepsilon_+^n)^2}{(k_+^n)^4} \\ \frac{1}{\eta^8 \alpha^2} \frac{(\varepsilon_+^n)^3}{(k_+^n)^6} \end{bmatrix} \quad (5.151)$$

converge to the fixed point (5.144) if and only if $\varepsilon_+^0 = \eta^2 \alpha (k_+^0)^2$. Therefore there does not exist an open ball S of (5.144) such that for any $(k_+^0, \varepsilon_+^0)^T \in S$, the sequence $\{(k_+^n, \varepsilon_+^n)^T\}$ converges to (5.144), that is (5.144) is not a point of attraction for (5.151) (see also Figure 5.3). \square

Theorem 5.3.6 finally implies the following result:

Theorem 5.3.7. *The solution $(\alpha/C_\mu^{1/2}, 1/\eta^2, \alpha/\eta^2)^T$ to (5.137) is not a point of attraction for the iterates (5.139)-(5.140)-(5.141).*

Chapter 6

Fully developed turbulent flows in expanding channels

The mesh grading towards the artificial wall (see (3.101)) which greatly improves the accuracy of the numerical solution and the robustness of Newton's method in the finite element computation of turbulent flows in straight channels (see respectively §3.7 and §5.2), is now tested in the much more challenging and practical context of fully developed turbulent flows in expanding channels. We will pursue this by solving the RANS and k - ε equations on expanding flow domains discretised by orthogonal meshes which, in the direction perpendicular to the artificial wall (now a curved boundary), are graded as (3.101). We will see that, even in the case of widely expanded channels, on such meshes it is possible to resolve, accurately and practically, complex flow features, such as recirculation and the blow-up of the ε -solution component as $h_+ \rightarrow 0$.

This chapter is organised as follows. In §6.1.1 we discuss the properties of the transformation we have used in order to construct expanding channels from straight ones, in §6.1.2 we present the specific weak form of the RANS and k - ε equations we have considered, together with the boundary conditions and in §6.1.3 we describe the numerical strategy employed in the finite element computations. Finally in §6.2.1 we briefly explain the technique we have adopted to generate graded, boundary-fitted, orthogonal meshes (this is described in details in [63]) and in §6.2.2 we discuss the outcome of the numerical experiments.

6.1 Formulation of the problem

Now, first we discuss the properties of the mapping we have used to generate expanding flow domains from a straight channel (see §6.1.1), then give the boundary conditions for the variables \mathbf{u} , k , ε and recast the RANS and k - ε equations into the weak form. This will differ from the one presented in Chapter 2 mainly in the fact that it will contain the normal component of the stress vector at the artificial wall as new variable and, therefore, will also comprise an extra equation (see §6.1.2).

6.1. Formulation of the problem

6.1.1 The flow domain

The RANS and k - ε equations (2.1)-(2.4), together with appropriate boundary conditions (see §6.1.2), will be considered in the domain Ω which consists of the lower half of a symmetric expanding channel. This, as explained below, is generated by a special mapping of the lower half of the symmetric straight channel introduced in §2.1, which is represented by the domain $\tilde{\Omega} = [0, L] \times [h_+, d]$ and whose boundary will be denoted by $\tilde{\Gamma} = \tilde{\Gamma}_{\text{in}} \cup \tilde{\Gamma}_{\text{cl}} \cup \tilde{\Gamma}_{\text{out}} \cup \tilde{\Gamma}_{\text{w}}$ (in §2.1 the corresponding notation without “tilde” is used). We now define the mapping on $\tilde{\Omega}$ and discuss its properties. Let (ξ, η) be the Cartesian coordinates in $\tilde{\Omega}$, we consider the following continuous, one-to-one transformation $(x(\xi, \eta), y(\xi, \eta))$ from $\tilde{\Omega}$ onto Ω :

$$\begin{aligned} x(\xi, \eta) &:= \xi \\ y(\xi, \eta) &:= \eta - \left(\frac{\alpha}{2}\right) (d - \eta)(\tanh(\beta(\xi - \gamma)) + 1), \end{aligned} \quad (6.1)$$

with α , β and γ parameters such that $\alpha \geq 0$, $\beta \geq 1$, and $\gamma > 0$. The precise role of these parameters will be examined in the following, we now discuss the shape of Ω by determining an expression for its boundary Γ . This is given by the transformation of $\tilde{\Gamma}$ through the mapping (6.1), and, like $\tilde{\Gamma}$, can be divided into four parts: $\Gamma = \Gamma_{\text{in}} \cup \Gamma_{\text{cl}} \cup \Gamma_{\text{out}} \cup \Gamma_{\text{w}}$, with Γ_{in} the image of $\tilde{\Gamma}_{\text{in}}$ and similarly the other parts. The curves which Γ consists of can be expressed as now shown.

Property 6.1.1. *If $\gamma \gg 1$, then, at a first order approximation, Γ_{in} coincides with $\tilde{\Gamma}_{\text{in}}$ and is therefore given by*

$$x = 0, \quad y \in [h_+, d]. \quad (6.2)$$

Proof. Applying the mapping (6.1) to $\tilde{\Gamma}_{\text{in}}$, given by $\xi = 0$ and $\eta \in [h_+, d]$, yields:

$$\begin{aligned} x &= 0 \\ y &= \eta - \left(\frac{\alpha}{2}\right) (d - \eta)(\tanh(-\beta\gamma) + 1), \quad \eta \in [h_+, d]. \end{aligned} \quad (6.3)$$

Now, since $\beta \geq 1$, for $\gamma \gg 1$ we have that:

$$\tanh(-\beta\gamma) \approx -1,$$

and using this in (6.3) gives:

$$\begin{aligned} x &= 0 \\ y &\approx \eta, \quad \eta \in [h_+, d]. \end{aligned} \quad (6.4)$$

That is, at a first order approximation, (6.1) maps $\tilde{\Gamma}_{\text{in}}$ into itself. \square

In practical computations we have used $\gamma = 10$, thus, for all $\beta \geq 1$, we have: $-1 < \tanh(-\beta\gamma) = \tanh(-10\beta) \leq \tanh(-10) = -0.9999999958$.

6.1. Formulation of the problem

Property 6.1.2. Γ_{cl} coincides with $\tilde{\Gamma}_{\text{cl}}$ and is then given by

$$x \in [0, L] , \quad y = d .$$

Proof. The result follows from applying (6.1) to $\tilde{\Gamma}_{\text{cl}}$, characterized by $\xi \in [0, L]$ and $\eta = d$. \square

We also have:

Property 6.1.3. If $(L - \gamma) \gg 1$, then, at a first order approximation, Γ_{out} is given by:

$$x = L , \quad y \in [h_+ - \alpha(d - h_+), d] . \quad (6.5)$$

Proof. First we observe that the mapping (6.1) transforms $\tilde{\Gamma}_{\text{out}}$, given by $\xi = L$ and $\eta \in [h_+, d]$, into:

$$\begin{aligned} x &= L \\ y &= \eta - \left(\frac{\alpha}{2}\right) (d - \eta)(\tanh(\beta(L - \gamma)) + 1) , \quad \eta \in [h_+, d] . \end{aligned} \quad (6.6)$$

Now, since $\beta \geq 1$, when $(L - \gamma) \gg 1$, we have that

$$\tanh(\beta(L - \gamma)) \approx 1 ,$$

and using this in (6.6) yields:

$$\begin{aligned} x &= L \\ y &= (1 + \alpha)\eta - \alpha d , \quad \eta \in [h_+, d] , \end{aligned} \quad (6.7)$$

from which the result follows. \square

In practical computations we have used $L - \gamma = 240$ and this, in the machine arithmetic, gives $\tanh(\beta(L - \gamma)) = 1$, for all $\beta \geq 1$. From (6.5) it is easy to see that, for all $\alpha > 0$, Γ_{out} is wider than $\tilde{\Gamma}_{\text{out}}$, in fact the first has width $(1 + \alpha)(d - h_+)$ whilst the second has width $(d - h_+)$. Finally, simply by applying the mapping (6.1) to $\tilde{\Gamma}_{\text{w}}$, given by $\xi \in [0, L]$ and $\eta = h_+$, we have:

Property 6.1.4. Γ_{w} , the image of $\tilde{\Gamma}_{\text{w}}$ through (6.1), is represented by the curve $(x, b(x))$ with

$$x \in [0, L] , \quad b(x) := h_+ - \left(\frac{\alpha}{2}\right) (d - h_+)(\tanh(\beta(x - \gamma)) + 1) . \quad (6.8)$$

The domain Ω is plotted in Figure 6.1.

We now discuss how α , β and γ affect the geometry of the channel. The parameter α controls the expansion of the channel. In fact, it is easy to see that for $\alpha = 0$, (6.1) becomes the identity mapping and Ω then coincides with $\tilde{\Omega}$ for all values of β and γ ; it also makes sense to define the expansion factor r as the ratio between the widths of the outlet Γ_{out} and of the inlet

6.1. Formulation of the problem

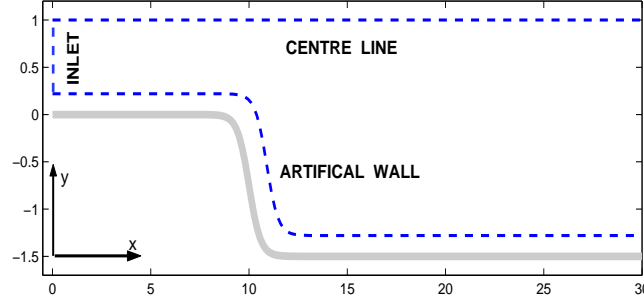


Figure 6.1: The expanding channel, for $\alpha = 1.5$, $\beta = 1.7$ and $\gamma = 10$.

Γ_{in} , and from their first order expressions (6.5) and (6.2) we have:

$$r \approx \frac{d - h_+ + \alpha(d - h_+)}{d - h_+} = \frac{(1 + \alpha)(d - h_+)}{d - h_+} = 1 + \alpha. \quad (6.9)$$

The parameter γ , instead, represents the x -coordinate of the point where the slope of the boundary Γ_w is maximum. To see this note that from (6.8) the gradient of the profile of Γ_w is:

$$b'(x) = -\frac{\alpha}{2}(d - h_+) \frac{\beta}{[\cosh(\beta(x - \gamma))]^2}, \quad (6.10)$$

and, clearly, $|b'(x)|$ is maximum when $x = \gamma$. In particular, for $x = \gamma$ we have:

$$|b'(\gamma)| = \frac{\alpha}{2}(d - h_+) \beta, \quad (6.11)$$

which shows that, for fixed α , the slope of Γ_w increases with $\beta \geq 1$.

As will be discussed in more detail in §6.1.3, we will compute a numerical solution to the k - ε model for flows in expanding channels, using continuation from the straight channel $\alpha = 0$, when a numerical solution to Poiseuille flow can confidently be computed starting from the analytical solution to Couette flow, as discussed in §2.5.

We now give the expressions for the unit tangent vector \mathbf{t} and the unit outward normal vector \mathbf{n} to the artificial wall Γ_w , these will be needed in the boundary conditions and in the weak form of the equations, which are presented in the following subsection. Recalling, from Property 6.1.4, that Γ_w is represented by the curve $(x, b(x))$, with $b(x)$ specified in (6.8), we have

$$\mathbf{t} := \frac{(1, b'(x))^T}{\sqrt{1 + (b'(x))^2}}, \quad \mathbf{n} := \frac{(b'(x), -1)^T}{\sqrt{1 + (b'(x))^2}}, \quad (6.12)$$

with $b'(x)$ given in (6.10). Note that, in the case of a straight channel, Γ_w is a straight line along the x -direction and $b'(x) = 0$ for all $x \in [0, L]$, therefore from (6.12) we consistently obtain: $\mathbf{t} = (1, 0)^T = \mathbf{e}_x$ and $\mathbf{n} = (0, -1)^T = -\mathbf{e}_y$.

6.1. Formulation of the problem

6.1.2 Boundary conditions and weak form

We now discuss the boundary conditions for the dynamical and turbulent variables and the weak form of the RANS and k - ε equations.

For given $\mathcal{G}_0 > 0$, let $U_p(y)$, $k_p(y)$ and $\varepsilon_p(y)$ be a solution to the boundary value problem (2.94)-(2.102) describing Poiseuille flow in straight channels, and let $\mathbf{u}_p = (U_p(y), 0)^\top$. Then, at the inlet of the channel, for $(x, y) \in \Gamma_{\text{in}}$, we impose the following Dirichlet conditions for the variables $\mathbf{u} = (U, V)$, k and ε :

$$\mathbf{u} = \mathbf{u}_p(y) , \quad (6.13)$$

$$k = k_p(y) , \quad (6.14)$$

$$\varepsilon = \varepsilon_p(y) , \quad (6.15)$$

(in practical computations the inlet profiles are obtained by a continuous piecewise linear interpolation of the numerical solution to (2.94)-(2.102) with $\mathcal{G}_0 = 12$, computed by the continuation strategy discussed in §2.5, see the plots on the left-hand side of Figure 6.4 and of Figure 6.8). At the centre line, for $(x, y) \in \Gamma_{\text{cl}}$, we prescribe the symmetry boundary conditions:

$$\frac{\partial U}{\partial y} = 0 , \quad (6.16)$$

$$V = 0 , \quad (6.17)$$

$$\frac{\partial k}{\partial y} = 0 , \quad (6.18)$$

$$\frac{\partial \varepsilon}{\partial y} = 0 , \quad (6.19)$$

and at the outlet of the channel, for $(x, y) \in \Gamma_{\text{out}}$, we impose:

$$p - \nu_\Gamma \frac{\partial U}{\partial x} = 0 , \quad (6.20)$$

$$\frac{\partial V}{\partial x} = 0 , \quad (6.21)$$

$$\frac{\partial k}{\partial x} = 0 , \quad (6.22)$$

$$\frac{\partial \varepsilon}{\partial x} = 0 . \quad (6.23)$$

Finally we give the boundary conditions at the artificial wall and explain their meaning. For

6.1. Formulation of the problem

$(x, y) \in \Gamma_w$, we have:

$$\boldsymbol{\tau}_w \cdot \mathbf{t} = \frac{\kappa C_\mu^{1/4} k^{1/2}}{\ln \left[(C_\mu^{1/4} k^{1/2} h_+) / \nu \right] + \kappa C} \mathbf{u} \cdot \mathbf{t} , \quad (6.24)$$

$$\mathbf{u} \cdot \mathbf{n} = 0 , \quad (6.25)$$

$$\nabla k \cdot \mathbf{n} = 0 , \quad (6.26)$$

$$\varepsilon = \frac{C_\mu^{3/4} k^{3/2}}{\kappa h_+} . \quad (6.27)$$

Above, \mathbf{t} and \mathbf{n} are respectively the tangential and normal vector to Γ_w (see (6.12)), h_+ , in (6.24) and (6.27), represents the perpendicular distance of the artificial from the physical wall, and $\boldsymbol{\tau}_w$, in (6.24), is the stress vector at Γ_w :

$$\boldsymbol{\tau}_w := \boldsymbol{\sigma} \cdot (-\mathbf{n}) \Big|_{\Gamma_w} , \quad (6.28)$$

with $\boldsymbol{\sigma}$ the total stress tensor defined in (2.2). The boundary condition (6.24) states that at the artificial wall the tangential component of the force per unit area and mass exerted by the fluid is proportional to the tangential component of the velocity field. It represents a generalization of (2.121) and reduces to it in the case of a straight channel geometry, as next shown. At the artificial wall of a straight channel, we have that

$$\mathbf{u} \cdot \mathbf{t} \Big|_{\Gamma_w} = \mathbf{u} \cdot \mathbf{e}_x \Big|_{y=h_+} = U(x, h_+) , \quad x \in [0, L]$$

and using this in (6.24) yields the right-hand side of (2.121), also, the left-hand side of (6.24) becomes

$$\begin{aligned} \boldsymbol{\tau}_w \cdot \mathbf{t} &= \mathbf{t} \cdot [\boldsymbol{\sigma} \cdot (-\mathbf{n})] \Big|_{\Gamma_w} \\ &= \mathbf{e}_x \cdot [\boldsymbol{\sigma} \cdot \mathbf{e}_y] \Big|_{y=h_+} \\ &= \nu_T \left(\frac{\partial U}{\partial y} + \frac{\partial V}{\partial x} \right) \Big|_{y=h_+} . \end{aligned} \quad (6.29)$$

We then observe that, in a straight channel, (6.25) reduces to

$$V(x, h_+) = 0 , \quad x \in [0, L] ,$$

from which it follows that

$$\frac{\partial V}{\partial x}(x, h_+) = 0 , \quad x \in [0, L] ,$$

6.1. Formulation of the problem

and this can then be used in (6.29) to get:

$$\boldsymbol{\tau}_w \cdot \mathbf{t} = \nu_T \left. \frac{\partial U}{\partial y} \right|_{y=h_+}$$

the same as the left-hand side of (2.121). Similarly to (2.121), (6.24) can be obtained from appropriate generalizations of the laws of the wall presented in §1.5. Specifically, the laws of the wall along curved boundaries corresponding to (1.63), (1.66) and (1.52) are respectively:

$$\boldsymbol{\tau}_w \cdot \mathbf{t} = [u_*(x)]^2, \quad (x, y) \in \Gamma_w, \quad (6.30)$$

$$k(x, y) = C_\mu^{-1/2} [u_*(x)]^2, \quad (x, y) \in \Gamma_w, \quad (6.31)$$

$$\frac{\mathbf{u} \cdot \mathbf{t}}{u_*(x)} = \frac{1}{\kappa} \ln \left(\frac{u_* h_+}{\nu} \right) + C, \quad (x, y) \in \Gamma_w, \quad (6.32)$$

and then, by following the same procedure as in §2.6.2, (6.24) can be derived from (6.30) by eliminating $[u_*(x)]^2$, using both (6.31) and (6.32). Finally we observe that (6.27) represents the “usual” implementation of the law of the wall for ε (compare it with (2.132)).

Next we derive the weak formulation of the dynamical and model equations subject to the above boundary conditions. As in the case of straight channel flows, we will recast into the weak form the RANS equations (2.103), and the turbulence equations (2.4). In deriving the weak formulation of the RANS equations, we will use some of the results presented in §2.6.1. In particular, we will start with the expression (2.108) for the weak form of the first equation in (2.103). In fact, as can be seen from its derivation, (2.108) does not depend on the special shape of the domain Ω , and we will also use (2.109), (2.110), (2.111). These expressions also apply to the expanding channel flow domain, since its centre line, inlet and outlet boundaries have the same orientation with respect to the coordinate axes as those of the straight channel. The difference from the formulation of §2.6.1, is that now the boundary condition (6.25):

$$\mathbf{u} \cdot \mathbf{n} = U n_1 + V n_2 = 0, \quad (x, y) \in \Gamma_w, \quad (6.33)$$

is treated as an extra equation for the new variable τ_n , defined as

$$\tau_n := \boldsymbol{\tau}_w \cdot \mathbf{n} = \mathbf{n} \cdot \boldsymbol{\sigma} \cdot (-\mathbf{n}) \Big|_{\Gamma_w}, \quad (6.34)$$

and representing the normal component of the stress vector at the artificial wall (we emphasize the fact that both equation (6.33) and the variable τ_n are defined only on the boundary Γ_w). The introduction of the variable τ_n is now discussed in conjunction with the derivation of the weak form of the first equation in (2.103). As observed above, an initial expression for this is

6.1. Formulation of the problem

given by (2.108):

$$\begin{aligned} & \int_{\Omega} [\mathbf{u} \cdot \nabla \mathbf{u} - \nabla \nu_T \cdot (\nabla \mathbf{u})^T] \cdot \mathbf{w} \, d\Omega + \int_{\Omega} \nu_T \nabla \mathbf{u} : (\nabla \mathbf{w})^T \, d\Omega - \\ & - \int_{\Omega} p \nabla \cdot \mathbf{w} \, d\Omega + \int_{\Gamma} [\mathbf{n} \cdot (p\mathbf{I} - \nu_T \nabla \mathbf{u})] \cdot \mathbf{w} \, d\Gamma = 0, \end{aligned} \quad (6.35)$$

the boundary term in (6.35) can again be expressed as the sum of four integrals each over one of the four parts of Γ . The integrals over Γ_{in} , Γ_{out} and Γ_{cl} can be expressed respectively as in (2.109), (2.110) and (2.111) whilst, by using (2.2) and (6.28), the integral over Γ_{w} can be written as:

$$\begin{aligned} \int_{\Gamma_{\text{w}}} [\mathbf{n} \cdot (p\mathbf{I} - \nu_T \nabla \mathbf{u})] \cdot \mathbf{w} \, d\Gamma &= - \int_{\Gamma_{\text{w}}} [\boldsymbol{\sigma} \cdot \mathbf{n} - \nu_T (\nabla \mathbf{u}) \cdot \mathbf{n}] \cdot \mathbf{w} \, d\Gamma \\ &= \int_{\Gamma_{\text{w}}} [\boldsymbol{\tau}_{\text{w}} + \nu_T (\nabla \mathbf{u}) \cdot \mathbf{n}] \cdot \mathbf{w} \, d\Gamma \end{aligned} \quad (6.36)$$

where we have also used the fact that $\mathbf{n} \cdot \boldsymbol{\sigma} = \boldsymbol{\sigma} \cdot \mathbf{n}$, due to the symmetry of $\boldsymbol{\sigma}$, and that $\mathbf{n} \cdot (\nabla \mathbf{u})^T = (\nabla \mathbf{u}) \cdot \mathbf{n}$. We then decompose $\boldsymbol{\tau}_{\text{w}}$ into its parallel and orthogonal components to Γ_{w} and, by using (6.24) and (6.34), express it as follows:

$$\begin{aligned} \boldsymbol{\tau}_{\text{w}} &= (\boldsymbol{\tau}_{\text{w}} \cdot \mathbf{t}) \mathbf{t} + (\boldsymbol{\tau}_{\text{w}} \cdot \mathbf{n}) \mathbf{n} \\ &= (f(k) \mathbf{u} \cdot \mathbf{t}) \mathbf{t} + \tau_n \mathbf{n}, \quad (x, y) \in \Gamma_{\text{w}}, \end{aligned} \quad (6.37)$$

where

$$f(k) := \frac{\kappa C_{\mu}^{1/4} k^{1/2}}{\ln \left[(C_{\mu}^{1/4} k^{1/2} h_{+}) / \nu \right] + \kappa C}, \quad (x, y) \in \Gamma_{\text{w}},$$

finally, by substituting (6.37) into (6.36), we get

$$\int_{\Gamma_{\text{w}}} [\mathbf{n} \cdot (p\mathbf{I} - \nu_T \nabla \mathbf{u})] \cdot \mathbf{w} \, d\Gamma = \int_{\Gamma_{\text{w}}} [(f(k) \mathbf{u} \cdot \mathbf{t}) \mathbf{t} + \tau_n \mathbf{n} + \nu_T (\nabla \mathbf{u}) \cdot \mathbf{n}] \cdot \mathbf{w} \, d\Gamma. \quad (6.38)$$

We now specify the spaces in which (6.35) is posed. Let $H^1(\Omega)$ be the Sobolev space of square integrable functions whose first derivatives are also square integrable over Ω and let $\mathbf{H}^1(\Omega) := H^1(\Omega) \times H^1(\Omega)$, then we seek the velocity field \mathbf{u} in:

$$\mathbf{H}_{E_P}^1(\Omega) = \{ \mathbf{v} \in \mathbf{H}^1(\Omega) : \mathbf{v} = \mathbf{u}_p \text{ on } \Gamma_{\text{in}} \text{ and } v_2 = 0 \text{ on } \Gamma_{\text{cl}} \},$$

and correspondingly require that \mathbf{w} is in the space:

$$\mathbf{H}_{0_P}^1(\Omega) = \{ \mathbf{v} \in \mathbf{H}^1(\Omega) : \mathbf{v} = \mathbf{0} \text{ on } \Gamma_{\text{in}} \text{ and } v_2 = 0 \text{ on } \Gamma_{\text{cl}} \}.$$

It is then not difficult to see that the only contribution to the boundary term in (6.35) which does not vanish, is the one corresponding to Γ_{w} , (6.38). In fact, the integral (2.109) is zero

6.1. Formulation of the problem

because $\mathbf{w} = \mathbf{0}$ on Γ_{in} , while (2.110) vanishes because of the boundary conditions (6.20) and (6.21), and finally (2.111) is also zero due to the boundary condition (6.16) and to the fact that $w_2 = 0$ on Γ_{cl} . Hence, using (6.38), (6.35) becomes:

$$\begin{aligned} a(\mathbf{u}, p, k, \varepsilon, \tau_n, \mathbf{w}) &:= \int_{\Omega} [\mathbf{u} \cdot \nabla \mathbf{u} - \nabla \nu_T \cdot (\nabla \mathbf{u})^T] \cdot \mathbf{w} \, d\Omega + \int_{\Omega} \nu_T \nabla \mathbf{u} : (\nabla \mathbf{w})^T \, d\Omega - \\ &- \int_{\Omega} p \nabla \cdot \mathbf{w} \, d\Omega + \int_{\Gamma_w} [(f(k) \mathbf{u} \cdot \mathbf{t}) \mathbf{t} + \tau_n \mathbf{n} + \nu_T (\nabla \mathbf{u}) \cdot \mathbf{n}] \cdot \mathbf{w} \, d\Gamma = 0 . \end{aligned} \quad (6.39)$$

As said before, τ_n in (6.39) is interpreted as a new variable and (6.33) as the equation for it. If one was going to attempt a theoretical discussion of (6.39), the natural space for τ_n would be $H^{-1/2}(\Gamma_w)$. For technical reasons our computed approximations will be smoother than that (see Remark 6.1.1). Finally, recalling (2.115), we can express the weak form of the RANS equations (2.103) subject to the boundary conditions (6.13), (6.16)-(6.17), (6.20)-(6.21) and (6.24)-(6.25) as

$$\begin{cases} a(\mathbf{u}, p, k, \varepsilon, \tau_n, \mathbf{w}) = 0 \\ b(\mathbf{u}, \psi) = 0 \\ \mathbf{u} \cdot \mathbf{n} = 0 , \quad \text{on } \Gamma_w . \end{cases}$$

We now briefly recast into the weak form of the transport equations for k and ε . An initial expression for the weak form of the equations in (2.4) is given by (2.130) and (2.131), respectively:

$$\begin{aligned} &\int_{\Omega} (\mathbf{u} \cdot \nabla k) z_1 \, d\Omega + \int_{\Omega} C_{\mu} \frac{k^2}{\varepsilon} \nabla k \cdot \nabla z_1 \, d\Omega + \int_{\Omega} \varepsilon z_1 \, d\Omega - \\ &- \int_{\Omega} C_{\mu} \frac{k^2}{\varepsilon} S(\mathbf{u}) z_1 \, d\Omega - \int_{\Gamma} C_{\mu} \frac{k^2}{\varepsilon} (\nabla k \cdot \mathbf{n}) z_1 \, d\Gamma = 0 \end{aligned} \quad (6.40)$$

and

$$\begin{aligned} &\int_{\Omega} (\mathbf{u} \cdot \nabla \varepsilon) z_2 \, d\Omega + \int_{\Omega} \frac{C_{\mu} k^2}{\sigma_{\varepsilon} \varepsilon} \nabla \varepsilon \cdot \nabla z_2 \, d\Omega + \int_{\Omega} C_{\varepsilon 2} \frac{\varepsilon^2}{k} z_2 \, d\Omega \\ &- \int_{\Omega} C_{\mu} C_{\varepsilon 1} k S(\mathbf{u}) z_2 \, d\Omega - \int_{\Gamma} \frac{C_{\mu} k^2}{\sigma_{\varepsilon} \varepsilon} (\nabla \varepsilon \cdot \mathbf{n}) z_2 \, d\Gamma = 0 . \end{aligned} \quad (6.41)$$

The turbulence variables (k, ε) are sought in the space

$$\mathbf{H}_{E_T}^1(\Omega) = \{\mathbf{s} \in \mathbf{H}^1(\Omega) : \mathbf{s} = (k_p(y), \varepsilon_p(y))^T \quad \text{on } \Gamma_{\text{in}}\} ,$$

and must satisfy the law of the wall:

$$\varepsilon(x, y) - \frac{C_{\mu}^{3/4} (k(x, y))^{3/2}}{\kappa h_+} = 0 , \quad (x, y) \in \Gamma_w , \quad (6.42)$$

6.1. Formulation of the problem

correspondingly the test function $\mathbf{z} = (z_1, z_2)^\top$ is chosen in the space:

$$\mathbf{H}_{0T}^1(\Omega) = \{\mathbf{q} \in \mathbf{H}^1(\Omega) : \mathbf{q} = \mathbf{0} \text{ on } \Gamma_{\text{in}} \text{ and } q_2 = 0 \text{ on } \Gamma_{\text{w}}\}.$$

From the boundary conditions (6.18), (6.22) and (6.26) (which are equivalent to $\nabla k \cdot \mathbf{n} = 0$ on $\Gamma_{\text{cl}} \cup \Gamma_{\text{out}} \cup \Gamma_{\text{w}}$) and the fact that $z_1 = 0$ on Γ_{in} , it follows that the boundary term in (6.40) vanishes, therefore we write the weak form of the transport equation for k as:

$$\begin{aligned} c(\mathbf{u}, k, \varepsilon, \mathbf{z}) &:= \int_{\Omega} (\mathbf{u} \cdot \nabla k) z_1 \, d\Omega + \int_{\Omega} C_{\mu} \frac{k^2}{\varepsilon} \nabla k \cdot \nabla z_1 \, d\Omega + \\ &+ \int_{\Omega} \varepsilon z_1 \, d\Omega - \int_{\Omega} C_{\mu} \frac{k^2}{\varepsilon} S(\mathbf{u}) z_1 \, d\Omega = 0. \end{aligned}$$

Also the boundary term in (6.41) is zero because of the boundary conditions (6.19) and (6.23) (which are equivalent to $\nabla \varepsilon \cdot \mathbf{n} = 0$ on $\Gamma_{\text{cl}} \cup \Gamma_{\text{out}}$) and of the fact that $z_2 = 0$ on $\Gamma_{\text{in}} \cup \Gamma_{\text{w}}$, thus we express the weak form of the transport equation for ε as:

$$\begin{aligned} d(\mathbf{u}, k, \varepsilon, \mathbf{z}) &:= \int_{\Omega} (\mathbf{u} \cdot \nabla \varepsilon) z_2 \, d\Omega + \int_{\Omega} \frac{C_{\mu} k^2}{\sigma_{\varepsilon} \varepsilon} \nabla \varepsilon \cdot \nabla z_2 \, d\Omega + \\ &+ \int_{\Omega} C_{\varepsilon 2} \frac{\varepsilon^2}{k} z_2 \, d\Omega - \int_{\Omega} C_{\mu} C_{\varepsilon 1} k S(\mathbf{u}) z_2 \, d\Omega = 0. \end{aligned}$$

Summarizing we have that the weak form of the RANS and k - ε equations is: find $\mathbf{u} \in \mathbf{H}_{EP}^1(\Omega)$, $p \in L_2(\Omega)$, $\tau_n \in H^{1/2}(\Gamma_{\text{w}})$, $(k, \varepsilon) \in \mathbf{H}_{ET}^1(\Omega)$ such that

$$\left\{ \begin{array}{l} a(\mathbf{u}, p, k, \varepsilon, \tau_n, \mathbf{w}) = 0 \\ b(\mathbf{u}, \psi) = 0 \\ \mathbf{u} \cdot \mathbf{n} = 0, \text{ on } \Gamma_{\text{w}} \\ c(\mathbf{u}, k, \varepsilon, \mathbf{z}) = 0 \\ \varepsilon - \frac{C_{\mu}^{3/4} k^{3/2}}{\kappa h_+} = 0, \text{ on } \Gamma_{\text{w}} \\ d(\mathbf{u}, k, \varepsilon, \mathbf{z}) = 0 \end{array} \right. \quad (6.43)$$

for all $\mathbf{w} \in \mathbf{H}_{0P}^1(\Omega)$, $\psi \in L_2(\Omega)$ and $\mathbf{z} \in \mathbf{H}_{0T}^1(\Omega)$.

6.1.3 The numerical strategy

We now briefly discuss the finite element discretisation of (6.43) and the continuation technique used to solve the resulting algebraic system of equations. We first make the following observation:

Remark 6.1.1. As for the corresponding cases of 2D turbulent Couette and Poiseuille flows in straight channels, the discretisation of (6.43) and the computation of the solution to the resulting algebraic system have been carried out using the industrial code ENTWIFE. But, this

6.1. Formulation of the problem

code does not allow variables to be defined only on the boundary or on parts of the boundary of a given domain, such is τ_n ; hence, a practical version of (6.43) has been obtained by introducing the harmonic extension of τ_n to Ω , which we denote by $\hat{\tau}_n$. We have then required that $\hat{\tau}_n$ satisfies

$$-\Delta \hat{\tau}_n = 0, \quad \text{on } \Omega, \quad (6.44)$$

subject to homogeneous Neumann condition on Γ_{in} , Γ_{cl} , Γ_{out} and equation (6.33) on Γ_w . Clearly, only the values of $\hat{\tau}_n$ on Γ_w are meaningful for our problem and correspond to the values of τ_n . Therefore, considering that the weak formulation of (6.44) is:

$$\hat{a}(\hat{\tau}_n, v) := \int_{\Omega} \nabla \hat{\tau}_n \cdot \nabla v \, d\Omega = 0$$

with $\hat{\tau}_n \in H^1(\Omega)$ and the test function v in the space:

$$H_{0\tau_n}^1(\Omega) := \{s \in H^1(\Omega) : s = 0 \text{ on } \Gamma_w\},$$

in our practical implementation we have discretised the following weak form: find $\mathbf{u} \in \mathbf{H}_{EP}^1(\Omega)$, $p \in L_2(\Omega)$, $\hat{\tau}_n \in H^1(\Omega)$, $(k, \varepsilon) \in \mathbf{H}_{ET}^1(\Omega)$ such that

$$\left\{ \begin{array}{l} a(\mathbf{u}, p, k, \varepsilon, \tau_n, \mathbf{w}) = 0 \\ b(\mathbf{u}, \psi) = 0 \\ \hat{a}(\hat{\tau}_n, v) = 0 \\ \mathbf{u} \cdot \mathbf{n} = 0, \quad \text{on } \Gamma_w \\ c(\mathbf{u}, k, \varepsilon, \mathbf{z}) = 0 \\ d(\mathbf{u}, k, \varepsilon, \mathbf{z}) = 0 \\ \varepsilon - \frac{C_\mu^{3/4} k^{3/2}}{\kappa h_+} = 0, \quad \text{on } \Gamma_w \end{array} \right. \quad (6.45)$$

for all $\mathbf{w} \in \mathbf{H}_{0P}^1(\Omega)$, $\psi \in L_2(\Omega)$, $v \in H_{0\tau_n}^1(\Omega)$ and $\mathbf{z} \in \mathbf{H}_{0T}^1(\Omega)$.

We now briefly discuss the finite element approximation to (6.45) on the expanding domain Ω (we are assuming that $\alpha > 0$, $\beta \geq 1$ and $\gamma > 0$ have been prescribed in (6.1)). This is carried out in two steps. First the weak form (6.45) is approximated on the straight domain $\tilde{\Omega}$ discretised via a mesh of quadrilateral elements defined by a bilinear map from the unit quadrilateral and then the resulting equations are mapped onto the expanding domain Ω using the orthogonal mapping which is described in §6.2.1.

As mentioned at the end of §6.1.1, we will compute a numerical solution to the fully developed Poiseuille flow in expanding channels using continuation from the straight channel (identified by $\alpha = 0$). In this case, in fact, Poiseuille flow can confidently be solved numerically using the analytical solution to Couette flow as initial guess, as described in §2.5. The computed solution to Poiseuille flow in a straight domain will then be used as starting point for a continuation process based on two homotopy transformations one on the parameter α , from

6.2. A graded boundary-fitted orthogonal mesh

$\alpha = 0$ to $\alpha_0 > 0$ and the other on the parameter β , from $\beta = 1$ to $\beta = \beta_0 > 1$. First we will perform the transformation on α and therefore solve the finite element system on a sequence of channels with increasingly bigger expansion factor r (see (6.9)) and increasingly steeper slope at $x = \gamma$ (see (6.11)). Then, reached the desired expansion of the channel, its maximum slope at $x = \gamma$ will be increased by performing the homotopy transformation on β (see (6.11)).

6.2 A graded boundary-fitted orthogonal mesh

This section consists of two parts. Initially we give a brief overview of the theoretical issues related to the generation of boundary-fitted, orthogonal meshes and explain how we will practically discretise expanding channels by appropriately graded, orthogonal grids. Then we will present the numerical experiments we have performed to assess the quality of such meshes. (In this section, as in the previous one, the domains Ω and $\tilde{\Omega}$ will denote respectively the lower half of an expanding channel and of a straight one, with boundaries $\Gamma = \Gamma_{\text{in}} \cup \Gamma_{\text{cl}} \cup \Gamma_{\text{out}} \cup \Gamma_{\text{w}}$ and $\tilde{\Gamma} = \tilde{\Gamma}_{\text{in}} \cup \tilde{\Gamma}_{\text{cl}} \cup \tilde{\Gamma}_{\text{out}} \cup \tilde{\Gamma}_{\text{w}}$. On Ω we will consider the curvilinear coordinates (x, y) , while on $\tilde{\Omega}$ we will consider the cartesian coordinates (ξ, η)).

6.2.1 Orthogonal mapping technique

The procedure followed in Chapter 3 for constructing one-dimensional equidistributed meshes, can also be used to generate graded, boundary-fitted, orthogonal mesh on Ω . These, in fact, can be considered as the image of certain cartesian meshes on $\tilde{\Omega}$ through an appropriate transformation $(x, y): \tilde{\Omega} \mapsto \Omega$ (according to the terminology introduced in Chapter 3, $\tilde{\Omega}$ represents the computational domain while Ω is the physical domain). The properties of the mapping (x, y) and the specific discretisation of $\tilde{\Omega}$ we have considered, are illustrated below.

The orthogonal mapping technique which we now outline, is discussed in detail in [63], where it was initially proposed for the finite element computation of a viscous free-surface flow along an undulating inclined plane. The mapping (x, y) is obtained by solving the system of elliptic PDE's:

$$\left\{ \begin{array}{l} \frac{\partial}{\partial \xi} \left(\lambda(\xi, \eta) \frac{\partial x}{\partial \xi} \right) + \frac{\partial}{\partial \eta} \left(\frac{1}{\lambda(\xi, \eta)} \frac{\partial x}{\partial \eta} \right) = 0 \\ \frac{\partial}{\partial \xi} \left(\lambda(\xi, \eta) \frac{\partial y}{\partial \xi} \right) + \frac{\partial}{\partial \eta} \left(\frac{1}{\lambda(\xi, \eta)} \frac{\partial y}{\partial \eta} \right) = 0 \\ \frac{\partial^2 \lambda}{\partial \xi^2} + \frac{\partial^2 \lambda}{\partial \eta^2} = 0 \end{array} \right. \quad (6.46)$$

for unknowns $x = x(\xi, \eta)$, $y = y(\xi, \eta)$ and $\lambda = \lambda(\xi, \eta)$; with (x, y) subject to the boundary

6.2. A graded boundary-fitted orthogonal mesh

conditions

$$x = 0 \quad \frac{\partial y}{\partial \xi} = 0 \quad \text{on } \xi = 0 \quad (6.47)$$

$$\frac{\partial x}{\partial \eta} = -\lambda \frac{\partial y}{\partial \xi} \quad y = b(x) \quad \text{on } \eta = h_+ \quad (6.48)$$

$$x = L \quad \frac{\partial y}{\partial \xi} = 0 \quad \text{on } \xi = L \quad (6.49)$$

$$\frac{\partial x}{\partial \eta} = 0 \quad y = d \quad \text{on } \eta = d \quad (6.50)$$

and λ subject to the boundary condition

$$\nabla \lambda \cdot \mathbf{n} = 0 \quad \text{on } \tilde{\Gamma} \quad (6.51)$$

and to the additional constraint:

$$\frac{\partial x}{\partial \eta} + \frac{\partial y}{\partial \eta} = \lambda \left(\frac{\partial x}{\partial \xi} - \frac{\partial y}{\partial \xi} \right) \quad \text{at } (\xi, \eta) = (\xi_c, \eta_c) . \quad (6.52)$$

In (6.48), $b(x)$ is the curved boundary of the expanding channel (see (6.8)) and \mathbf{n} , in (6.51), is the outward normal vector to the boundary $\tilde{\Gamma}$. In the following we will not give a detailed derivation of (6.46) (this can be found in [63]) and of (6.47)-(6.52), but we shall simply explain the rational behind them.

It can be shown (see [63] and also [64]) that, under appropriate boundary conditions, the solution to the system:

$$\begin{cases} \frac{\partial}{\partial \xi} \left(\lambda(\xi, \eta) \frac{\partial x}{\partial \xi} \right) + \frac{\partial}{\partial \eta} \left(\frac{1}{\lambda(\xi, \eta)} \frac{\partial x}{\partial \eta} \right) = 0 \\ \frac{\partial}{\partial \xi} \left(\lambda(\xi, \eta) \frac{\partial y}{\partial \xi} \right) + \frac{\partial}{\partial \eta} \left(\frac{1}{\lambda(\xi, \eta)} \frac{\partial y}{\partial \eta} \right) = 0 \end{cases} \quad (6.53)$$

(note that (6.53) consists of the first two equations in (6.46)) gives an orthogonal transformation from $\tilde{\Omega}$ to Ω (provided a solution actually exists for the particular boundary shape of Ω). In (6.53), λ is a strictly positive, smooth function, representing the aspect ratio of a small rectangle in the (x, y) plane, that is the image of a small square in the (ξ, η) plane; we will explain below how we have determined it. In [63], the system (6.53) is derived from the equations expressing the orthogonality constraint on the curvilinear coordinates (x, y) :

$$\frac{\partial x}{\partial \eta} = -\lambda \frac{\partial y}{\partial \xi} \quad (6.54)$$

$$\frac{\partial y}{\partial \eta} = \lambda \frac{\partial x}{\partial \xi} , \quad (6.55)$$

6.2. A graded boundary-fitted orthogonal mesh

(also known as generalized Cauchy-Riemann equations) using:

$$\frac{\partial}{\partial \xi} \left(\frac{\partial y}{\partial \eta} \right) = \frac{\partial}{\partial \eta} \left(\frac{\partial y}{\partial \xi} \right), \quad \frac{\partial}{\partial \xi} \left(\frac{\partial x}{\partial \eta} \right) = \frac{\partial}{\partial \eta} \left(\frac{\partial x}{\partial \xi} \right).$$

(It should be noted that in [64], differently from [63], the equations in (6.53) are obtained by means of a covariant Laplace equation method). We also observe that (6.47)-(6.50) follow from imposing the orthogonality condition (6.54)-(6.55) and from prescribing that $\tilde{\Gamma}_{\text{in}}$, $\tilde{\Gamma}_{\text{cl}}$, $\tilde{\Gamma}_{\text{out}}$, $\tilde{\Gamma}_{\text{w}}$ are transformed respectively into Γ_{in} , Γ_{cl} , Γ_{out} , Γ_{w} . For example, (6.48) expresses the condition that $\tilde{\Gamma}_{\text{w}}$ is mapped into Γ_{w} and that the coordinates (x, y) are orthogonal along Γ_{w} .

Finally, as in [63], we require that λ in (6.53) takes a constant value on $\tilde{\Omega}$. This is achieved by solving the Laplace equation:

$$\Delta \lambda = 0 \quad \text{on } \tilde{\Omega} \quad (6.56)$$

(this is the third equation in (6.46)) under the boundary condition

$$\nabla \lambda \cdot \mathbf{n} = 0 \quad \text{on } \tilde{\Gamma} \quad (6.57)$$

and the constraint:

$$\frac{\partial x}{\partial \eta} + \frac{\partial y}{\partial \eta} = \lambda \left(\frac{\partial x}{\partial \xi} - \frac{\partial y}{\partial \xi} \right) \quad \text{at } (\xi, \eta) = (\xi_c, \eta_c). \quad (6.58)$$

(respectively (6.51) and (6.52)). Note that any constant function λ is a solution to (6.56)-(6.57) and that equation (6.58), obtained from the sum of (6.54) and (6.55), is needed to determine uniquely the constant value of λ ; the point (ξ_c, η_c) is the centre of the domain $\tilde{\Omega}$ (in practical computation it will be the coordinates of the node at the centre of the mesh on $\tilde{\Omega}$). It should be noted that there are other possible procedures of determining λ (see for example [64], [65], [66] and [67]) and that the technique described above may not be the most efficient. It was chosen because it represents the most natural way of treating the equations for the mapping as a system of elliptic PDE's to be discretised and solved, together with (6.45), by the finite element code ENTWIFE.

The weak form of the boundary value problem for determining the orthogonal mapping is then given by:

$$\begin{cases} \mathbf{a}_M(x, y, \mathbf{v}) = 0 \\ b_M(\lambda, q) = 0 \\ y - b(x) = 0, \quad \text{on } \tilde{\Gamma}_{\text{w}} \\ \frac{\partial x}{\partial \eta} + \frac{\partial y}{\partial \eta} = \lambda \left(\frac{\partial x}{\partial \xi} - \frac{\partial y}{\partial \xi} \right), \quad \text{at } (\xi_c, \eta_c) \end{cases} \quad (6.59)$$

6.2. A graded boundary-fitted orthogonal mesh

where

$$(\mathbf{a}_M(x, y, \mathbf{v}))_1 := \int_{\tilde{\Omega}} \lambda \frac{\partial x}{\partial \xi} \frac{\partial v_1}{\partial \xi} d\tilde{\Omega} + \int_{\tilde{\Omega}} \frac{1}{\lambda} \frac{\partial x}{\partial \eta} \frac{\partial v_1}{\partial \eta} d\tilde{\Omega} - \int_{\tilde{\Gamma}_w} \frac{\partial y}{\partial \xi} v_1 d\tilde{\Gamma}_w ,$$

$$(\mathbf{a}_M(x, y, \mathbf{v}))_2 := \int_{\tilde{\Omega}} \lambda \frac{\partial y}{\partial \xi} \frac{\partial v_2}{\partial \xi} d\tilde{\Omega} + \int_{\tilde{\Omega}} \frac{1}{\lambda} \frac{\partial y}{\partial \eta} \frac{\partial v_2}{\partial \eta} d\tilde{\Omega} ,$$

and

$$b_M(\lambda, q) := \int_{\tilde{\Omega}} \nabla \lambda \cdot \nabla q d\tilde{\Omega} .$$

The variables (x, y) are sought in the space

$$\mathbf{H}_{EM}^1(\tilde{\Omega}) := \{ \mathbf{w} \in \mathbf{H}^1(\tilde{\Omega}) : w_1 = 0 \text{ on } \tilde{\Gamma}_{in}, w_1 = L \text{ on } \tilde{\Gamma}_{out} \text{ and } w_2 = d \text{ on } \tilde{\Gamma}_{cl} \}$$

while λ is sought in $H^1(\tilde{\Omega})$. Correspondingly the test function \mathbf{v} is chosen in the space

$$\mathbf{H}_{0M}^1(\tilde{\Omega}) := \{ \mathbf{u} \in \mathbf{H}^1(\tilde{\Omega}) : u_1 = 0 \text{ on } \tilde{\Gamma}_{in} \cup \tilde{\Gamma}_{out} \text{ and } u_2 = 0 \text{ on } \tilde{\Gamma}_w \cup \tilde{\Gamma}_{cl} \}$$

and q is chosen in $H^1(\tilde{\Omega})$.

As for the RANS and $k-\varepsilon$ equations, the weak form (6.59) is discretised on the domain $\tilde{\Omega}$ using continuous piecewise biquadratic finite elements and the resulting nonlinear algebraic system is solved by Newton's method (the entries of the Jacobian of the nonlinear system were computed using the 3×3 Gauss-Jacobi quadrature applied element wise). The solution to the finite element system then provides the mapping from the straight channel to the expanding one to be applied to the dynamical and model equations initially discretised on the straight domain $\tilde{\Omega}$, as discussed in §6.1.3.

The computational domain is discretised as now explained: first $\tilde{\Omega}$ is divided into disjoint sub-domains, and on each sub-domain the tensor product of the following two grids is considered: a mesh graded as (3.101) in the η -direction, and an exponentially graded mesh (see (3.104)) in the ξ -direction. Finally the mesh on $\tilde{\Omega}$ is obtained by taking the union of all subdomains. The transformation of the mesh on $\tilde{\Omega}$ will produce a grid on Ω which will have the right grading for resolving profiles as (6.27) in the direction orthogonal to the artificial wall and be appropriately refined in the longitudinal direction according to geometry of the channel (for example, finer in a neighbourhood of the expansion of the channel and increasingly coarser towards the outlet of the channel).

6.2.2 Numerical experiments

In this section we present the outcomes of the finite element computations of fully developed turbulent flows in expanding channels, discretised by graded, boundary-fitted, orthogonal meshes.

First, we observe that, in order to validate the computations performed on orthogonal grids (see Figure 6.3 and Figure 6.6), we have also considered non-orthogonal discretisations of Ω ,

6.2. A graded boundary-fitted orthogonal mesh

see Figure 6.2. These were obtained simply by transforming the computational grid on $\tilde{\Omega}$, through the mapping (6.1), therefore, using a procedure much more straightforward and less prone to mistakes than the one used for generating orthogonal grids.

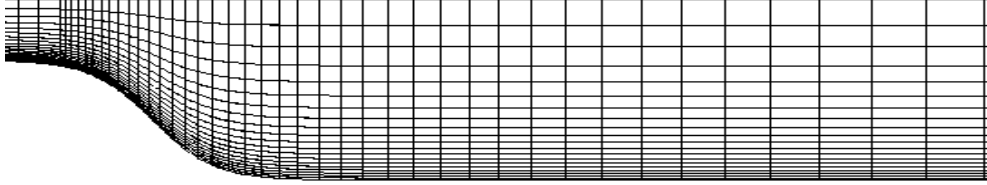


Figure 6.2: Zoom of the non-orthogonal mesh on the the expanding channel with $h_+ = 10^{-1}$, $\alpha = 2.0$, $\beta = 1.5$ and $\gamma = 10$.

For $h_+ = 10^{-1}$, the numerical results obtained on these two discretisations of Ω (derived from the same grid on $\tilde{\Omega}$) were identical; this then gave clear indication of the fact that the method for creating graded, orthogonal mesh was correctly implemented. In the case of $h_+ = 10^{-2}$, only for values of α sufficiently small (i.e. for flow domains with sufficiently small expansions, see (6.9)) could the computations performed on the non-orthogonal mesh reproduce the results obtained on the orthogonal one. In fact, at the stage of the continuation procedure when $\alpha = 0.8$, Newton's method for the finite element system obtained on the non-orthogonal mesh, failed to converge. At this point only by reducing the size of the continuation steps or by increasing the number of elements could Newton's method attain convergence. As the expansion of the channel was increased the computations on the non-orthogonal grid became more and more unpractical and it was not possible to consider values of α as big as in the case of orthogonal meshes. In the orthogonal case, it took 20 continuation steps on a mesh with 200×25 elements, to reach the values $\alpha = 2.0$, $\beta = 1.5$, and then to obtain the outlet U -, k -, ε -profiles plotted in the left-hand side of Figure 6.4. As it can be clearly seen, these have the same trend as the inlet profiles but are scaled by a factor proportional to the expansion of the channel. It was also possible to resolve the flow recirculating immediately after the expansion as the contour plot of the streamlines, in Figure 6.5, shows.

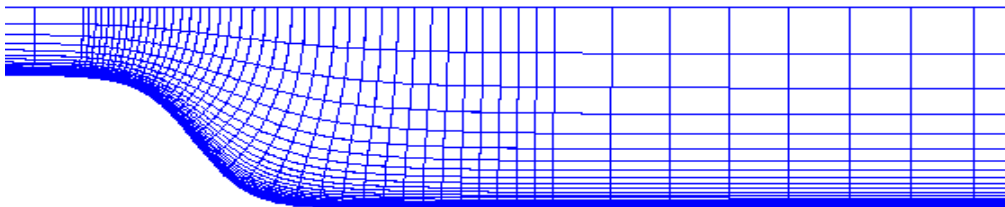


Figure 6.3: Zoom of the graded, orthogonal mesh on the the expanding channel with $h_+ = 10^{-2}$, $\alpha = 2.0$, $\beta = 1.5$ and $\gamma = 10$. The number of elements in the y -direction is 25.

Qualitatively similar results were also obtained for $h_+ = 10^{-3}$, $\alpha = 1.3$ and $\beta = 1.55$ on a graded, orthogonal mesh with 200×35 elements. For this case, the pressure profile along the centre line and the outlet profiles are represented respectively in Figure 6.7 and in Figure 6.8,

6.2. A graded boundary-fitted orthogonal mesh

while the streamlines contour plot is in Figure 6.9.

Our numerical experiments then show that the h_+ -dependent nodes' distribution in the direction of the blow-up of ε , identified from the study of "simple" $1D$ problems, performs extremely well also in the much more challenging situation of $2D$ flows in expanding channels. It allows, in fact, to perform practical computations of the RANS and k - ε equations when channels with big expansions and small values of h_+ are considered.

6.2. A graded boundary-fitted orthogonal mesh

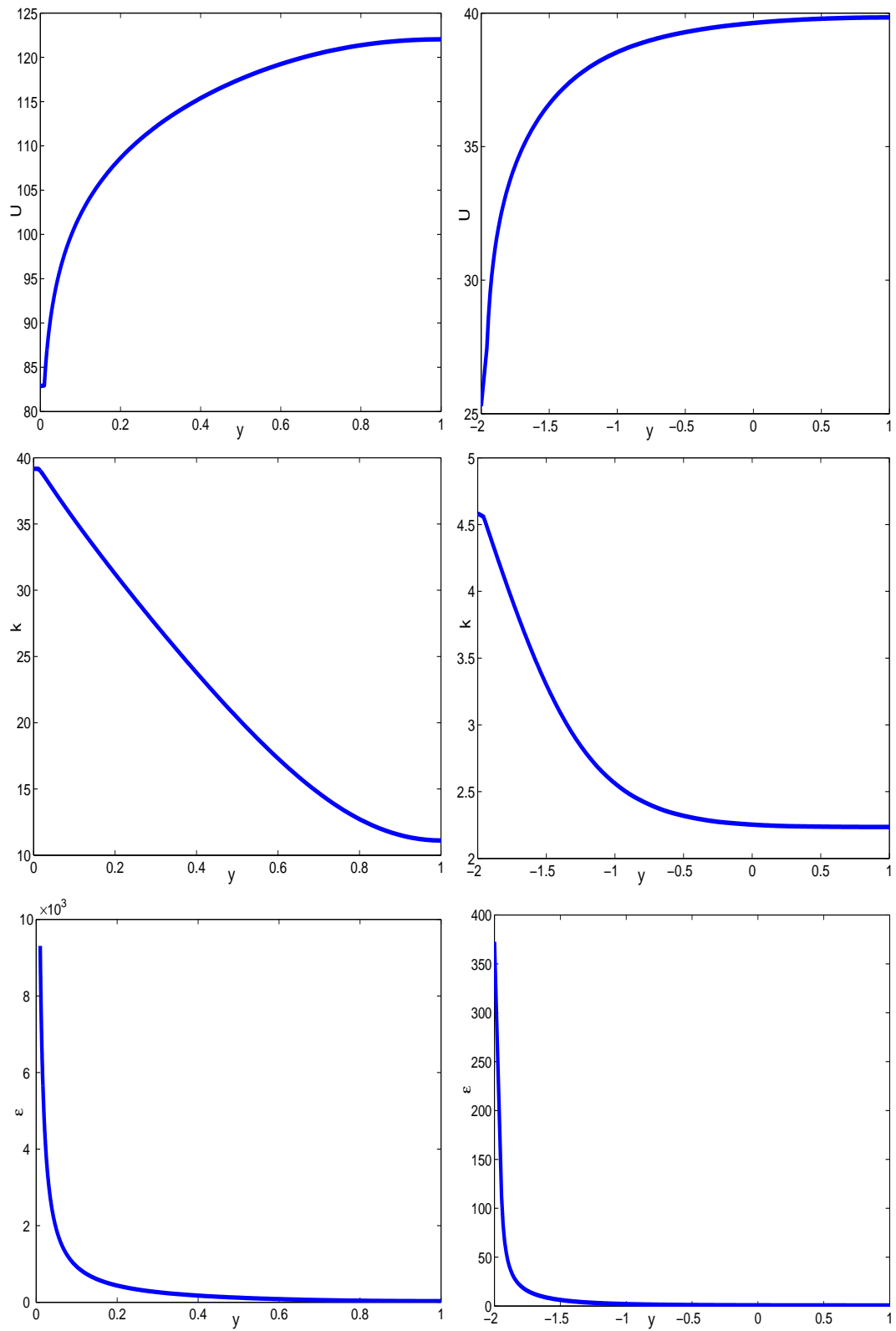


Figure 6.4: Left (from top to bottom): inlet U -, k -, ε -profile. Right (from top to bottom): outlet U -, k -, ε -solution components, computed on an expanding channel with $h_+ = 10^{-2}$, $\alpha = 2.0$, $\beta = 1.5$ and $\gamma = 10$.

6.2. A graded boundary-fitted orthogonal mesh

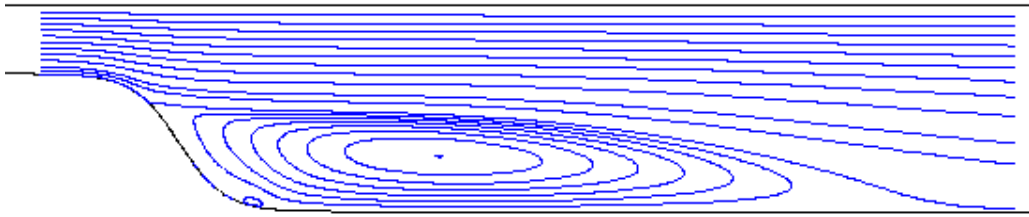


Figure 6.5: Contour plot of the streamlines obtained on the expanding channel with $h_+ = 10^{-2}$, $\alpha = 2.0$, $\beta = 1.5$ and $\gamma = 10$.

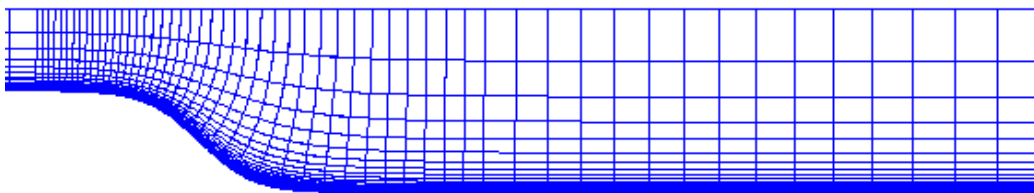


Figure 6.6: Zoom of the graded, orthogonal mesh on the the expanding channel with $h_+ = 10^{-3}$, $\alpha = 1.3$, $\beta = 1.55$ and $\gamma = 10$. The number of elements in the y -direction is 35.

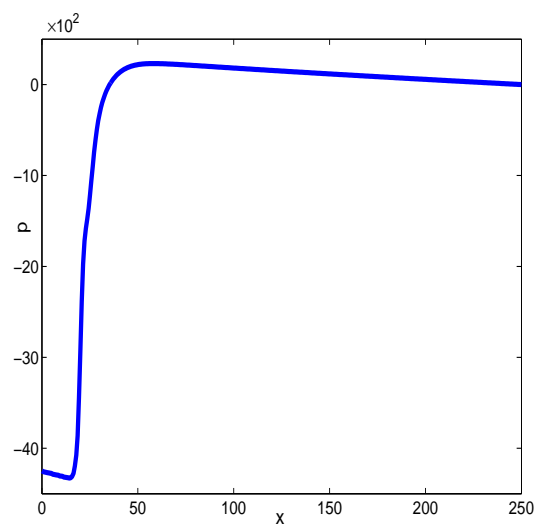


Figure 6.7: Pressure profile along the centre line of the expanding channel with $h_+ = 10^{-3}$, $\alpha = 1.3$, $\beta = 1.55$ and $\gamma = 10$.

6.2. A graded boundary-fitted orthogonal mesh

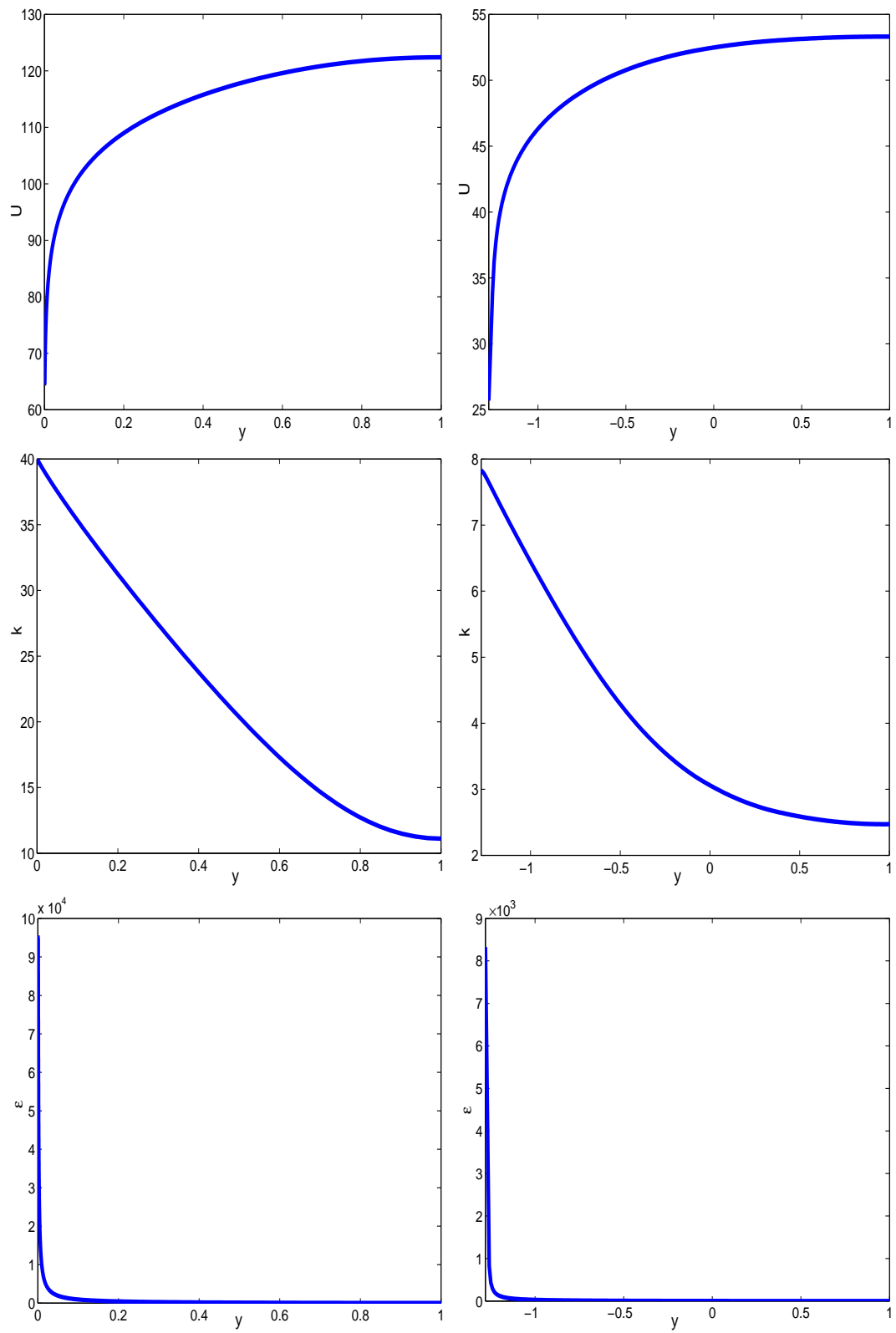


Figure 6.8: Left (from top to bottom): inlet U -, k -, ε -profile. Right (from top to bottom): outlet U -, k -, ε -solution components, obtained on an expanding channel with $h_+ = 10^{-3}$, $\alpha = 1.3$, $\beta = 1.55$ and $\gamma = 10$.

6.2. A graded boundary-fitted orthogonal mesh

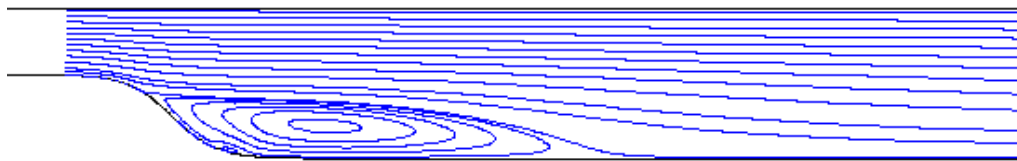


Figure 6.9: Contour plot of the streamlines obtained on the expanding channel with $h_+ = 10^{-3}$, $\alpha = 1.3$, $\beta = 1.55$ and $\gamma = 10$.

Bibliography

- [1] H. Tennekes and J.L. Lumley. *A First Course in Turbulence*. The MIT Press, Cambridge, Massachusetts, 1972.
- [2] S.B. Pope. *Turbulent Flows*. Cambridge University Press, Cambridge, 2000.
- [3] C. Foias, O.P. Manley, R. Rosa and R. Temam. *Navier-Stokes Equations and Turbulence*, volume 83 of *Encyclopedia of Mathematics and its Applications*. Cambridge University Press, Cambridge, 2001.
- [4] J. Mathieu and J. Scott. *An Introduction to Turbulent Flow*. Cambridge University Press, Cambridge, 2000.
- [5] C.-J. Chen and S.-Y. Jaw. *Fundamentals of Turbulence Modelling*. Taylor & Francis Ltd., London, 1998.
- [6] T.B. Gatski, M.Y. Hussaini, J.L. Lumley, editor. *Simulation and Modelling of Turbulent Flows*. ICASE/LaRC Series in Computational Science and Engineering. Oxford University Press, Inc., New York, 1996.
- [7] P.M. Gresho and R.L. Sani. *Incompressible Flow and the Finite Element Method*, volume 2: Isothermal Laminar Flow. John Wiley and Sons, LTD, Chichester, 2000.
- [8] C.C. Lin and L.A. Segel. *Deterministic Problems in the Natural Sciences*. Macmillan Publishing Co., Inc., New York, 1974.
- [9] E.N. Lorenz. Deterministic nonperiodic flow. *J. Atmospheric Sci.*, 20:130–141, 1963.
- [10] C. Foias and G. Prodi. Sur les solutions statistiques des équations de Navier-Stokes. *Ann. Mat. Pura Appl.*, 111(4):307–330, 1976.
- [11] M.J. Feigenbaum. The transition to aperiodic behaviour in turbulent systems. *Comm. Math. Phys.*, 77:65–86, 1980.
- [12] J. Guckenheimer and P. Holmes. *Nonlinear Oscillations, Dynamical Systems and Bifurcations of Vector Fields*. Springer-Verlag, New York, 1983.
- [13] Moon. F.C. *Chaotic and fractal dynamics: an introduction for applied scientists and engineers*. Wiley, New York, 1992.

BIBLIOGRAPHY

- [14] J. Gleick. *Chaos: Making a New Science*. Penguin, New York, 1988.
- [15] A.N. Kolmogorov. The local structure of turbulence in incompressible viscous fluid at very high Reynolds number. *Dokl. Akad. Nauk. SSSR*, 30(4):301–305, 1941.
- [16] A.N. Kolmogorov. On the decay of isotropic turbulence in an incompressible viscous liquid. *Dokl. Akad. Nauk. SSSR*, 31:538–540, 1941.
- [17] A.N. Kolmogorov. Energy dissipation in locally isotropic turbulence. *Dokl. Akad. Nauk. SSSR*, 32:16–18, 1941.
- [18] L. Onsager. The distribution of energy in turbulence. *Phys. Rev.*, 68:285, 1945.
- [19] C. Foias, O.P. Manley, R. Rosa and R. Temam. Cascade of energy in turbulent flows. *Comptes Rendus Acad. Sci. Paris, Série I-Mathématique*, 332(6):509–514, 2001.
- [20] C. Foias, O.P. Manley, R. Rosa and R. Temam. Estimates for the energy cascade in three-dimensional turbulent flows. *Comptes Rendus Acad. Sci. Paris, Série I-Mathématique*, 333(5):499–504, 2001.
- [21] C. Foias, M.S. Jolly, O.P. Manley, R. Rosa and R. Temam. Kolmogorov theory via finite-time averages. *Physica D-Nonlinear Phenomena*, 212(3-4):245–270, 2005.
- [22] H.L. Grant, R.W. Stewart and A. Moilliet. Turbulence spectra from a tidal channel. *Journal of Fluid Mechanics*, 12:241–268, 1962.
- [23] G. Zocchi, P. Tabeling, J. Maurer and H. Willaime. Applied mathematics and turbulence modelling. *Physical Review E*, 50(5):3693–3700, 1994.
- [24] K.R. Sreenivasan. On the universality of the Kolmogorov constant. *Phys. Fluids*, 7(11):2778–2784, 1995.
- [25] G.K. Batchelor. *The Theory of Homogeneous Turbulence*. Cambridge University Press, Cambridge, 1953.
- [26] W.P. Jones and B.E. Launder. Prediction of laminarization with a two-equation model of turbulence. *International Journal of Heat and Mass Transfer*, 15(2):301–314, 1972.
- [27] B.E. Launder and B.I. Sharma. Application of the energy-dissipation model of turbulence to the calculation of flow near a spinning disc. *Lett. Heat Mass Trans.*, 1:131–138, 1974.
- [28] R. M. Smith. On the finite-element calculation of turbulent flow using the k - ε model. *Int. J. Numer. Methods Fluids*, 4(4):303–319, 1984.
- [29] R. M. Smith. A practical method of two-equation turbulence modelling using finite elements. *Int. J. Numer. Methods Fluids*, 4(4):321–336, 1984.

BIBLIOGRAPHY

- [30] R. M. Hutton, A.G. Smith and S. Hickmott. The computation of turbulent flows of industrial complexity by the finite element method - Progress and prospects. *Int. J. Numer. Methods Fluids*, 7(11):1277–1298, 1987.
- [31] B. Mohammadi and O. Pironneau. *Analysis of the K-Epsilon Model*. Jhon Wiley and Sons Ltd, Chichester, 1994.
- [32] B. Mohammadi and O. Pironneau. Applied mathematics and turbulence modelling. *Int. J. Numer. Methods Fluids*, 20:819–829, 1995.
- [33] Z.N. Wu and S. Fu. Positivity of k -epsilon turbulence models for incompressible flow. *Mathematical Models and Methods in Applied Sciences*, 12(3):393–406, 2002.
- [34] R. Lewandowski and B. Mohammadi. Existence and positivity results for the phi, teta and a modified k, epsilon two-equation turbulence models. Technical Report 1395, INRIA, 1991.
- [35] R. Lewandowski and B. Mohammadi. Existence and positivity results for the $\varphi - \theta$ and a modified $k - \varepsilon$ two-equation turbulence models. *Mathematical Models and Methods in Applied Sciences*, 3(2):195–215, 1993.
- [36] M. Gómez Mármol and F. Órtegon Gallego. Coupling the Stokes and Navier-Stokes equations with two scalar nonlinear parabolic equations. *Mathematical Modelling and Numerical Analysis*, 33(1):157–167, 1999.
- [37] M. Gómez Mármol and F. Órtegon Gallego. Existence of solution to nonlinear elliptic systems arising in turbulence modelling. *Mathematical Models and Methods in Applied Sciences*, 10(2):247–260, 2000.
- [38] K.A. Cliffe. Some simple solutions of the $k - \varepsilon$ model of turbulence. Technical Report AERE R10241, Harwell, 1981.
- [39] F.S. Henry and A.J. Reynolds. Analytical solution of two gradient-diffusion models applied to turbulent couette flow. *Journal of Fluids Engineering-Transactions of the ASME*, 106(2):211–216, 1984.
- [40] D.J. Tritton. *Physical Fluid Dynamics*. Van Nostrad Reinhold Company, New York, 1977.
- [41] F.C. Carey and H.T. Dinh. Grading functions and mesh redistribution. *SIAM J. Numer. Anal.*, 22(5):1028–1040, 1985.
- [42] J.F. Thompson. A survey of dynamically-adaptive grids in the numerical solution of partial differential equations. *Applied Numerical Mathematics*, 1(1):3–27, 1985.
- [43] P. Knupp and S. Steinberg. *Fundamentals of Grid Generation*. CRC Press, Boca Raton, FL, 1993.

BIBLIOGRAPHY

- [44] J.F. Thompson, Z.U.A. Warsi and C.W. Mastin. *Numerical Grid Generation*. North-Holland, New York, 1985.
- [45] B. van Brunt. *The Calculus of Variations*. Springer-Verlag, New York, 2004.
- [46] A. Winslow. Numerical solution of the quasi-linear poisson equation. *J. Comput. Phys.*, 1:149–172, 1967.
- [47] J.U. Brackbill and J.S. Saltzman. Adaptive zoning for singular problems in two dimensions. *J. Comput. Phys.*, 46(3):342–368, 1982.
- [48] J.U. Brackbill. An adaptive grid with directional control. *J. Comput. Phys.*, 108(1):38–50, 1993.
- [49] W. Huang. Variational mesh adaptation: isotropy and equidistribution. *Journal of Computational Physics*, 174(2):903–924, 2001.
- [50] W. Huang and W.W. Sun. Variational mesh adaptation II: error estimates and monitor functions. *Journal of Computational Physics*, 184(2):619–648, 2003.
- [51] S.C. Brenner and L.R. Scott. *The mathematical theory of finite elements methods*. Springer-Verlag, New York, Inc., 1994.
- [52] C.T. Kelley. *Iterative Methods for Linear and Nonlinear Equations*. SIAM, Philadelphia, 1995.
- [53] J.E. Dennis JR and R.B. Schnabel. *Numerical Methods for Unconstrained Optimization and Nonlinear Equations*. Prentice Hall, New Jersey, 1983.
- [54] E. Zeidler. *Nonlinear Functional Analysis and its Applications I*. Springer-Verlag, New York, 1986.
- [55] J.M. Ortega and W.C. Rheinboldt. *Iterative Solution of Nonlinear Equations in Several Variables*. Academic Press, New York, 1970.
- [56] M.A. Krasnosel'skii, G.M. Vainikko, P.P. Zabreiko, Ya. B. Rutitskii and V. Ya. Stetsenko. *Approximate Solution of Operator Equations*. Wolters-Noordhoff Publishing, Groningen, 1972.
- [57] L.B. Rall. *Computational Solution of Nonlinear Operator Equations*. John Wiley & Sons, Inc., New York, 1969.
- [58] P. Deuffhard. *Newton Methods for Nonlinear Problems*. Springer-Verlag, Berlin Heidelberg, 2004.
- [59] L.B. Rall. A note on the convergcnce of Newton's method. *SIAM J. Numer. Anal.*, 11(1):34–36, 1974.

BIBLIOGRAPHY

- [60] J.D. Pryce. *Basic Methods of Linear Functional Analysis*. Hutchinson & Co. LTD, London, 1973.
- [61] W.C. Rheinboldt. An adaptive continuation process for solving system of nonlinear equations. *Polish Academy of Science, Stefan Banach Center Publ.*, 3:129–142, 1977.
- [62] G. Bader. *Numerische Behandlung von Randwertproblemen für Funktionaldifferentialgleichungen*. PhD thesis, Universität Heidelberg, Inst. Angew. Math., 1983.
- [63] K.A. Cliffe, S.J. Tavener and A.A. Wheeler. An orthogonal mapping technique for the computation of a viscous free-surface flow. *Int. J. Numer. Methods Fluids*, 15(11):1243–1258, 1992.
- [64] G. Ryskin and L.G. Leal. Orthogonal mapping. *Journal of Computational Physics*, 50(1):71–100, 1983.
- [65] D.E. Potter and G.H. Tuttle. The construction of discrete orthogonal coordinates. *Journal of Computational Physics*, 13(4):483–501, 1973.
- [66] S.B. Pope. The calculation of recirculatory flows in general orthogonal coordinates. *Journal of Computational Physics*, 26(2):197–217, 1978.
- [67] P. Morice. Numerical generation of boundary-fitted coordinate systems with optimal control of orthogonality. In K.N. Ghia and U. Ghia, editors, *Advances in Grid Generation*, volume 5 of *ASME Applied Mechanics, Bioengineering and Fluid Engineering Conference*, page 71, Houston, 1983.